



UNIL | Université de Lausanne

Unicentre

CH-1015 Lausanne

<http://serval.unil.ch>

Year : 2013

CELLULAR AND MOLECULAR STUDY OF SUBCORTICAL BAND HETEROTOPIA IN THE MOUSE MUTANT HeCo

KIELAR Michel

KIELAR Michel, 2013, CELLULAR AND MOLECULAR STUDY OF SUBCORTICAL BAND
HETEROTOPIA IN THE MOUSE MUTANT HeCo

Originally published at : Thesis, University of Lausanne

Posted at the University of Lausanne Open Archive.
<http://serval.unil.ch>

Droits d'auteur

L'Université de Lausanne attire expressément l'attention des utilisateurs sur le fait que tous les documents publiés dans l'Archive SERVAL sont protégés par le droit d'auteur, conformément à la loi fédérale sur le droit d'auteur et les droits voisins (LDA). A ce titre, il est indispensable d'obtenir le consentement préalable de l'auteur et/ou de l'éditeur avant toute utilisation d'une oeuvre ou d'une partie d'une oeuvre ne relevant pas d'une utilisation à des fins personnelles au sens de la LDA (art. 19, al. 1 lettre a). A défaut, tout contrevenant s'expose aux sanctions prévues par cette loi. Nous déclinons toute responsabilité en la matière.

Copyright

The University of Lausanne expressly draws the attention of users to the fact that all documents published in the SERVAL Archive are protected by copyright in accordance with federal law on copyright and similar rights (LDA). Accordingly it is indispensable to obtain prior consent from the author and/or publisher before any use of a work or part of a work for purposes other than personal use within the meaning of LDA (art. 19, para. 1 letter a). Failure to do so will expose offenders to the sanctions laid down by this law. We accept no liability in this respect.

Département de Neuropsychologie et de Neuroréhabilitation

**CELLULAR AND MOLECULAR STUDY OF SUBCORTICAL BAND
HETEROTOPIA IN THE MOUSE MUTANT *HeCo***

Thèse de doctorat en Neurosciences

présentée à la

Faculté de Biologie et de Médecine
de l'Université de Lausanne

par

Michel KIELAR

Diplômé en Neurosciences à l'Université de Strasbourg, France

Jury

Prof. Jean-Pierre Hornung, Président
PD Alexandre Croquelois, Directeur
Prof. Egbert Welker, Co-Directeur
Prof. Denis Jabaudon, Expert
Prof. Philippe Maeder, Expert

Lausanne 2013

*Programme doctoral interuniversitaire en Neurosciences
des Universités de Lausanne et Genève*

**Programme doctoral interuniversitaire en Neurosciences
des Universités de Lausanne et Genève**

Imprimatur

Vu le rapport présenté par le jury d'examen, composé de

Président	Monsieur Prof. Jean-Pierre Hornung
Directeur de thèse	Monsieur Prof. Alexandre Croquelois
Co-directeur de thèse	Monsieur Prof. Egbert Welker
Experts	Monsieur Prof. Denis Jabaudon
	Monsieur Prof. Philippe Maeder

le Conseil de Faculté autorise l'impression de la thèse de

Monsieur Michel Kielar

master en neurosciences de l' Université Louis Pasteur de Strasbourg, France

intitulée

**CELLULAR AND MOLECULAR STUDY OF
SUBCORTICAL BAND HETEROTOPIA
IN THE MOUSE MUTANT *HECO***

Lausanne, le 15 avril 2013



pour Le Doyen
de la Faculté de Biologie et de Médecine

Prof. Jean-Pierre Hornung

Acknowledgements

First, I would like to thank my thesis director, Alexandre Croquelois, for welcoming me and hiring me to start this marvelous “*HeCo*” project. I appreciated his trust in me to manage this work. I am grateful for all the connections I could get with great people through Alexandre’s ability to collaborate. I also keep a great memory of Alexandre’s help in the analysis of results and for the jokes he shared to keep a joyful ambience at work.

My sincere gratitude to the Professor Egbert Welker who helped me through difficult times to keep looking in the right direction and for relevant conversations we had concerning science as well as funny moments we spent thank to his great sense of particular and recognizable humour ☺. I want to say that besides his scientific heart, he is a great man who even shared his personal belongings with me (huge THANK for the BUS!) which translates his great support when someone needs concrete help. I am also very conscious of the great advices and the precious correction process he lead me through which are just priceless, I couldn’t have done this manuscript without him...

I insist to share my greetings with the marvellous collaborators, Fiona Francis & Françoise Phan-din Tuy from the Institut du Fer à Moulin in Paris, with whom I exchanged great expertise and who have done a fantastic work during my thesis journey. For sure we will stay in contact with them in the future. I would also like to thank Cécile Lebrand who helped me with her technical skills and methodological approach of the scientific work as well as adventurous collaborative moments.

My thankfulness goes also to the members of the Jury, Pr. Denis Jabaudon, Pr. Jean-Pierre Hornung and Pr. Philippe Maeder who kindly accepted to evaluate my thesis work which makes me feel very honored and proud.

Isabel, my love, wife, my coach, my friend, my punching-ball, the mother who gave me my extremely cute daughter Annaëlle...Isabel, my partner of life who is closely and lovely there to answer my needs...I love you! You are very unique and precious to me.

To my family who was really helpful and supportive, I give you all a big HUG especially to my parents who prayed for me and took care of Annaëlle so I could finish this work. Catherine, thanks for your advices and corrections. Marie, thanks for motivating me.

A special thank goes to people who helped me in different ways to achieve my thesis work and publications Gwendolline Boillat, Delphine Valloton, Christiane Desvenoges, Mathieu Niquille, Jean-Pierre Hornung, Julien Puyal, Vanessa Ginet Puyal, Rudolf Kraftsik, Joerg Kleeberg, Paola Bezzi, Nicolas Toni, Peter Clarke, Hubert Fiumelli, Yannick Krempp, Thidung Hau-Iuliano and Romano Regazzi.

A warmhearted THANKS! goes to my former and present colleagues: Mathieu Niquille, Delphine Valloton, Nathalie Wenger, Christine Savary, Aouatef Abaza, Ines Khadimalla, Charles Guilliéron, Hugues Cadas, Marie Pertin, Alexandre Pinault, Sonia Naegele-Tollardo, Alexabdre Sandoval, Eric Bernardi, the DNF technical crew and the secretary team.

Abstract

The *HeCo* mouse model is characterized by a subcortical heterotopia formed by misplaced neurons normally migrating into the superficial cortical layers. The mutant mouse has a tendency to epileptic seizures. In my thesis project we discovered the mutated *Eml1* gene, a member of the echinoderm microtubule-associated protein (EMAP) family, in *HeCo* as well as in a family of three children showing complex malformation of cortical development. This discovery formed an important step in exploring the pathogenic mechanisms underlying the *HeCo* phenotype. *In vitro* results showed that during cell division the EML1 protein is associated with the midbody and a mutated version of *Eml1* highlighted an important role of the protein in the astral MT array during cell cycle. *In vivo*, we found that already at an early age of cortical development (E13), ectopic progenitors such as RGs (PAX6) and IPCs (TBR2) accumulate in the IZ along the entire neocortex. We demonstrated that in the VZ of the *HeCo* mouse, spindle orientation and cell cycle exit are perturbed. In later stages (E17), RG fibers are strongly disorganized with deep layer (TBR1) and upper layer (CUX1) neurons trapped within an ectopic mass. At P3, columns of upper layer neurons were present between the heterotopia and the developing cortex; these columns were also present at P7 but at lesser extent. Time lapse video recording (E15.5) revealed that the parameters characterizing the migration of individual neurons are not disturbed in *HeCo*; however, this analysis showed that the density of migrating neuron was smaller in *HeCo*. In conclusion, truncated EML1 is likely to play a prominent role during cell cycle but also acts on the cytoskeletal architecture altering the shape of RG fibers thus influencing the pattern of neuronal migration. The signal transduction between external cues and intracellular effector pathways through MTs may be secondary but sustains the heterotopia development and further studies are needed to clarify the impact of EML1 in progenitors versus post-mitotic cells.

Résumé

Le modèle de la souris *HeCo* est caractérisé par une hétérotopie subcorticale formée par des neurones, qui migrent normalement vers les couches corticales superficielles. La souris mutante a une tendance à manifester des crises d'épilepsie. Dans mon projet de thèse, nous avons découvert le gène muté *Eml1*, membre de la famille des protéines associées aux microtubules chez les échinodermes (EMAP), aussi bien chez la souris *HeCo* que dans une famille de trois enfants présentant une malformation complexe du développement cortical. Cette découverte a constitué une étape importante pour explorer les mécanismes pathogènes sous-jacents au phénotype *HeCo*. Les résultats *in vitro* ont montré que pendant la division cellulaire, la protéine EML1 était associée avec le « midbody » et jouait un rôle important pendant le cycle cellulaire dans la structure astrale formée par les microtubules. *In vivo*, nous avons trouvé que dès le développement cortical précoce (E13), des progéniteurs ectopiques tels que la glie radiaire (PAX6) et les cellules progénitrices intermédiaires (TBR2) s'accumulent dans la IZ et le neocortex tout entier. Nous avons démontré que dans la VZ du mutant *HeCo*, l'orientation du plan de division ainsi que la sortie du cycle cellulaire étaient perturbés. Dans des stades de développement plus tardifs (E17), les fibres radiaires étaient fortement désorganisées avec des neurones des couches profondes (TBR1) et des couches supérieures (CUX1) formant une masse ectopique. A P3, des colonnes de neurones des couches supérieures étaient présentes entre l'hétérotopie et le cortex en développement ; ces colonnes étaient également visibles à P7 mais formé par moins de neurones. Les enregistrements vidéo en time lapse (E15.5) ont révélé que les paramètres caractéristiques de la migration de neurones individuels n'étaient pas perturbés dans la souris *HeCo*; cependant, cette analyse a montré que la densité des neurones en migration était moindre chez *HeCo*. En conclusion, la version tronquée d'EML1 semble jouer un rôle important pendant le cycle cellulaire, mais en agissant également sur le cytosquelette en altérant la forme des fibres radiaires, influençant ainsi le pattern de la migration neuronale. Tout en maintenant le développement de l'hétérotopie, la transduction du signal entre les informations externes et l'action des effecteurs intracellulaires via les microtubules pourrait être secondaire. Des recherches supplémentaires sont nécessaires pour clarifier l'impact d'EML1 dans les progéniteurs et les cellules post-mitotiques.

List of Abbreviations

ABL1	Abelson 1
AJ	adherens junctions
APC	adenomatous polyposis coli
aPKC λ	atypical protein kinase C λ
Ara-C	cytosine arabinoside
<i>Arfgef2</i>	ADP-ribosylation factor guanine nucleotide-exchange factor 2
aRG	apical radial glia
<i>Arx</i>	aristaless related homeobox
Aspm	abnormal spindle-like microcephaly-associated
BCNU	1-3-bis-chloroethylnitrosurea
bRG	basal radial glia
BXD29	mouse strain selectively used as an animal model for heterotopia
CDC42	cell division control 42
CD133	prominin 1
CGE	caudal glanglionic eminence
CP	cortical plate
Ct	centrosome
CUX1	cut-like homeobox 1
Div	days in vitro
DiI	1, 1'-dioctadecyl-3,3,3',3'-tetramethylindocarbocyanine perchlorate
DCX	doublecortin
DNA	deoxyribonucleic acid
dP	dorsal pallium
E13	embryonic day 13
EGFP	exogenous green fluorescent protein
EMAP	echinoderm microtubule-associated protein
EML1	echinoderm microtubule-associated protein like 1
<i>Emx2</i>	empty spiracles homeobox 2
FAK	focal adhesion kinase
FGF	fibroblast growth factor
<i>Flna</i>	filamin A, alpha
G α i	heterotrimeric G-protein alpha subunit
GABA	gamma aminobutyric acid
GFAP	glial fibrillary acidic protein
GPR56	G protein-coupled receptor 56
GW	gestational week
HeCo	heterotopic cortex mouse model of SBH
HELP	hydrophobic echinoderm-like protein
HES1	hairy and enhancer of split-1
hGFAP	human glial fibrillary acidic protein
Hipp	hippocampus
IFL	inner fiber layer
INM	interkinetic nuclear migration

IPC	intermediate progenitor cell
ISVZ	inner subventricular zone
IZ	intermediate zone
LGE	lateral ganglionic eminence
LIS	lissencephaly
LIS1	lissencephaly 1
Lmx1a	LIM homeobox transcription factor 1, alpha
MAM	methylazoxymethanol
MAP	microtubule associated proteins
MARCKS	myristoylated alanine-rich protein kinase C substrate
MARK	microtubule-affinity-regulating-kinase
MCD	malformation of cortical development
MEG	megalencephaly
MGE	medial ganglionic eminence
mGluR	metabotropic glutamate receptor
MIC	microcephaly
MRI	magnetic resonance imaging
MS	mitotic spindle
MST	mitotic somal translocation
MT	microtubule
MZ	marginal zone
NCK	non-catalytic region of tyrosine kinase adaptor protein
NDE1	nuclear distribution E homolog 1
NeSC	neuroepithelial stem cell
NeuN	neuronal nuclear antigen
NMDA	N-Methyl-D-aspartate
NOR-CD1	mouse strain which <i>HeCo</i> mouse model for SBH derives from
NOTCH	notch (<i>Drosophila</i>) homolog (translocation-associated)
NUMB	numb (<i>Drosophila</i>) homolog
NuMA	NuMA, nuclear mitotic apparatus protein
OFC	occipital-frontal cortex
OFL	outer fiber layer
oRG	outer radial glia
OSVZ	outer subventricular zone
P3	Postnatal age
PAFAH1B1	platelet-activating factor acetylhydrolase 1b, regulatory subunit 1
PAR3	partitioning defective 3
PAX6	paired box 6
Pins	Partner of Inscuteable
PMC	primary motor cortex
PMG	polymicrogyria
<i>Pou3f2/3</i>	POU class 3 homeobox transcription factor 2/3
PS	pial surface
PVC	primary visual cortex
<i>Ra-gef1</i>	guanine Nucleotide Exchange Factor for Rap1
<i>Reln</i>	reelin
RG	radial glia

<i>RhoA</i>	ras homolog family member A
RNAi	ribonucleic acid interference
SBH	subcortical band heterotopia
SD	standard deviation
SNP	short neural precursor
SOX2	SRY-related HMG-box 2
sP	subpallium
SP	subplate
SPARC	secreted protein, acidic, cysteine-rich (osteonectin)
SVZ	subventricular zone
T α 1	gene promoter
TBR1	T-box brain factor 1
TBR2	T-box Eomes 2
TUBA1A	tubulin, alpha 1a
VZ	ventricular zone
WD	tryptophan aspartate
<i>Wnt3a</i>	wingless-type MMTV integration site family, member 3A
WT	wild type

Contents

List of Figures and Tables	i
Introduction	1
I. The human brain.....	3
I.1. Structure of the cerebral cortex	4
I.1a. Cortical cells.....	4
I.1b. The layer pattern of the cerebral cortex	5
The concept of layer	5
Cellular distribution between layers.....	7
Layer connectivity	7
I.2. Development of the Cerebral cortex	8
I.2a. Neural tube formation.....	8
I.2b. Neural proliferation	10
Neuroepithelial stem cells	10
Radial glial cells	12
Intermediate progenitor cells	16
I.2c. Neuronal migration	16
Radial and tangential migration.....	16
Multipolar migration.....	19
I.2d. Neuronal Differentiation	20
II. Background of cerebral malformations	20
II.1. Human malformations of cortical development	21
II.1a. Clinical aspects	21
II.1b. Classification of MCDs	23
II.2. Basic mechanisms of pathologic cortical development	24
II.2a. Pathologic mechanisms leading to MCDs	24
Group I: malformations secondary to abnormal neuronal and glial proliferation or apoptosis	24
Group II: malformations of abnormal migration	25
Group III: malformations of abnormal postmigrational development	26

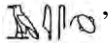
II.2b. Comparison of genes involved in MCDs: animal VS human	27
II.2c. Animal Models of MCD	27
Models including proliferation defects	27
Models including migration defects	28
Epileptic phenotype in animal models	28
The <i>HeCo</i> mouse	30
Aim of this study.....	31
Results	32
Results-Part1: characterization of the <i>HeCo</i> mutant mouse: a new model of subcortical band heterotopia associated with seizures and behaviour deficits.....	32
Summary	32
Results-Part2: mutations in EML1/Eml1 lead to misplaced neuronal progenitors during cortical development and massive heterotopia in mouse and human.....	35
Summary	35
General Discussion	39
I. Proliferation and cell cycle defects	40
I.1. Longer cell cycle may delay the engagement in neuronal migration and contribute to <i>HeCo</i> pathology	40
I.2. Mitotic spindle disorientation drives progenitors misplacement	41
I.3. The role of the neurogenetic gradient in heterotopic location	41
II. Altered migration patterns in <i>HeCo</i>	42
II.1. Altered radial glial guided migration does not totally abort the formation of cortical layers in <i>HeCo</i>	42
II.2. Late RGC fibers alterations during embryogenesis may affect predominantly superficial neurons in the adult <i>HeCo</i> mouse	43
II.3. Columns of immature cells could promote <i>HeCo</i> phenotype	44
II.4. Misplaced apical and basal progenitors participate to <i>HeCo</i> pathogenesis	45
III. EML1 role in the <i>HeCo</i> mouse.....	46
III.1. EML1 role in proliferation.....	46
III.2. EML1 role in migration	47
IV. Conclusion and perspectives	48

References	51
References to webpages.....	71
Articles	72
Croquelois <i>et al.</i> , 2009.....	73
Kielar <i>et al.</i> , 2013	86

List of Figures and Tables

Figure 1: Two sketches of the human brain by Leonardo di ser Piero da Vinci (1508)	2
Figure 2: Major neuronal cell types of the adult cerebral cortex	5
Figure 3: Neocortex organization in the human adult brain	6
Figure 4: Neural tube development during human embryogenesis	9
Figure 5: Molecular segregation and mitotic spindle orientation in mouse cell fate specification .	11
Figure 6: The development of the cerebral cortex	13
Figure 7: bRG in human OSVZ during neocortical development	15
Figure 8: Radial glial scaffold	17
Figure 9: Contrasting rodent and human neocortical development	18
Figure 10: Magnetic Resonance Imaging micrographs of different typical MCDs	22
Figure 11: Cx26-dependent glial-guided migration is regulated by FAK	43
Figure 12: Hypotheses for the development of the SBH in <i>HeCo</i>	50
Table 1: Simplified classification scheme of Barkovich	24
Table 2: Malformations of cortical development with associated genes and clinical features	26
Table 3: Animal models of focal cortical dysplasia and related malformations of cortical development	29

INTRODUCTION

The brain is known as the most important, complex and mysterious organ. Ancient Egyptians handled it through ancestral mummification procedure for hundreds of years but they did not consider this marvelous organ of great value. This practice consisted of extracting as much of the brain as possible with an iron hook to throw it away. Nevertheless, a document talking about the nervous system was found in Egypt by E. Smith in 1822; a papyrus record written around 1700 B.C. using the word brain for the first time, hieroglyphic “” (Kandel *et al.*, 2000). Indeed, it describes a few lesions related to the nervous system, even mentioning neuroanatomical parts of the brain such as meninges (coverings of the brain) and cerebrospinal fluid with texts going back to 3000 B.C. One thousand years later, the ancient greeks focused their work on the mind and the spirit according to brain functions for philosophical interest. Alcmeon of Croton, 6th and 5th centuries B.C., was the first to consider the brain as the location of the mind. In the 4th century B.C., Hippocrates believed the brain to be the “seat of intelligence”. In the antic Rome, Galen dissected the brains of different mammals and concluded that the strong density of the cerebellum reflects muscles control whereas the softness of the cerebrum permits senses processing (Bear *et al.*, 2001). During the Renaissance, Andreas Vesalius worked on human cadavers and discovered many anatomical features such as the “Putamen” and “Corpus Callosum” (*De humani corporis fabrica*, 1543) and proposed that the brain was made up of seven pairs of functionally specialized “brain nerves” (Van Laere, 1993). Leonardo da Vinci also did great anatomical findings and drew detailed sketches of the human brain (Figure 1) but never published his work.

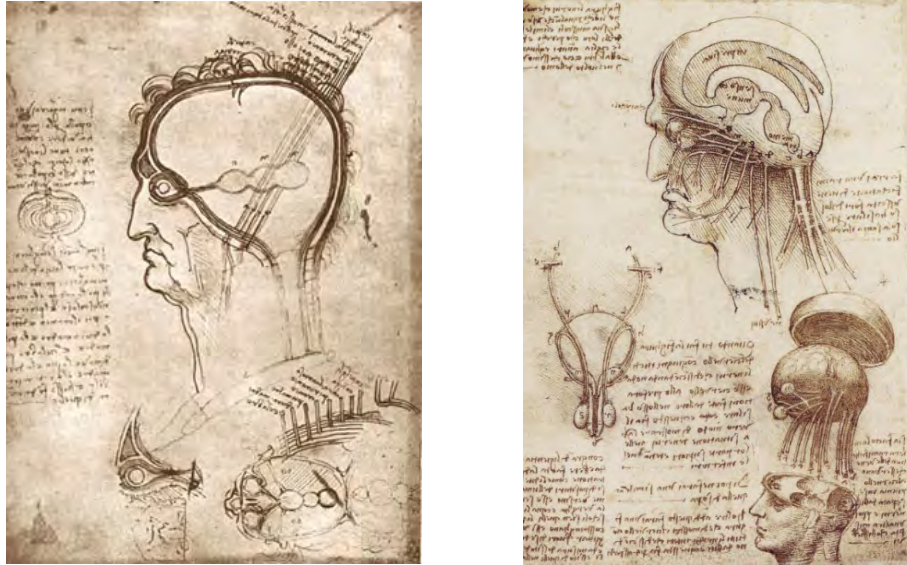


Figure 1: Two sketches of the human brain by Leonardo di ser Piero da Vinci (1508). (Left) Brain study. (Right) Study of brain physiology. Sourced from <http://www.drawingsofleonardo.org/http://davincighost.buzznet.com/photos/default/?id=1404298>

Descartes formulated mechanisms responsible for circulating cerebrospinal fluid and developed the theory of dualism suggesting that the pineal gland was where the mind interacted with the body (Lokhorst, 2011). Studying the brain became more sophisticated since the invention of the microscope by Galileo in 1609 and its further development by Christian Huygens at the end of the 17th century. Staining procedure invented by Golgi in 1873 had a huge impact on histological approach of science that revealed the intricate structures of single neurons with silver chromate. Santiago Ramon y Cajal, used Golgi's technique and established the neuron doctrine in 1880: the neuron is the functional unit of the brain. This hypothesis opened the way for numerous scientists to perform pioneering work in electrophysiology like Emil du Bois-Reymond or Hermann von Helmholtz who showed that neurons were electrically excitable cells and that their activity modulated the electrical state of adjacent neurons in a foreseeable manner. In parallel with this research, Paul Broca worked with patients with cerebral damages and suggested a link between regions of the brain and certain functions. Furthermore, Carl Wernicke (1874) has developed the theory of specialization after discovering that specific brain structures are related to language comprehension and production.

In the same period of time, Jean-Martin Charcot introduced “Neurology” (term invented by Thomas Willis), as a medical specialty studying diseases of the nervous system, in particular in the brain. He made the link between lesions of certain cortical regions and motor deficiencies and thus decided to separate the neurology from the psychiatric field. In 1882, the first chair of neurology was established for Charcot and he launched his school of neurology at the Hôpital de la Salpêtrière in Paris. Meanwhile, Brodmann described the parcellation of the cerebral cortex into different cortical areas on the basis of cytoarchitectonic criteria (distribution of cell types and laminar organization; Brodmann K., 1909). Brodmann proposed that each area would be activated during the execution of specific tasks. His work resulted in a complex and precise map of 52 discrete areas of the human brain that is still used by modern science. Interest in the brain increased exponentially in the 20th century and a new era of research emerged in the 1960’s known as “Neurosciences”. This modern field began principally with an electrophysiological approach as mentioned before (du Bois-Reymond, von Helmholtz) and has carried a variety of titles through the years depending on the techniques used. However, it is nowadays a very interdisciplinary domain encompassing, a diversity of research areas such as biology, medicine, psychology, physics, chemistry, mathematics, informatics and computational science, all together directing efforts to try to unravel the mystery of the human brain.

I. The human brain.

Among many important cerebral structures, like the thalamus involved as a relay for external stimuli or the medulla regulating autonomic vital functions, the neocortex is a very determinant one (Kandel *et al.*, 2000). It is a six-layered organized sheet of neural tissue at the outermost part of the telencephalic hemispheres and forms phylogenetically, the most recent part of the cerebral cortex in mammalian evolution. Depending on the species, it can be folded with convolutions (gyrencephalic species) or almost smooth (lissencephalic species) (see review, Lui *et al.*, 2011; Borell and Reillo, 2012). The neocortex is involved in several higher cognitive, motor and sensory functions, coordinating external and internal informations to build and communicate programmed tasks to subcortical regions (thalamus, medulla, spinal cord) in order for the body to effectuate an adapted response. These complex activities are regulated by molecular processes that

control the identity, positioning and connections of nervous cells. (Borello and Pierani, 2010; Manzini and Walsh, 2011; Rubenstein, 2011; Kwan *et al.*, 2012).

1.1. Structure of the cerebral cortex

1.1a. Cortical cells

The adult cerebral cortex (further referred to as “cortex”) is composed of different cell types organized in a network. The cortex is part of “the grey matter” because of its natural darker tint when dissected. Indeed, the grey matter contains the cell bodies of “excitable cells” called neurons, the sole capable to create the nervous message (Kandel *et al.*, 2000). However, to sustain and modulate this neuronal circuitry, “non-excitable cells” called glia (astrocytes, oligodendrocytes, macro- and microglia) are integrated within the grey matter and constitute 50% of adult brain cells. A neuron is generally described as a polarized structure with a spherical body shape (soma) from which emerge fibers: a long one, the axon (generation and conduction of the electric nervous message) and several small ones at the opposite side of the soma, the dendrites. The subcortical white matter is called “white” because it is formed by a large proportion of axonal fibers coated with myelin protein, produced by oligodendrocytes, it also contains other glial cells. The connections between axons and dendrites are generally made by synapses and are (partially) surrounded by processes of glial cells (Kandel *et al.*, 2000). There are two major neuronal cell types in the human adult cortex with distinct morphological aspects and molecular signatures: projection neurons and interneurons (Figure 2) (Jones, 1986; DeFelipe and Farinas, 1992; Kwan *et al.*, 2012). Projection neurons use glutamate as neurotransmitter and are therefore excitatory. Morphologically, these neurons are characterized by a long axonal fiber that projects to another part of the brain but that also provides local axonal projections via axonal collaterals. Their dendrites contain spines with which the cell makes excitatory synapses. In contrast, the axon of an interneuron remains within the same part of the brain as where the cell body and dendrites are localized to participate in local neuronal circuitry. These neurons can be either excitatory (using glutamate as neurotransmitter) or inhibitory (using GABA -gamma aminobutyric acid- as neurotransmitter).

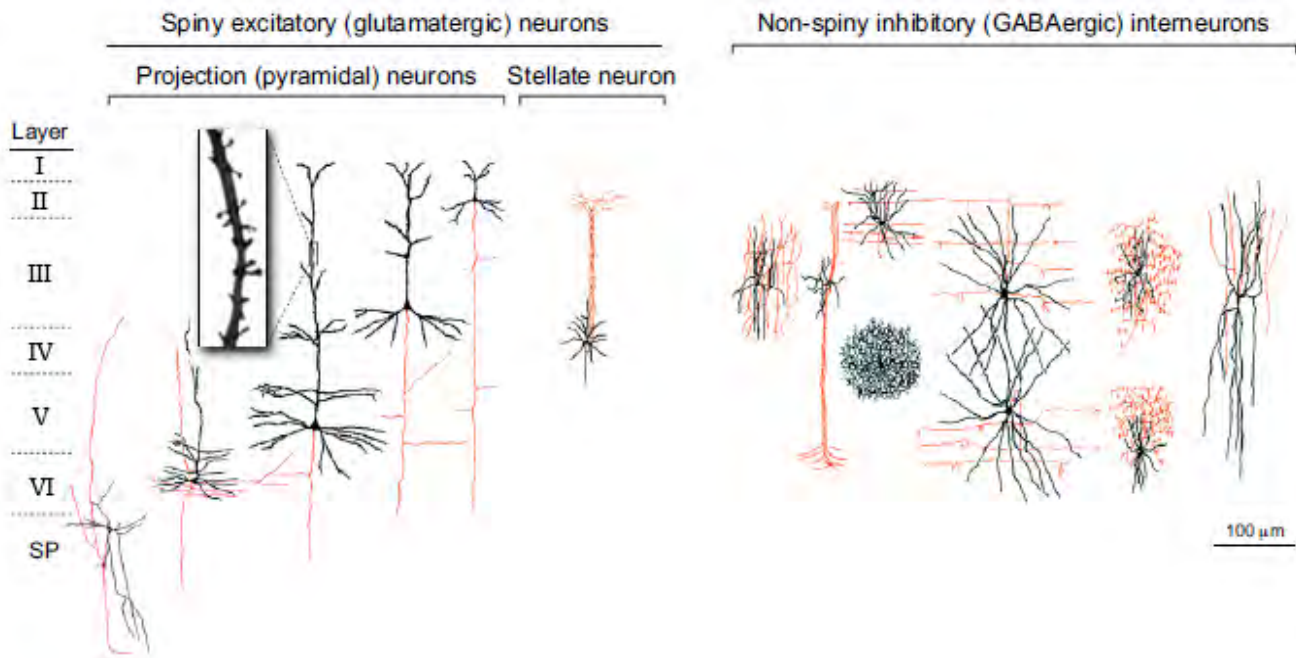


Figure 2: Major neuronal cell types of the adult primate cerebral cortex. Cortical neurons are categorized into two major classes: spiny excitatory (glutamatergic) neurons (left panel) and non-spiny inhibitory (GABAergic) interneurons (right panel). The former, the dendrites of which are decorated by numerous post-synaptic membranous protrusions termed spines, include the projection (pyramidal) neurons, the principal cells of the neocortex, and stellate neurons, which are mostly found in layer IV of primary sensory areas. Projection neurons display marked layer- and subtype-specific differences in the morphology of their dendrites (black) and in the targets of their axonal projections (red) connecting different layers and structures (cortical or subcortical regions). The non-spiny interneurons, which are highly diverse in morphology, neurochemistry and electrophysiology, project axons within a local circuit. Subtypes of interneurons also display laminar preferences, thereby contributing to layer differences in cortical circuitry. SP, subplate. Adapted from Jones, 1986 and Kwan *et al.*, 2012.

1.1b. The layer pattern of the cerebral cortex

The concept of layer

The neocortex is composed of 6 horizontal layers (Figure 3). Although the cortex appears globally uniform, the distribution of cell bodies among the cortical layers is varied. On the basis of these differences, cortical areas can each be distinguished with a well characterized laminar pattern. These cytoarchitectonic differences reflect the diversity in the functional organization between cortical areas, each possessing a special function (Brodmann, 1909; Kandel *et al.*, 2000). For example, the primary visual cortex (PVC) distinguishes its cerebral function (processing ocular information) from other specialized cortices by its unique laminar and cellular organization as well as its input. First, layer IV of the PVC is thicker than the layer IV of the primary motor (PMC) and parietal-temporal-occipital association cortices (Figure 3, A). Plus, the preferential response of neu-

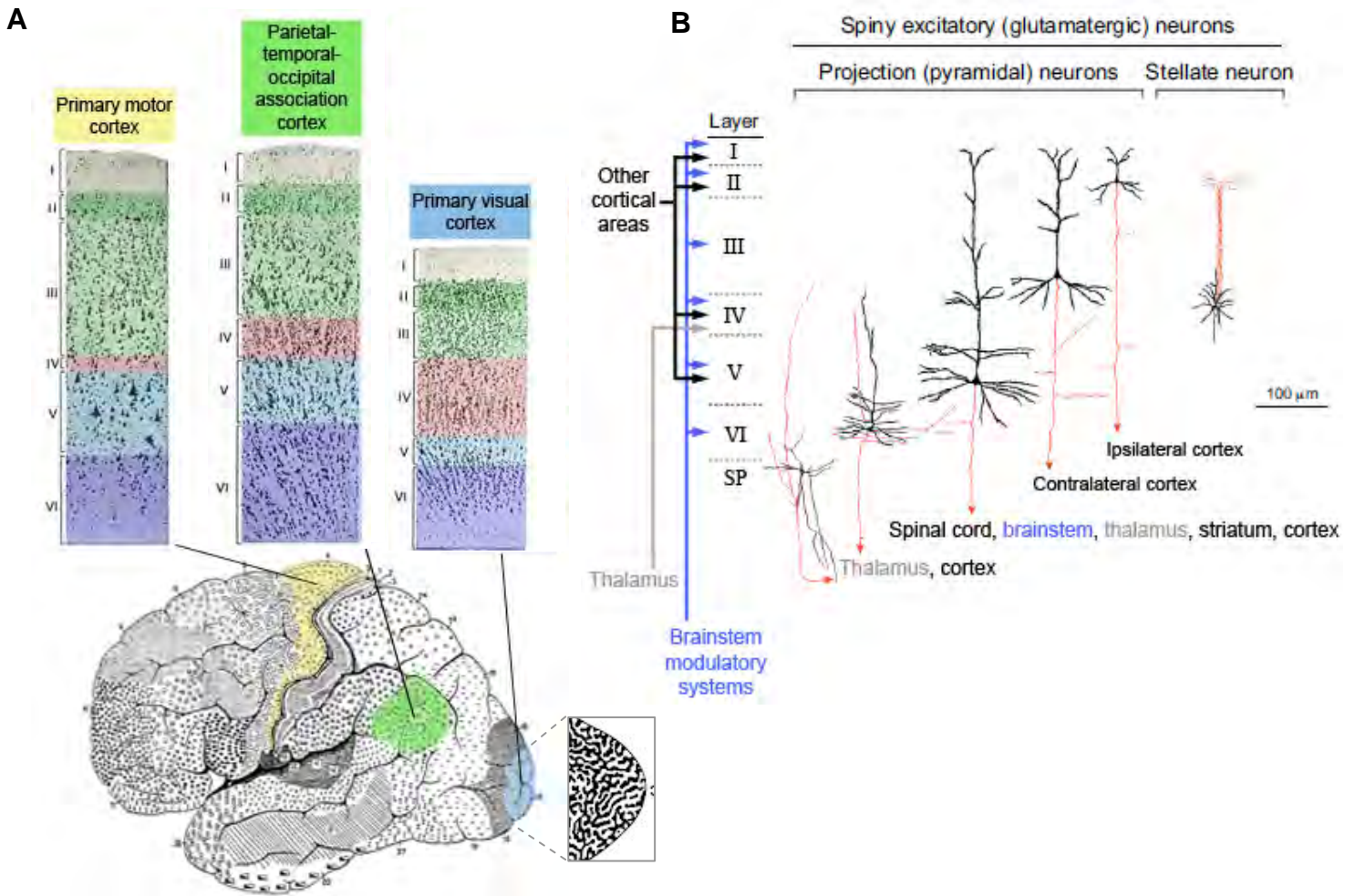


Figure 3: Neocortex organization in the human adult brain. (A) Representations of different regions of the neocortex according to Brodmann's cytoarchitectonic map of the brain (lateral view). It is composed of 6 layers, layer I (molecular) being the most superficial one and layer VI (polymorphous) the deeper one. Layer I is very singular and contains just a few scattered neuronal and glial cells. Note the large thickness of layer IV in the primary visual cortex which cellular distribution (traced with radioactive molecules injected in one eye; black stripes) is organized in ocular dominance columns resulting in a striped cortex complementary of each hemisphere. (B) Connectivity scheme of the neocortex. Layer II (external granular) and III (external pyramidal) project to other cortical regions either by intrahemispherical axonal fibers (ipsilateral) or interhemispherical (contralateral) connections through the corpus callosum which is the main communicating conduit linking both hemispheres. Layer V (internal pyramidal) projects to subcortical regions and layer VI mainly to the Thalamus. Layer IV (internal granular) is mainly a receptive band of cells with projections coming from the thalamus. Arrows representing connections between layers and other structures of the brain. Adapted from Brodmann, 1909; Carpenter, 1985 and Kwan *et al.*, 2012.

-rons to the input of the connected eye, also known as retinotopy, results in a particular striped cortical sheet configuration restricted selectively to the PVC layer IV (LeVay *et al.*, 1980). This phenomenon is due to the recruitment of cells organized together in functional units, so-called ocular dominance columns. A cortical layer is hence recognizable by a more or less specific group

of cells with a relative homogeneity in their morphology, density, molecular identity, inputs and outputs determining its specialized function (Jones, 1986; DeFelipe and Farinas, 1992).

Cellular distribution between layers

Pyramidal neurons and interneurons are mainly settled through the five horizontal layers (II-VI) of the neocortex, layer I being the most superficial and layer VI the deepest (Figure 3). The morphological cellular differences observed in the six layers lead to separate them histologically: layer VI is called polymorphous; layer V, internal pyramidal, layer IV, internal granular; layer III, external pyramidal; layer II, external granular; and layer I, molecular. The molecular layer consists in majority of dendritic branches and horizontal axons, only a few dispersed neurons as well as some glial cells are present. In contrary, large pyramidal projection neurons, called “Betz cells” (Vladimir Alekseyevich Betz described them in 1874) are present exclusively in layer V especially in the primary motor cortex. Furthermore, projection neurons exhibit layer specific markers due to expression of particular genes (most of the time specific transcription factors), i.e. T-box brain factor 1 (TBR1) is expressed by the post-mitotic cells of layer VI (Hevner *et al.*, 2001); cut-like homeobox 1 (CUX1) protein expressed by layer II-IV neurons (Cubelos *et al.*, 2010). These molecular markers together with differences in electric firing and neuronal connections determine the specific properties of neurons within a given layer (DeFelipe and Farinas, 1992; O’Leary and Koester, 1993). Interneurons do also have their own particularities with a layer-specific segregation in the neocortex according to distinct morphological, neurochemical and electrophysiological features. For example, calretinin expressing neurons are found in layers II-IV and somatostatin expressing interneurons are concentrated in layers V-VI (Wonders and Anderson, 2006; Rudy *et al.*, 2010). These differences among neuronal cells in terms of distribution and molecular characteristics are contributing to layer differences in local and global circuits building specific networks in the neocortex (Miyoshi *et al.*, 2007; Miyoshi and Fishell, 2011; Lodato *et al.*, 2011).

Layer connectivity

The connectivity between two cortical layers or between a layer and a distinct anatomical structure comprises afferent (incoming information) and efferent (outgoing information) axonal projections (Figure 3, B). Generally, layer IV is considered as the main “afferent” layer because in sensory areas it is the layer that receives the sensory information from the subcortical level whereas layers II-III and V-VI are the main efferent layers redirecting the information to other parts of the brain

and subcortical regions, respectively (Kandel *et al.*, 2000). The global afferent and efferent connections segregate neocortical layers into two groups: deep layers (V-VI) and upper-layers (I-IV). More precisely, layer VI has a major efferent connection with the thalamus, but it also sends long horizontal axonal fibers along deep layers of the cortex (Thomson, 2010). Layer V is a large output layer with efferent connections to a variety of subcortical structures such as striatum, tectum, pons, medulla and spinal cord (Bannister, 2005). Layer IV is essentially present in primary sensory areas as a singular band of granular cells (small stellate neurons) that receive sensory inputs from the thalamus (Miller *et al.*, 2001). Layer III is an important cortical layer that dispatches axons through the corpus callosum, the biggest bundle of commissural fibers, to communicate with the opposite hemisphere and thus coordinating the whole cortical tissue (Payne *et al.*, 1984; Rajkowska *et al.*, 1998). Layer II is also restricted to interact only intracortically but uniquely in the same hemisphere thus sustaining associational connections in partnership with layer III of other cortical areas (auditory, visual, somatosensory areas; Bannister, 2005) to facilitate cognitive processes as face recognition (Young and Yamane, 1992). In addition to other cortical and subcortical inputs, the six layers receive afferent projections from the modulatory systems of the brainstem (catecholaminergic, cholinergic and serotonergic) (Purves *et al.*, 2004).

1.2. Development of the Cerebral cortex

Widely studied in rodents, monkeys and humans (Molnár *et al.*, 2006; Bystron *et al.*, 2008; reviewed in Lui *et al.*, 2011, Borell and Reillo, 2012), corticogenesis is based on successive finely tuned cellular processes such as proliferation, migration and connectivity formation. In 1889, Wilhelm His was the first to raise the idea that during development proliferating cells lining the ventricles of the neural tube will shape the structure and organization of the mature adult neocortex.

1.2a. Neural tube formation

After implantation of the zygote in the uterine wall, the embryo grows and forms a sphere of 3 germinal sheets (gastrula stage) the endoderm, the mesoderm and the ectoderm from which will derive the “neural tube”. The neural tube is an open tubular structure that will establish the nervous system of the entire body under the control of specific genes expression (Rowitch and Kriegstein, 2010). After the closure of both distal parts of the neural tube during the 4th gestational week (GW), 3 primary vesicles increase their size and differentiate at the rostral neuropore (Figure 4, A):

prosencephalon (forebrain), mesencephalon (midbrain) and rhombencephalon (hindbrain). Then, the prosencephalon divides into telencephalon and diencephalon, the mesencephalon does not change its identity but is still evolving and the rhombencephalon splits into metencephalon and myelencephalon (Figure 4, B). These 5 secondary vesicles will rapidly increase their size to build the future adult brain thanks to regulated cellular processes such as proliferation (Dehay and Kennedy, 2007) and migration (Huang, 2009).

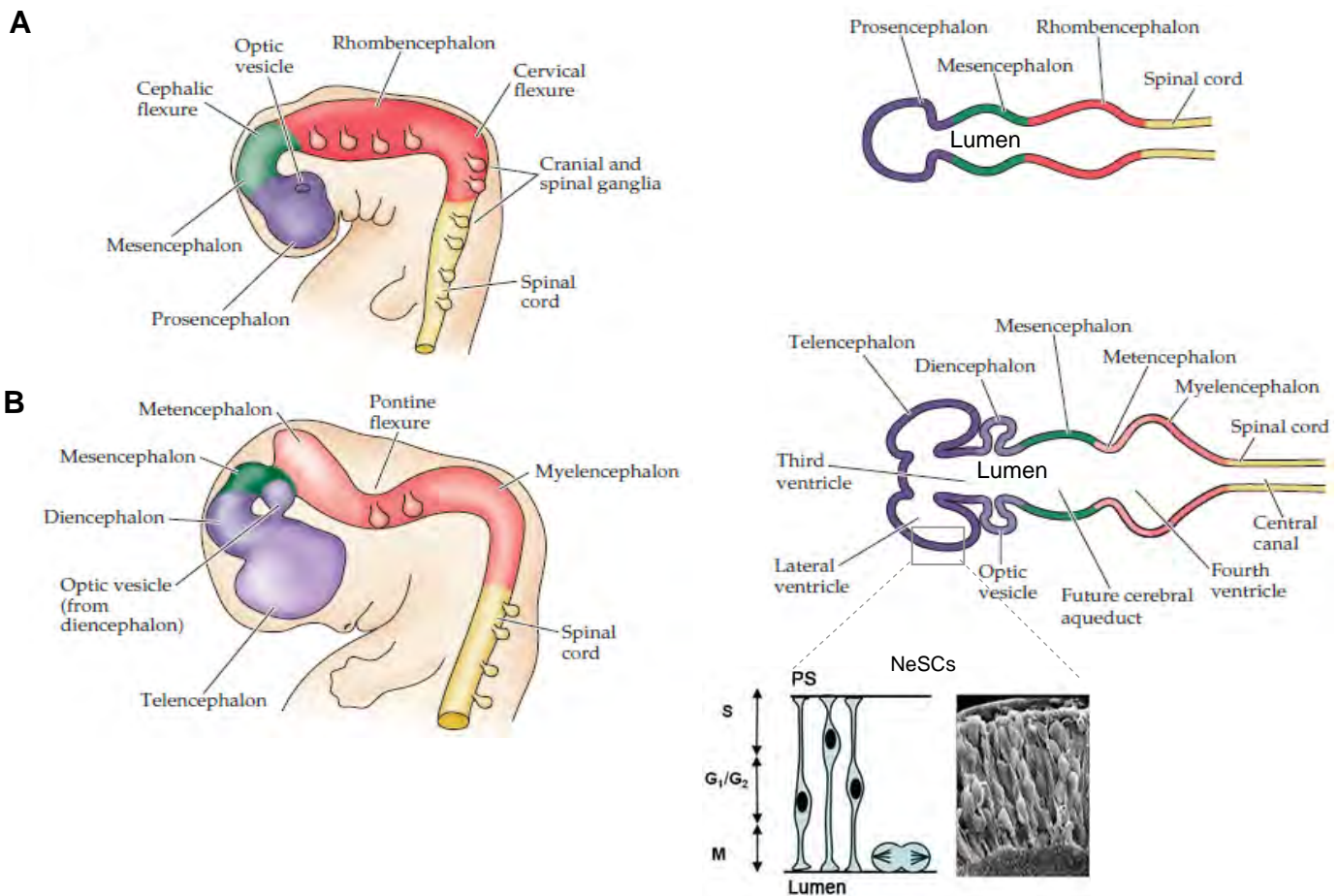


Figure 4: Development of the Neural tube during human embryogenesis. (A) At embryonic day E35-38, the neural tube begins the differentiation of its anterior neuropore into 3 primary vesicles: Prosencephalon, Mesencephalon and Rhombencephalon. (B) At E37-42, it keeps developing to form 5 elaborated secondary vesicles which will constitute the final human brain organization: Telencephalon, Diencephalon, Mesencephalon, Metencephalon and Myelencephalon. The box represents a high magnification of the telencephalic vesicle containing neuroepithelial stem cells (NeSC) undergoing different phases of the cell cycle (left panel) also illustrated by a scanning electron microscope snapshot (right panel). PS, pial surface. Adapted from Purves *et al.*, 2004.

1.2b. Neural proliferation

Neuroepithelial stem cells

Between the 4th and 5th GW, a monolayer of neuroepithelial stem cells (NeSC) lines the ventricular borders of the telencephalic vesicles (Figure 4, B). NeSCs express the intermediate filament Nestin. They are bipolar and multipotent which means that they can give birth to a variety of specialized cells destined to build the future cortex (Gotz and Huttner, 2005). In addition, along the successive phases of the cell cycle (G1, S, G2 and M), NeSCs undergo interkinetic nuclear migration (INM), an ascending and descending movement of their nucleus between the apical (facing the ventricle surface) and basal (opposite extremity directed towards the pial surface [PS]) compartments. Prior to corticogenesis, NeSCs proliferate thanks to symmetric mitosis (division phase of the cell cycle) generating two similar daughter stem cells thus auto-amplifying the NeSCs pool which increases the epithelial area.

One of the key regulatory mechanisms of the cortical formation is based on a controlled distribution of cell fate determinants during mitosis according to two major ways: symmetric or asymmetric cell division (Figure 5) (Morin and Bellaïche, 2011). The difference relies on the segregation of molecules, as symmetric division distributes the genetic information equally (proliferative) whereas asymmetric division results in an unequal distribution (neurogenic). Thus, asymmetric division changes the molecular balance between daughter cells defining the cellular identity of the post-mitotic cell and its subsequent laminar position; numb (*Drosophila*) homolog (*Numb*) gene is favoring neuronal fate during the asymmetric division (Figure 5, B) (Rasin *et al.*, 2007).

Furthermore, mitotic spindle (MS) and centrosome (Ct) functions are very important factors influencing neurogenesis hence playing a key role in proliferation and cell fate, neuronal differentiation and migration (Huttner and Kosodo, 2005; Fish *et al.*, 2006; Buchman and Tsai, 2007; Higginbotham and Gleeson, 2007; Zhong and Chia, 2008; Wang *et al.*, 2009; Peyre *et al.*, 2011; Morin and Bellaïche, 2011). The MS is a dynamic structure composed of arranged microtubules (MT) spanned between the two spindle poles, called centrosomes (Figure 5, A) (Glotzer, 2009; Tanaka, 2010). During cellular divisions, the orientation of the MS influences the inheritance of progenitor long basal fibers, the distribution of Cts between daughter cells and the detachment of progenitors from the ventricular surface (Feng and Walsh, 2004; Wang *et al.*, 2009; Lizarraga *et al.*, 2010). Thus, when MS is oriented in an oblique or horizontal cleavage plane there

is an increased tendency to generate one basal radial glial cell and one neuron or intermediate progenitor cell (Figure 5, B) (Shitamukai *et al.*, 2011). In addition, recent work showed that impaired asymmetric inheritance of daughter Ct in mouse cortical progenitors results in neuronal overproduction due to altered cell fate (Wang *et al.*, 2009). Furthermore, the lineage from NeSCs to radial glial progenitors is tightly controlled by fibroblast growth factor (FGF) and NOTCH signaling (Figure 5, A) (Yoon *et al.*, 2004; Yoon and Gaiano, 2005; Mizutani *et al.*, 2007; Kang *et al.*, 2009; Sahara and O'Leary, 2009; Wu *et al.*, 2012).

MOUSE

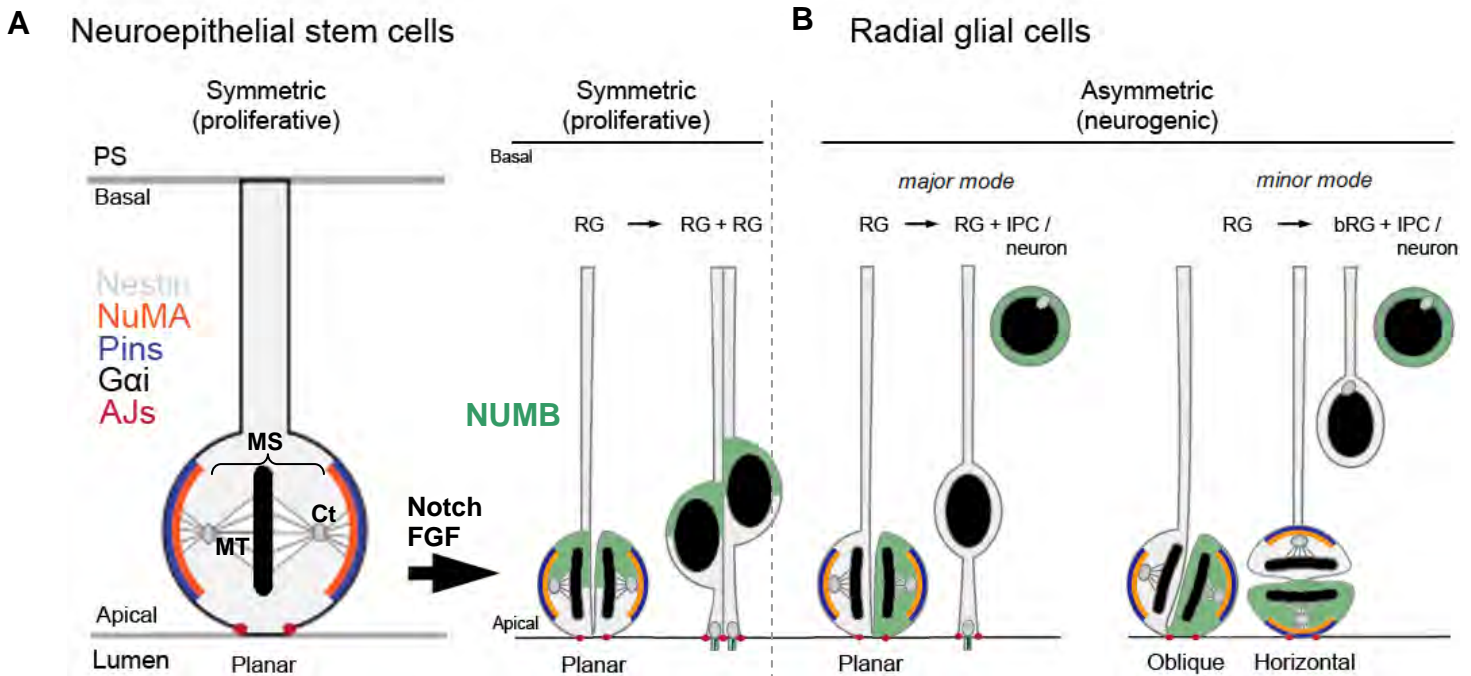


Figure 5: Molecular segregation and mitotic spindle orientation in mouse cell fate specification. (A) Side view of a neuroepithelial progenitor, expressing Nestin; important proteins influencing the mitotic spindle (MS) orientation such as adherens junctions (AJs) and polarity markers Pins and NuMA enriched in a lateral ring. The centrosomes (Ct) are participating to the maintenance and nucleation of microtubule arrays (MT) applying pulling forces on the MS to hold it. (B) Illustration of Radial glial cells with *Numb* gene segregation as an example of both symmetric proliferative (left) and asymmetric neurogenic (middle) planar divisions. A minority of divisions (10% in mouse) is slightly oblique or horizontal (right), so that the cell that inherits the basal process loses the apical attachment. This cell retains the molecular signature of RG and is proposed to become an outer radial glia (oRG) (Shitamukai *et al.*, 2011). It is not clear whether oRG and RG are a single cell type with two different localizations or whether they have different properties. oRG cells are present in low quantity in the mouse cortex (Shitamukai *et al.*, 2011; Wang *et al.*, 2011) but are much more frequent in the ferret and primates (Hansen *et al.*, 2010; Fietz *et al.*, 2010). The sister cell probably delaminates and becomes a neuron or a basal progenitor (although Wang *et al.* [2011] propose that it remains a RG). FGF, fibroblast growth factor; G α i, heterotrimeric G-protein alpha subunit; NuMA, nuclear mitotic apparatus protein; Pins, partner of inscuteable; PS, Pial surface. Adapted from Morin and Bellaïche, 2011.

Radial glial cells

The production of neurons, or neurogenesis, begins around 5-6th GW (E10-11 in mouse; Jaglin and Chelly, 2009) when first neurogenic (asymmetric) mitoses appear in the dorsal telencephalon. Indeed, NeSCs start to gradually divide asymmetrically (Figure 5, B) generating this time a self-renewed stem cell plus either one projection neuron or one intermediate progenitor cell (IPC) (Noctor *et al.*, 2001, 2004; Haubensak *et al.*, 2004). During neurogenic mitosis, NeSCs acquire new markers such as glial fibrillary acidic protein (GFAP; not in mice where it is selectively expressed after neurogenesis in astrocytes; Sancho-Tello *et al.*, 1995), Paired box 6 (PAX6) and SRY-related HMG-box 2 (SOX2) transcription factors to progressively become a new type of progenitor called the Radial glial (RG) cell (Levitt and Rakic, 1980; Voigt, 1989; Götz and Huttner, 2005; Arai *et al.*, 2011). RG cells are keeping an epithelial organization with their cell bodies, attached to each other by adherens junctions. They are residing in the vicinity of the apical membrane or ventricular zone (VZ; Figure 6). The ventricular positioned RGs, called apical RGs (aRG) (Hevner and Haydar, 2012; Kelava *et al.*, 2012) have a protruding short apical endfoot facing the VZ and a very long basal process along the intermediate zone (IZ) up to the pial surface conferring them a bipolar shape.

Newborn IPCs coming from the VZ rapidly accumulate right above the VZ and build together a supplementary germinal layer, the subventricular zone (SVZ) (Figure 6) (Doetsch and Alvarez-Buylla, 1996). Specifically in gyrencephalic mammals, the SVZ develops extensively to become the major germinal layer and splits first into inner SVZ (ISVZ, thin with high cellular density) overlaying the VZ and then at 11th GW into outer SVZ (OSVZ, thicker with lower cellular density) that faces the PS (Figure 6, B) (Smart *et al.*, 2002; Lui *et al.*, 2011). In contrast, SVZ remains monolayered during all embryogenesis in lissencephalic species (Figure 6, A) (Dehay and Kennedy, 2007).

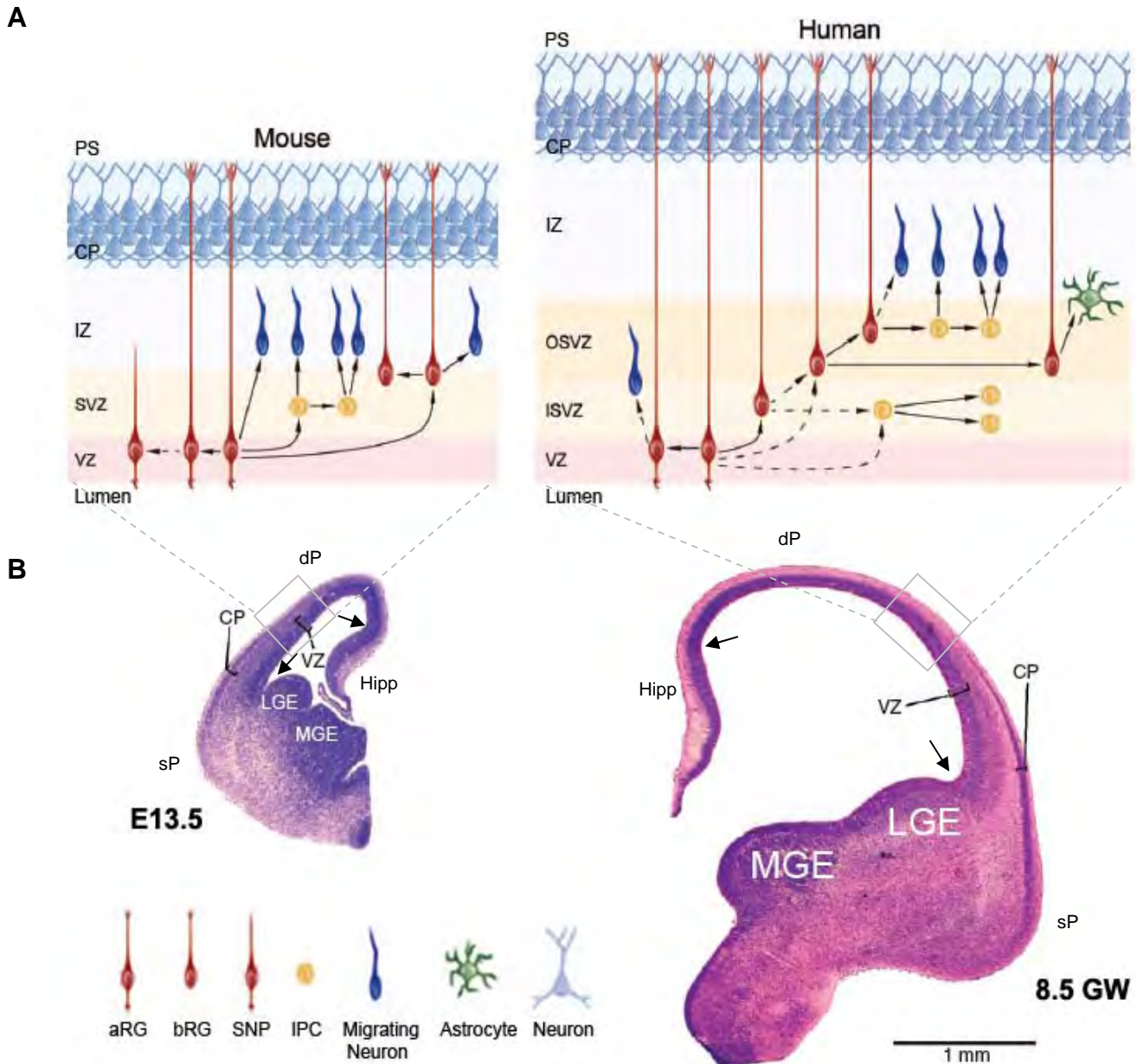


Figure 6: The development of the cerebral cortex. (A) Stem cells of mouse and human dorsal pallium (dP) with lineage relationships. Mouse apical radial glia (aRG), basal radial glia (bRG), and short neural precursors (SNP) express mostly PAX6 and SOX2; plus GFAP in human aRG (red). Intermediate progenitor cells (IPC) express only TBR2 in both species yet PAX6 expression has to be clarified in human (yellow). Solid line arrows indicate demonstrated lineage relationships. Dashed line arrows indicate not yet demonstrated lineage relationships. (B) Comparison of germinal zones in mouse (left) and human (right) embryonic neocortex; coronal view. In human, the subventricular zone (SVZ) overlaying the ventricular zone (VZ) splits into two distinct germinal compartments: the inner SVZ (ISVZ) and the outer SVZ (OSVZ). In mice, most interneurons migrate from the subpallium (sP): medial and lateral ganglionic eminences (MGE, LGE); from both dP and sP in human. Arrows indicate the presumptive hippocampus/dorsal pallium and dorsal pallium/subpallium boundaries. PS, pial surface; CP, cortical plate; IZ, intermediate zone; E, embryonic day; GW, gestational week. Adapted from Tyler and Haydar, 2010; Borrell and Reillo, 2012.

During subsequent stages of corticogenesis when layers VI-V are obvious, asymmetric divisions of aRGs give rise to new unipolar RGs which colonize the OSVZ, known as basal radial glia cells (bRG) (Figure 6) (Ramon y Cajal, 1891; Noctor *et al.*, 2001, 2004; Rakic, 2003a,b; Hevner and Haydar, 2012; Kelava *et al.*, 2012). bRGs are similar to aRGs in expressing typically Pax6 plus retaining a basal fiber up to the PS but they are distinct from aRGs in lacking apical membrane markers such as prominin 1 (CD133), partitioning defective 3 (PAR3), or atypical protein kinase C λ (aPKC λ) and missing the apical endfoot (Figure 6, A; 7) (Fietz *et al.*, 2010; Hansen *et al.*, 2010; Reillo *et al.*, 2011). Moreover, bRG population is very heterogeneous expressing multiple possibilities of transcription factors such as PAX6, TBR2, SOX2, OLIG2, NKX2.1, and HES1, reflecting the outstanding complexity of human cortical development in contrast to mouse relative simplistic molecular identity including PAX6, SOX2 and HES1 (Figure 7, A) (Zecevic *et al.*, 2005; Howard *et al.*, 2006; Mo *et al.*, 2007; Bayatti *et al.*, 2008a,b; Fish *et al.*, 2008; Mo and Zecevic, 2008; Fietz *et al.*, 2010; Hansen *et al.*, 2010; Jakovcevski *et al.*, 2011; Reillo *et al.*, 2011). Moreover, a unique bRGs feature is that they undergo mitotic somal translocation (MST) (Figure 7, B) where their soma rapidly ascends along the radial fiber before mitosis (Hansen *et al.*, 2010); different from INM where mitosis is located only at the VZ, plus MST always induces inheritance of the basal process to the more basal daughter cell. In addition, bRGs in human appear to undergo mostly indirect neurogenesis through IPCs generation when compared to murine bRGs which are rare and directly neurogenic (Shitamukai *et al.*, 2011; Wang *et al.*, 2011).

Another mouse singularity resides in the existence of a new class of progenitors, known as short neural precursors (SNP), expressing an additional distinct molecular signature, the T α 1 promoter (Gal *et al.*, 2006). As opposed to RGs, SNPs carry a shorter basal process preventing any contact with the PS, they are transient (E13.5–E16.5) and also less numerous, finally they are directly and uniquely neurogenic (Notch pathway promoting proliferation is absent) (Mizutani *et al.*, 2007; Stancik *et al.*, 2010). Although SNPs have a longer cell cycle compared to RGs (Stancik *et al.*, 2010), they are thought to finely adjust the cortical layer thickness during mid-neurogenesis, due to their direct neurogenic divisions avoiding the IPC passage thus shortening the embryonic time scale to produce neurons.

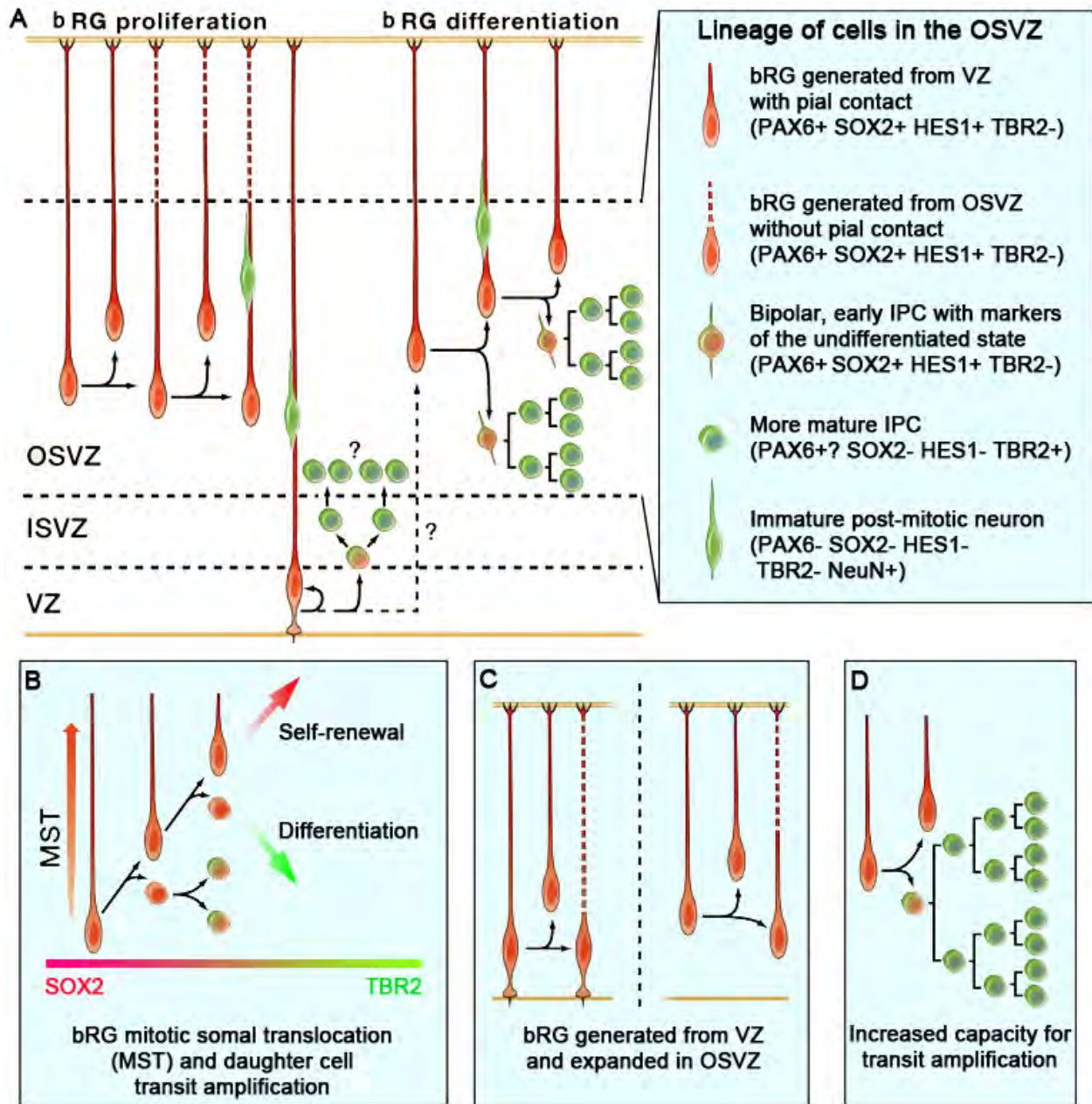


Figure 7: bRG in human OSVZ during neocortical development. (A) OSVZ is composed of both stem and transit amplifying cell types: basal radial glia (bRG) and intermediate progenitor cells (IPC), respectively. 45% of the OSVZ population is neuronal at 15.5 GW, expressing NeuN but never the progenitor cell marker SOX2. The differentiation of bRG daughter cells is marked by the loss of SOX2 expression and Notch activation (HES1), with a gain in TBR2 expression. Together, these observations explain how the combination of bRG proliferation and differentiation expands the OSVZ over the course of midgestation and gives rise to an increased number of neurons. The lineage and molecular signatures of cells that form the OSVZ are shown (inset). (B) Illustration of cell division and behavior of bRGs. (C) The RG population increases through the generation of bRG cells from the ventricular zone (VZ) and their expansion in the OSVZ. Dashed lines indicate the unknown length of newborn radial fibers. (D) bRG daughter cells exhibit protracted differentiation and have an increased capacity for transit amplification. HES1, hairy and enhancer of split-1; NeuN, neuronal nuclear antigen; PAX6, paired box 6; SOX2, SRY-related HMG-box 2; TBR2, T-box Eomes 2 protein. Adapted from Lui et al., 2011.

Intermediate progenitor cells

In mice IPCs are located in the SVZ and adopt a multipolar morphology (Noctor *et al.*, 2004, 2008; Miyata *et al.*, 2004), contacting neither the VZ nor the PS hence never undergoing INM or MST; rather freely moving. IPCs are derived from asymmetric RG divisions and selectively express the T-box Eomes 2 (TBR2) transcription factor following quick downregulation of *Pax6* (Smart *et al.*, 2002; Hevner *et al.* 2006; Arnold *et al.*, 2008; Bayatti *et al.*, 2008). Although, Tbr2 expression appears to be a general feature of IPCs, both in rodents and humans (Kowalczyk *et al.* 2009; Hansen *et al.* 2010), human IPCs are principally located in the ISVZ. They represent a transit self-amplifying population that migrates away from the VZ constituting the most part of progenitors (Figure 7, A and D) (Haubensak *et al.*, 2004; Englund *et al.*, 2005; Kowalczyk *et al.*, 2009; Hansen *et al.*, 2010). Indeed, IPCs increase the neurogenic capacity of each RG cell mitosis thanks to their one or two rounds of cell division thus contributing to two or four post-mitotic neurons (Kriegstein *et al.*, 2006; Sessa *et al.*, 2010; Fietz and Huttner, 2011). As a result, ISVZ/OSVZ cycling progenitors dramatically surpass the number of VZ progenitors with an accumulation of IPCs that can reach 85% of all progenitors during late human neurogenesis compared to 15–30% in lissencephalic rodents (Dehay and Kennedy, 2007; Kowalczyk *et al.*, 2009; Reillo *et al.*, 2011). This phenomenon indicates that IPCs, with the help of relative abundant bRGs, are the major progenitors of glutamatergic neurons although RGs may directly generate some post-mitotic neurons (Figure 7, A and D) (Alvarez-Buylla *et al.*, 1988; 1990; Malatesta *et al.*, 2000; Noctor *et al.*, 2001, 2004; Anthony *et al.*, 2004; Kowalczyk *et al.*, 2009; Sessa *et al.*, 2010). This might explain how human neocortex sustains its fast and extensive growth compared to mouse where IPCs divide only once to give two immature neurons (Noctor *et al.*, 2004, 2008).

1.2c. Neuronal migration

Radial and tangential migration

At the beginning of neurogenesis, the cortical wall is very thin and post-mitotic neurons born from aRGs and IPCs migrate for a short distance from the VZ to the PS with a simple translocation of their soma (Nadarajah *et al.*, 2001). Gradually, a uniform layer of immature neurons forms, the cortical plate (CP) (Figure 9) and abundant continuous flow of incoming IPCs with newborn neurons are shaping the SVZ and IZ, respectively. The cortical wall thus progressively thickens and aRGs lengthen their basal processes to guide migrating neurons toward the CP thanks to a second mechanism, “radial migration” (Gadisseux *et al.*, 1989, 1992; Rakic 1972, 1974, 2007). In this

process, post-mitotic neurons adhere to the parent cell's radial fiber, with the help of a small prolonged axonal arm enrolled around it (Figure 8), all radial fibers creating together a scaffold serving as a columnar "route" (Morest, 1970; Anton *et al.*, 1997, 1999; Nadarajah and Parnavelas, 2002; Rakic, 2003a; Borrell *et al.*, 2006; Elias *et al.*, 2007). The neuronal migration is based on an inside-out pattern, so that first born neurons build the deep cortical layers whereas late born neurons will populate the superficial cortical layers (Meyer 2007; Volpe, 2008). Thus, last generated neurons get their way across the cortical laminas laid down earlier until they reach their final position to arrest their migration and undergo morphological and molecular differentiation (D'Arcangelo and Curran, 1998; Lambert de Rouvroit and Goffinet, 1998; Anton *et al.*, 1999; Yokota *et al.*, 2007a).

Besides the columnar migration provided by aRG units also the bRGs seem to contribute to the extensive and highly curved gyrencephalic corticogenesis (Reillo *et al.*, 2010). In this context, recent data suggest that additional OSVZ bRG processes may help neurons to spread over a greater tangential surface although immature neurons were not directly observed migrating on bRG fibers but rather a lateral dispersion as in ferrets (Ware *et al.*, 1999; Reid *et al.*, 1997) and primates (Kornack and Rakic, 1995) (Figure 9, B). As a result of the large neuronal production in the human OSVZ, many newborn neurons begin migration from the OSVZ. Thus, post-mitotic neurons may follow a variable discontinuous relay of fibers to reach the CP rather than the trajectory of a single trajectory determined by RG fibers. Therefore, in gyrencephalic species, the birth date and location of the parent cell plus the orientation/trajectory of the radial fibers are intimately associated with future laminar identity and connectivity of the pyramidal neuron (Diaz and Gleason, 2009, Miyoshi *et al.*, 2010; Miyoshi and Fishell, 2011). In contrary, this dispersion is relatively modest in rodents (Walsh and Cepko, 1988; Austin and Cepko, 1990; Tan and Breen, 1993; Torii *et al.*, 2009) confirming a more simple cortical configuration in lissencephalic mammals. For example in mice,

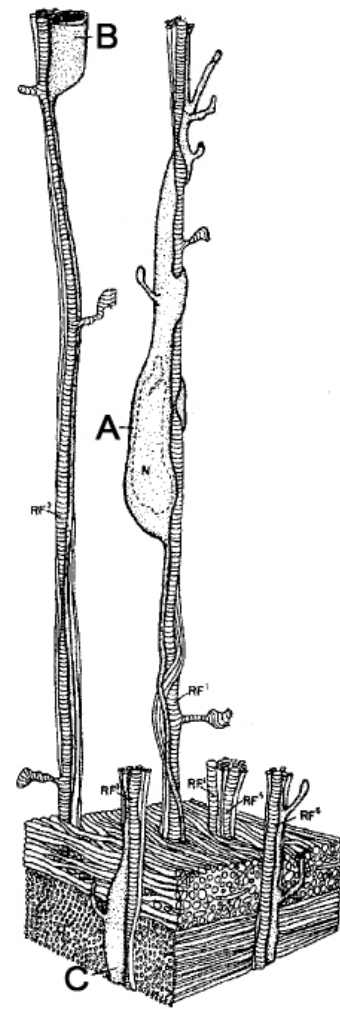


Figure 8: Radial glial scaffold. (A, B and C) Migrating post-mitotic neurons adhering to radial fibers (RF). N, nucleus. Adapted from Rakic, 1972.

Introduction

RG fibers are almost in a parallel axis (Gadisseux *et al.*, 1992), and bRGs fraction is low thus the location of their mother cell at the time of birth essentially determines the final position of projection neurons (O'Leary and Borngasser, 2006).

In contrast to excitatory neurons coming from the dorsal telencephalon, mouse inhibitory neurons arise from ventral telencephalic areas, referred to ganglionic eminences (medial, MGE; lateral, LGE and caudal, CGE) and septal region (Figure 6) (Wonders and Anderson, 2006; Gelman and Marin, 2010). Although it has been suggested that some interneurons are derived from dorsal progenitors in the human fetal neocortex (Letinic *et al.*, 2002; Yu and Zecevic, 2011), certain human interneuron subtypes are probably generated in the ventral telencephalon and enter the cortex via tangential migration (Fertuzinhos *et al.*, 2009). In the forebrain of rodents, interneurons have the particularity to first disperse tangentially towards the neocortex following two main migratory routes in the marginal zone (MZ) above the CP and in the SVZ (Lavdas *et al.* 1999; Lopez-Bendito *et al.* 2008) before migrating radially to reach their final laminar destination. Recent evidence suggests that a laminar-specific transcription factor in projection neurons might play a non-cell-autonomous role in the positioning and distribution of tangentially migrating interneurons (Lodato *et al.*, 2011).

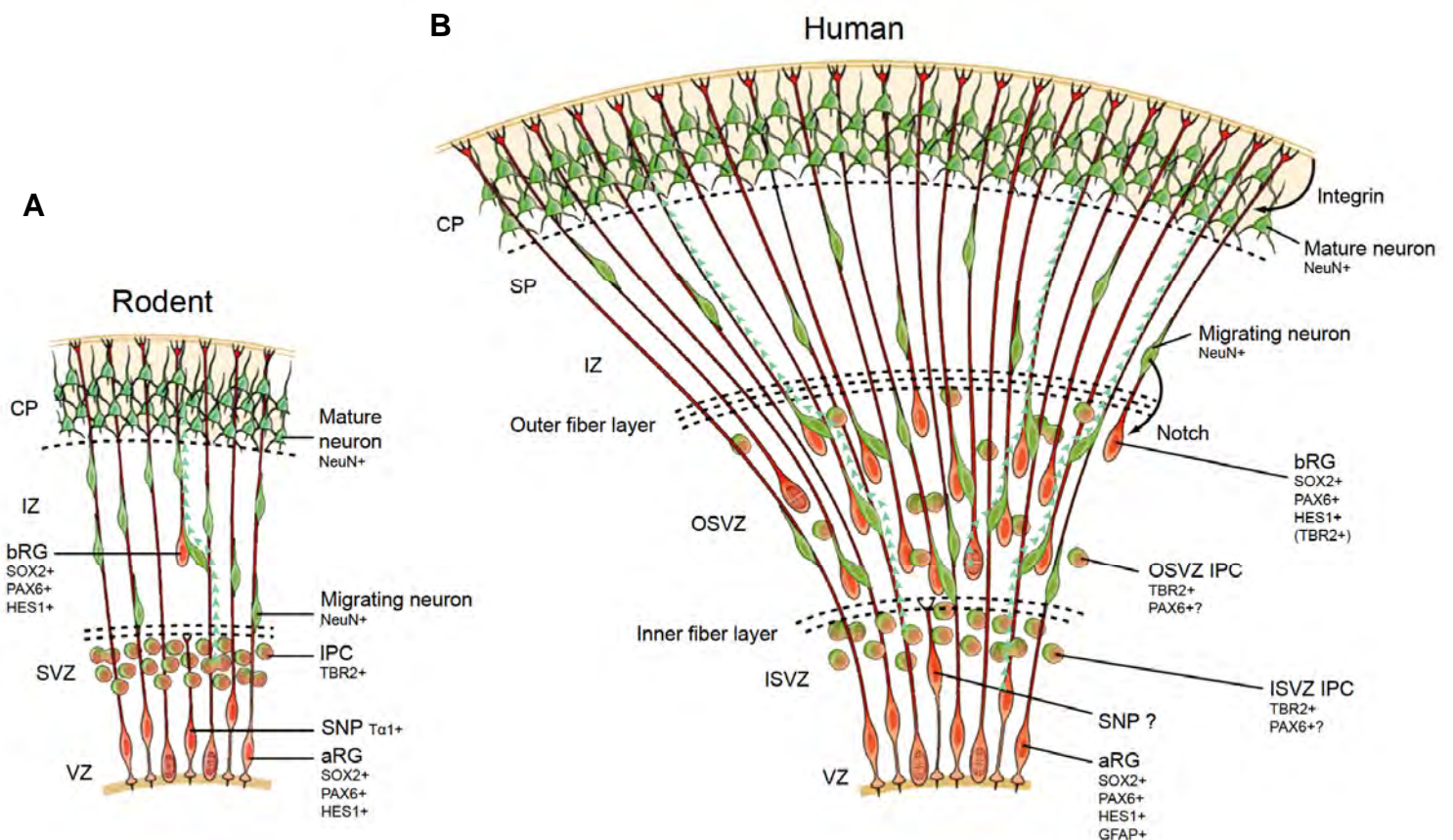


Figure 9: Contrasting Rodent and Human Neocortical Development. (A) Rodent corticogenesis: radial glial (RG) cells most often generate intermediate progenitor cells (IPC) that divide to produce pairs of neurons. These neurons use RG fibers to migrate to the cortical plate. Small numbers of basal radial glial cells (bRG) exist in the mouse SVZ. (B) Highlight of the lineage of bRG cells, IP cells, and migrating neurons (red to green) in the human outer subventricular zone (OSVZ). The number of ontogenetic ‘units’ is significantly increased with the addition of bRG cells over apical RG (aRG) cells in human compared to rodents; human bRGs express TBR2 indicating a longer transitional state vs mouse bRGs where co-expression of TBR2 and Pax6 is very scarce. Notch and integrin signaling maintain bRG cells. Short neural precursors (SNP), a transitional cell form between RGs and IPCs. Green arrows represent migrating neurons pathways illustrating more tangential possibilities in human neocortex versus rodent.

Multipolar migration

During embryogenesis, the migration of projection neurons from the VZ to the CP is overall radial. However, projection neurons also transition from bipolar to multipolar morphology in the SVZ and move nonradially in the IZ (Nowakowski and Rakic, 1979; Loturco and Bai, 2006; Jossin and Cooper, 2011). Therefore, radial migration of projection neurons in rodents does not follow a unidirectional route and includes phases of temporary migratory arrest and retrograde migration prior to entering the CP (Tabata and Nakajima, 2003; Noctor *et al.*, 2004). Multipolar stage was later confirmed by other studies demonstrating a relevant role for normal cortical development (Kriegstein and Noctor, 2004; Loturco and Bai, 2006, Sasaki *et al.*, 2008). Multipolar neurons express the selective Svet1 protein (Tarabykin *et al.*, 2001) and they incessantly extend and retract their processes. During their migration they frequently change direction as if searching for environmental guidance cues to direct axonal growth or eventually to “re-engage” in radial migration to the CP. Sometimes, multipolar cells seem to be free to move tangentially during their radial migration slowing down their speed in the SVZ and IZ, at about one-fifth the rate of the bipolar cells in the neocortex (Bayer and Altman, 1991; Tabata and Nakajima, 2003). This flexibility may help the migrating neurons to pass the obstacles in the IZ, such as previous radially moving neurons, tangentially migrating neurons and afferent and efferent fibers. Indeed, after ISVZ and OSVZ get established, a thick axonal bundle forms at the basal level of the OSVZ, the outer fiber layer (OFL) and in later ages additional stripes of axons make their way between ISVZ and OSVZ creating the inner fiber layer (IFL; Figure 9, B) (Smart *et al.*, 2002) which newborn neurons will traverse to reach the overlying developing human neocortex.

1.2d. Neuronal Differentiation

To form the neocortical mantle, neurons differentiate in their corresponding layer after migration. To do so, recent data have shown that the proper detachment of migrating neurons from their RG fibers in the CP is a crucial step in the arrest of migration. This phenomenon might require the coordination of RG-based anti-adhesion signals, such as SPARC-like 1, adapted changes of neurons to ambient glutamate and GABA (Gongidi *et al.*, 2004; Bortone and Polleux, 2009) and the induction of neuronal cytoskeletal modulators, such as NCK-associated protein 1 which converts the motile cytoskeleton into a more stable state favoring axonal and dendritic outgrowth (Yokota *et al.*, 2007b). The telencephalon continues to develop, with an end of neuronal migration around the 5th month of intra-uterine human development and neurons initiate the formation of dendrites and synaptic connections. This differentiation will provide neurons of each cortical layer gaining more specialized electrophysiological properties to establish and strengthen a mature neuronal network (Parnavelas *et al.*, 1991; Anderson and Price, 2002). Following neuronal production, RGs generate oligodendrocytes (forming the myelin sheath around axons in the CNS) and astrocytes (providing nutrients, maintaining extracellular ion balance, modulating neuronal network plus involved in repair and scarring process of the brain) (Bentivoglio and Mazarello, 1999; Kriegstein and Alvarez-Buylla, 2009; Okano and Temple, 2009; Rowitch and Kriegstein, 2010). Meanwhile, the external morphology of the cortex becomes more folded with fissures and its surface increases without changing the brain volume by the process of sulcation and gyration (Welker, 1990). The nature and timing of a disturbance in cortical development are important factors that determine the type of cerebral malformations (Kriegstein *et al.*, 2006; de Wit *et al.*, 2008; d’Arcangelo, 2009; Valiente and Marin, 2010).

II. Background of cerebral malformations

The term malformation of cortical development (MCD) was introduced to point out a common group of disorders in children with developmental delay and in young people with epilepsy (Barkovich, 1996). The rapid evolution of molecular biology, genetics and brain imaging has helped to understand the normal brain development but has also increased our knowledge of the pathogenesis of different cerebral pathologies.

II.1. Human malformations of cortical development

II.1a. Clinical aspects

MCD forms a group of neuropathologies that result from internal (genetic inheritance) or external (alcohol, virus, irradiation, lack of vitamin) aberrations affecting the normal process of brain development such as microcephaly (Mochida, 2008), lissencephaly (LIS) (Dobyns, 1999) or subcortical band heterotopia (SBH) (D'Agostino *et al.*, 2002; Pang *et al.*, 2008) (Figure 10). They are responsible for light to profound mental retardation, motor and learning difficulties, metabolic defects, spasticity, epilepsy to general milder forms with infrequent seizures and reduced longevity (Guerrini and Marini, 2006; Andrade, 2009; Barkovich *et al.*, 2012). The overall incidence of MCDs is not well known but for some of them it is estimated around >1% in the human population (Meencke and Veith, 1992). The diagnosis is mostly performed using high resolution magnetic resonance imaging (MRI) (Colombo *et al.*, 2009; Madan and Grant, 2009) which provides a clear topographic characterization of the cortical surface and allows more accurate analysis of the formation of white matter and stages of myelination as well as detection of brain lesions. Despite the difficulty to classify MCDs, epilepsy (often refractory) is rather a common clinical feature associated to patients with brain malformations (Meencke and Janz, 1984; Mischel *et al.*, 1995) and MCDs are observed in at least 14% of all epileptic cases (Meencke and Veith, 1992). It is estimated that up to 40% of children with medically intractable epilepsy have a cortical malformation (Taylor *et al.*, 1971; Kuzniecky *et al.*, 1994; Lerner *et al.*, 2009) and that at least 75% of patients with MCD will suffer from epilepsy (Leventer *et al.*, 1999).

Another pathology often related to MCDs is schizophrenia (Zipursky *et al.*, 1992) where patients exhibit abnormal ventricle volumes with compressed gray matter but also neuronal circuitry defects during brain development (Lewis *et al.*, 2002). It is also discussed in that the clinical severity depends of the morphology and size of the MCD which affects the cerebrum. For example, the degree of agyria and cortical thickening may result in disparate anatomical changes, from small to prominent ones (Leventer *et al.*, 2008). Moreover, the time aspect of MCDs appearance is also crucial for the patients especially when occurring in childhood, people suffer from a wider spectrum of histopathological features and more varied, even more severe, clinical manifestations (Blümcke *et al.*, 2009).

Although gene chips and modern imaging techniques facilitate the diagnosis (Curatolo *et al.*, 2008; Datta *et al.*, 2008; Stefansson *et al.*, 2008), effective treatments are still scarce. Currently, the most used form of treatment aimed at controlling pharmacoresistant seizures consists of removing the parts of the brain identified as the epileptic foci (Lüders & Schuele, 2006; Vinters and Mathern). However, specific brain surgery cannot be considered for each patient, because of the number or the location of the epileptic foci, and the risk to induce functional damage. Therefore, we need to better understand this group of pathologies in order to develop new forms of therapeutic intervention and diagnostic techniques during embryogenesis that may replace or complement the surgical approach.

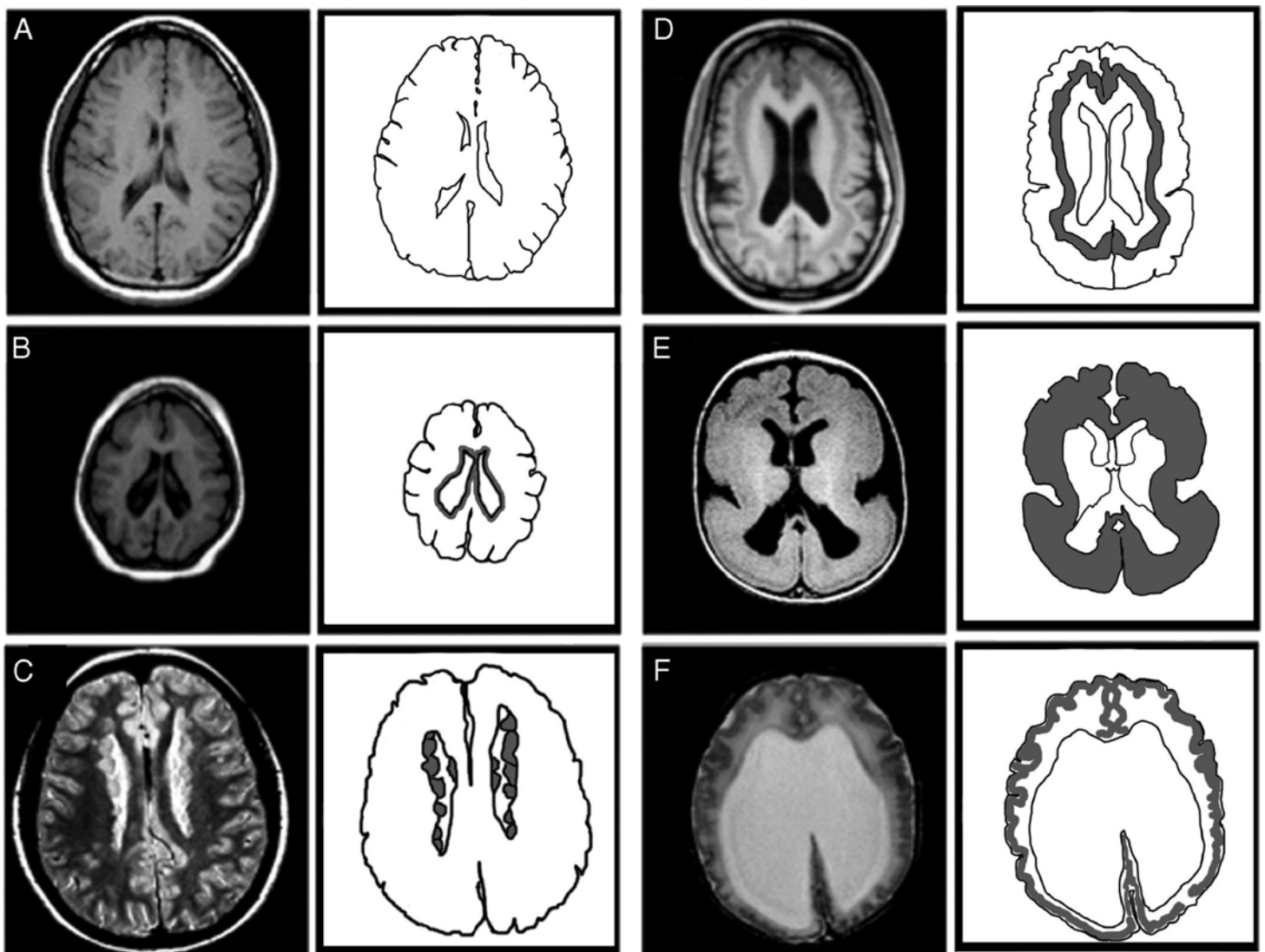


Figure 10: Magnetic Resonance Imaging micrographs of different typical MCDs. (A) Normal brain. Camera lucida rendering of the normal brain is to the right. (B) Microcephaly with ASPM mutation. Camera lucida rendering to the right shows the pathologic region (gray) along the ventricular zone. (C) Periventricular heterotopia with FLNA mutation. Note the nodules of heterotopic gray matter lining the lateral ventricles bilaterally. (D) Subcortical band heterotopia with DCX mutation. Note the thick band of gray matter running deep and parallel to the thinned outer cortex. A thin band of white matter separates the outer cortex and the inner subcortical band of heterotopic neurons. (E) Classic lissencephaly (type I) with LIS1 mutation. The brain has an “hour-glass” appearance with agyria and pachygyria. Note the greater severity of lissencephaly in the parietal and occipital lobes. (F) Cobblestone lissencephaly (type II lissencephaly). Note the cobblestone appearance with a thin cortex, absent corpus callosum, and severely enlarged ventricles with nodules of neurons in the dorsal part of the cortex. Pang *et al.*, 2008.

II.1b. Classification of MCDs

MCDs have a large spectrum of histopathological alterations, disparate clinical presentations and variable neuroradiological manifestations. Thus, MCDs are very difficult to study and classify because the same patient may have a combination of different malformations (Andrade and Leite, 2011). The most currently adopted categorization is the classification scheme introduced by Barkovich which was updated in 2012 (Table 1) (Barkovich *et al.*, 2012). It is based on three brain developmental processes and so divided into three groups: Group I: malformations secondary to abnormal neuronal and glial proliferation or apoptosis; Group II: malformations due to abnormal neuronal migration; and Group III: malformations secondary to abnormal post-migrational development. Further classification is based on the mode of inheritance (autosomal recessive, autosomal dominant, X-linked, polygenic...) and whether the disorder is clinically or genetically defined. With the explosive increase of gene discoveries through DNA microarray screening combined with powerful informatics analysis and imaging techniques, we see that different mutations of the same gene can result in different syndromes (Nadeau, 2001; Zeldenrust, 2012). Therefore, MCD defined by gene alone may quickly become excessive and confusing for scientists and clinicians. According to Barkovich, “the optimal classification will not be based on genes but pathways and mechanism of protein action, with variations based on how the specific gene mutation alters protein function in the affected pathway”.

Table 1. Simplified classification scheme of Barkovich		
GROUP I: MALFORMATIONS SECONDARY TO ABNORMAL NEURONAL AND GLIAL GLIAL PROLIFERATION OR APOPTOSIS	GROUP II: MALFORMATIONS OF ABNORMAL NEURONAL MIGRATION	GROUP III: MALFORMATIONS OF ABNORMAL POSTMIGRATIONAL DEVELOPMENT
(A) SEVERE CONGENITAL MICROCEPHALY (MIC), pre-migrational reduced proliferation or excess apoptosis	(A) MALFORMATIONS WITH NEUROEPENDYMAL ABNORMALITIES: PERIVENTRICULAR HETEROTOPIA	(A) MALFORMATIONS WITH PMG OR CORTICAL MALFORMATIONS RESEMBLING PMG
(B) MEGALENCEPHALY (MEG) including both congenital and early postnatal	(B) MALFORMATIONS DUE TO GENERALIZED ABNORMAL TRANSMANTLE MIGRATION (radial and non-radial)	(B) CORTICAL DYSGENESIS SECONDARY TO INBORN ERRORS OF METABOLISM (neuropathology differs from classic PMG)
(C) CORTICAL DYSGENESIS WITH ABNORMAL CELL PROLIFERATION BUT WITHOUT NEOPLASIA	(C) MALFORMATIONS PRESUMABLY DUE TO LOCALIZED ABNORMAL LATE RADIAL OR TANGENTIAL TRANSMANTLE MIGRATION	(C) FOCAL CORTICAL DYSPLASIAS (WITHOUT DYSMORPHIC NEURONS) DUE TO LATE DEVELOPMENTAL DISTURBANCES
(D) CORTICAL DYSPLASIAS WITH ABNORMAL CELL PROLIFERATION AND NEOPLASIA	(D) MALFORMATIONS DUE TO ABNORMAL TERMINAL MIGRATION AND DEFECTS IN PIAL LIMITING MEMBRANE	(D) POSTMIGRATIONAL DEVELOPMENTAL MICROCEPHALY (PREVIOUSLY POSTNATAL MIC) WITH BIRTH OFC -3 SD OR LARGER, LATER OFC BELOW -4 SD AND NO EVIDENCE OF BRAIN INJURY

OFC = occipital-frontal cortex; MEG = megalencephaly; MIC = microcephaly; SD = standard deviation score compared to age- and gender matched controls

Sourced from Barkovich *et al.*, 2012

II.2. Basic mechanisms of pathologic cortical development

The human corticogenesis is a very complex and extraordinary biological process, with highly regulated expression of key genes, plenty of molecular partners and intriguing signaling cascades.

II.2a. Pathologic mechanisms leading to MCDs

Group I: malformations secondary to abnormal neuronal and glial proliferation or apoptosis

The mechanisms sustaining MCDs are diverse but some of them often represent a unique signature leading to the associated pathologic phenotype (Barkovich *et al.*, 2012). For instance, Group I patients suffering microcephaly present proliferation and apoptosis (cellular programmed death)

disorders resulting in size reduction of a part of the fetal brain due to a reduced production of neurons (Table 2) (Takano *et al.*, 2006; Pang *et al.*, 2008). The *Microcephalin* gene is thought to play a role in deoxyribonucleic acid (DNA) repair because its loss of function induce abnormal DNA repair causing increased neural progenitor cell death along the ventricles. Additional studies suggest that MICROCEPHALIN is a Ct protein (Zhong *et al.*, 2006) and plays a role in the control of cell cycle timing (Trimborn *et al.*, 2004). Cyclin dependent kinase-5 regulatory subunit associated protein 2 and centromere protein J encode for Ct proteins that are found at the spindle poles of mitotic apical progenitors. Thus, many genes for microcephaly play an important role in neurogenesis by regulation of microtubules and cell cycle progression during cell division (Hung *et al.*, 2000; Bond *et al.*, 2005).

Group II: malformations of abnormal migration

It is interesting to note that mutations affecting genes encoding cytoskeletal regulators that control different aspects of neuronal migration can lead to dramatic brain malformations (Kriegstein and Noctor, 2004; Hand *et al.*, 2005; Ge *et al.*, 2006; LoTurco and Bai, 2006; Kawauchi and Hoshino, 2008; Kawauchi *et al.*, 2010; Valiente and Marín, 2010; Alfano *et al.*, 2011; Pacary *et al.*, 2011; Westerlund *et al.*, 2011). Indeed, patients undergoing abnormal neuronal migration patterns can declare LIS Type I creating a poorly structured cortex with four immature layers instead of the normal six bands (Kato and Dobyns, 2003) or other diseases belonging to a group of disorders, Heterotopias. The latter is characterized by an aggregate of disorganized neurons in abnormal regions of the brain including three main groups: periventricular nodular heterotopias, SBH and marginal glioneural heterotopia. In LIS, the platelet-activating factor acetylhydrolase 1b, regulatory subunit 1 (*Pafah1b1*, formerly *Lis1*) gene controls MS orientation in both the NeSCs and RGs; its deletion causes dysfunction of dynein, a microtubular cytoplasmic protein involved in neuronal migration (Table 2) (Pang *et al.*, 2008; Yingling *et al.*, 2008). Other essential genes such as *Cdk5*, *p35* have a dual role modulating the cell cycle but also impacting neuronal migration here in LIS (Toyo-oka *et al.*, 2003). Mutations of doublecortin (*Dcx*) gene also cause classical LIS in males while heterozygous mutations in females are associated with SBH (Bernardi *et al.*, 2002). *Dcx* is expressed in newborn neurons encoding a MT-associated protein which stabilizes MT confirming that regulation of the cytoskeleton dynamics is important for proper neuronal migration (Francis *et al.*, 1999, 2006; Gleeson, 1999). Other genetic causes for SBH remain unclear and *Dcx* might still be involved in large deletions or duplications and cryptic chromosomal defects (Mei *et al.*, 2007).

Group III: malformations of abnormal postmigrational development

Polymicrogyria (PMG) is characterized by an irregular brain surface with an excessive number of small and partly fused gyri separated by shallow sulci. Two types of polymicrogyria involving G-protein coupled receptor 56 exist: a simplified four layered form (intracortical laminar necrosis with subsequent alterations of late migration and postmigratory defects of cortical organization) and a complex un-layered form (continuous molecular layer without following the borders of convolutions, no laminar organization whereas neurons adopt a radial distribution) (Table 2) (Jansen and Andermann, 2005; Pang *et al.*, 2008). PMG is actually the final stage of different etiological processes arriving at various times of corticogenesis such as congenital cytomegalovirus infection, placental hypoperfusion, prenatal cerebral hypoxia–ischemia, twin–twin transfusion, loss of twin in utero or maternal drug ingestion (Guerrini and Carrozzo, 2001).

TABLE 1. Malformations of Cortical Development With Associated Genes and Clinical Features

Developmental Stage	Cortical Malformation	Genetic Cause	Clinical Features
Abnormal neurogenesis	Microcephaly	<i>ASPM</i> <i>Microcephalin</i> <i>CDK5RAP2</i> <i>CENPJ</i>	Mental retardation, not generally associated with epilepsy, autosomal recessive inheritance
	Hemimegalencephaly	Unknown	Mental retardation, early onset seizures (frequently intractable epilepsy), ±neurocutaneous syndrome
Abnormal neuronal migration	Focal cortical dysplasia	Unknown	Most common, focal and generalized Seizures
	Periventricular heterotopia	<i>FLNA</i>	Normal intelligence, adolescent onset seizures, X-linked disorder with male lethality
		<i>ARFGEF2</i>	Mental retardation, microcephaly, autosomal recessive inheritance, rare
	Subcortical band heterotopia	<i>DCX</i>	Subcortical band heterotopia in females, mental retardation, epilepsy, X-linked disorder
	Lissencephaly	<i>LIS1</i>	Miller-Dieker syndrome (characteristic facial features), autosomal dominant inheritance
		<i>DCX</i>	Lissencephaly in males, X-linked
		<i>TUBA1A</i>	Lissencephaly, clinical features similar those caused by <i>LIS1</i> and <i>DCX</i> , de novo mutations
		<i>ARX</i>	Associated with ambiguous genitalia, hypothalamic dysfunction, neonatal epilepsy, X-linked disorder
		<i>RELN</i>	Associated with cerebellar hypoplasia, epilepsy, autosomal recessive inheritance
		<i>Fukutin</i>	Fukuyama congenital muscular dystrophy
Abnormal arrest in neuronal migration	Cobblestone lissencephaly	<i>POMGnT1</i> <i>POMT1</i>	Muscle-eye-brain disease Walker-Warburg syndrome
Abnormal neuronal organization	Polymicrogyria	<i>GPR56</i>	Bilateral frontoparietal polymicrogyria, epilepsy
	Schizencephaly	<i>EMX2</i>	Type 2 (open cleft)

II.2b. Comparison of genes involved in MCDs: animal VS human

Every step of the brain development could be an “open door” to mutations which could occur both during the prenatal or postnatal period. The identification of genes tends to show a major role for genetic inheritance even if it is known that MCD are a multifactor pathologies. Genes coding for microtubule associated proteins (MAP) such as DCX or PAFAH1B1 and a tubulin isoform 1A (TUBA1A) highlights the involvement of MT hence cytoskeletal perturbations in neuronal migration disorders (Sapir *et al.*, 1997; Francis *et al.*, 1999; Gleeson *et al.*, 1999, Keays *et al.*, 2007; Jaglin and Chelly, 2009). However, DCX, PAFAH1B1 or TUBA1A mouse mutants do not reproduce aberrant location of neurons in the neocortical white matter as in human and their severest anatomical abnormalities are found in the hippocampus (Hirotsune *et al.*, 1998; Corbo *et al.*, 2002; Kappeler *et al.*, 2007; Keays *et al.*, 2007). Other genes involved in actin filament association (*Flna*), in guanine nucleotide-exchange (*Arfgef2*) or coding for homeobox genes (*Arx*, *Emx2*), for a secreted extracellular matrix protein (*Reln*) and G protein-coupled receptor (*Gpr56*) show the broad spectrum of targets involved in MCDs which complicates the elucidation and comprehension of underneath mechanisms. Moreover, smooth brain species (mouse, rat, zebra fish, rabbit) do not possess as much bRG progenitors as gyrencephalic species (ferret, monkey, human), which lead to a different way of cortical development in time and space as seen previously underscoring the difficulty to transpose animal results to human (Lui *et al.*, 2011; Borrell and Reillo, 2012). Indeed, mutations observed in patients are rarely corresponding to those studied in current animal models (Andrade *et al.*, 2011), meanwhile keeping in mind that other compensatory genetic processes present in animals, not found in human (where a great variability already exists), may interfere.

II.2c. Animal Models of MCD

There are many animal models mimicking different types of MCD mostly studied in mice and rats (Table 3) (Chevassus-au-Louis and Represa, 1999; Wong, 2009).

Models including proliferation defects

Disruption of genes involved in microtubule and centrosome function in mice results in impairments in neural progenitor proliferation and causes microcephaly (Feng and Walsh, 2004). For example, NDE1 is a microtubule-associated protein required for centrosome duplication, and the formation and function of the mitotic spindle. *Nde1* expression is also associated with the

centrosome, kinetochore, and spindle. Loss of *Nde1* function in cortical progenitors causes defects in mitotic progression and orientation, and mitotic chromosome localization. This disruption in centrosome duplication and mitotic spindle assembly produces a small brain. Abnormal spindle-like, microcephaly-associated (*Aspm*) is a gene that encodes for a very large centrosomal protein (Zong *et al.*, 2005) that is essential for normal mitotic spindle function in *Drosophila* neuroblasts thus regulating cell fate (do Carmo Avides and Glover, 1999).

Models including migration defects

The most studied model of cortical malformation is the “reeler mouse” which mutated *Reelin* gene induces an inverted cortical layer pattern (Caviness 1982). Other knockout or deficient mice for different transcription factors of selective neuronal layer are studied such as the *Sox5* deficient cortex (only the deep layers are inverted) (Kwan *et al.*, 2008; Lai *et al.*, 2008), the *Tbr1* deficient mouse (deep layer neurons form abnormal clusters and upper layer neurons fail to migrate) (Han *et al.*, 2011; McKenna *et al.*, 2011), the *Pou3f2/3* double knockout mouse (migration of V-II projection neurons is stalled below the subplate) (Sugitani *et al.*, 2002) and the *Lmx1a* “Dreher mouse” (abnormalities of the glial limiting membrane with a heterotopic layer I) (Costa *et al.*, 2001).

Other mutants form large numbers of ectopic neurons grouped together in so-called heterotopias. For example, a mouse model of heterotopia is available after administering cytosine arabinoside (Ara-C) but is also accompanied by microcephaly (Takano *et al.*, 2006). The rat models of prenatal exposure to methylazoxymethanol (MAM), 1-3-bis-chloroethylnitrosurea (BCNU) or γ -ray also present different types of heterotopias. Alternatively, acute inactivation of *Dcx* by RNAi in the developing rat cortex (Bai *et al.*, 2003) and *Wnt3a* overexpression in the mouse neocortex (Munji *et al.*, 2011) lead to SBH. Conditional knockout mice for *Ra-gef1* (Bilasy *et al.*, 2009) and for *RhoA* (Cappello *et al.*, 2012) also result in SBH, associated with other brain malformations. There are only two spontaneous mutants, the *tish* rat and BXD29 mouse, who are presenting SBH (Lee *et al.*, 1997; Rosen *et al.*, 2012) but their genetic defects are still unknown.

Epileptic phenotype in animal models

Some of these animal models are presenting interesting epileptic phenotypes enabling to study seizures genesis in malformed brains as it is the case in human patients (Andrade, 2009). The rats

MAM, BCNU or γ -ray, as well as DCX knockdown and *tish* phenotype show different epileptic related features. They include NMDA receptor complex defects, lower threshold compared to normal response for convulsive-inducing chemicals (Pilocarpine, Pentylentetrazol) with sometimes spontaneous seizures but more often the dysplastic cortex is exhibiting both hyperexcitability and decreased sensitivity to inhibition (Benardete and Kriegstein, 2002; Battaglia *et al.*, 2009). According to the recent literature, both heterotopia and overlying cortex sustain epileptic manifestations (Gabel and LoTurco, 2001; Trotter *et al.*, 2006; Ackman *et al.*, 2009; Lapray *et al.*, 2010).

Table 3. Animal models of focal cortical dysplasia and related malformations of cortical development

Animal model	Pathologic features	Epilepsy/hyperexcitability
<i>Malformations due to abnormal neuronal glial proliferation</i>		
Focal cortical dysplasia		
In utero irradiation rat	Abnormal cortical lamination Heterotopic/dysmorphic neurons	Rare (<20%) spontaneous epilepsy
In utero methylazoxymethanol (MAM) rat	Abnormal cortical lamination Heterotopic neurons	Rare (<20%) spontaneous epilepsy
In utero carmustine (BCNU) rat	Abnormal cortical lamination Dysmorphic neurons	In vitro hyperexcitability
Neonatal focal ibotenate	Abnormal cortical lamination Heterotopic neurons	In vitro hyperexcitability
Prenatal/in utero freeze lesion rat	Abnormal cortical lamination	Interictal spikes/increased kindling
Tuberous sclerosis		
Eker rat (spontaneous <i>Tsc2</i> ^{+/-})	Rare subcortical and Subependymal hamartomas	None
<i>Tsc1</i> -synapsin conditional knockout mice	Abnormal cortical lamination Large, dysmorphic neurons	Spontaneous epilepsy
<i>Tsc1</i> -GFAP conditional knockout mice	Glial proliferation	Spontaneous epilepsy
<i>Malformations due to abnormal neuronal migration</i>		
Lissencephaly		
<i>Lis1</i> ^{+/-} knockout mice	Abnormal cortical lamination	In vitro hyperexcitability
Heterotopia		
<i>Tish</i> spontaneous mutant rat	Subcortical band heterotopias	Spontaneous epilepsy
p35 knockout mice	Heterotopic neurons	Spontaneous epilepsy
In utero irradiation or MAM rat	Nodular heterotopias	Rare spontaneous epilepsy
<i>Malformations due to abnormal cortical organization</i>		
Polymicrogyria		
Postnatal/neonatal freeze-lesion rat	Microsulcus	In vitro hyperexcitability

^aCategorized according to presumed developmentally based pathophysiology (based on Barkovich *et al.*, 2005 classification). This table highlights only representative examples from each category and is not intended to be a comprehensive listing of all animal models; see the text for references to selected animal models and more comprehensive reviews with additional references.

The HeCo mouse

The *HeCo* mouse arose spontaneously in a colony of NOR-CD1 outbred stock (Croquelois *et al.*, 2009). This mouse presents a bilateral and anterior-posterior mass of erroneously placed neurons sheathed in the white matter, and suffers from mild spontaneous epileptic seizures with subtle learning deficits, closely resembling SBH in human (Croquelois *et al.*, 2009). *HeCo* mouse model therefore constitutes an important tool to further study the causes and consequences of SBH and formed the subject of my thesis work.

AIM OF THIS STUDY

The project aims to elucidate the mechanisms underlying the cortical malformation in the *HeCo* mouse. This study was divided into two parts: molecular characterization of the genetic mutation and the morphogenesis of the cortical heterotopia. We first focused our work on characterizing the *HeCo* mouse using a battery of behavioral tests coupled to immunocytochemistry techniques to determine global integrated and selective cellular features describing its phenotype. Subsequently, we studied the *HeCo* mouse at the genetic and cellular level to identify the responsible candidate gene for *HeCo* phenotype and finely study the role of neural progenitors in proliferation and migration through embryonic development. The genetic approach was lead by Fiona Francis's group (Institut du Fer à Moulin, Paris), a collaboration using the single nucleotide polymorphism technique, to target the region of interest of hypothetic involved genes and their expression was determined by transcriptome analysis on whole genome of dissected embryonic brains. Moreover, immunocytochemistry on cultured progenitors targeting intracellular components such as cytoskeleton was analyzed to elucidate potential molecular mechanisms sustaining a pathological cortical development *in vitro*. In parallel, in Lausanne we studied early and late embryogenesis plus early postnatal stages with immunocytochemistry and time lapse video recordings to characterize progenitor cells and their fate determinants to elucidate their role in SBH formation *in vivo*. This collaborative study allowed us to better understand molecular and cellular mechanisms crucial for the development of the human brain.

Results

Results – Part 1:

Characterization of the HeCo Mutant Mouse: A New Model of Subcortical Band Heterotopia Associated with Seizures and Behavioral Deficits.

Croquelois A, Giuliani F, Savary C, Kielar M, Amiot C, Schenk F, Welker E. (2009).
Cereb. Cortex 19(3):563-75.

Summary

This paper forms the first description of the *HeCo* phenotype. My contribution to this work consisted in tissue preparation (mouse breeding, animal perfusion, brain removal and slice section for adults and embryos mostly; phenotyping) and immunocytochemistry procedure to characterize the heterotopia.

The *HeCo* phenotype generated spontaneously in our mouse colony. Cross-breeding tests revealed an autosomal recessive inheritance. *HeCo* morphology is characterized by the presence of a bilateral ectopic neuronal mass sheathed in the white matter and displayed medially in an anterior-posterior axis, known in human as subcortical band heterotopia. Tracing and immunostaining experiments showed connectivity between the heterotopia and the overlaying homotopic cortex (HoCo), thalamus and opposite hemisphere; *HeCo* cortex containing parvalbumin positive interneurons and mostly neurons that correspond to those in the most superficial cortical layers (CUX2).

To determine the cortical organization in *HeCo* and to analyze how the different layers are affected, I performed Nissl stainings on coronal brain sections of adult mice combined with morphometric analysis using NeuroLucida software (MBF bioscience©) in collaboration with Christine Savary who did the most part of tissue preparation and analysis. Results revealed a decrease in both thickness and cell density in layers II-III of the *HeCo* cortex demonstrating that SBH affects mostly superficial layers without changing the cellular global morphology.

To determine the birthdate of cells in the heterotopia, I used 5-bromo 2-deoxyuridine (BrdU) injections at different embryonic ages (E13, E15, E18) with animal sacrifice always at the same postnatal age (P13); BrdU injection at E18 revealed a large number of positive cells in the ectopic mass which disrupts the formation of HoCo in both wild-type (WT) and *HeCo*.

To study the development of the heterotopia as well as the overlying cortex, I analyzed Nissl-stained sections at various embryonic stages. This quantitative analysis showed an increase of IZ thickness with an accumulation of cells already at E16 in this region until E19. This part of the study demonstrated that the heterotopia is forming in the IZ. At P0, the size and configuration of the heterotopia was very similar to that observed in adults.

Using TBR1 immunocytochemistry as a marker for the projection neurons of the deep cortical layers, I identified that the pattern of migration of these neurons is altered. In *HeCo*, the deep layer neurons stay for longer time within the IZ. Moreover, the IZ is significantly enlarged in the *HeCo*. This observation is likely to be at the basis of the fact that in *HeCo* the deeper cortical layers have a larger thickness and suggests that the *HeCo* phenotype could, at least partially, be the consequence of altered radial migration.

In addition, I performed pulsed BrdU experiments that revealed a large dispersion of proliferating cells in the IZ of *HeCo* at E16 and E17. These results identified a second factor that could contribute to the *HeCo* phenotype: the presence of a high number of proliferating cells in *HeCo* is contributing to the IZ enlargement and participates to SBH formation. I then assessed the morphology of RG cells (RC2, GLAST) and immature neurons (DCX) by immunostaining. However, no obvious differences were found between *HeCo* and WT mice during midneurogenesis (E15,E17).

Results

Further experiments were conducted to assess the *HeCo* epileptic phenotype using the pilocarpine-induced model of epilepsy (Cavalheiro *et al.*, 1996). Data showed that HeCo mice develop seizures at a lower dose (200mg/kg body weight) of pilocarpine compared to WT (300-350mg/kg body weight). This result indicates the susceptibility of HeCo to generate epileptic activity likely to be due to a problem in altered neuronal circuitry related to the SBH.

Behavioural tests demonstrated developmental difficulties such as a significant delay in hair growth, eye opening, a slower locomotor development, a decreased general activity (only until 2 month), a lower performance in task acquisition in later aged animals.

Results – Part 2:

Mutations in EML1/Eml1 Lead to Misplaced Neuronal Progenitors during Cortical Development and Massive Heterotopia in Mouse and Human.

Kielar M*, Phan Dinh Tuy F*, Lebrand C, Poirier K, Olaso Robert, Bizzotto S, Boutourlinsky K, Bahi-Buisson N, Le Moing A G, de Juan C, Boucher D, Borrell V, Berquin P, Carpentier W, Gut I, Welker E, Chelly J, Croquelois A[#], Francis F[#].

Submitted

* These authors contributed equally to the work

These authors jointly directed the project

Summary

This study allowed the identification of a candidate gene, *Eml1*, coding for a microtubule associated protein important in *HeCo* pathogenesis. My contribution to this work consisted in determining the development and origins of progenitors in *HeCo* embryonic cortex *in vivo* thanks to tissue preparation (mouse breeding, animal perfusion, dissection, brain slicing, organotypic culture), immunostaining, *in situ* hybridization and time lapse video microscopy; whereas Francis's group in Paris (Institut du Fer à Moulin) performed the molecular analysis and studied *Eml1* expression *in vitro*.

To determine the genomic region of the mutation in *HeCo*, mice were crossed and I performed brain sections of each F2 mouse to phenotype the offspring. Then I dissected tails of F1 and F2 mice for screening arrays and analysis of SNP markers performed by Francis's group. Results showed a 13.7 Mb genomic region on chromosome 12. A second round of genotyping within this region refined it to 4.4 Mb without mutations found; however, additional SNPs gained a further refinement of the candidate region. Subsequently, I dissected embryonic WT and *HeCo* hemispheres (E18) for Francis's group to carry out transcriptome experiments. Mouse gene microarray revealed *Eml1* transcripts, mapping to the refined 4.4 Mb region being differentially expressed and RT-qPCR analyses showed that *Eml1* full length transcripts were more than 96 fold decreased. This result, together with the location of *Eml1* in the identified genomic region, demonstrates that *Eml1* is the mutant gene in *HeCo* mice.

To investigate mutated products, Francis's group searched for disruptions of *Eml1* in genomic DNA in RT-PCR experiment, and identified abnormalities in intron 22. Data showed that although transcripts up to and including exon 22 are detected in *HeCo* brains, normal full-length transcripts were absent, replaced by trace levels of shortened transcripts, predicted to lead to truncated Eml1 with potentially perturbed protein conformation.

To determine the type of mutation, sequencing of a fragment amplified from *HeCo* genomic DNAs revealed an early retrotransposon (ETn) element in *Eml1* highly similar to ETn type II retrotransposons. The ETn is in the same transcriptional orientation as *Eml1* and chimeric *Eml1*-ETn transcripts were identified, thus predicted to truncate and perturb the protein in *HeCo*.

To search for human *Eml1* mutations, a panel of non-consanguineous and consanguineous sporadic and familial cortical malformation cases were screened by PCR. Results showed one family that had a striking phenotype with compound heterozygote mutations in their three affected children, combining giant bilateral periventricular and subcortical heterotopia (mostly frontal), as well as polymicrogyria and corpus callosum agenesis. Human *Eml1* mutations are thus associated with an atypical form of severe heterotopia, epilepsy and intellectual disability. Francis's group then studied the effect of the T243A patient mutation on EML1 MT association. The subcellular localization was assessed in transfected Vero or COS7 cells for WT-EML1 showing cytoplasmic and MT localization during the cell cycle but not for the T243A mutant protein. This proves that the T243A human mutation affects the MT association of EML1.

To further investigate the role of *Eml1* during cortical development, its expression pattern was checked in the brain of lissencephalic (mouse) and gyrencephalic (ferret) animals. *In situ* hybridization performed by Francis's group revealed *Eml1* transcripts in both neuronal progenitors and post-mitotic neurons. I performed a similar experiment with full-length *Eml1* transcripts showing no presence of such copies in *HeCo* (E17). In the adult, sparse *Eml1* labeling persists in the brain, notably in the cingulate, infra-limbic, prelimbic and piriform cortices, hippocampus and in the thalamic nuclei. These combined data suggest that *Eml1* may play several roles during cortical development, in proliferation of several progenitor types, and in migration, differentiation and mature neuronal function.

Then, EML1's role in cortical cells was addressed and subcellular localization in neuronal progenitors showed a cell cycle-dependent, punctate presence of the YFP-EML1 transfected construct; enriched in perinuclear regions in interphase cells and the region of spindle MTs during metaphase. During telophase and cytokinesis, YFP-EML1 labeled puncta accumulated in the midbody region. In neurons, tagged Eml1 appeared distributed throughout the cell, aligning with MTs, and prominent in perinuclear regions and growth cones (co-localizing partially with dynein). In contrast, considering all proliferating cells together, the percentage of Ki-67⁺ cells was found reduced in *HeCo* cultures.

To further study *in vivo* aspects of *HeCo* embryogenesis, I labelled RG fibers (Nestin), deep layer (TBR1) and upper layer (CUX1) neurons. Data showed ectopic cells forming a heterotopia including both early-born (TBR1) and late-born (CUX1) neurons in contrast to WT where neurons formed corresponding cortical layers. In addition, RG fibers appeared disorganized in heterotopic regions. Strikingly, in postnatal *HeCo cortex*, CUX1 neurons failed to reach cortical layers II-IV and were present both in the heterotopia, and in a zone between the heterotopia and the CP. In this zone the CUX1 labeled neurons were spatially organized in columns. These data indicate that all types of cortical projection neurons successively populate the heterotopia with a migrating delay compared to WT.

I then investigated the migration *per se* to detect defects in *HeCo* using GFP-electroporation performed at E15.5 embryos. Unexpectedly, the parameters defining migration, i.e. average migration speed and number and duration of pauses, were found to be identical between *HeCo* and WT. As only difference between the two strains, I found a diminished density of migrating neurons in *HeCo*. The GFP-electroporated migrating neurons showed a similar morphology in postnatal WT and *HeCo* CP (P3); however many mutant cells formed an ectopic compact mass.

To further investigate the origin of the defects, I assessed progenitors with pulsed BrdU (marker for S-phase of the cell cycle) injections revealing misplaced cells throughout the *HeCo* cortical wall from very early (E13) to later embryonic stages (E19); similar results were obtained with cells labeled for Ki-67 (marker for entire cell cycle) confirming altered distribution of progenitors in *HeCo*. The labeling index (percentage of Ki-67⁺ cells that are also labeled with BrdU; (Chenn and Walsh, 2002) was found significantly higher in *HeCo* progenitors. This indicates that *HeCo*

progenitors have a reduced cell cycle exit (quantified by identifying after 24 h those BrdU⁺ cells which showed no Ki-67 expression), particularly in ectopic regions (same at E19). These data demonstrated a perturbed cell cycle in *HeCo*. In addition, I found an increased number of apoptotic (Caspase-3) cells in *HeCo* proving an increased apoptosis during embryogenesis. These data showed the extensive proliferative character of ectopic progenitors from almost the beginning (E13) to the end of neurogenesis (E19).

Using a marker for mitosis (PH3) I confirmed that both RGs (PAX6) and IPCs (TBR2) progenitors were generating cells in ectopic positions (IZ and CP). Therefore, to further search for abnormalities *in vivo*, I used a cytoplasmic marker of RG mitotic progenitors, (P-vim), revealing less cells in mitosis at the ventricular lining in *HeCo* brains despite normal anchoring (β -catenin) and polarity (PAR3) proteins distribution at the apical membrane. P-vim detection during early stages of embryogenesis also showed RG ectopic progenitors (PAX6) with basal fibers extending towards the PS with some cases having disoriented processes. However, at the VZ, most metaphasic cells showed significantly oblique oriented MS in *HeCo*, indicating the detachment of progenitors in *HeCo*. These results clearly demonstrate that a defect in spindle orientation in cells lining the apical membrane is involved in progenitor misplacement. This forms an important element in our hypothesis on formation of the subcorical heterotopia.

General Discussion

The *HeCo* mouse model is characterized by a subcortical heterotopia formed by misplaced neurons normally migrating into the superficial cortical layers. The mutant mouse has a tendency to epileptic seizures. In my thesis project we discovered the mutated *Eml1* gene in *HeCo* as well as in a family of three children showing complex MCD. This discovery formed an important step in exploring the pathogenic mechanisms underlying the *HeCo* phenotype. *In vitro* results showed that during cell division the EML1 protein is associated with the midbody and a mutated version of *Eml1* highlighted an important role of the protein in the astral MT array during cell cycle. *In vivo*, we found that already at an early age of cortical development (E13), ectopic progenitors such as RGs (PAX6) and IPCs (TBR2) accumulate in the IZ along the entire neocortex. We demonstrated that in the SVZ of the *HeCo* mouse cell cycle exit and spindle orientation are perturbed. In later stages (E17), RG fibers are strongly disorganized with deep layer (TBR1) and upper layer (CUX1) neurons trapped within an ectopic mass. At P3, columns of upper layer neurons were present between the heterotopia and the developing cortex; these columns were also present at P7 but at lesser extent. Time lapse video recording (E15.5) revealed that the parameters characterizing the migration of individual neurons are not disturbed in *HeCo*; however, this analysis showed that the density of migrating neuron is smaller in *HeCo*. In conclusion, truncated EML1 is likely to play a prominent role during cell cycle but also acts on the cytoskeletal architecture altering the shape of RG fibers thus influencing the pattern of neuronal migration. The signal transduction between external cues and intracellular effector pathways through MTs may be secondary but sustains the heterotopia development and further studies are needed to clarify the impact of *Eml1* in progenitors versus post-mitotic cells.

The general discussion will first focus on neuronal proliferative disorders that disturb embryonic development and influence secondary processes including neuronal migration that will be addressed subsequently. The third part will raise the question of *Eml1* candidate gene in these two biological events to try to understand its role in the SBH formation in the *HeCo* mouse.

I. Proliferation and cell cycle defects

I.1. Longer cell cycle may delay the engagement in neuronal migration and contribute to HeCo pathology

Our results showed that *HeCo* mouse progenitors present a longer duration of the cell cycle during embryogenesis. It is known that progenitors exit the cell cycle at a precise time point during embryonic development to differentiate into post-mitotic neurons that migrate towards corresponding neocortical layers (Dehay and Kennedy, 2007). Indeed, in mice, 11 successive cell cycles produce the majority of projection neurons, meanwhile a decline in VZ and SVZ progenitors pool takes place (Caviness *et al.*, 2003). The cell cycle exit is hence forming the successive overlapping cortical layers with terminal mitosis specifying layer-specific cytological features of the pyramidal neurons including its pattern of connectivity (Parnavelas *et al.*, 1991; Takahashi *et al.*, 1999; Anderson *et al.*, 2002). Therefore, when the time-orchestrated exit phase is delayed, the entry of progenitors into migration is retarded which, as a consequence, will reduce the overall population of migrating neurons.

Our observations in *HeCo* illustrate these general aspects of cortical development. We found in the mutant a decreased density in migrating cells in organotypic culture slices that were taken at E15.5, but interestingly there was no alteration in other parameters that characterize migration (average speed, number and frequency of pauses) compared to WT. These latter findings suggest that an abnormal long cell cycle does not affect the migration mechanism *per se*.

These observations made us focus on the mechanism by which the cell cycle is delayed in *HeCo* progenitors. As normal brain development is limited in time, perturbing its cell cycle exit may partially explain the lower cellular density observed in *HeCo* adult cortical layers II-III (Croquelois *et al.*, 2009) and highlight the importance of this crucial phase in heterotopia formation.

1.2. Mitotic spindle disorientation drives progenitors misplacement

During embryonic development we found a significant amount of apical progenitors to divide in an oblique oriented plane during mitosis at the apical membrane of the ventricular zone in *HeCo*. A hypothesis towards cellular detachment linked to SBH formation could explain progenitor misplacement. MS orientation is important for VZ structural identity and partial cell fate specification, since it is well known that cleavage planes modulate the proliferation, cell fate, neuronal differentiation and consecutive migration activity (Huttner and Kosodo, 2005; Fish *et al.*, 2006; Buchman and Tsai, 2007; Higginbotham and Gleeson, 2007; Zhong and Chia, 2008; Konno *et al.*, 2008; Wang *et al.*, 2009; Peyre *et al.*, 2011). In this context, one daughter cell would detach from the apical membrane and the other sister cell might stay or even leave the neuroepithelial surface as a bRG. This could be similar in *HeCo* where a decrease in apical progenitors at the ventricular surface is observed at the apical lamina but we also noticed misplaced, disoriented and proliferating RGs and IPCs in IZ, and CP. We do not know the exact cellular processes responsible for the oblique orientation of the MS (through pulling forces on spindle poles or via specific polarity proteins). In this context it is important to note that we did not observe any difference in the total number of neurons or progenitors in *HeCo* compared to WT, indicating a pure detachment process contributing to heterotopic mass rather than a cell fate change. Further experiments are needed to dissect the precise mechanism of MS orientation in *HeCo*.

1.3. The role of the neurogenetic gradient in heterotopic location

The operations of time, cell production and specification do not proceed concurrently across the entire dorsal pallium. The sequence of neurogenesis is initiated at the rostro-lateral margin of the neocortical epithelium at E10 and progresses caudo-medially with initiation in dorso-medial cortex at E11 (Miyama *et al.*, 1997) corresponding to the “neurogenetic gradient” (Bayer and Altman, 1991; Caviness *et al.*, 2000b). Thus, the same classes of neurons will arise at different times with progression along the caudo-medial axis, meaning that different classes of neurons will be formed at the same time in positions arrayed along this axis. This may partially explain why we observe at the same embryonic time, deep and superficial layer neurons in the heterotopia whereas the adult *HeCo* mouse present a bilateral and medial SBH composed mostly of upper layer cells. This could be the consequence of the cellular -lateral to medial- gradient through which the production of the last (most superficial) layers will be most affected. The neurogenetic gradient may also partially resolve the fact that superficial neurons are still able to form an upper neocortical layer as they are

not produced all together thus migrating successively to the CP with relative chances to avoid “pathologic traps” formed by the heterotopia.

II. Altered migration patterns in HeCo

II.1. Altered radial glial guided migration does not totally abort the formation of cortical layers in HeCo

Recent data published by Valiente *et al.* (2011) on the role of focal adhesion kinase (FAK) in glial-guided neuronal migration (Figure 11), showed a partial attachment of the post-mitotic neuron to the RGC scaffold when FAK was mutated. This phenomenon is due to a lack of adhesion points on the surface of migrating neurons which FAK normally provides through a recruitment process. Their results showed that FAK is not required for tangential migration but more in radial migration where most FAK-deficient pyramidal cells managed to reach the upper layers of the cortex in postnatal mice; however with some FAK-deficient neurons accumulating in ectopic locations. In our study we observed no significant differences during the migration phase at E15.5 Div3 between WT and *HeCo* but still a heterotopia was formed thus suggesting that pure migration is not touched. We could also consider the fact that there are neurons migrating around the ectopic mass which acts like a physical barrier obliging migrating neurons to increase the distance of migration. This could be an additional factor explaining the diminished density of neurons in layer II-IV of the adult *HeCo* mice.

In addition, TBR1 deep layer neurons and CUX1 upper layer neurons are present in the heterotopia at E17 but at P3 the heterotopia is only populated by CUX1 neurons. This clearly demonstrates that sequential waves of neurons that are populating the ectopic mass through embryonic development. Therefore, a similar possible “FAK-deficient paradigm” may occur in *HeCo* despite highly disorganized RGC fibers. The FAK mechanism may however be accountable for some but not all ectopic neurons as we find an impoverished but still formed cortical layers II-III in adult *HeCo* (Croquelois *et al.*, 2009).

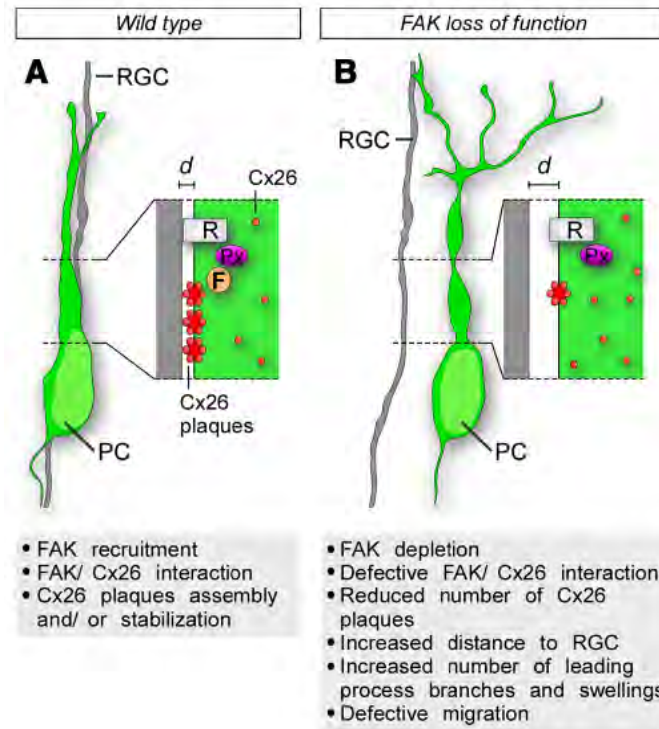


Figure 11. Cx26-dependent glial-guided migration is regulated by FAK. (A) Recruitment of FAK (F) to adhesion points through its interaction with Paxillin (Px) is necessary for the recruitment of Cx26 to the membrane and/or to stabilize its aggregation in discrete plaques. Note that the schema only represents FAK and connexins present in migrating neurons, as the present study has not investigated their role in RGCs. (B) FAK ablation leads to a failure in the formation/ stabilization of Cx26 plaques at the membrane and disruption of radial migration. Pyramidal cells (PC) continue to migrate in the absence of FAK, but they are no longer able to maintain its attachment to the radial glia and the distance (d) between PCs and their parental RGC increases. Detachment from RGC also leads to important morphological modifications (multiple swelling, increased number of processes) in migrating neurons. R, Receptor. Valiente et al., 2011.

II.2. Late RGC fibers alterations during embryogenesis may affect predominantly superficial neurons in the adult HeCo mouse

The adult *HeCo* mouse model is characterized by an ectopic mass of layers II-IV neurons sheathed bilaterally in the subcortical white matter bordering the lateral ventricles. At late embryonic stages radial fibers in *HeCo* are twisted and disoriented. This altered spatial configuration is likely to alter the glial-guided migration for a number of immature neurons leading to SBH. However, in *HeCo* mouse, we do not observe a complete damage of RGs scaffold in its structure neither at E13 nor at E15 and E17, in the latter age only RGs inside the heterotopia are damaged. Thus, one part of the explanation in favor of mildly preserved superficial layer in *HeCo* may be due to the fact that the disorganization of RG fibers takes place in late embryonic days at a time point at which upper layer

cells proliferate and migrate (Molyneaux *et al.*, 2007). This will have the largest impact on the formation of layers II-IV since a major part of the population of pyramidal cells for these layers will remain in the SBH. We still need to explore what mechanism could compensate or hijack the development of the heterotopia for the projection neurons generated at earlier embryonic days.

II.3. Columns of immature cells could promote HeCo phenotype

It is well known that in mammals neurogenesis and neuronal migration are still active after birth in olfactory bulb, ventricular areas and hippocampus (Luskin 1993; Lois and Alvarez-Buylla, 1994; Lim *et al.*, 1997; Kirschenbaum *et al.*, 1999; Gage 2002, Alvarez-Buylla and Lim 2004, Nottebohm 2004, Ming and Song 2005; Zraggen *et al.*, 2011). Strikingly, our data showed columns of superficial cells in the early postnatal neocortex between the heterotopia and superficial layers, a phenomenon that has never been observed in the WT. As we proposed a delayed migration in *HeCo*, these columns are likely to consist of ectopic neurons trapped at the end of the migration period. For the moment we do not know the significance and the identity of these misplaced (columnar) cells. Given that we do not find these neurons in that position in the adult cortex two possibilities come to mind; between P3 and adulthood these neurons either descend to the heterotopia or ascend to the cortex. A number of these neurons at P3 are PAX6 positive whereas this marker does not label cells within the heterotopia at this time point (data not shown). In many vertebrates, some RGs do not convert into astrocytes at the end of development but persist postnatally to generate neurons and guide them through migration (Stevenson and Yoon 1981; Alvarez-Buylla *et al.*, 1990, 1998; Goldman *et al.* 1996; Kálmán, 1998; Garcia-Verdugo *et al.*, 2002; Weissman *et al.*, 2003; Zupanc, 2006). Supplemental double labelling experiments are necessary to determine exactly the cell type of these columnar neurons and identify their connectivity.

On the other hand, the columnar migration at P3 and P7 was also already observed in EGFP positive progenitors shaped together in bundles and columns at E15.5 Div4 in transfected *HeCo* cortices (data not shown), suggesting that this aggregate migration is determined during embryogenic stages. In addition, these misplaced cells may modulate the normal cortical circuitry and could contribute to the epileptic symptoms. Indeed, it is interesting to note that we do not see these columns in adult *HeCo* mice (Croquelois *et al.*, 2009) but only in young animals P3 and P7. As a result, this phenomenon could clarify in human why children and young adults (P3, P7 mouse

$\approx 2, 7$ years human; Flurkey *et al.*, 2007) present more recurrent and severe epileptic clinical manifestations compared to adults (Blümcke *et al.*, 2009).

II.4. Misplaced apical and basal progenitors participate to HeCo pathogenesis

Apical PAX6 and basal TBR2 progenitors are located ectopically and colonize the entire cortical hem in *HeCo* embryonic brains during corticogenesis. Observations in the Tish-rat (Lee *et al.*, 1998; Fitzgerald *et al.*, 2011) have led to the hypothesis of the existence of two distinct germinative zones. This hypothesis may be applied to the *HeCo* mouse where we observed many PAX6 and TBR2 progenitors not only ectopically distributed but also as active mitotic cells. In this context, the accumulation of newborn ectopic pyramidal neurons in the SVZ-IZ region may account for a pseudo supplemental germinal layer leading to heterotopia.

These data raise the question which progenitors are involved in the SBH formation? TBR2 identified misplaced IPCs hence suggesting their involvement but in the RG population there are several candidates as RG family is composed of aRGs, bRGs and SNPs in the mouse (Stancik *et al.*, 2010; Borell and Reillo, 2012). The three latter cells have similar molecular signature PAX6 and SOX2, except for SNPs differing only by the *Ta1* promoter. We therefore need to assess in which proportions each RG type is participating in SBH formation. bRGs have a great role in the developing cortex of primates, including human, and other species (Fietz *et al.*, 2010; Hansen *et al.*, 2010; Reillo *et al.*, 2011; Kelava *et al.*, 2012) but they are quite rare in the mouse brain (Wang *et al.*, 2011; Shitamukai *et al.*, 2011). Interestingly, *Eml1* expression in the ferret OSVZ suggests that this gene could be expressed in bRGs. Since bRGs lack apical end-feet they would be preferential subjects to defects such as observed in the *HeCo*. Moreover, the secretion of attracting guidance cues by adjacent progenitors around the ectopic mass and by post-mitotic cells already present inside the heterotopia, may further contribute to the SBH development in the IZ as it is well known that neurons attract other neurons (Lui *et al.*, 2011).

Actually, we cannot exclude another possibility that neurons originating from misplaced and mitotic delayed IPCs and RGs could rearrange the global RG scaffolding and damage it during corticogenesis. Thus, the question is to know if RGs disorganized fibers induce SBH or is it the inverse.

III. EML1 role in the HeCo mouse

Studies of the Echinoderm microtubule-associated protein (EMAP) family pointed to impact cell division, mechanotransduction and sensory function (Brisch *et al.*, 1996; Ly *et al.*, 2002; Eichenmuller *et al.*, 2002; Pollmann *et al.*, 2006; Hueston *et al.*, 2008; Bechstedt *et al.*, 2010); EML1 belongs to the EMAP family but its function in brain development is unknown. In addition, a variety of diseases have been linked to defects in the MT cytoskeleton which include developmental disorders (see Introduction), issues in symmetric and asymmetric cell divisions, genomic instability, and ciliopathies (Konno *et al.*, 2008; Andrade *et al.*, 2009; Lizarraga *et al.*, 2010; Postiglione *et al.*, 2011; Benadiba *et al.*, 2012).

III.1. EML1 role in proliferation

In our study, EML1 was shown to bind directly to MTs and had interesting subcellular localizations during mitosis at the MS poles during metaphase and at the midbody (characteristic bridge structure linking the separating daughter cells, [Guizetti *et al.*, 2011]) during telophase. In addition, a human mutation which targets EML1 specific domain involved in MT interactions (HELP region, [Tegha-Dunghu *et al.*, 2008]), resulted *in vitro* in the loss of the particular MT aster structure. Thus, truncated EML1 copies found in *HeCo* may induce an important lack of protein-protein interactions which may prolong the cell cycle duration either by preventing the transduction of a “stop” signal to arrest the proliferative state or by slowing down the speed of the global cellular machinery. On one hand, these data clearly show the relevance of EML1 as an essential protein for normal cellular functioning during cell cycle (mitosis and interphase). On the other hand, however, these experiments raise the questions of how and when does EML1 influence the cell cycle? Indeed, our results showed chimeric EML1 variants in *HeCo* brains due to retrotransposon mutation and progenitors having a defect in cell cycle exit but we do not know at which moment of the cell cycle EML1 interferes; at the interphase (G1, S and G2 phase) or during mitosis (M-phase)? Moreover, EML1 also contains several WD-repeats regions that are crucial domains for mediating other protein-protein interactions. These repeats lead to a huge diversity of cellular events in which EML1 can interact offering more possibilities for future complex, but exciting investigations.

As mentioned, *in vivo HeCo* progenitors are more obliquely oriented at the VZ during metaphase suggesting a prominent role for EML1 during mitotic phases. Several studies showed that spindle polarity disorientations, according to normal vertical cleavage planes, determine the detachment of

progenitors from the apical surface which might be the fact here in *HeCo* to promote SBH pathology in spite of normal distribution of adhesion (B-catenin) and polarity (PAR-3) proteins at the ventricular membrane.

III.2. EML1 role in migration

It is known that preserved microtubules are one of the essential features leading to normal neuronal migration (Jaglin and Chelly, 2009) including RG motility and their orientation (Li *et al.*, 2003). Li reported that the unique morphology of RG is due to the composition and organization of their cytoskeleton. Indeed, treated RGs with nocodazole and cytochalasin D showed that microtubules are critical for their polarized morphology. In addition, other experiments indicated that certain transcripts specific for MT associated proteins are selectively expressed in RG. Further studies are needed to determine whether it would be the case for *Eml1* but if yes it could be central for RG scaffold organization and RG body orientation.

Recent studies reinforce the role of the cytoskeleton components in normal cortical development. For example, Cdc42, a cytoskeleton molecule participating in neuronal motility, showed disrupted radial glia development when inactivated specifically in RGs (Yokota *et al.*, 2010). Indeed, hGFAP-Cre-mediated recombination used to inactivate Cdc42 showed defects with more branched endfeet, less fasciculated processes and misplaced soma less densely packed hence compromising inter-RG interactions. Furthermore, TBR1 labeling indicated misplaced deep layer neurons and moderate to severe misplacement of neurons within the disrupted RG scaffold (Yokota *et al.*, 2010). Gsk3, another interacting protein with the cytoskeleton, deletion perturbs prominently symmetric proliferative axis and the overall organization of RGs (Kim *et al.*, 2009). In addition, loss of APC, a multifunctional protein involved in cell migration, proliferation and differentiation, provokes a huge disarrangement of the whole RG scaffold (Yokota *et al.*, 2009). Strikingly, a variety of protein having no obvious direct relations between them can affect the polarity of RGs in a non-overlapping and hierarchical way because they target the same structure, the cytoskeleton. Plus, Cdc42 and Gsk3 aberrant regulations have been reported in psychiatric disorders (Mao *et al.*, 2009; Ide and Lewis, 2010). Therefore, EML1 that associates with MTs could play a role in RG shape but also link other molecules controlling RG polarization through cytoskeleton structure and influence the degree of neurodevelopmental disorders such as SBH.

IV. Conclusion and perspectives

Characterizing *HeCo* mouse phenotype in adults and embryos lead to the identification of a novel gene important in cortical development, *Eml1*, encoding a MT associated protein related to giant bilateral heterotopia in human and SBH in mouse. In addition, MT dynamics coordinate MS orientation, midbody function and cell cycle properties during embryogenesis (Kosodo *et al.*, 2004; Paramasivam *et al.*, 2007; Dubreuil *et al.*, 2007; Asami *et al.*, 2011) thus truncated EML1 may disturb these finely-tuned processes to generate ectopic progenitors. As a result, EML1 suggest an important role in progenitor anchoring at the VZ and in cell cycle duration which strongly highlight the fact that progenitor misplacement may represent the primary pathologic feature in *HeCo*.

One point of investigation would lead us to study events occurring in the VZ and SVZ regions where progenitors divide and immature neurons enter the multipolar stage before migrating to the CP. Interestingly, results showed that mutated genes encoding cytoskeleton interacting molecules, can arrest neuronal migration either near the VZ/SVZ (*Flna* mutation) or near the IZ (*Dcx* and *Pafah1b1* mutations). These observations are indicating that multipolar stage has at least two sub-stages susceptible to interruption with different degrees of vulnerability depending on the gene involved; it could be the case with mutated *Eml1*. Due to our experimental time lapse window (E15.5) and selected area studied (IZ/CP), we might have missed a plausible “arrested multipolar” mechanism in SVZ but also pathologic defects happening at later embryonic stages (E17-E19). RGs transplant experiments might help to determine cell-autonomous or non-cell-autonomous events related to EML1. Further time lapse experiments coupled to cristal DiI-labeled RG fibers will also help to elucidate how the RG scaffold interacts with migrating cells in and around the ectopic mass.

To go further and confirm the involvement of *Eml1* in the *HeCo* phenotype, a complete deletion of the gene by knockout technique in the *HeCo* genome would be necessary. It would show the degree of *Eml1* impact in SBH formation and even more if new features would appear after *Eml1* extinction. Combined rescue experiment with a WT-*Eml1* transcript would also tell us if it is possible to reverse the pathology to consider new therapeutic treatments targeting this EMAP.

Studying *Eml1* gene pathway to find its upstream and downstream effectors would help us to better understand how and in which process they are specifically involved. Recent data are pointing to EML1 fusion with Abelson 1 (ABL1) in a patient with T-cell acute lymphoblastic leukemia (de

Keersmaecker *et al.*, 2005) that is transforming normal cells into carcinogenic ones. This is highlighting EMAPs important role in regulating cell cycle. Still, we need to address how EML1 does influence MT array and more important at what time it does modulate the cellular pathways in particular, only during proliferation? Interestingly, recent data demonstrated that appropriate RG placement, proliferation, organization (orientation and polarized shape) and localization of anchoring and polarity proteic complexes depend also on myristoylated alanine-rich C-kinase substrate (MARCKS). Its dysfunction during corticogenesis leads to aberrant cortical lamination and cobblestone lissencephaly (Weimer *et al.*, 2009). Thus EML1 association with MARCKS could be a plausible explanation for *HeCo* phenotype. Another close interaction may involve MARK, a microtubule-associated proteins/microtubule affinity-regulating kinase that binds to the MT network and to centrosomes (Trinczek *et al.*, 2003; Sapir *et al.*, 2008). Reduced MARK levels resulted in multipolar neurons stalled in the IZ and affected centrosomal dynamics in migrating neurons. These are important associations because MARCKS and MARK are interacting with MTs and centrosomes where EML1 also associates.

Concerning the epileptic phenotype, studying *HeCo* neuronal network will help us to understand the epileptic tendency observed previously (Croquelois *et al.*, 2009). In a first step, electrophysiology experiments could show us how the neuronal circuitry responds to different stimuli and we could answer the question of how mature/immature are the excitatory and inhibitory systems and investigate the ectopic mass role in the epileptogenesis. Interestingly, studies on the *Dcx*-inactivated rat model of cortical band heterotopia showed ectopic neurons retaining immature properties with a delayed maturation of GABA-mediated signalling and that the heterotopia act rather as a modulator than being the source of seizures (Ackman *et al.*, 2009). These results showed that cortical dysplasia produce major alterations not only in neurons that fail to migrate but also in their electrical properties that bring complementary insights on cortical plasticity.

The most striking finding in this study is ectopic location of progenitors which changes our classical view of SBH formation caused directly by disturbed neuronal migration (Barkovich *et al.*, 2012). In human, severe heterotopias also present polymicrogyria thus highlighting defects in progenitors in the pathogenesis of certain MCDs. Whether pathologic mechanisms inducing heterotopias are orchestrated successively or happening synchronally in relative proportions, it still needs clarification and further studies are required to identify the precise role of ectopic progenitors in pathologic and pseudo-normal cortex. Identification of EML1 provides a new key to unravel the

molecular and cellular mechanisms underlying progenitor dynamics at the apical surface during normal cortical development. A simplified scheme of heterotopic formation during mouse embryogenesis is suggested in Figure 12 below.

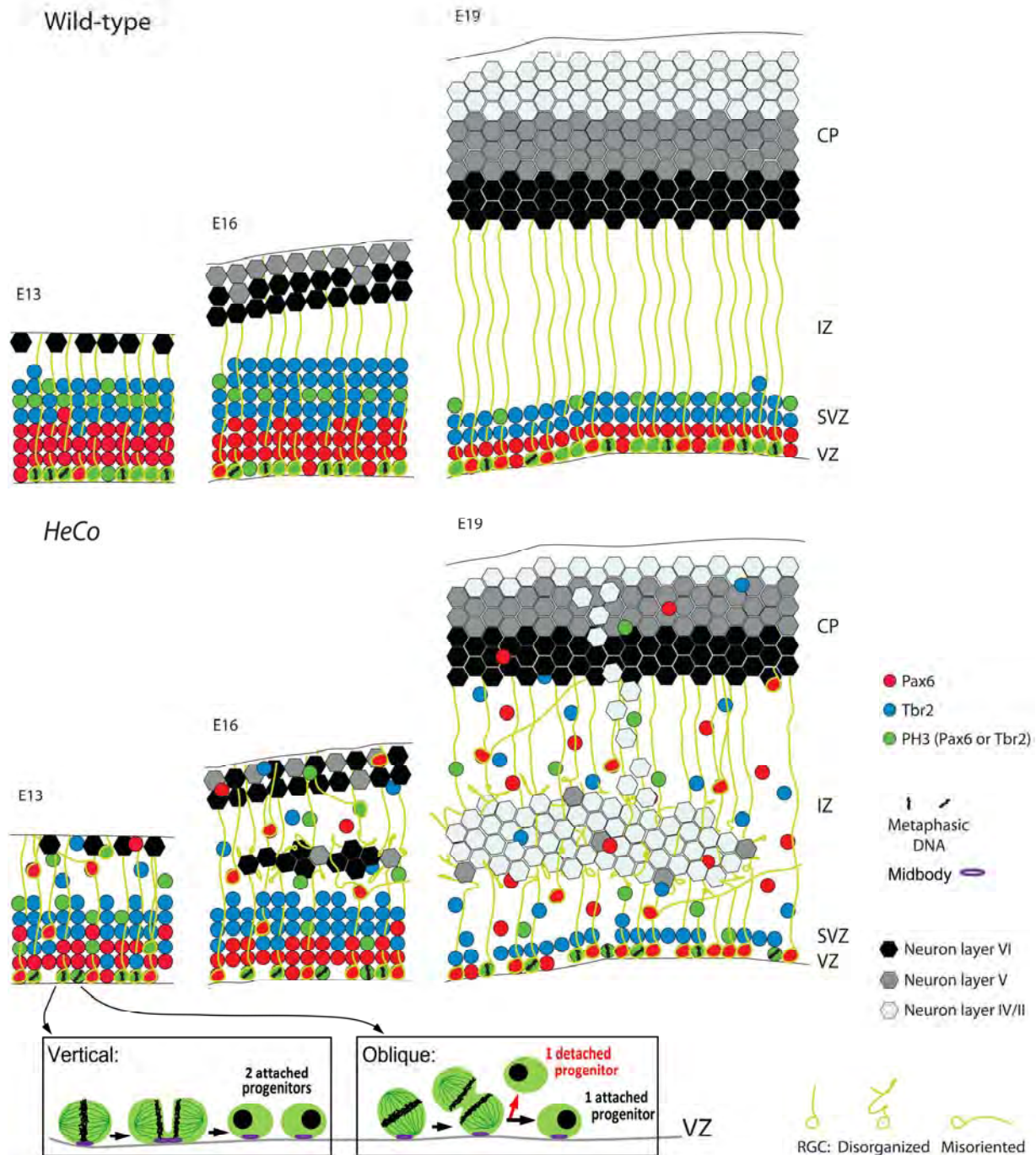


Fig12. Hypotheses for the development of the SBH in *HeCo*. Subcortical band heterotopia development is occurring since early neurogenesis (E13) up to end of postnatal migration (P7). Several hypotheses involving truncated EM11 may be responsible for *HeCo* pathogenesis such as prolonged cell cycle duration, increased oblique oriented mitosis and defects in RG fibers organization. All together, these mechanisms may lead to misplaced apical and basal proliferating progenitors thus to ectopic post-mitotic neurons forming a subcortical heterotopia.

References

- Ackman, J.B., Aniksztejn, L., Crépel, V., Becq, H., Pellegrino, C., Cardoso, C., Ben-Ari, Y., and Represa, A. (2009). Abnormal network activity in a targeted genetic model of human double cortex. *J. Neurosci.* 29(2):313-27
- Alfano, C., Viola, L., Heng, J.I., Pirozzi, M., Clarkson, M., Flore, G., De Maio, A., Schedl, A., Guillemot, F., and Studer, M. (2011). COUP-TFI promotes radial migration and proper morphology of callosal projection neurons by repressing *Rnd2* expression. *Development* 138(21):4685-97.
- Alvarez-Buylla, A., Theelen, M., and Nottebohm, F. (1988). Mapping of radial glia and of a new cell type in adult canary brain. *J. Neurosci.* 8, 2707–2712.
- Alvarez-Buylla, A., Theelen, M., and Nottebohm, F. (1990). Proliferation ‘‘hot spots’’ in adult avian ventricular zone reveal radial cell division. *Neuron* 5, 101–109.
- Alvarez-Buylla, A., García-Verdugo, J.M., Mateo, A.S., and Merchant-Larios, H. (1998). Primary neural precursors and intermitotic nuclear migration in the ventricular zone of adult canaries. *J. Neurosci.* 18(3):1020-37.
- Alvarez-Buylla, A., and Lim, D.A. (2004). For the long run: maintaining germinal niches in the adult brain. *Neuron* 41(5):683-6.
- Anderson, G., and Price, D.J. (2002). Layer-specific thalamocortical innervation in organotypic cultures is prevented by substances that alter neural activity. *Eur. J. Neurosci.* 16(2):345-9.
- Andrade DM. (2009). Genetic basis in epilepsies caused by malformations of cortical development and in those with structurally normal brain. *Hum Genet.* 126(1):173-93.
- Andrade, C.S., and Leite, C. da C. (2011). Malformations of cortical development: current concepts and advanced neuroimaging review. *Arq. Neuropsiquiatr.* 69(1):130-8.
- Anthony, T.E., Klein, C., Fishell, G., and Heintz, N. (2004). Radial glia serve as neuronal progenitors in all regions of the central nervous system. *Neuron* 41(6):881-90.
- Anton, E.S., Marchionni, M.A., Lee, K.F., and Rakic, P. (1997). Role of GGF/neuregulin signaling in interactions between migrating neurons and radial glia in the developing cerebral cortex. *Development* 124(18):3501-10.
- Anton, E.S., Kreidberg, J.A., and Rakic, P. (1999). Distinct functions of $\alpha3$ and $\alpha(v)$ integrin receptors in neuronal migration and laminar organization of the cerebral cortex. *Neuron* 22, 277-289.
- Arai, Y., Pulvers, J.N., Haffner, C., Schilling, B., Nusslein, I., Calegari, F., and Huttner, W.B. (2011). Neural stem and progenitor cells shorten S-phase on commitment to neuron production. *Nat. Commun.* 2:154.

- Arnold., S.J., Huang., G.J., Cheung, A.F., Era, T., Nishikawa, S., Bikoff, E.K., Molnár, Z., Robertson, E.J., and Groszer, M. (2008). The T-box transcription factor Eomes/Tbr2 regulates neurogenesis in the cortical subventricular zone. *Genes Dev.* 22, 2479–2484.
- Asami, M., Pilz, G.A., Ninkovic, J., Godinho, L., Schroeder, T., Huttner, W.B., and Götz, M. (2011). The role of Pax6 in regulating the orientation and mode of cell division of progenitors in the mouse cerebral cortex. *Development* 23, 5067-5078.
- Austin., C.P., and Cepko, C.L. (1990). Cellular migration patterns in the developing mouse cerebral cortex. *Development* 110, 713–732.
- Bai, J., Ramos, R.L., Ackman, J.B., Thomas, A.M., Lee, R.V., and LoTurco, J.J. (2003). RNAi reveals doublecortin is required for radial migration in rat neocortex. *Nat. Neurosci.* 6, 1277-1283.
- Bannister, A.P. (2005). Inter- and intra-laminar connections of pyramidal cells in the neocortex. *Neurosci. Res.* 53(2):95-103.
- Barkovich, A.J. (1996). Subcortical heterotopia: a distinct clinico-radiologic entity. *AJNR. Am. J. Neuroradiol.* 17: 1315–22
- Barkovich, A.J., Guerrini, R., Kuzniecky, R.I., Jackson, G.D., and Dobyns, W.B. (2012). A developmental and genetic classification for malformations of cortical development: update 2012. *Brain* 135(Pt 5):1348-69.
- Battaglia, G., Becker, A.J., LoTurco, J., Represa, A., Baraban, S.C., Roper, S.N., and Vezzani, A. (2009). Basic mechanisms of MCD in animal models. *Epileptic Disord.* 11(3):206-14.
- Bayatti, N., Moss, J.A., Sun, L., Ambrose, P., Ward, J.F., Lindsay, S., and Clowry, G.J. (2008). A molecular neuroanatomical study of the developing human neocortex from 8 to 17 postconceptional weeks revealing the early differentiation of the subplate and subventricular zone. *Cereb. Cortex* 18, 1536–1548.
- Bayer, S.A., and Altman, J. (1991). *Neocortical Development* (New York:Raven Press).
- Bear, M.F., Connors, B.W., and Paradiso, M.A. (2001). *Neuroscience: Exploring the Brain*. Baltimore: Lippincott.
- Bechstedt, S., Albert, J.T., Kreil, D.P., Müller-Reichert, T., Göpfert, M.C., and Howard, J. (2010). A doublecortin containing microtubule-associated protein is implicated in mechanotransduction in *Drosophila* sensory cilia. *Nat. Commun.* 1:11.
- Benadiba, C., Magnani, D., Niquille, M., Morlé, L., Valloton, D., Nawabi, H., Ait-Lounis, A., Otsmane, B., Reith, W., Theil, T., Hornung, J.P., Lebrand, C., and Durand, B. (2012). The ciliogenic transcription factor RFX3 regulates early midline distribution of guidepost neurons required for corpus callosum development. *PLoS Genet.* 8(3):e1002606.
- Benardete, E.A., and Kriegstein, A.R. (2002). Increased excitability and decreased sensitivity to GABA in an animal model of dysplastic cortex. *Epilepsia* 43(9):970-82.

- Bentivoglio, M., and Mazzarello, P. (1999). The history of radial glia. *Brain Res. Bull.* 49:305-315.
- Bernardi, B., Volpi, L., Tassinari, C.A., Guggenheim, M.A., Ledbetter, D.H., Gleeson, J.G., Lopes-Cendes, I., Vossler, D.G., Malaspina, E., Franzoni, E., Sartori, R.J., Mitchell, M.H., Mercho, S., Dubeau, F., Andermann, F., Dobyns, W.B., and Andermann, E. (2002). Subcortical band heterotopia (SBH) in males: clinical, imaging and genetic findings in comparison with females. *Brain* 125(Pt 11):2507-22.
- Bilasy, S.E., Satoh, T., Ueda, S., Wei, P., Kanemura, H., Aiba, A., Terashima, T., and Kataoka, T. (2009). Dorsal telencephalon-specific RA-GEF-1 knockout mice develop heterotopic cortical mass and commissural fiber defect. *Eur. J. Neurosci.* 29(10):1994-2008.
- Blümcke, I., Vinters, H.V., Armstrong, D., Aronica, E., Thom, M., and Spreafico, R. (2009). Malformations of cortical development and epilepsies: neuropathological findings with emphasis on focal cortical dysplasia. *Epileptic Disord.* 11(3):181-93.
- Bond, J., Roberts, E., Springell, K., Lizarraga, S.B., Scott, S., Higgins, J., Hampshire, D.J., Morrison, E.E., Leal, G.F., Silva, E.O., Costa, S.M., Baralle, D., Raponi, M., Karbani, G., Rashid, Y., Jafri, H., Bennett, C., Corry, P., Walsh, C.A., and Woods, C.G. (2005). A centrosomal mechanism involving CDK5RAP2 and CENPJ controls brain size. *Nat. Genet.* 37(4):353-5.
- Borrell, V., Kaspar, B.K., Gage, F.H., and Callaway, E.M. (2006). In vivo evidence for radial migration of neurons by long-distance somal translocation in the developing ferret visual cortex. *Cereb. Cortex* 16, 1571–1583.
- Borrell, V., and Reillo, I. (2012). Emerging roles of neural stem cells in cerebral cortex development and evolution. *Dev. Neurobiol.* 72(7):955-71.
- Borello, U., and Pierani, A. (2010). Patterning the cerebral cortex: traveling with morphogens. *Curr. Opin. Genet. Dev.* 20(4):408-15.
- Bortone, D., and Polleux, F. (2009). KCC2 expression promotes the termination of cortical interneuron migration in a voltage-sensitive calcium-dependent manner. *Neuron* 62, 53-71.
- Brisch, E., Daggett, M.A., and Suprenant, K.A. (1996). Cell cycle-dependent phosphorylation of the 77 kDa echinoderm microtubule-associated protein (EMAP) in vivo and association with the p34cdc2 kinase. *J. Cell Sci.* 109, 2885-2893.
- Brodmann, K. (1909). *Vergleichende Lokalisationslehre der Grosshirnde*. Barth, Leipzig.
- Buchman, J.J., and Tsai, L.H. (2007). Spindle regulation in neural precursors of flies and mammals. *Nat. Rev. Neurosci.* 8(2):89-100.
- Bystron, I., Blakemore, C., and Rakic, P. (2008). Development of the human cerebral cortex: Boulder Committee revisited. *Nat. Rev. Neurosci.* 9(2):110-22.

- Cappello, S., Böhringer, C.R., Bergami, M., Conzelmann, K.K., Ghanem, A., Tomassy, G.S., Arlotta, P., Mainardi, M., Allegra, M., Caleo, M., van Hengel, J., Brakebusch, C., and Götz, M. (2012). A radial glia-specific role of RhoA in double cortex formation. *Neuron* 73, 911-924.
- Carpenter, M.B., and Cowie, R.J. (1985). Connections and oculomotor projections of the superior vestibular nucleus and cell group 'y'. *Brain Res.* 336(2):265-87.
- Caviness, V.S., Jr (1982). Neocortical histogenesis in normal and reeler mice: a developmental study based upon [3H]thymidine autoradiography. *Brain Res.* 256, 293-302.
- Caviness, V.S., Jr., Takahashi, T., and Nowakowski, R.S. (2000b). Neuronogenesis and the early events of neocortical histogenesis. *Results Probl. Cell. Differ.* 30:107-43.
- Caviness, V.S. Jr., Goto, T., Tarui, T., Takahashi, T., Bhide, P.G., and Nowakowski, R.S. (2003). Cell output, cell cycle duration and neuronal specification: a model of integrated mechanisms of the neocortical proliferative process. *Cereb. Cortex.* 13(6):592-8.
- Chenn, A., and Walsh, C.A. Regulation of Cerebral Cortical Size by Control of Cell Cycle Exit in Neural Precursors. *Science.* 2002; 297 (5580): 365-369.
- Chevassus-au-Louis, N., and Represa, A. (1999). The right neuron at the wrong place: biology of heterotopic neurons in cortical neuronal migration disorders, with special reference to associated pathologies. *Cell. Mol. Life Sci.* 55(10):1206-15.
- Colombo, N., Salamon, N., Raybaud, C., Ozkara, C., and Barkovich, A.J. (2009). Imaging of malformations of cortical development. *Epileptic Disord.* 11(3):194-205.
- Corbo, J.C., Deuel, T.A., Long, J.M., LaPorte, P., Tsai, E., Wynshaw-Boris, A., and Walsh, C.A. (2002). Doublecortin is required in mice for lamination of the hippocampus but not the neocortex. *J. Neurosci.* 22(17):7548-57.
- Costa, C., Harding, B., and Copp, A.J. (2001). Neuronal migration defects in the Dreher (Lmx1a) mutant mouse: role of disorders of the glial limiting membrane. *Cereb. Cortex* 11(6):498-505.
- Croquelois, A., Giuliani, F., Savary, C., Kielar, M., Amiot, C., Schenk, F., and Welker, E. (2009). Characterization of the HeCo mutant mouse: a new model of subcortical band heterotopia associated with seizures and behavioral deficits. *Cereb. Cortex* 19(3):563-75.
- Cubelos, B., Sebastián-Serrano, A., Beccari, L., Calcagnotto, M. E., Cisneros, E., Kim, S., Dopazo, A., Alvarez-Dolado, M., Redondo, J. M., Bovolenta, P., et al. (2010). Cux1 and Cux2 regulate dendritic branching, spine morphology, and synapses of the upper layer neurons of the cortex. *Neuron* 66, 523-535.
- Curatolo, P., Bombardieri, R., and Cerminara, C. (2008). Medical treatment in children with central nervous system malformations. *Handb. Clin. Neurol.* 87:555-68.
- Datta, A.N., Hahn, C.D., and Sahin, M. (2008). Clinical presentation and diagnosis of tuberous sclerosis complex in infancy. *J. Child. Neurol.* 23(3):268-73.

- D'Agostino, M.D., Bernasconi, A., Das, S., Bastos, A., Valerio, R.M., Palmini, A., Costa da Costa, J., Scheffer, I.E., Berkovic, S., Guerrini, R., Dravet, C., Ono, J., Gigli, G., Federico, A., Booth, F., D'Arcangelo, G., and Curran, T. (1998). Reeler: new tales on an old mutant mouse. *BioEssays* 20, 235-244.
- D'Arcangelo, G. (2009). From human tissue to animal models: Insights into the pathogenesis of cortical dysplasia. *Epilepsia*. 50 Suppl 9:28-33
- DeFelipe, J., and Farinas, I. (1992). The pyramidal neuron of the cerebral cortex: morphological and chemical characteristics of the synaptic inputs. *Prog. Neurobiol.* 39, 563-607.
- Dehay, C., and Kennedy, H. (2007). Cell-cycle control and cortical development. *Nat Rev Neurosci.* 8(6):438-50.
- De Keersmaecker, K., Graux, C., Odero, M.D., Mentens, N., Somers, R., Maertens, J., Wlodarska, I., Vandenberghe, P., Hagemeyer, A., Marynen, P., Cools, J. (2005). Fusion of EML1 to ABL1 in T-cell acute lymphoblastic leukemia with cryptic t(9;14)(q34;q32). *Blood* 105, 4849-4852.
- de Wit M.C., Lequin, M.H., de Coo, I.F., Brusse, E., Halley, D.J., van de Graaf, R., Schot, R., Verheijen, F.W., and Mancini, G.M. (2008). Cortical brain malformations: effect of clinical, neuroradiological, and modern genetic classification. *Arch. Neurol.* 65(3):358-66.
- Diaz, A.L., and Gleeson, J.G. (2009). The molecular and genetic mechanisms of neocortex development. *Clin. Perinatol.* 36(3):503-12.
- Dobyns, W.B., Truwit, C.L., Ross, M.E., Matsumoto, N., Pilz, D.T., Ledbetter, D.H., Gleeson, J.G., Walsh, C.A., and Barkovich, A.J. (1999). Differences in the gyral pattern distinguish chromosome 17-linked and X-linked lissencephaly. *Neurology* 53(2):270-7.
- do Carmo Avides, M., and Glover, D.M. (1999). Abnormal spindle protein, Asp, and the integrity of mitotic centrosomal microtubule organizing centers. *Science* 283(5408):1733-5.
- Doetsch, F., and Alvarez-Buylla, A. (1996). Network of tangential pathways for neuronal migration in adult mammalian brain. *Proc. Natl. Acad. Sci. U S A.* 93(25):14895-900.
- Dubreuil, V., Marzesco, A.M., Corbeil, D., Huttner, W.B., and Wilsch-Bräuninger, M. (2007). Midbody and primary cilium of neural progenitors release extracellular membrane particles enriched in the stem cell marker prominin-1. *J. Cell Biol.* 176, 483-495
- Eichenmüller, B., Everley, P., Palange, J., Lepley, D., and Suprenant, K.A. (2002). The human EMAP-like protein-70 (ELP70) is a microtubule destabilizer that localizes to the mitotic apparatus. *J. Biol. Chem.* 277, 1301-1309.
- Elias, L.A., Wang, D.D., and Kriegstein, A.R. (2007). Gap junction adhesion is necessary for radial migration in the neocortex. *Nature* 448(7156):901-7.

- Englund, C., Fink, A., Lau, C., Pham, D., Daza, R.A., Bulfone, A., Kowalczyk, T., and Hevner, R.F. (2005). Pax6, Tbr2, and Tbr1 are expressed sequentially by radial glia, intermediate progenitor cells, and postmitotic neurons in developing neocortex. *J. Neurosci.* 25, 247–251.
- Feng, Y., and Walsh, C.A. (2004). Mitotic spindle regulation by Nde1 controls cerebral cortical size. *Neuron* 44(2):279-93.
- Fertuzinhos, S., Krsnik, Z., Kawasawa, Y. I., Rasin, M. R., Kwan, K. Y., Chen, J. G., Judas, M., Hayashi, M., and Sestan, N. (2009). Selective depletion of molecularly defined cortical interneurons in human holoprosencephaly with severe striatal hypoplasia. *Cereb. Cortex* 19, 2196-2207.
- Fietz, S.A., Kelava, I., Vogt, J., Wilsch-Brauninger, M., Stenzel, D., Fish, J.L., Corbeil, D., Riehn, A., Distler, W., Nitsch, R., and Huttner, W.B. (2010). OSVZ progenitors of human and ferret neocortex are epithelial-like and expand by integrin signaling. *Nat. Neurosci.* 13, 690–699.
- Fietz, S.A., and Huttner, W.B. (2011). Cortical progenitor expansion, selfrenewal and neurogenesis—a polarized perspective. *Curr. Opin. Neurobiol.* 21, 23–35.
- Fish, J.L., Kosodo, Y., Enard, W., Pääbo, S., and Huttner, W.B. (2006). Aspm specifically maintains symmetric proliferative divisions of neuroepithelial cells. *Proc. Natl. Acad. Sci. U S A.* 103(27):10438-43.
- Fish, J.L., Dehay, C., Kennedy, H., and Huttner, W.B. (2008). Making bigger brains—the evolution of neural-progenitor-cell division. *J. Cell Sci.* 121, 2783–2793.
- Fitzgerald, M.P., Covio, M., and Lee, K.S. (2011). Disturbances in the positioning, proliferation and apoptosis of neural progenitors contribute to subcortical band heterotopia formation. *Neuroscience* 176:455-71.
- Flurkey, K., Curren, J.M., and Harrison, D.E. (2007). The Mouse in Aging Research. From “The Mouse in Biomedical Research 2nd Edition”. Fox *et al.*, editors. American College Laboratory Animal Medicine (Elsevier), Burlington, MA. 637–672.
- Francis, F., Koulakoff, A., Boucher, D., Chafey, P., Schaar, B., Vinet, M.C., Friocourt, G., McDonnell, N., Reiner, O., Kahn, A., McConnell, S.K., Berwald-Netter, Y., Denoulet, P., and Chelly, J. (1999). Doublecortin is a developmentally regulated, microtubule-associated protein expressed in migrating and differentiating neurons. *Neuron* 23(2):247-56.
- Gabel, L.A., and LoTurco, J.J. (2001). Electrophysiological and morphological characterization of neurons within neocortical ectopias. *J. Neurophysiol.* 85(2):495-505.
- Gadisseux, J.F, Evrard, P., Misson, J.P., and Caviness, V.S. (1989). Dynamic structure of the radial glial fiber system of the developing murine cerebral wall. An immunocytochemical analysis. *Brain Res Dev Brain Res.* 50(1):55-67.
- Gadisseux, J.F, Evrard, P., Mission, J.P., and Caviness, V.S. Jr. (1992). Dynamic changes in the density of radial glial fibers of the developing murine cerebral wall: a quantitative immunohistological analysis. *J Comp Neurol.* 322(2):246-54.

- Gage, F.H. (2002). Neurogenesis in the adult brain. *J Neurosci.* 22(3):612-3.
- Gal, J.S., Morozov, Y.M., Ayoub, A.E., Chatterjee, M., Rakic, P., and Haydar, T.F. (2006). Molecular and morphological heterogeneity of neural precursors in the mouse neocortical proliferative zones. *J. Neurosci.* 26, 1045–1056.
- García-Verdugo, J.M., Ferrón, S., Flames, N., Collado, L., Desfilis, E., and Font, E. (2002). The proliferative ventricular zone in adult vertebrates: a comparative study using reptiles, birds, and mammals. *Brain Res. Bull.* 57(6):765-75.
- Ge, W., He, F., Kim, K. J., Bianchi, B., Coskun, V., Nguyen, L., Wu, X., Zhao, J., Heng, J. I., Martinowich, K., Tao, J., Wu, H., Castro, D., Sobeih, M.M., Corfas, G., Gleeson, J.G., Greenberg, M.E., Guillemot, F., and Sun, Y.E. (2006). Coupling of cell migration with neurogenesis by proneural bHLH factors. *Proc. Natl. Acad. Sci. USA* 103, 1319-1324.
- Gelman, D.M, and Marín, O. (2010). Generation of interneuron diversity in the mouse cerebral cortex. *Eur J Neurosci.* 31(12):2136-41.
- Gleeson, J.G, Lin, P.T., Flanagan, L.A., and Walsh, C.A. (1999). Doublecortin is a microtubule-associated protein and is expressed widely by migrating neurons. *Neuron* 23(2):257-71.
- Glotzer, M. (2009). The 3Ms of central spindle assembly: microtubules, motors and MAPs. *Nat Rev Mol Cell Biol.* 10(1):9-20.
- Goldman, S.A., Zukhar, A., Barami, K., Mikawa, T., and Niedzwiecki, D. (1996). Ependymal/subependymal zone cells of postnatal and adult songbird brain generate both neurons and nonneuronal siblings in vitro and in vivo. *J. Neurobiol.* 30(4):505-20.
- Gongidi, V., Ring, C., Moody, M., Brekken, R., Sage, E. H., Rakic, P., and Anton, E. S. (2004). SPARC-like 1 regulates the terminal phase of radial gliaguided migration in the cerebral cortex. *Neuron* 41, 57-69.
- Götz, M., and Huttner, W.B. (2005). The cell biology of neurogenesis. *Nat Rev Mol Cell Biol.* 6(10):777-88.
- Guerrini, R., and Carrozzo, R. (2001). Epilepsy and genetic malformations of the cerebral cortex. *Am. J. Med. Genet.* 106(2):160-73.
- Guerrini R, Marini C. (2006). Genetic malformations of cortical development. *Exp. Brain Res.* 173(2):322-33.
- Guizetti, J., Schermelleh, L., Mäntler, J., Maar, S., Poser, I., Leonhardt, H., Müller-Reichert, T., and Gerlich, D.W. (2011). Cortical constriction during abscission involves helices of ESCRT-III-dependent filaments. *Science* 331, 1616-1620.
- Han, W., Kwan, K. Y., Shim, S., Lam, M. M., Shin, Y., Xu, X., Zhu, Y., Li, M., and Sestan, N. (2011). TBR1 directly represses Fezf2 to control the laminar origin and development of the corticospinal tract. *Proc. Natl. Acad. Sci. USA* 108, 3041-3046.

Hand, R., Bortone, D., Mattar, P., Nguyen, L., Heng, J.I., Guerrier, S., Boutt, E., Peters, E., Barnes, A.P., Parras, C., Schuurmans, C., Guillemot, F., and Polleux, F. (2005). Phosphorylation of Neurogenin2 specifies the migration properties and the dendritic morphology of pyramidal neurons in the neocortex. *Neuron* 48(1):45-62.

Hansen, D.V., Lui, J.H., Parker, P.R., and Kriegstein, A.R. (2010). Neurogenic radial glia in the outer subventricular zone of human neocortex. *Nature* 464, 554–561.

Haubensak, W., Attardo, A., Denk, W., and Huttner, W.B. (2004). Neurons arise in the basal neuroepithelium of the early mammalian telencephalon: a major site of neurogenesis. *Proc. Natl. Acad. Sci. USA* 101, 3196–3201.

Hevner, R.F., Shi, L., Justice, N., Hsueh, Y., Sheng, M., Smiga, S., Bulfone, A., Goffinet, A.M., Campagnoni, A.T., and Rubenstein, J.L. (2001). *Tbr1* Regulates Differentiation of the Preplate and Layer 6. *Neuron* 29 (2), 353–366.

Hevner, R.F., Hodge, R.D., Daza, R.A., and Englund, C. (2006). Transcription factors in glutamatergic neurogenesis: conserved programs in neocortex, cerebellum, and adult hippocampus. *Neurosci. Res.* 55(3):223-33.

Hevner, R.F., and Haydar, T.F. (2012). The (not necessarily) convoluted role of basal radial glia in cortical neurogenesis. *Cereb. Cortex.* 22(2):465-8.

Higginbotham, H.R., and Gleeson, J.G. (2007). The centrosome in neuronal development. *Trends Neurosci.* 30(6):276-83.

Hirotsune, S., Fleck, M.W., Gambello, M.J., Bix, G.J., Chen A, Clark, G.D., Ledbetter, D.H., McBain, C.J., and Wynshaw-Boris, A. (1998). Graded reduction of *Pafah1b1* (*Lis1*) activity results in neuronal migration defects and early embryonic lethality. *Nat. Genet.* 19(4):333-9.

Howard, B., Chen, Y., and Zecevic, N. (2006). Cortical progenitor cells in the developing human telencephalon. *Glia* 53:57--66.

Huang, Z. (2009). Molecular regulation of neuronal migration during neocortical development. *Mol Cell Neurosci.* 42(1):11-22.

Hueston, J.L., Herren, G.P., Cueva, J.G., Buechner, M., Lundquist, E.A., Goodman, M.B., and Suprenant, K.A. (2008). The *C. elegans* EMAP-like protein, ELP-1 is required for touch sensation and associates with microtubules and adhesion complexes. *BMC Dev. Biol.* 8, 110.

Hung, L.Y., Tang, C.J., and Tang, T.K. (2000). Protein 4.1 R-135 interacts with a novel centrosomal protein (CPAP) which is associated with the gamma-tubulin complex. *Mol. Cell. Biol.* 20(20):7813-25.

Huttner, W.B., and Kosodo, Y. (2005). Symmetric versus asymmetric cell division during neurogenesis in the developing vertebrate central nervous system. *Curr Opin Cell Biol.* 17(6):648-57.

- Ide, M., and Lewis, D.A. (2010). Altered cortical CDC42 signaling pathways in schizophrenia: implications for dendritic spine deficits. *Biol. Psychiatry*. 68(1):25-32.
- Jaglin, X.H., and Chelly, J. (2009). Tubulin-related cortical dysgeneses: microtubule dysfunction underlying neuronal migration defects. *Trends Genet*. 25, 555-566.
- Jansen, A., and Andermann, E. (2005). Genetics of the polymicrogyria syndromes. *J. Med. Genet*. 42(5):369-78.
- Jakovcevski, I., Mayer, N., and Zecevic, N. (2011). Multiple origins of human neocortical interneurons are supported by distinct expression of transcription factors. *Cereb. Cortex* 21(8):1771-82.
- Jones, E. G. (1986). Neurotransmitters in the cerebral cortex. *J. Neurosurg*. 65, 135-153.
- Jossin, Y., and Cooper, J.A. (2011). Reelin, Rap1 and N-cadherin orient the migration of multipolar neurons in the developing neocortex. *Nat. Neurosci*. 14(6):697-703.
- Kálmán, M. (1998). Astroglial architecture of the carp (*Cyprinus carpio*) brain as revealed by immunohistochemical staining against glial fibrillary acidic protein (GFAP). *Anat. Embryol. (Berl)*. 198(5):409-33.
- Kandel, E.R; Schwartz JH, Jessell TM. (2000). *Principles of Neural Science* (4th ed.). New York: McGraw-Hill.
- Kang, W., Wong, L.C., Shi, S.H., and Hébert, J.M. (2009). The transition from radial glial to intermediate progenitor cell is inhibited by FGF signaling during corticogenesis. *J Neurosci*. 29(46):14571-80.
- Kappeler, C., Dhenain, M., Phan Dinh Tuy, F., Saillour, Y., Marty, S., Fallet-Bianco, C., Souville, I., Souil, E., Pinard, J.M., Meyer, G., Encha-Razavi, F., Volk, A., Beldjord, C., Chelly, J., and Francis, F. (2007). Magnetic resonance imaging and histological studies of corpus callosal and hippocampal abnormalities linked to doublecortin deficiency. *J. Comp. Neurol*. 500(2):239-54.
- Kato, M., and Dobyns, W.B. (2003). Lissencephaly and the molecular basis of neuronal migration. *Hum. Mol. Genet*. 12 Spec No 1:R89-96.
- Kawauchi, T., and Hoshino, M. (2008). Molecular pathways regulating cytoskeletal organization and morphological changes in migrating neurons. *Dev. Neurosci*. 30(1-3):36-46.
- Kawauchi, T., Sekine, K., Shikanai, M., Chihama, K., Tomita, K., Kubo, K., Nakajima, K., Nabeshima, Y., and Hoshino, M. (2010). Rab GTPases-dependent endocytic pathways regulate neuronal migration and maturation through N-cadherin trafficking. *Neuron* 67(4):588-602.
- Keays, D.A. et al. (2007). Mutations in alpha-tubulin cause abnormal neuronal migration in mice and lissencephaly in humans. *Cell* 128, 45-57.

- Kelava, I., Reillo, I., Murayama, A.Y., Kalinka, A.T., Stenzel, D., Tomancak, P., Matsuzaki, F., Lebrand, C., Sasaki, E., Schwamborn, J.C., Okano, H., Huttner, W.B., and Borrell, V. (2012). Abundant occurrence of basal radial glia in the subventricular zone of embryonic neocortex of a lissencephalic primate, the common marmoset *Callithrix jacchus*. *Cereb. Cortex* 22(2):469-81.
- Kim, W.Y., Wang, X., Wu, Y., Doble, B.W., Patel, S., Woodgett, J.R., and Snider, W.D. (2009). GSK-3 is a master regulator of neural progenitor homeostasis. *Nat. Neurosci.* 12, 1390–1397.
- Kirschenbaum, B., Doetsch, F., Lois, C., and Alvarez-Buylla, A. (1999). Adult subventricular zone neuronal precursors continue to proliferate and migrate in the absence of the olfactory bulb. *J. Neurosci.* 19, 2171–2180.
- Konno, D., Shioi, G., Shitamukai, A., Mori, A., Kiyonari, H., Miyata, T., and Matsuzaki, F. (2008). Neuroepithelial progenitors undergo LGN-dependent planar divisions to maintain self-renewability during mammalian neurogenesis. *Nat. Cell Biol.* 10, 93–101.
- Kornack, D.R., and Rakic, P. (1995). Radial and horizontal deployment of clonally related cells in the primate neocortex: relationship to distinct mitotic lineages. *Neuron* 15, 311–321.
- Kosodo, Y., Röper, K., Haubensak, W., Marzesco, A.M., Corbeil, D., Huttner, W.B. (2004). Asymmetric distribution of the apical plasma membrane during neurogenic divisions of mammalian neuroepithelial cells. *EMBO J.* 23(11):2314-2324 (2004).
- Kowalczyk, T., Pontious, A., Englund, C., Daza, R.A., Bedogni, F., Hodge, R., Attardo, A., Bell, C., Huttner, W.B., and Hevner, R.F. (2009). Intermediate neuronal progenitors (basal progenitors) produce pyramidal-projection neurons for all layers of cerebral cortex. *Cereb. Cortex* 19, 2439–2450.
- Kriegstein, A.R., and Noctor, S.C. (2004). Patterns of neuronal migration in the embryonic cortex. *Trends Neurosci.* 27, 392-399.
- Kriegstein, A., Noctor, S., and Martinez-Cerdeno, V. (2006). Patterns of neural stem and progenitor cell division may underlie evolutionary cortical expansion. *Nat. Rev. Neurosci.* 7, 883–890.
- Kriegstein, A., and Alvarez-Buylla, A. (2009). The glial nature of embryonic and adult neural stem cells. *Annu. Rev. Neurosci.* 32:149-84.
- Kuzniecky, R., Andermann, F., and Guerrini, R. (1994). The epileptic spectrum in the congenital bilateral perisylvian syndrome. CBPS Multicenter Collaborative Study. *Neurology* 44(3 Pt 1):379-85.
- Kwan, K.Y., Lam, M.M., Krsnik, Z., Kawasawa, Y.I., Lefebvre, V., and Sestan, N. (2008). SOX5 postmitotically regulates migration, postmigratory differentiation, and projections of subplate and deep-layer neocortical neurons. *Proc. Natl. Acad. Sci. USA* 105, 16021-16026.
- Kwan, K.Y., Sestan, N., and Anton, E.S. (2012). Transcriptional co-regulation of neuronal migration and laminar identity in the neocortex. *Development* 139(9):1535-46.

- Lai, T., Jabaudon, D., Molyneaux, B.J., Azim, E., Arlotta, P., Menezes, J.R., and Macklis, J.D. (2008). SOX5 controls the sequential generation of distinct corticofugal neuron subtypes. *Neuron* 57, 232-247.
- Lambert de Rouvroit, C., and Goffinet, A.M. (1998). A new view of early cortical development. *Biochem Pharmacol.* 56(11):1403-9.
- Lapray, D., Popova, I.Y., Kindler, J., Jorquera, I., Becq, H., Manent, J.B., Luhmann, H.J., and Represa, A. (2010). Spontaneous epileptic manifestations in a DCX knockdown model of human double cortex. *Cereb. Cortex* 20(11):2694-701.
- Lavdas, A.A., Grigoriou, M., Pachnis, V., and Parnavelas, J.G. (1999). The medial ganglionic eminence gives rise to a population of early neurons in the developing cerebral cortex. *J. Neurosci.* 19(18):7881-8.
- Lee, K.S., Schottler, F., Collins, J.L., Lanzino, G., Couture, D., Rao, A., Hiramatsu, K., Goto, Y., Hong, S.C., Caner, H., Yamamoto, H., Chen, Z.F., Bertram, E., Berr, S., Omary, R., Scrable, H., Jackson, T., Goble, J., and Eisenman, L. (1997). A genetic animal model of human neocortical heterotopia associated with seizures. *J Neurosci.* 17(16):6236-42.
- Lee, K.S., Collins, J.L., Anzivino, M.J., Frankel, E.A., and Schottler, F. (1998). Heterotopic neurogenesis in a rat with cortical heterotopia. *J. Neurosci.* 18(22):9365-75.
- Lerner, J.T., Salamon, N., Hauptman, J.S., Velasco, T.R., Hemb, M., Wu, J.Y., Sankar, R., Donald Shields, W., Engel, J. Jr, Fried, I., Cepeda, C., Andre, V.M., Levine, M.S., Miyata, H., Yong, W.H., Letinic, K., Zoncu, R., and Rakic, P. (2002). Origin of GABAergic neurons in the human neocortex. *Nature* 417, 645-649.
- LeVay, S., Wiesel, T.N., and Hubel, D.H.. (1980). The development of ocular dominance columns in normal and visually deprived monkeys. *J. Comp. Neurol.* 191, 1-51.
- Leventer, R.J., Phelan, E.M., Coleman, L.T., Kean, M.J., Jackson, G.D., and Harvey, A.S. (1999). Clinical and imaging features of cortical malformations in childhood. *Neurology* 53(4):715-22.
- Leventer, R.J., Guerrini, R., and Dobyns, W.B. (2008). Malformations of cortical development and epilepsy. *Dialogues Clin. Neurosci.* 10(1):47-62.
- Levitt, P., and Rakic, P. (1980). Immunoperoxidase localization of glial fibrillary acidic protein in radial glial cells and astrocytes of the developing rhesus monkey brain. *J. Comp. Neurol.* 193(3):815-40.
- Lewis, D.A., and Levitt, P. (2002). Schizophrenia as a disorder of neurodevelopment. *Annu. Rev. Neurosci.* 25:409-32
- Li, H., Berlin, Y., Hart, R.P., and Grumet, M. (2003). Microtubules are critical for radial glial morphology: possible regulation by MAPs and MARKs. *Glia* 44(1):37-46.

- Lim, D.A., Fishell, G.J., and Alvarez-Buylla, A. (1997). Postnatal mouse subventricular zone neuronal precursors can migrate and differentiate within multiple levels of the developing neuraxis. *Proc. Natl. Acad. Sci. U S A.* 94(26):14832-6.
- Lizarraga, S.B., Margossian, S.P., Harris, M.H, Campagna, D.R., Han, A.P., Blevins, S., Mudbhary, R., Barker, J.E., Walsh, C.A., and Fleming, M.D. (2010). *Cdk5rap2* regulates centrosome function and chromosome segregation in neuronal progenitors. *Development* 137(11):1907-17.
- Lodato, S., Rouaux, C., Quast, K. B., Jantrachotechatchawan, C., Studer, M., Hensch, T. K., and Arlotta, P. (2011). Excitatory projection neuron subtypes control the distribution of local inhibitory interneurons in the cerebral cortex. *Neuron* 69, 763-779.
- Lois, C., and Alvarez-Buylla, A. (1994). Long-distance neuronal migration in the adult mammalian brain. *Science* 264, 1145–1148.
- Lokhorst, G.Jan. (2011). "Descartes and the Pineal Gland". *The Stanford Encyclopedia of Philosophy* Edward N. Zalta (ed.)
- López-Bendito, G., Sánchez-Alcañiz, J.A., Pla R, Borrell V, Picó E, Valdeolmillos M, and Marín, O. (2008). Chemokine signaling controls intracortical migration and final distribution of GABAergic interneurons. *J. Neurosci.* 28(7):1613-24.
- LoTurco, J.J., and Bai, J. (2006). The multipolar stage and disruptions in neuronal migration. *Trends Neurosci.* 29, 407-413.
- Lüders, H., and Schuele, S.U. (2006). Epilepsy surgery in patients with malformations of cortical development. *Curr. Opin. Neurol.* 19(2):169-74.
- Lui, J.H., Hansen, D.V., and Kriegstein, A.R. (2011). Development and evolution of the human neocortex. *Cell* 146(1):18-36.
- Luskin, M.B. (1993). Restricted proliferation and migration of postnatally generated neurons derived from the forebrain subventricular zone. *Neuron* 11(1):173-89.
- Ly, C.D., Roche, K.W., Lee, H.K., and Wenthold, R.J. (2002). Identification of rat EMAP, a delta-glutamate receptor binding protein. *Biochem. Biophys. Res. Commun.* 291(1):85-90.
- Madan, N., and Grant, P.E. (2009). New directions in clinical imaging of cortical dysplasias. *Epilepsia* 50 Suppl. 9:9-18.
- Malatesta, P., Hartfuss, E., and Götz, M. (2000). Isolation of radial glial cells by fluorescent-activated cell sorting reveals a neuronal lineage. *Development* 127, 5253–5263.
- Manzini, M.C., and Walsh, C.A. (2011). What disorders of cortical development tell us about the cortex: one plus one does not always make two. *Curr. Opin. Genet. Dev.* 2011; 21(3):333-9.

- Mao, Y., Ge, X., Frank, C.L., Madison, J.M., Koehler, A.N., Doud, M.K., Tassa, C., Berry, E.M., Soda, T., Singh, K.K., Biechele, T., Petryshen, T.L., Moon, R.T., Haggarty, S.J., and Tsai, L.H. (2009). Disrupted in schizophrenia 1 regulates neuronal progenitor proliferation via modulation of GSK3beta/beta-catenin signaling. *Cell* 136(6):1017-31
- McKenna, W.L., Betancourt, J., Larkin, K.A., Abrams, B., Guo, C., Rubenstein, J.L., and Chen, B. (2011). *Tbr1* and *Fezf2* regulate alternate corticofugal neuronal identities during neocortical development. *J. Neurosci.* 31,549-564.
- Meencke, H.J., and Janz, D. (1984). Neuropathological findings in primary generalized epilepsy: a study of eight cases. *Epilepsia* 25: 8-21.
- Meencke, H.J., and Veith, G. (1992). Migration disturbances in epilepsy. *Epilepsy Res. Suppl.* 9:31-9; discussion 39-40.
- Mei, D., Parrini, E., Pasqualetti, M., Tortorella, G., Franzoni, E., Giussani, U., Marini, C., Migliarini, S., and Guerrini, R. (2007). Multiplex ligation-dependent probe amplification detects DCX gene deletions in band heterotopia. *Neurology* 68(6):446-50.
- Meyer, G. (2007). Genetic control of neuronal migrations in human cortical development. *Adv Anat Embryol Cell Biol.* 189:1 p preceding 1, 1-111.
- Miller, K.D., Pinto, D.J., and Simons, D.J. (2001). Processing in layer 4 of the neocortical circuit: new insights from visual and somatosensory cortex. *Curr. Opin. Neurobiol.* 11(4):488-97.
- Ming, G.L., and Song, H. (2005). Adult neurogenesis in the mammalian central nervous system. *Annu. Rev. Neurosci.* 28:223-50.
- Mischel, P.S., Nguyen, L.P., and Vinters, H.V. (1995). Cerebral cortical dysplasia associated with pediatric epilepsy. Review of neuropathologic features and proposal for a grading system. *J. Neuropathol. Exp. Neurol.* 54: 137-53.
- Miyama, S., Takahashi, T., Nowakowski, R.S., and Caviness, V.S. Jr. (1997). A gradient in the duration of the G1 phase in the murine neocortical proliferative epithelium. *Cereb. Cortex.* 7(7):678-89.
- Miyata, T., Kawaguchi, A., Saito, K., Kawano, M., Muto, T., and Ogawa, M. (2004). Asymmetric production of surface-dividing and non-surface-dividing cortical progenitor cells. *Development* 131, 3133-3145.
- Miyoshi, G., Butt, S. J., Takebayashi, H., and Fishell, G. (2007). Physiologically distinct temporal cohorts of cortical interneurons arise from telencephalic Olig2-expressing precursors. *J. Neurosci.* 27, 7786-7798.
- Miyoshi, G., and Fishell, G. (2011). GABAergic interneuron lineages selectively sort into specific cortical layers during early postnatal development. *Cereb. Cortex* 21, 845-852.

- Mizutani, K., Yoon, K., Dang, L., Tokunaga, A., and Gaiano, N. (2007). Differential Notch signalling distinguishes neural stem cells from intermediate progenitors. *Nature* 449, 351–355.
- Mochida, G.H. (2008). Molecular genetics of lissencephaly and microcephaly. *Brain Nerve* 60(4):437-44.
- Molnár, Z., Métin, C., Stoykova, A., Tarabykin, V., Price, D.J., Francis, F., Meyer, G., Dehay, C., and Kennedy, H. (2006). Comparative aspects of cerebral cortical development. *Eur. J. Neurosci.* 23(4):921-34.
- Molyneaux, B.J., Arlotta, P., Menezes, J.R. and Macklis, J.D. (2007). Neuronal subtype specification in the cerebral cortex. *Nat. Rev. Neurosci.* 8, 427-437.
- Morest, D.K. (1970). A study of neurogenesis in the forebrain of opossum pouch young. *Z Anat Entwicklungsgesch.* 130(4):265-305.
- Morin, X., and Bellaïche, Y. (2011). Mitotic spindle orientation in asymmetric and symmetric cell divisions during animal development. *Dev. Cell* 21(1):102-19.
- Mo, Z., Moore, A.R., Filipovic, R., Ogawa, Y., Kazuhiro, I., Antic, S.D., and Zecevic, N. (2007). Human cortical neurons originate from radial glia and neuron-restricted progenitors. *J. Neurosci.* 27(15):4132-45.
- Mo, Z., and Zecevic, N. (2008). Is Pax6 critical for neurogenesis in the human fetal brain? *Cereb. Cortex* 18, 1455–1465.
- Munji, R.N., Choe, Y., Li, G., Siegenthaler, J.A., and Pleasure, S.J. (2011). Wnt signaling regulates neuronal differentiation of cortical intermediate progenitors. *J. Neurosci.* 31(5):1676-87.
- Nadarajah, B., Brunstrom, J.E., Grutzendler, J., Wong, R.O., and Pearlman, A.L. (2001). Two modes of radial migration in early development of the cerebral cortex. *Nat. Neurosci.* 4(2):143-50.
- Nadarajah, B., and Parnavelas, J.G. (2002). Modes of neuronal migration in the developing cerebral cortex. *Nat. Rev. Neurosci.* 3, 423-432.
- Nadeau, J. H. (2001). Modifier genes in mice and humans. *Nature Reviews Genetics* 2, 165–174.
- Noctor, S.C., Flint, A.C., Weissman, T.A., Dammerman, R.S., and Kriegstein, A.R. (2001). Neurons derived from radial glial cells establish radial units in neocortex. *Nature* 409, 714–720.
- Noctor, S.C., Martinez-Cerdeno, V., Ivic, L., and Kriegstein, A.R. (2004). Cortical neurons arise in symmetric and asymmetric division zones and migrate through specific phases. *Nat. Neurosci.* 7, 136-144.
- Noctor, S.C., Martinez-Cerdeno, V., and Kriegstein, A.R. (2008). Distinct behaviors of neural stem and progenitor cells underlie cortical neurogenesis. *J. Comp. Neurol.* 508, 28–44.

Nottebohm, F. (2004). The road we travelled: discovery, choreography, and significance of brain replaceable neurons. *Ann. N. Y. Acad. Sci.* 1016:628-58.

Nowakowski, R.S., and Rakic, P.. (1979). The mode of migration of neurons to the hippocampus: a Golgi and electron microscopic analysis in foetal rhesus monkey. *J. Neurocytol.* 8(6):697-718.

Okano, H., and Temple, S. (2009). Cell types to order: temporal specification of CNS stem cells. *Curr. Opin. Neurobiol.* 19(2):112-9.

O'Leary, D.D., and Koester, S.E. (1993). Development of projection neuron types, axon pathways, and patterned connections of the mammalian cortex. *Neuron* 10, 991-1006.

O'Leary, D.D., and Borngasser, D. (2006). Cortical ventricular zone progenitors and their progeny maintain spatial relationships and radial patterning during preplate development indicating an early protomap. *Cereb. Cortex* 16 Suppl 1:i46-56.

Pacary, E., Heng, J., Azzarelli, R., Riou, P., Castro, D., Lebel-Potter, M., Parras, C., Bell, D. M., Ridley, A. J., Parsons, M., and Guillemot, F. (2011). Proneural transcription factors regulate different steps of cortical neuron migration through Rnd mediated inhibition of RhoA signaling. *Neuron* 69, 1069-1084.

Pang, T., Atefy, R., and Sheen, V. (2008). Malformations of cortical development. *Neurologist* 14(3):181-91.

Paramasivam, M., Chang, Y.J., and LoTurco, J.J. (2007). ASPM and citron kinase co-localize to the midbody ring during cytokinesis. *Cell Cycle* 6, 1605-1612

Parnavelas, J.G., Barfield, J.A., Franke, E., and Luskin, M.B. (1991). Separate progenitor cells give rise to pyramidal and nonpyramidal neurons in the rat telencephalon. *Cereb. Cortex* 1(6):463-8.

Payne, B.R., Pearson, H.E., and Cornwell, P. (1984). Transneuronal degeneration of beta retinal ganglion cells in the cat. *Proc. R. Soc. Lond. B. Biol. Sci.* 222(1226):15-32.

Peyre, E., Jaouen, F., Saadaoui, M., Haren, L., Merdes, A., Durbec, P., and Morin, X. (2011). A lateral belt of cortical LGN and NuMA guides mitotic spindle movements and planar division in neuroepithelial cells. *J. Cell. Biol.* 193(1):141-54.

Pollmann, M., Parwaresch, R., Adam-Klages, S., Kruse, M.L., Buck, F., Heidebrecht, H.J. (2006). Human EML4, a novel member of the EMAP family, is essential for microtubule formation. *Exp. Cell Res.* 312, 3241-3251.

Postiglione, M.P., Jüschke, C., Xie, Y., Haas, G.A., Charalambous, C., and Knoblich, J.A. (2011). Mouse *inscuteable* induces apical-basal spindle orientation to facilitate intermediate progenitor generation in the developing neocortex. *Neuron.* 72(2):269-84.

Purves, D., Augustine, G.J., Fitzpatrick, D., LaMantia, A.S., McNamara, J.O., Williams, S.M., et al., editors. (2004). *Neurosciences.* (3rd ed.). Sunderland (MA): Sinauer Associates; 2004.

- Rakic, P. (1972). Mode of cell migration to the superficial layers of fetal monkey neocortex. *J. Comp. Neurol.* 145, 61–83.
- Rakic, P. (1974). Neurons in rhesus monkey visual cortex: systematic relation between time of origin and eventual disposition. *Science* 183, 425–427.
- Rakic, P. (2003a). Developmental and evolutionary adaptations of cortical radial glia. *Cereb. Cortex.* 13(6):541-9.
- Rakic, P. (2003b). Elusive radial glial cells: historical and evolutionary perspective. *Glia* 43(1):19-32.
- Rakic, P. (2007). The radial edifice of cortical architecture: from neuronal silhouettes to genetic engineering. *Brain Res. Rev.* 55(2):204-19.
- Ramon y Cajal, S. (1891). Pequeñas y comunicaciones técnicas. *Rev. Trimest. Microgr.* 5.
- Rajkowska, G., Selemon, L.D., Goldman-Rakic, P.S. (1998). Neuronal and glial somal size in the prefrontal cortex: a postmortem morphometric study of schizophrenia and Huntington disease. *Arch. Gen. Psychiatry.* 55(3):215-24.
- Rasin, M.R., Gazula, V.R., Breunig, J.J., Kwan, K.Y., Johnson, M.B., Liu-Chen, S., Li, H.S., Jan, L.Y., Jan, Y.N., Rakic, P., and Sestan, N. (2007). Numb and Numbl are required for maintenance of cadherin-based adhesion and polarity of neural progenitors. *Nat. Neurosci.* 10, 819–827.
- Reid, C.B., Tavazoie, S.F., and Walsh, C.A. (1997). Clonal dispersion and evidence for asymmetric cell division in ferret cortex. *Development* 124, 2441–2450.
- Reillo, I., de Juan Romero, C., García-Cabezas, M.Á., and Borrell, V. (2011). A role for intermediate radial glia in the tangential expansion of the mammalian cerebral cortex. *Cereb Cortex.* 21(7):1674-94.
- Rosen, G.D., Azoulay, N.G., Griffin, E.G., Newbury, A., Koganti, L., Fujisaki, N., Takahashi, E., Grant, P.E., Truong, D.T., Fitch, R.H., Lu, L., and Williams, R.W. (2012) Bilateral Subcortical Heterotopia with Partial Callosal Agenesis in a Mouse Mutant. *Cereb. Cortex.* [Epub ahead of print]
- Rowitch, D.H., and Kriegstein, A.R. (2010). Developmental genetics of vertebrate glial-cell specification. *Nature* 468(7321):214-22.
- Rubenstein, J.L. (2011). Annual Research Review: Development of the cerebral cortex: implications for neurodevelopmental disorders. *J. Child Psychol. Psychiatry* 52(4):339-55.
- Rudy, B., Fishell, G., Lee, S., and Hjerling-Leffler, J. (2011). Three groups of interneurons account for nearly 100% of neocortical GABAergic neurons. *Dev. Neurobiol.* 71(1):45-61.
- Sahara, S., and O’Leary, D.D. (2009). Fgf10 regulates transition period of cortical stem cell differentiation to radial glia controlling generation of neurons and basal progenitors. *Neuron* 63, 48–62.

- Sancho-Tello, M., Vallés, S., Montoliu, C., Renau-Piqueras, J., and Guerri, C. (1995). Developmental pattern of GFAP and vimentin gene expression in rat brain and in radial glial cultures. *Glia* 15(2):157-66.
- Sapir, T., Elbaum, M., and Reiner, O. (1997). Reduction of microtubule catastrophe events by LIS1, platelet-activating factor acetylhydrolase subunit. *EMBO J.* 16(23):6977-84.
- Sapir, T., Sapoznik, S., Levy, T., Finkelshtein, D., Shmueli, A., Timm, T., Mandelkow, E.M., and Reiner, O. (2008). Accurate balance of the polarity kinase MARK2/Par-1 is required for proper cortical neuronal migration. *J. Neurosci.* 28(22):5710-20.
- Sasaki, S., Tabata, H., Tachikawa, K., and Nakajima, K. (2008). The cortical subventricular zone-specific molecule Svet1 is part of the nuclear RNA coded by the putative netrin receptor gene *Unc5d* and is expressed in multipolar migrating cells. *Mol. Cell. Neurosci.* 38(4):474-83.
- Sessa, A., Mao, C.A., Colasante, G., Nini, A., Klein, W.H., and Broccoli, V. (2010). *Tbr2*-positive intermediate (basal) neuronal progenitors safeguard cerebral cortex expansion by controlling amplification of pallial glutamatergic neurons and attraction of subpallial GABAergic interneurons. *Genes Dev.* 24, 1816-1826.
- Shitamukai, A., Konno, D., and Matsuzaki, F. (2011). Oblique radial glial divisions in the developing mouse neocortex induce self-renewing progenitors outside the germinal zone that resemble primate outer subventricular zone progenitors. *J. Neurosci.* 31, 3683–3695.
- Smart, I.H., Dehay, C., Giroud, P., Berland, M., and Kennedy, H. (2002). Unique morphological features of the proliferative zones and postmitotic compartments of the neural epithelium giving rise to striate and extrastriate cortex in the monkey. *Cereb. Cortex* 12, 37–53.
- Stancik, E.K., Navarro-Quiroga, I., Sellke, R., and Haydar, T.F. (2010). Heterogeneity in ventricular zone neural precursors contributes to neuronal fate diversity in the postnatal neocortex. *J. Neurosci.* 30, 7028–7036.
- Stefansson, H., Rujescu, D., Cichon, S., Pietiläinen, O.P., Ingason, A., Steinberg, S., Fossdal, R., Sigurdsson, E., Sigmundsson, T., Buizer-Voskamp, J.E., Hansen, T., Jakobsen, K.D., et al. (2008). Large recurrent microdeletions associated with schizophrenia. *Nature* 455(7210):232-6.
- Stevenson, J.A., and Yoon, M.G. (1981). Mitosis of radial glial cells in the optic tectum of adult goldfish. *J Neurosci.* 1981 Aug;1(8):862-75.
- Sugitani, Y., Nakai, S., Minowa, O., Nishi, M., Jishage, K., Kawano, H., Mori, K., Ogawa, M., and Noda, T. (2002). *Brn-1* and *Brn-2* share crucial roles in the production and positioning of mouse neocortical neurons. *Genes Dev.* 16, 1760-1765.
- Tabata, H., and Nakajima, K. (2003). Multipolar migration: the third mode of radial neuronal migration in the developing cerebral cortex. *J. Neurosci.* 23, 9996-10001.

- Takahashi, K., MacDonald, D., Murayama, Y., and Kinane, D. (1999). Cell synthesis, proliferation and apoptosis in human dental periapical lesions analysed by in situ hybridisation and immunohistochemistry. *Oral Dis.* 5(4):313-20.
- Takano, T., Akahori, S., Takeuchi, Y., and Ohno, M. (2006). Neuronal apoptosis and gray matter heterotopia in microcephaly produced by cytosine arabinoside in mice. *Brain Res.* 1089(1):55-66.
- Tan, S.S., and Breen, S. (1993). Radial mosaicism and tangential cell dispersion both contribute to mouse neocortical development. *Nature* 362, 638–640.
- Tanaka, T.U. (2010). Kinetochore-microtubule interactions: steps towards bi-orientation. *EMBO. J.* 29, 4070–4082.
- Tarabykin, V., Stoykova, A., Usman, N., and Gruss, P. (2001). Cortical upper layer neurons derive from the subventricular zone as indicated by *Svet1* gene expression. *Development* 128, 1983-1993.
- Taylor, D.C., Falconer, M.A., Bruton, C.J., and Corsellis, J.A. (1971). Focal dysplasia of the cerebral cortex in epilepsy. *J. Neurol. Neurosurg. Psychiatry* 34(4):369-87.
- Tegha-Dunghu, J., Neumann, B., Reber, S., Krause, R., Erfle, H., Walter, T., Held, M., Rogers, P., Hupfeld, K., Ruppert, T., Ellenberg, J., and Gruss, O.J. (2008). EML3 is a nuclear microtubule-binding protein required for the correct alignment of chromosomes in metaphase. *J. Cell Sci.* 121, 1718-1726.
- Thomson, A.M. (2010). Neocortical layer 6, a review. *Front. Neuroanat.* 31;4:13.
- Torii, M., Hashimoto-Torii, K., Levitt, P., and Rakic, P. (2009). Integration of neuronal clones in the radial cortical columns by EphA and ephrin-A signalling. *Nature* 461, 524–528.
- Toyo-oka, K., Shionoya, A., Gambello, M.J., Cardoso, C., Leventer, R., Ward, H.L., Ayala, R., Tsai, L.H., Dobyns, W., Ledbetter, D., Hirotsune, S., and Wynshaw-Boris, A. (2003). 14-3-3epsilon is important for neuronal migration by binding to NUDEL: a molecular explanation for Miller-Dieker syndrome. *Nat. Genet.* 34(3):274-85.
- Trimborn, M., Bell, S.M., Felix, C., Rashid, Y., Jafri, H., Griffiths, P.D., Neumann, L.M., Krebs, A., Reis, A., Sperling, K., Neitzel, H., and Jackson, AP. (2004). Mutations in microcephalin cause aberrant regulation of chromosome condensation. *Am. J. Hum. Genet.* 75: 261–6.
- Trinczek, B., Brajenovic, M., Ebner, A., and Drewes, G. (2004). MARK4 is a novel microtubule-associated protein/microtubule affinity-regulating kinase that binds to the cellular microtubule network and to centrosomes. *J. Biol. Chem.* 279(7):5915-23.
- Trotter, S.A., Kapur, J., Anzivino, M.J., and Lee, K.S. (2006). GABAergic synaptic inhibition is reduced before seizure onset in a genetic model of cortical malformation. *J. Neurosci.* 26(42):10756-67.
- Tyler, W.A., and Haydar, T.F. (2010). A new contribution to brain convolution: progenitor cell logistics during cortex development. *Nat. Neurosci.* 13(6):656-7.

- Valiente, M., and Marín, O. (2010). Neuronal migration mechanisms in development and disease. *Curr. Op. Neurobiol.* 20:68-78.
- Valiente, M., Ciceri, G., Rico, B., and Marín, O. (2011). Focal adhesion kinase modulates radial glia-dependent neuronal migration through connexin-26. *J. Neurosci.* 31(32):11678-91.
- Van Laere, J. (1993). Vesalius and the nervous system. *Verh K Acad Geneeskdg Belg.* 55(6):533-76.
- Vinters, H.V., and Mathern, G.W. (2009). Assessment and surgical outcomes for mild type I and severe type II cortical dysplasia: a critical review and the UCLA experience. *Epilepsia* 50(6):1310-35.
- Voigt, T. (1989). Development of glial cells in the cerebral wall of ferrets: direct tracing of their transformation from radial glia into astrocytes. *J. Comp. Neurol.* 289, 74–88.
- Volpe, J. (2008). *Neurology of the Newborn.* 5th ed. Philadelphia: Elsevier, pp. 1-1042.
- Walsh, C., and Cepko, C.L. (1988). Clonally related cortical cells show several migration patterns. *Science* 241, 1342–1345.
- Wang, K., Zhang, H., Ma, D., Bucan, M., Glessner, J. T., Abrahams, B. S., Salyakina, D., Imielinski, M., Bradfield, J. P., Sleiman, P. M. et al. (2009). Common genetic variants on 5p14.1 associate with autism spectrum disorders. *Nature* 459, 528-533.
- Wang, Y., Li, G., Stanco, A., Long, J.E., Crawford, D., Potter, G.B., Pleasure, S.J., Behrens, T., and Rubenstein, J.L. (2011). CXCR4 and CXCR7 have distinct functions in regulating interneuron migration. *Neuron* 69, 61-76.
- Ware, M.L., Tavazoie, S.F., Reid, C.B., and Walsh, C.A. (1999). Coexistence of widespread clones and large radial clones in early embryonic ferret cortex. *Cereb. Cortex* 9, 636–645.
- Weimer, J.M., Yokota, Y., Stanco, A., Stumpo, D.J., Blackshear, P.J., and Anton, E.S. (2009). MARCKS modulates radial progenitor placement, proliferation and organization in the developing cerebral cortex. *Development* 136, 2965–2975.
- Weissman, T., Noctor, S.C., Clinton, B.K., Honig, L.S., and Kriegstein, A.R. (2003). Neurogenic radial glial cells in reptile, rodent and human: from mitosis to migration. *Cereb. Cortex.* 13(6):550-9.
- Welker, W.I. (1990). The significance of foliation and fissuration of cerebellar cortex. The cerebellar folium as a fundamental unit of sensorimotor integration. *Arch. Ital. Biol.* 128(2-4):87-109.
- Wang, K., Zhang, H., Ma, D., Bucan, M., Glessner, J. T., Abrahams, B. S., Salyakina, D., Imielinski, M., Bradfield, J. P., Sleiman, P. M. et al. (2009). Common genetic variants on 5p14.1 associate with autism spectrum disorders. *Nature* 459, 528-533.

Westerlund, N., Zdrojewska, J., Padzik, A., Komulainen, E., Björkblom, B., Rannikko, E., Tararuk, T., Garcia-Frigola, C., Sandholm, J., Nguyen, L., Kallunki, T., Courtney, M.J., and Coffey, E.T. (2011). Phosphorylation of SCG10/stathmin-2 determines multipolar stage exit and neuronal migration rate. *Nat. Neurosci.* 14, 305-313.

Wonders, C.P., and Anderson, S.A. (2006). The origin and specification of cortical interneurons. *Nat. Rev. Neurosci.* 7, 687-696.

Wong, M. (2009). Animal models of focal cortical dysplasia and tuberous sclerosis complex: recent progress toward clinical applications. *Epilepsia* 50 Suppl 9:34-44.

Wu, F., Xu, T., He, G., Ouyang, L., Han, B., Peng, C., Song, X., and Xiang, M. (2012). Discovery of novel focal adhesion kinase inhibitors using a hybrid protocol of virtual screening approach based on multicomplex-based pharmacophore and molecular docking. *Int. J. Mol. Sci.* 13(12):15668-78.

Yingling, J., Youn, Y.H., Darling, D., Toyo-Oka, K., Pramparo, T., Hirotsune, S., and Wynshaw-Boris, A. (2008). Neuroepithelial stem cell proliferation requires LIS1 for precise spindle orientation and symmetric division. *Cell* 132(3):474-86

Yokota, Y., Gashghaei, H.T., Han, C., Watson, H., Campbell, K. J., and Anton, E.S. (2007a). Radial glial dependent and independent dynamics of interneuronal migration in the developing cerebral cortex. *PLoS ONE* 2, e794.

Yokota, Y., Ring, C., Cheung, R., Pevny, L., and Anton, E.S. (2007b). Nap1- regulated neuronal cytoskeletal dynamics is essential for the final differentiation of neurons in cerebral cortex. *Neuron* 54, 429-445.

Yokota, Y., Kim, W.Y., Chen, Y., Wang, X., Stanco, A., Komuro, Y., Snider, W., and Anton, E.S. (2009). The adenomatous polyposis coli protein is an essential regulator of radial glial polarity and construction of the cerebral cortex. *Neuron* 61(1):42-56.

Yokota, Y., Eom, T.Y., Stanco, A., Kim, W.Y., Rao, S., Snider, W.D., and Anton, E.S. (2010). Cdc42 and Gsk3 modulate the dynamics of radial glial growth, inter-radial glial interactions and polarity in the developing cerebral cortex. *Development* 137(23):4101-10.

Yoon, K., Nery, S., Rutlin, M.L., Radtke, F., Fishell, G., and Gaiano, N. (2004). Fibroblast growth factor receptor signaling promotes radial glial identity and interacts with Notch1 signaling in telencephalic progenitors. *J. Neurosci.* 24(43):9497-506.

Yoon, K., and Gaiano, N.(2005). Notch signaling in the mammalian central nervous system: insights from mouse mutants. *Nat. Neurosci.* 8(6):709-15.

Young, M.P., and Yamane, S. (1992). Sparse population coding of faces in the inferotemporal cortex. *Science* 256(5061):1327-31.

Yu, X., and Zecevic, N. (2011). Dorsal radial glial cells have the potential to generate cortical interneurons in human but not in mouse brain. *J. Neurosci.* 31, 2413-2420.

Zecevic, N., Chen, Y., and Filipovic, R. (2005). Contributions of cortical subventricular zone to the development of the human cerebral cortex. *J. Comp. Neurol.* 491, 109–122.

Zeldenrust SR. (2012). Genotype--phenotype correlation in FAP. *Amyloid.* 19 Suppl 1:22-4.

Zraggen, E., Boitard, M., Roman, I., Kanemitsu, M., Potter, G., Salmon, P., Vutskits, L., Dayer, A.G., and Kiss, J.Z. (2012). Early postnatal migration and development of layer II pyramidal neurons in the rodent cingulate/retrosplenial cortex. *Cereb. Cortex.* 22(1):144-57.

Zipursky, A., Poon, A., and Doyle, J. (1992). Leukemia in Down syndrome: a review. *Pediatr. Hematol. Oncol.* 9(2):139-49.

Zhong, X., Pfeifer, G.P., and Xu, X. (2006). Microcephalin encodes a centrosomal protein. *Cell Cycle* 5, 457-458.

Zhong, W., and Chia, W. (2008). Neurogenesis and asymmetric cell division. *Curr. Opin. Neurobiol.* 18(1):4-11.

Zong, H., Li, Z., Liu, L., Hong, Y., Yun, X., Jiang, J., Chi, Y., Wang, H., Shen, X., Hu, Y., Niu, Z., and Gu, J. (2005). Cyclin-dependent kinase 11(p58) interacts with HBO1 and enhances its histone acetyltransferase activity. *FEBS. Lett.* 579(17):3579-88.

Zupanc, GK. (2006). Neurogenesis and neuronal regeneration in the adult fish brain. *J. Comp. Physiol. A Neuroethol. Sens. Neural. Behav. Physiol.* 192(6):649-70.

References to webpages

<http://www.drawingsofleonardo.org/>

<http://davincighost.buzznet.com/photos/default/?id=1404298>

Articles

Characterization of the HeCo Mutant Mouse: A New Model of Subcortical Band Heterotopia Associated with Seizures and Behavioral Deficits

Alexandre Croquelois^{1,2}, Fabienne Giuliani^{3,4}, Christine Savary², Michel Kielar², Clotilde Amiot⁵, Françoise Schenk^{3,4} and Egbert Welker²

¹Service de Neuropsychologie et de Neuroréhabilitation, Centre Hospitalier Universitaire Vaudois (CHUV), Avenue Pierre Decker 5, 1011 Lausanne, Switzerland, ²Department de Biologie Cellulaire et de Morphologie, Université de Lausanne, Rue du Bugnon 9, CH-1005 Lausanne, Switzerland, ³Institut de Physiologie, Centre de Neurosciences Psychiatriques, Site de Cery, CH-1008 Prilly, Switzerland, ⁴Institut de Psychologie, Université de Lausanne, Quartier UNIL-Dorigny, Bâtiment Anthropole, 1015 Lausanne, Switzerland and ⁵Service de Génétique, Histologie, Biologie du Développement et de la Reproduction (EA 3922), Hôpital Saint-Jacques, Place Saint-Jacques, 25030 Besancon cedex, France

In human, neuronal migration disorders are commonly associated with developmental delay, mental retardation, and epilepsy. We describe here a new mouse mutant that develops a heterotopic cortex (HeCo) lying in the dorsolateral hemispheric region, between the homotopic cortex (HoCo) and subcortical white matter. Cross-breeding demonstrated an autosomal recessive transmission. Birthdating studies and immunochemistry for layer-specific markers revealed that HeCo formation was due to a transit problem in the intermediate zone affecting both radially and tangentially migrating neurons. The scaffold of radial glial fibers, as well as the expression of doublecortin is not altered in the mutant. Neurons within the HeCo are generated at a late embryonic age (E18) and the superficial layers of the HoCo have a correspondingly lower cell density and layer thickness. Parvalbumin immunohistochemistry showed the presence of gamma-aminobutyric acidergic cells in the HeCo and the mutant mice have a lowered threshold for the induction of epileptic seizures. The mutant showed a developmental delay but, in contrast, memory function was relatively spared. Therefore, this unique mouse model resembles subcortical band heterotopia observed in human. This model represents a new and rare tool to better understand cortical development and to investigate future therapeutic strategies for refractory epilepsy.

Keywords: cerebral cortex growth and development, migration disorder, models: animal, neuronal neurobehavioral manifestations

Introduction

Development of the neocortex involves complex cellular and molecular mechanisms, among them neuronal genesis, migration, cell differentiation and the development of afferent and efferent connections (Rakic 1988; Honda et al. 2003). Neuronal migration is controlled by cytoskeletal molecules that regulate the initiation of migration which is subsequently controlled by a set of extracellular signaling molecules, such as the reelin pathway, and other stop signals (Gressens 2006). The morphology of pyramidal neurons undergoes several modifications that reflect the various steps in the migratory pathway (LoTurco and Bai 2006). Whereas the progenitors in the ventricular zone (VZ) are bipolar, migrating neurons are multipolar within the subventricular zone (SVZ). Upon arrival in the deep intermediate zone (IZ), they adopt a bipolar morphology, a characteristic of the migrating pyramidal neuron that is maintained until they arrive in their final position in the cerebral cortex. Interestingly, LoTurco and Bai (2006) hypothesized that failure

to make the transition from the multipolar to the bipolar stage may be a characteristic of most neuronal migration disorders. Although some neocortical migrating neurons migrate almost exclusively radially, others initially take a tangential trajectory at the level of the VZ or SVZ before adopting a classical radial migration pathway (Gressens 2000). Radial migration of neurons is supported by radial glial cells (Rakic 2003) and concerns the development of cortical projection neurons, mainly glutamatergic. However, the important pool of gamma-aminobutyric acidergic (GABAergic) interneurons have their origin principally in the subcortical telencephalon, in non-primate mammals mainly in the medial ganglionic eminence (Wonders and Anderson 2005). In primates however, other sources have been proposed, including the caudal and lateral ganglionic eminences, the septal region, and the cortex itself (Wonders and Anderson 2005). Recent evidence suggests that the diversity of the origin of GABAergic interneurons can be correlated with the remarkable diversity in their differentiated state (Wonders and Anderson 2005).

In human, neuronal migration disorders form a group of brain malformations which primarily affect development of the cerebral cortex (Dobyns and Truwit 1995). They are mainly caused by genetic alterations (Clark 2004, for review). Other etiologies are infections during pregnancy as well as ischemic and toxic insults. Such alterations are likely to affect neuronal migration to the cortex during the third and fourth months of gestation (Dobyns and Truwit 1995). However, currently evidence exists that other pathogenic mechanisms could cause subcortical accumulation of neurons such as modified cellular proliferation and programmed cell death (Clark 2004). Neuronal migration disorders range in severity from minor displacements of a few neurons (Meencke and Veith 1999; Eriksson et al. 2005) to massive rearrangements of cortical structure including the formation of subcortical heterotopia, also called double cortex. This severe form of diffuse subcortical heterotopia is commonly associated with a delay in somatic development, mental retardation, and epilepsy. The incidence of cortical malformations is more than 1% in the human population. Fourteen percent of epileptic patients have a cortical malformation based on a migration disorder. This incidence rises to 40% in patients with intractable epilepsy, the majority of them already presenting seizures during infancy (Farrell et al. 1992; Meencke and Veith 1992; Guerrini 2005).

We here characterize the phenotype of a new and unique genetic mouse model of cortical heterotopia (the HeCo

[heterotopic cortex] mouse). The mutation appeared spontaneously in our colony of the NOR strain derived from ICR-stock (Van der Loos et al. 1986) and was discovered during an unrelated experiment (Croquelois et al. 2005). We identify and characterize here the cortical malformation, its mode of inheritance and its developmental schedule, as well as the associated neurological and behavioral deficits exhibited by HeCo mutant mice.

Materials and Methods

Mice of the NOR and C57/Black6 (C57/Bl6) strains were used in this study. All the procedures described beneath were reviewed and approved by the Office Vétérinaire Cantonal (Lausanne, Switzerland), following Swiss Federal Laws.

Cross-Breeding Experiments

The first HeCo mouse was discovered using histological brain sections performed for unrelated experiments. Selective inbreeding including crossing of living relatives and backcrossing were used to increase the occurrence of the phenotype in offspring. Crossings of HeCo females with C57/Bl6 unaffected males and of HeCo males with C57/Bl6 unaffected females were then performed to define the transmission mode. Phenotype was determined in Nissl-stained coronal sections throughout the forebrain.

BrdU Injections and Immunohistochemistry

Mutant and control pregnant females were injected intraperitoneally with 5-bromo-2'-deoxyuridine (BrdU) (100 µg/g body weight, in phosphate buffered saline [PBS] 0.1 M, Sigma, St Louis, MO). Injections were performed at either embryonic (E)13 (brain removal at postnatal [P]13), E14 (brain removal at E15), E15 (brain removal at E16 and P13), E16 (brain removal at E17), or E18 (brain removal at P13) stages. The day of vaginal plug detection was designated as day 0 of gestation (E0). For juvenile animals (brain removal at P6 or P13), mice received a lethal dose of pentobarbital and were immediately fixed via cardiac perfusion with a solution of paraformaldehyde (1% in phosphate buffer 0.1 M, pH 7.4, for 5 min, then 4% in phosphate buffer 0.1 M, pH 7.4, for another 10 min). For embryos, brains were removed and immersed in paraformaldehyde (4% in phosphate buffer 0.1 M, pH 7.4) for 4 h. After cryoprotection in sucrose (30% overnight), brains were serially cut at 40-µm thickness using a sliding cryotome. Alternate sections were either stained with Cresyl Violet, processed for BrdU immunohistochemistry or immunohistochemistry for Cux-2, Tbr1, RC2, GLAST, and Dcx (doublecortin). For Parvalbumin (PARV)-immunohistochemistry we used 4 adult HeCo mice that were not exposed to BrdU.

BrdU Immunohistochemistry

We used the protocol described by Takahashi et al. (1992). In brief, sections were immersed in 2 N HCl for 60 min, neutralized in tris-buffered saline (TBS) for 3 × 10 min, and then incubated with primary antibody (anti-BrdU, mouse monoclonal, clone Bu20a, Dako, Switzerland) at a dilution of 1:100 in TBS 0.05 M overnight at 4 °C. Sections were rinsed in TBS and incubated in biotinylated secondary antibody (Biotin-SP-conjugated AffiniPure Goat Anti-Mouse, Jackson Immuno-Research Europe, Newmarket, UK) for 60 min. The sections were then processed with avidin-biotin-peroxidase complex (ABC) (Vector Laboratories, Peterborough, UK) for 60 min, rinsed in PBS, and visualized with diaminobenzidine (DAB) (Sigma). Sections were dehydrated in a series of graded ethanols, cleared in xylene, and coverslipped using Permount.

Immunohistochemistry

PARV Immunohistochemistry

Sections were thoroughly rinsed in PBS, and incubated in a blocking solution containing 10% normal goat serum and 4% bovine serum albumin in PBST (0.2% Triton X-100 in PBS) for 1 h at room temperature. After rinsing, sections were incubated overnight at 4 °C with rabbit anti-PARV (1:1000) antibody. Thereafter, sections were

sequentially incubated with biotinylated goat anti-rabbit antibodies (1:200) and with the ABC (1:200). Peroxidase was developed with 0.05% diaminobenzidine in 0.1 M PB and 0.005% hydrogen peroxide. Thereafter, immunoreacted sections were mounted onto gelatinized slides.

Tbr-1, Cux-2, RC2, GLAST, Dcx Immunohistochemistry

Sections were blocked with 2% normal horse serum in PBST with azide (phosphate buffer 0.1 M, NaCl 0.9%, Triton 0.3%, Azide 1 g/L; blocking solution) then incubated overnight at 4 °C with primary antibodies diluted in blocking solution. Secondary antibodies diluted in PBS 0.9% with Triton 0.3% were applied for one hour. Sections were then rinsed in PBS, mounted with chrom-alun 4% and coverslipped. Primary antibodies used: anti-Cux-2 (Millipore Corporation) at 1:150, anti-Tbr-1 (Millipore AG, Zug, Switzerland) at 1:1000, anti-RC2 (Developmental Studies Hybridoma Bank, University of Iowa) at 1:200, anti-GLAST (Millipore Corporation) at 1:5000 and anti-Dcx (Santa Cruz Biotechnology, Santa Cruz, CA) at 1:100, all raised in rabbits. Secondary antibodies used: Alexa 488 Donkey anti-Rabbit (Invitrogen) at 1:300 for Cux-2 and GLAST and Alexa 594 Donkey anti-Rabbit (Invitrogen) at 1:300 for Tbr-1, RC2, and Dcx.

Reconstruction and Morphometric Analysis

To morphometrically characterize the neurons of the HeCo and those of the overlying homotopic cortex (HoCo), contours of neuronal cell body were drawn with a computer controlled microscope and the NeuroLucida Software (Microbrightfield, Magdeburg, Germany) in 4 consecutive Nissl-stained sections (spaced 80 µm from each other on the rostro-caudal axis) in both control ($n = 4$) and mutant ($n = 4$) mice. The most rostral section was taken at the level of the most rostral part of the hippocampal formation. Radial thickness of the HeCo and the cortical layers of the HoCo together with cell density were also recorded.

BrdU-positive cells in the cerebral cortex of the right hemisphere were quantitatively analyzed using the brains of 3 P13 mice for each injection date (E13, E15, and E18). Positive cells were plotted using the same device. Per brain, 3 sections (spaced 80 µm from each other on the rostro-caudal axis) were analyzed. The most rostral section was taken at the level of the most rostral part of the hippocampal formation. In mutant mice, 3 contours were drawn around the HeCo, the HoCo and the adjacent, more lateral, cortex (AdCo). In control mice contours corresponding to the HoCo and the AdCo as determined by distance to midline were also drawn. To define the relative position of BrdU-positive neurons within these different regions of interest, the position of the subcortical white matter was plotted for the HeCo and the AdCo. For the HoCo, the thin band of white matter lying between the HeCo and the HoCo was identified as well. These reference lines were used to extrapolate the different curves using Lagrange interpolating polynomial. Migration distance was defined for each cell by the minimal distance to the corresponding curve. To allow comparison of the number of BrdU-positive cells between the 3 regions of interest and across embryonic ages of BrdU injection, we divided each region of interest in 10 equivalent tangentially oriented stripes, stripe 1 being the deeper and stripe 10 the more superficial one. The mean number of positive cells for each stripe was obtained from the 4 sections of the 4 animals in each group.

PARV+ cells in the cerebral cortex of the right hemisphere were plotted using the brains of the 4 mutant mice in the same way. Cells were plotted in 3 different regions of interest: the HeCo, the HoCo, and the AdCo. The number of PARV+ cells per surface unit, cell size and distance to the closest PARV+ cell were determined.

Tracing Experiments

To study neuronal connectivity of the HeCo, 3 mutant mice were anaesthetized with pentobarbital (sodium pentobarbital 60 mg/kg body weight i.p.) and placed in a stereotaxic frame. Part of the skull overlying the medio-dorsal cortex was removed and the HeCo was identified using extracellular recording and stereotaxic coordinates. Biotinylated dextran amine (BDA, Molecular Probes D-7135, MW 3000, Eugene, OR) was injected into the HeCo. The pressure injection was made at 1000-µm cortical depth and lasted for 2 min using the following parameters: 70 nL of a 5% solution in PBS (phosphate buffer 0.1 M, 0.9% saline, pH 7.4). After 10 days survival time, the animals were deeply anaesthetized and

perfused with paraformaldehyde (4% in 0.1 M phosphate buffer, pH 7.4). Serial coronal sections were cut at 40- μ m thickness. Sections were processed for DAB reaction (Veenman et al. 1992) and counterstained with toluidine blue.

Histological Examination of Organs and Blood Tests

Adult mice (4 HeCo and 4 controls) received a lethal dose of pentobarbital and were immediately fixed via cardiac perfusion with a solution of paraformaldehyde (4% in phosphate buffer 0.1 M, pH 7.4, for 15 min). Following cryoprotection in 30% sucrose overnight, heart, liver, pancreas, spleen and kidney were removed and cut at 40- μ m thickness with a cryotome. Sections were stained with hematoxylin-eosin. Blood samples from 4 control and 4 HeCo mice were obtained after a 16-h fasting period and processed for analysis of electrolytes (Na^+ , K^+ , Cl^-), creatinin, glucose and cholesterol.

Pilocarpine Induced Status Epilepticus

Sensitivity for the development of epileptic seizures was compared between HeCo and control mice using the pilocarpine induced status epilepticus (SE) model (Cavalheiro et al. 1996). Seventeen mice (12-16 weeks of age) received an intraperitoneal injection (i.p.) of methylscopolamine at a dose of 1 mg/kg body weight 30 min prior to injection of pilocarpine to reduce its peripheral cholinergic effects. Animals were then intraperitoneally injected with a single dose of either 100 or 200 mg/kg of pilocarpine in 0.2-mL sterile saline vehicle (0.9% NaCl). Animals were observed continuously and epileptic seizures and/or SE were recorded. Mice that developed a SE were deeply anesthetized with sodium pentobarbital (60 mg/kg body weight i.p.) and subsequently perfused with paraformaldehyde (4% in phosphate buffer 0.1 M, pH 7.4). Coronal sections were cut at 40- μ m thickness and processed for Nissl staining.

Behavioral Experiments

A total of 92 mice were used, 23 HeCo and 35 control mice from P0 to P22, 5 HeCo and 5 control mice at the age of 2 months and finally 9 HeCo and 15 control mice aged more than 7 months. Behavior was analyzed in different situations in order to assess the early development of locomotor capacities and complementary aspects of potential cognitive deficits linked to the HeCo phenotype.

Two spatial tasks were adapted, the Morris navigation task and the 8-arm radial maze. In addition, one set-up was designed to assess locomotor activity (Grandchamp and Schenk 2006).

The early development of locomotion was assessed in 2 conditions. Contact righting was observed on a rough substrate of 25 \times 20 cm, limited on 3 sides by a 5 cm high wall. Negative geotaxis capacity was recorded on a rough substrate (25 \times 20 cm). Its surface was tilted 25° from the horizontal plane. The infant mouse was able to clutch the rough surface and was also prevented from passive slipping due to the enhanced friction.

The Y-maze was composed of 3 (6 \times 6 \times 50 cm) transparent Plexiglas runways (named A, B, and C) linked together in a symmetrical Y shape (120° of angular deviation from each other). The olfactory automated radial maze was made of 8 transparent Plexiglas tunnels (6 \times 6 \times 50 cm) placed on a circular table covered by a plastic sheet. Three arms were baited with a drop of diluted condensed milk deposited on a glass plate at the end of the tunnels. The olfactory cues were bands of blotting paper (2 \times 50 cm) affixed to the arms' ceiling. The cues were made by impregnating the blotting paper bands with 0.8 mL of solutions made with 8 different alimentary aromas (lemon, apricot, aniseed, orange, blackcurrant, apple, amend bitter, brandy). Guillotine doors closed the exit of each tunnel.

The Morris navigation task was performed using a circular pool (120 cm in diameter, 30 cm height) made of gray polyvinyl chloride that was situated in a dimly illuminated room. The pool was filled to a depth of 15 cm with water (27 °C) opacified with milk (0.5 L). Four orthogonal starting positions around the perimeter of the pool, divided its surface into 4 quadrants. A platform consisting of a transparent Plexiglas cylinder (15 cm tall and 8 cm diameter) and covered with a white aluminum perforated plate (14 cm diameter) was placed in the

center of the quadrants, approximately 0.5 cm under water level. The pool was located in a room containing numerous extra-maze cues.

Morphologic and motor developments were evaluated as follows. Body weight and hair growth was assessed daily. Time of eye opening was recorded for each mouse. The locomotor development included a description of locomotion strategies, the assessment of contact righting and negative geotaxis. Spontaneous locomotion was recorded daily during 2 min on a horizontal plan according to 5 items described by Altman and Sudarshan (1975), pivoting (the front legs push like paddles and the rear wheel-axle unit is practically motionless), punting (the head is posed over a leg, the leg is withdrawn and placed in the direction of the movement while the other leg pushes to help it), treading (the head is elevated, the movements of the front legs are not more constrained; at the same time, the posterior legs are more isolated and offer a better support), crawling (the belly rests by ground but the posterior legs become mobile) and walking (the belly does not touch any more by ground and there is a synchronization of the legs).

For the negative geotaxis test, the animal was deposited with the head oriented downwards, in the center of the tilted plan. The test lasted a maximum of 3 min and the position of the animal was recorded every 5 s with a precision of 15°, from the starting position (-90°), through the horizontal plan (0°) to the expected position with the head upwards (+90°). The test started at day 5 and was prolonged until the animal tried to escape from the apparatus.

To test general activity, mice were individually placed in the distal end of an arm of the Y-maze for 8 min free exploration. The starting position for each mouse was randomly A, B, or C runway. Two kinds of measures were recorded. First, the number of arm entries as an indication of general activity. Second, alternation behavior was assessed from the individual sequences of arm visits. The frequency of 3-arm alternations (ABC-type) was compared with the frequency of incomplete or null alternation patterns (ABA-, BAA-, or AAA-type). For the 20- and 22-day-old mice, a black cue was placed opposite the arm B.

Cognitive tasks were tested using the automated radial maze and the Morris water maze. Mice were trained over 9 consecutive daily sessions in an automated 8-arm radial maze to discriminate the 3 arms that were constantly baited with food and the 5 arms that were never baited. A first exploration session consisted of leaving each mouse during 10 min in the maze with free access to all the tunnels and with all arms baited with food to familiarize them with the maze and its environment. After that, the animals received 6 daily learning trials. Two different configurations of 3 baited arms were used, always the same for a given mouse throughout training. The baited and non baited arms were thus at fixed positions in space and could also be discriminated by a specific odor cue. An arm was baited or non baited depending on the test subject so that no particular arm could accumulate scent marks due to the presence or absence of reinforcement. Each subject was assigned a different set of 3 constantly baited arms (arms 1, 4, 6 or 2, 5, 7) with the sequence of angles between the baited arms being 135°-90°-135°. Mice were individually introduced into the central platform and each trial started by the opening of all 8 doors simultaneously. After each visit to an arm, the door giving access to that arm was automatically closed, preventing re-entries into an already visited arm. Each trial was terminated after the animal retrieved the third food pellet and had returned to the central platform; all 8 doors were closed simultaneously and the animal was left 1 min in the central platform. During the entire testing period, all the mice had restricted access to food and their weight was checked every day to prevent more than a 10% body weight loss. Discrimination performance was assessed by the mean of total errors for each trial (with a maximum of 5 errors) calculated for each day.

For the Morris water maze task, the mice received 4 daily learning trials during 5 days. The position of the hidden platform remained fixed for the entire period of the acquisition and each subject was assigned a different sector. Each trial started with the mice being placed into the water, at one of 4 starting points: N, E, S, W. Four different starting positions were pseudorandomly used in each training block. A trial ended when the mouse reached the hidden platform and it was allowed to remain there for 20 s. If a successful escape was not performed within 60 s, the mouse was guided to the platform and the trial was recorded as an escape failure. Between successive trials the test mouse

was left for a 30-s intertrial interval in a dry container. Each mouse was dried in the container with cellulose paper before being replaced in its home cage. At the end of the 20 training trials, each mouse received a probe trial. For this trial, the platform was removed from the pool and the mouse was allowed to swim for 60 s. Then the platform was replaced in the training location and the mouse was allowed to climb on it. For the learning and transfer stages, a variable was measured: the average number of errors across all days to find the platform (% errors). For the probe trials, we compared the time spent in the training half of the pool (containing the platform during training) with the opposite one.

For all the experiments, a video camera suspended directly above each apparatus was connected to a computer and used to record the mice behavior. Experiments took place during the light phase between 7:00 a.m. and 7:00 p.m.

Statistics

The statistical analysis was performed using the SAS package (SAS Institute Inc., Cary, NC) and StatView (version 4.5). Data were checked for the normality of distribution. Comparisons of means in 2 groups were made using the unpaired Student's *t*-test. When comparison was based on the means of more than 2 groups we applied an analysis of variance (ANOVA). For the BrdU study, data related to the different stripes defined above were analyzed with the multivariate ANOVA using the generalized linear model procedure. For the behavioral experiments, ANOVAs were performed on the raw data with the genotype as the between-subjects and repeated measures such as day, session, area,

as within-subject factors. The ANOVAs were confirmed by unpaired *t*-test and other pair comparisons were performed by a post hoc test (Fisher post-hoc least significant difference, $P < 0.05$), when necessary. Parametric correlations (r) and Spearman rank correlation were computed. The limit of significance, if unspecified, was $P < 0.05$ for all tests.

Results

HeCo Morphology

The HeCo phenotype is defined by the presence of a subcortical band heterotopia, that is located bilaterally beneath the medial part of the neocortex and extends from the frontal lobe to the occipital lobe (see Fig. 1A,B). The HeCo is separated from the overlying neocortex (HoCo) by a thin layer of white matter, and from subcortical structures by a thicker layer of white matter, resembling normal subcortical white matter. Even though the medio-lateral as well as the rostro-caudal extension of the cortical heterotopia varies between animals (for comparison see Fig. 1A,B), its general appearance and location is constant. Interestingly, notable differences in severity were identified between animals of the same offspring and, to a lesser extent, between hemispheres of the same animal. Underlying subcortical structures, including the hippocampus, striatum and thalamus as well as the cerebellum and brainstem have

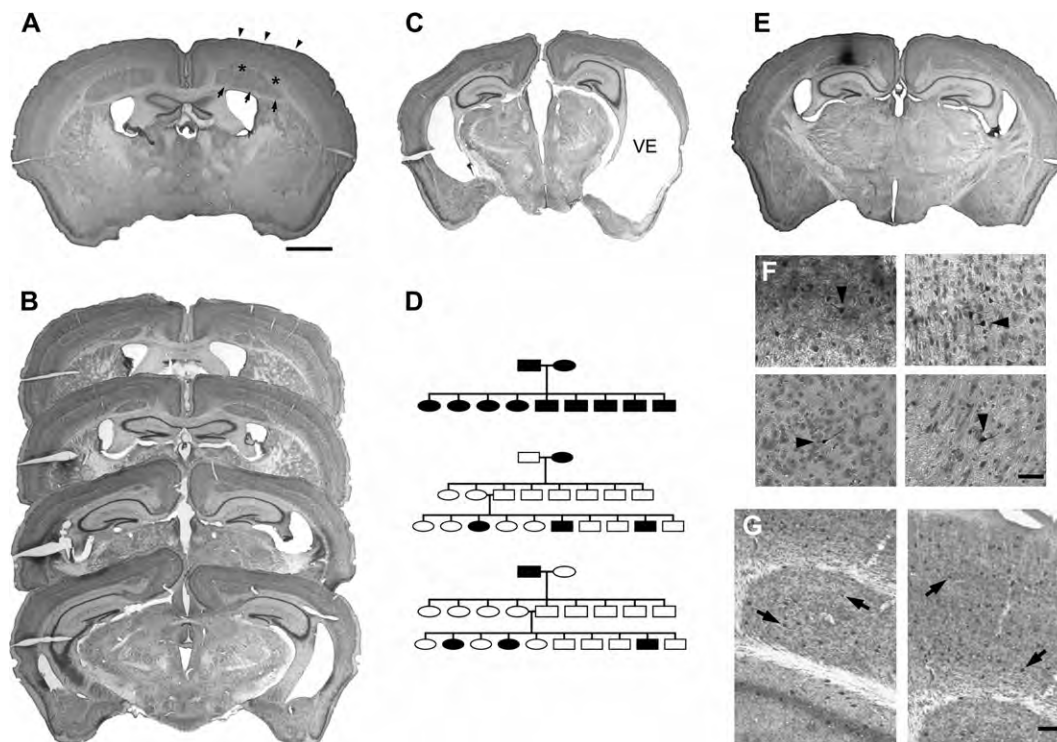


Figure 1. (A) Nissl-stained coronal section from a HeCo mouse. Arrows point to HeCo, asterisks to subcortical white matter and arrowheads to HoCo. (B) Photomicrograph of 4 consecutive Nissl-stained coronal sections of a HeCo mouse brain from rostral to caudal, showing the antero-posterior extension of the cortical heterotopia. (C) Photomicrograph of a coronal section of a HeCo mouse brain with severe lateral cortical atrophy and subsequent ventricular enlargement (VE). (D) Pedigree of different crossings between HeCo and control animals. Crossings between 2 affected mice (15 breeding pairs) revealed a 100% positive HeCo phenotype in offspring ($n = 110$). Results of the crossing of a HeCo female (black oval) with a C57/BL6 unaffected male (open square) and F2 generation from this offspring, with subsequently the reverse crossing with a HeCo male (black square) with a C57/BL6 unaffected female (open oval). Note that in either of these cases none of the F1 offspring had the HeCo phenotype, excluding a dominant or sex-linked trait. The frequency of affected mice in the F2 generation of the 2 crossings (60/247 and 10/47, respectively) indicates that the HeCo phenotype is due to an autosomal recessive disorder of a single locus. (E and F) Results of BDA-tracing in a HeCo mouse. (E) Photomicrograph at low power of a coronal section counterstained for Nissl-substance. Note the injection site located in the HeCo in the right hemisphere. (F) Photomicrographs at higher magnification showing cell labeling (black arrowheads) in the ipsilateral HeCo (upper left), the ipsilateral HoCo (upper right), the contralateral HeCo (lower left) and the ipsilateral thalamus (lower right). (G) Results of immunocytochemistry for PARV in an experimental mouse. Photomicrographs at high magnification showing the ipsilateral HeCo (left) and the ipsilateral HoCo (right). Black arrows indicate PARV+ cells. Scale bars: (A-D) 1000 μ m, (E) 50 μ m, (F) 100 μ m.

a normal microscopic appearance but a discrete ventricular enlargement is observed as compared with mice of the NOR strain that do not display the HeCo phenotype. In a small number of animals, a more severe malformation was present with a lateral cortical atrophy and huge ventricular enlargement (see Fig. 1C). During general animal inspection, HeCo and control mice are hard to distinguish, except for these more severe cases where mice are small and have a low body weight with sometimes a cranial malformation and brady- and hypokinesia. Other organs, including the heart, liver, pancreas, spleen and kidney have a normal microscopic appearance and no differences were found in the serum levels of electrolytes (Na^+ , K^+ , Cl^-), creatinin, glucose and cholesterol between HeCo and control age and sex matched mice (results not shown).

Cross-Breeding Experiments

In these experiments the phenotype was determined in histological sections through the forebrain taken after the adult mouse had given off-spring. Crossings between 2 affected mice (15 breeding pairs) revealed a 100% positive HeCo phenotype in offspring ($n = 110$). Crossings between affected HeCo mice and unaffected C57/Bl6 mice (10 breeding pairs) revealed no HeCo-phenotypes in the offspring ($n = 78$ for all crossings, $n = 56$ for crossings between C57/Bl6 male and HeCo female, $n = 22$ for crossings between HeCo male and C57/Bl6 female). These results exclude a dominant or sex-linked trait. F2 generations from these crossings between HeCo and C57/Bl6 mice demonstrated that 70 out of 294 mice (24%) were affected which exclude a multiloci origin and demonstrate the autosomal recessive nature of the HeCo phenotype (see Fig. 1D).

Tracing Experiments

After BDA injections in the HeCo of the right hemisphere, retrogradely labeled cells were found in the HoCo, in the contralateral HeCo and HoCo and in the ipsilateral thalamus (see Fig. 1E,F). Afferent connections to the HeCo are therefore comparable to connections of the HoCo.

PARV Immunostaining

PARV+ cells were found in the HoCo, in the hippocampus, in subcortical structures as well as in the HeCo, demonstrating the presence of GABA cells in the cortical heterotopia (see Fig. 1G). Density (60, 63, 65 [cells/mm²]) and distribution, defined by the mean distance to the closest positive cell (65, 64, 65 [μm]) of PARV+ cells were not significantly different in the HeCo, HoCo, and the adjacent cortex (AdCo), respectively. It has to be noted that this analysis does not take into account the absence of layering in the HeCo and the layer-dependent density differences in the HoCo and AdCo.

Morphometric Analysis

The thickness of the HoCo is slightly smaller in the HeCo mouse compared with cortical thickness in the control (Fig. 2A), but this difference did not reach significance. However, the HeCo together with the HoCo gives a total cortical thickness that is larger in HeCo than in control mice (Mann-Whitney test, $P < 0.0001$). To determine if all layers of the HoCo are equally affected, we compared individual layer thickness with its corresponding cortical layer in control mice. Figure 2B displays the results of this analysis showing that the only significantly affected layer is layer II/III (Mann-Whitney

test, $P = 0.0003$). We completed this morphometric investigation of the various cortical layers by determining the cell density in each layers (Fig. 2C). Analysis revealed that the cell density in layer II/III of the HeCo was significantly lower than in controls (Mann-Whitney test, $P = 0.0275$). Finally, we made a comparison of cell size between the heterotopia and layer II/III and observed that there was no significant difference in cell size between both regions (Fig. 2D).

Cell Markers

Immunolabeling by anti-Cux-2 (a marker of supragranular and granular layers) and anti-Tbr-1 (a marker of infragranular layers) antibodies are shown in Figure 3. The Tbr-1 antibody strongly labels cells in the deep cortical layers of both the normal cortex of control mice and the HoCo of mutant mice, with no cell labeling within the HeCo. Intense cell labeling by anti-Cux-2 antibodies was noted in superficial cortical layers in both the normal cortex of control mice and the HoCo of mutant mice, but this antibody also labeled virtually all the cells that form the HeCo.

Analysis of the Birth Dates of Cells in Heco, HoCo, and AdCo

At P13, BrdU-positive cells were present in infragranular, granular and supragranular layers of the HoCo and AdCo when the BrdU injection took place at E13, E15, and E18, respectively (see Fig. 4A). We found very few BrdU-positive cells in the HeCo after injection at E13 and E15. However, BrdU injection at E18 revealed a large number of positive cells in the HeCo (see Fig. 4A).

The quantitative analysis of the number of BrdU-positive cells in the HeCo demonstrated that this number was significantly different between embryonic ages of injection (multivariate ANOVA [MANOVA], $P < 0.0001$). Univariate comparisons revealed that the number of positive cells in the HeCo was higher for the E18 injection group than for E13 and E15 injection groups. No statistical differences were found between the 10 analyzed stripes in the HeCo (see Fig. 4B).

Analyzing data from the HoCo and AdCo revealed that HeCo formation disrupts the formation of the overlying cerebral cortex. MANOVA indicated that the number of BrdU-positive cells in the HoCo was significantly different between HeCo and control mice with an important drop in the number of labeled cells in the superficial stripes in HeCo mice ($P < 0.05$, see Fig. 4C). The same analysis in the AdCo also showed a less pronounced but significant drop in the number of labeled cells in the superficial stripes (see Fig. 4D).

Development of the Cerebral Cortex and Heterotopia

Histology of coronal sections at E16, 17, and 19 revealed an increase in the IZ thickness in HeCo mice compared with control animals, with a high cell density area beneath the subplate, and therefore within the IZ (see Fig. 5A). At P0, the size and extent of the cortical heterotopia was very similar to that observed in adult animals (see Fig. 5B). Results of immunocytochemistry for Tbr-1 at E17 and E19 confirmed this increase of the IZ and demonstrated a wider distribution of positive cells within this zone (see Fig. 6A) in HeCo mice. BrdU immunocytochemistry also revealed a wider distribution of positive cells within the IZ in HeCo animals (see Fig. 6B). Finally, immunocytochemistry for RC2 and GLAST (here used as marker for the radial glia) and Dcx showed no obvious differences

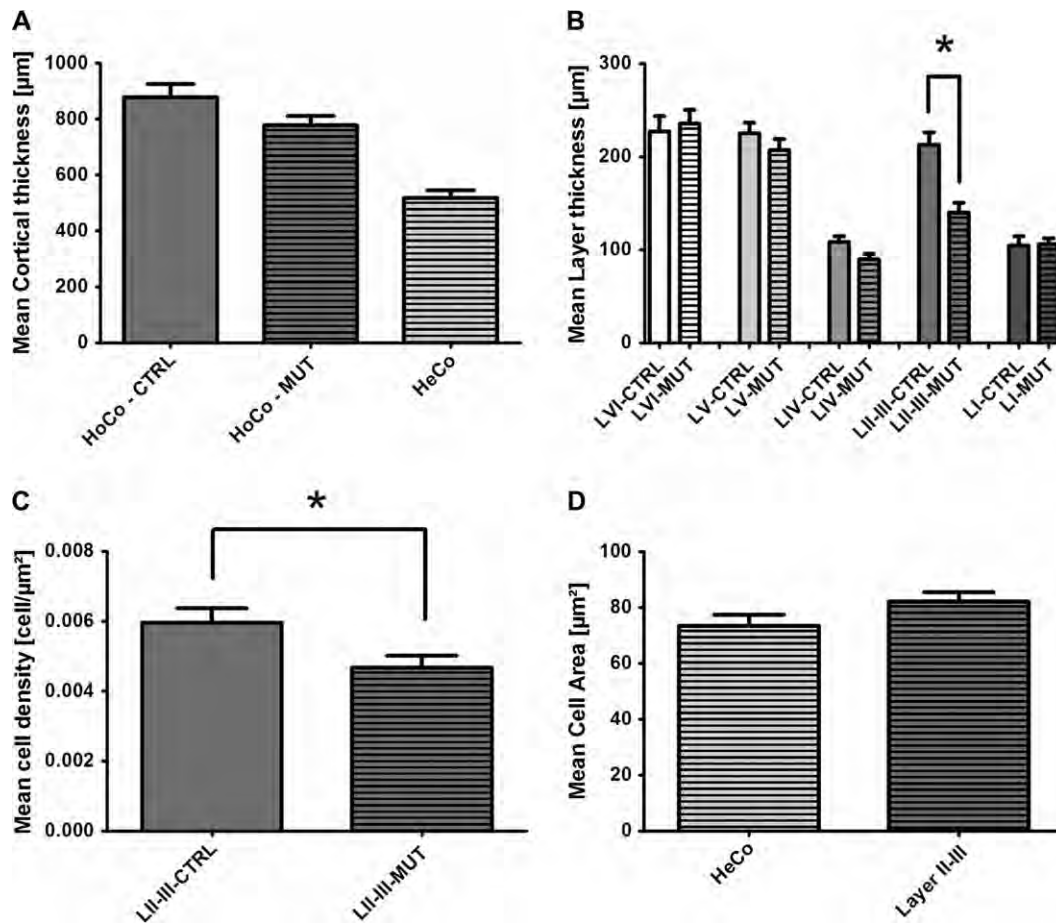


Figure 2. Results of the morphometric analysis. (A) Mean thickness (\pm SD) of the normal cortex in control animals (HoCo—CTRL, $n = 16$), and the HoCo (HoCo—MUT) and the radial extent of the heterotopia (HeCo—MUT) in mutant mice ($n = 16$). A slight, non significant, decrease in HoCo thickness was observed in mutant mice. (B) Comparison of the mean layer thickness within the HoCo of both the control (CTRL, $n = 16$) and mutant (MUT, $n = 16$) mice. Note that a significant decrease in layer thickness was only observed for layers II–III. (C) Comparison of the mean cell density (\pm SD) within layers II–III of the HoCo of both the control and HeCo mice. A significant decrease in cell density was observed in mutant animals. (D) Comparison of cell size (here represented by cell area) between the heterotopia (HeCo) and layers II–III of the HoCo of mutant animals; no significant differences were detected.

between control and HeCo mice at E15 and confirmed the increase in IZ thickness in HeCo mice at E17 (see Fig. 7).

Spontaneous Seizures

At 8–12 weeks of age, no epileptic seizures were observed during the 24-h video recording period ($n = 24$). In younger animals (4–5 weeks of age), spontaneous myoclonic jerks associated with interruption in exploratory behavior were observed in all of the 23 HeCo animals, but never in control age matched animals ($n = 35$). In 3 out of the 23 HeCo animals spontaneous seizures similar to pilocarpine induced seizures (see below) occurred after behavioral experiments. This never occurred in age matched controls ($n = 35$).

Pilocarpine Induced SE

Compared with wild-type animals, the HeCo mice showed a significant increase in tendency to develop epileptic seizures in the pilocarpine-induced model of epilepsy. In this model, a SE is obtained at a dose of 300–350 mg/kg body weight (Cavalheiro et al. 1996). When injected with a dose of 100 mg/kg body weight, none of the 4 mutants tested developed a SE. On the other hand, all the 9 HeCo mice developed a SE when injected with the dose of 200 mg/kg body weight, whereas none of the 4 control mice did with the same dose.

Behavioral Experiments

The results of the tests for somatic growth and sensorimotor activity are presented in Figures 8 and 9. The mice of the 2 genotypes do not differ in growth rate (see Fig. 8A). Despite their apparently normal growth rate, the HeCo showed a significant delay in hair growth (see Fig. 8B) and eye opening (see Fig. 8C). Separate one-way ANOVAs revealed significant effects of genotype on hair growth ($F_{1,34} = 25.850$, $P < 0.0001$) and eye opening ($F_{1,34} = 7.855$, $P = 0.0083$).

The slower development of locomotion in some of the HeCo mice is illustrated in Figures 8D and 9. In fact, all of the control mice ($n = 35$) displayed a normal locomotion pattern at the age of 10 days, whereas only 14 of 23 HeCo mice reached the same criterion. This was related to a one-day delay in the development of efficient righting response and to a more marked delay in geotaxis reflexes (see Fig. 8E,F). The behavior in sensorimotor tests was significantly correlated with the development of walking. Individual results for the righting test (see Fig. 9) were correlated with the onset of walking ($r = 0.669$, $P < 0.0001$) and the response in negative geotaxis tested at 9 days ($r = 0.278$, $P = 0.0343$). These analyses were confirmed by Spearman rank correlations.

General activity assessed by the Y-Maze was significantly different between control and HeCo mice, but this difference

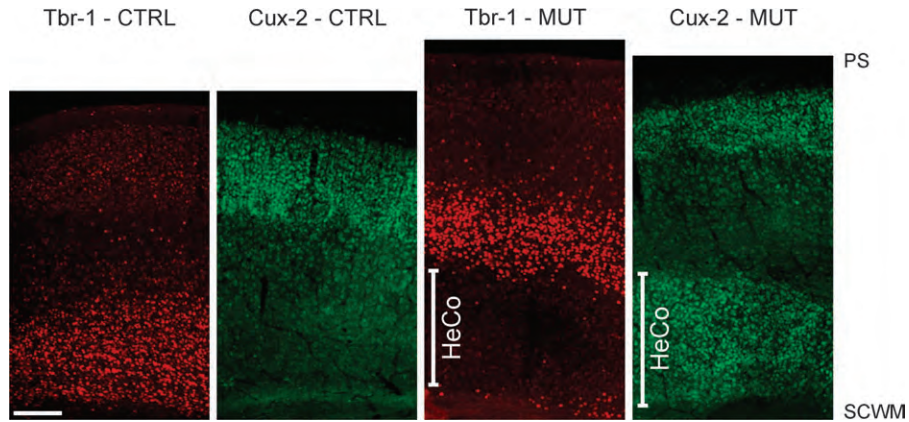


Figure 3. Results of immunohistochemistry for Tbr-1 and Cux-2 at P6. Note the strong cell labeling of deep cortical layers by anti-Tbr-1 antibody in both the normal cortex of the control (CTRL) mouse and the HoCo of the mutant (MUT) mouse, with almost no cell labeling of the HeCo. Intense cell labeling by anti-Cux-2 antibody is observed in superficial cortical layers in both the normal cortex of the control mouse and the HoCo of the HeCo mouse but also in the HeCo. Scale bar represents 200 μ m. SCWM: Subcortical white matter, PS: pial surface.

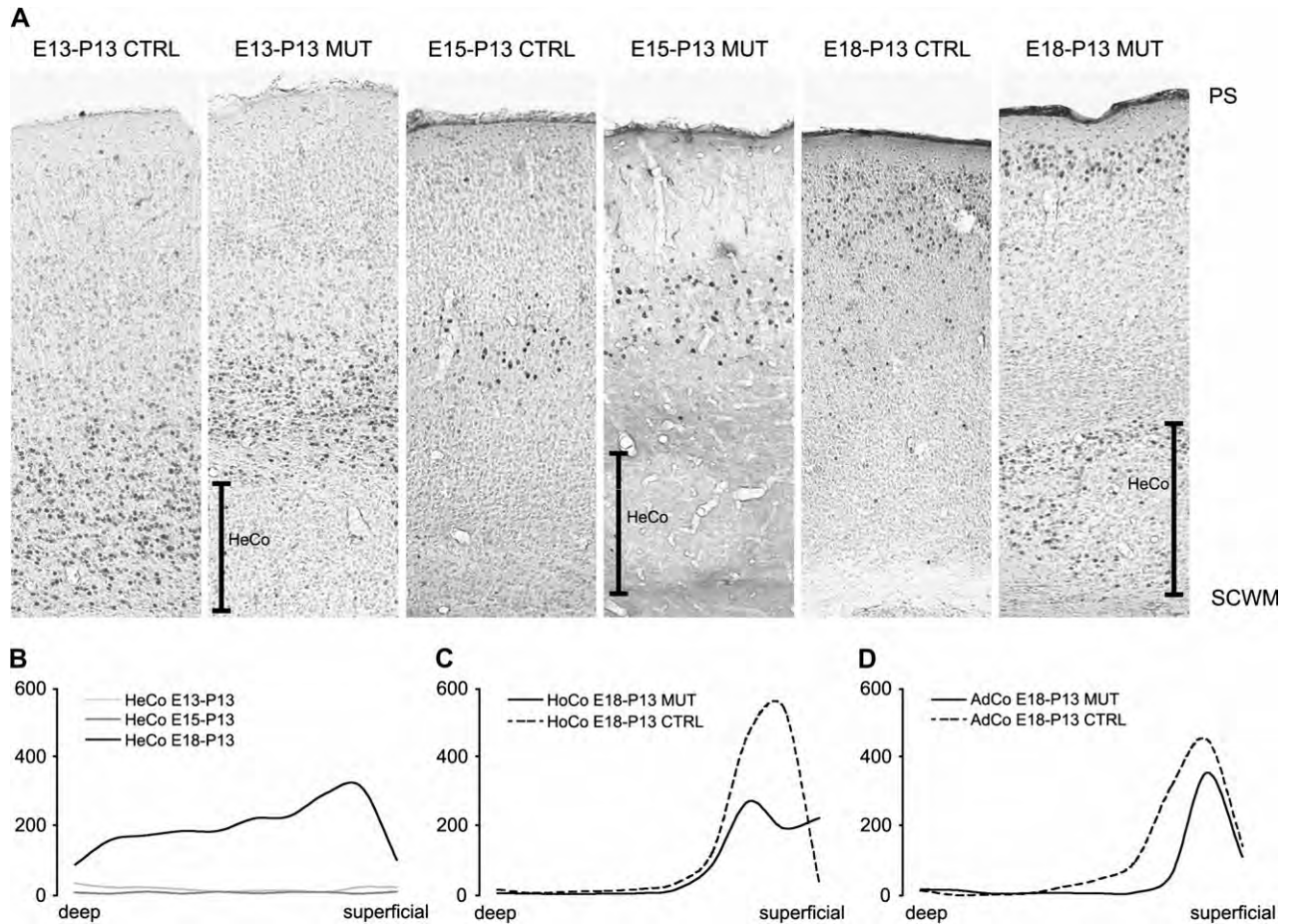


Figure 4. Results of immunohistochemistry for BrdU injected at embryonic day 13 (E13) 15 (E15) and 18 (E18) in both control (CTRL) and mutant (MUT) mice. (A) Photomicrographs at low magnification showing after injection at E13 labeling in lower layers in both control mice and HoCo of mutant mice with almost no labeling in HeCo; after injection at E15, labeling in intermediate layers in both control mice and HoCo of mutant mice with again almost no labeling in HeCo; and, after injection at E18, labeling in upper layers in both control mice and HoCo of mutant mice, together with intense labeling in the HeCo. (B–D) Line graphs of BrdU analysis. (B) Comparison of the number of labeled cells in HeCo between animals of the 3 injection time groups, embryonic age 13 (E13), 15 (E15), and 18 (E18) and determined at P13. Note the relatively low number of cells at E13 and E15 and the important number of labeled cells when the injection took place at E18. (C) Comparison of the number of labeled cells in the HoCo in mutant (MUT) and control (CTRL) mice when the injection was performed at E18 with determination at P13. Note the important drop in labeled cells in the superficial part in the HoCo of mutant mice. (D) Comparison of the number of labeled cells in AdCo in mutant mice and control animals when the injection was performed at E18 with determination at P13. Note the significant drop in labeled cells in the superficial stripes in mutant mice.

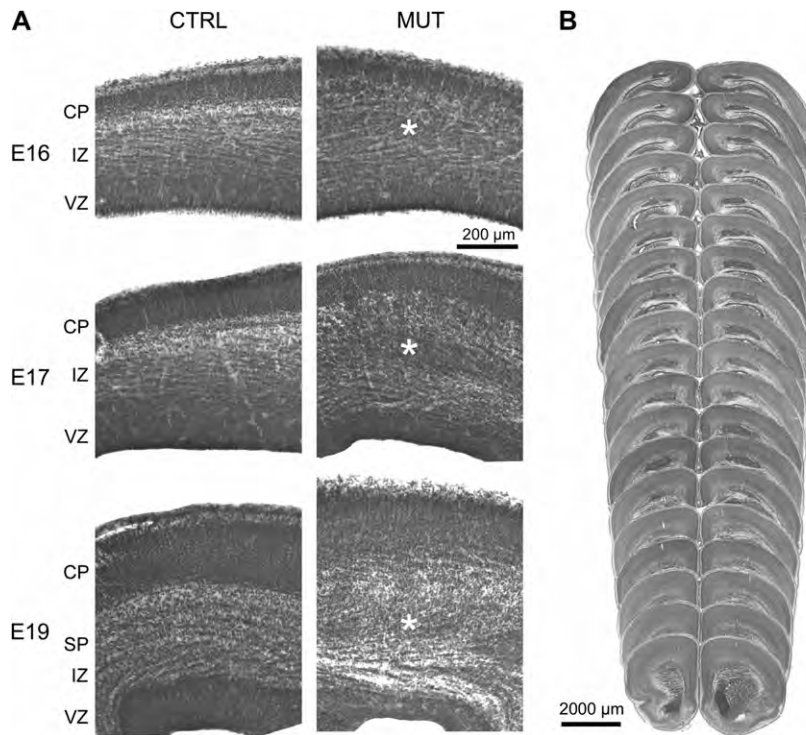


Figure 5. (A) Photomicrographs of coronal Nissl-stained sections through the developing cerebral cortex of control (CTRL) and mutant (MUT) mice at embryonic age 16 (E16), 17 (E17), and 19 (E19). Note the increase in IZ thickness in HeCo mice at all ages with normal thickness of the VZ and the cortical plate (CP) as compared with the control animals. Asterisks highlight a condensation of cell bodies within the IZ in HeCo mice, which is already present at E16. (B) Photomicrographs of consecutive coronal sections through the forebrain of a new born HeCo mouse. Note the presence of the cortical heterotopia throughout the antero-posterior axis, which is very similar to the observed heterotopia distribution in adults.

was only observed at the age of 2 months (see Fig. A in Supplemental Data). This was confirmed by a 2-way ANOVA (4 ages \times 2 genotypes) revealing a significant effect of age ($F_{3,28} = 68.017$, $P < 0.0001$) but not of genotype, and a significant interaction between age and genotype ($F_{3,84} = 8.674$, $P < 0.0001$). Unpaired T-tests revealed a significant effect of genotype at 2 months only ($P = 0.0191$). The frequency of complete alternations (e.g., ABC pattern vs. ABA, BAA, or AAA) was lower in the HeCo than in control mice at 20 days only (see Fig. A in supplemental data). This was confirmed by a 2-way ANOVA (4 ages \times 2 genotypes) revealing a significant effect of age ($F_{3,28} = 6.342$, $P = 0.0006$) but not of genotype, and a significant interaction between age and genotype ($F_{3,84} = 2.913$, $P = 0.0391$). Unpaired T-tests revealed a significant effect of genotype at 20 days only ($P = 0.0044$). Arm selection analyzed on the combined 20- and 22-day-old mice with the 2-way ANOVA (3 arms, 2 genotypes) revealed a significant arm effect ($F_{2,56} = 11.945$, $P < 0.0001$), no effect of genotype nor of interaction between these 2 factors (see Fig. A in Supplemental Data). It was interesting to note that the mice preferred on the one hand the arm near the cue, as well as the starting arm, in comparison with the supposed neutral third arm. In addition, an unpaired T-test carried out on the cued arm revealed that the preference for this arm was significantly higher in the HeCo than in the control mice at P20 ($P = 0.0210$).

Figure B of the supplemental data illustrates the performance during task acquisition in the automated radial maze based on the number of visits in non baited arms (reference errors) until the mice had visited the 3 baited arms. The 2-way repeated measure ANOVA (genotype \times 3-trials blocks) con-

ducted on the 2-month-old group revealed a significant effect of the repetition ($F_{2,25} = 20.375$, $P < 0.0001$) and genotype ($F_{1,25} = 4.285$, $P = 0.0489$) indicating better performance in controls but no interaction between genotype and repetition. The same analysis conducted in the groups aged above 7 months revealed also a significant effect of repetition ($F_{2,67} = 96.783$, $P < 0.0001$) and genotype ($F_{1,67} = 7.655$, $P = 0.0073$) without interaction but in this case results of control mice were worse.

During the Morris water maze task, the acquisition of spatial learning was assessed from the average number of errors (failures) in reaching the platform (see Fig. 10A,B). Separate 2-way repeated measure ANOVAs (genotype \times days) were conducted as an indication of task acquisition in each age groups. There was a significant effect of genotype in the 7-month-old group ($F_{4,22} = 5.967$, $P = 0.0231$), but not in the 2-month-old group. Indeed, the HeCo mice aged above 7 months were significantly impaired. A 2-way repeated measure ANOVA (age \times days) revealed a significant effect of age ($F_{1,12} = 6.155$, $P = 0.0289$) in the HeCo mice but not in the control group.

For the Probe trial, a 2-way measure ANOVA (genotype \times age) on the bias toward the training position (i.e., % time in the reinforced half of the pool) during the probe trial did not reveal a significant effect (see Fig. 10C). However, a 2-way measure ANOVA (genotype \times age) on the velocity during the probe trial (see Fig. 10D) revealed a significant effect of genotype ($F_{1,18} = 19.776$, $P = 0.0003$) and of age ($F_{1,18} = 34.996$, $P < 0.0001$).

In summary, when compared with controls, HeCo mice do not differ in overall growth rate, but show a significant delay in

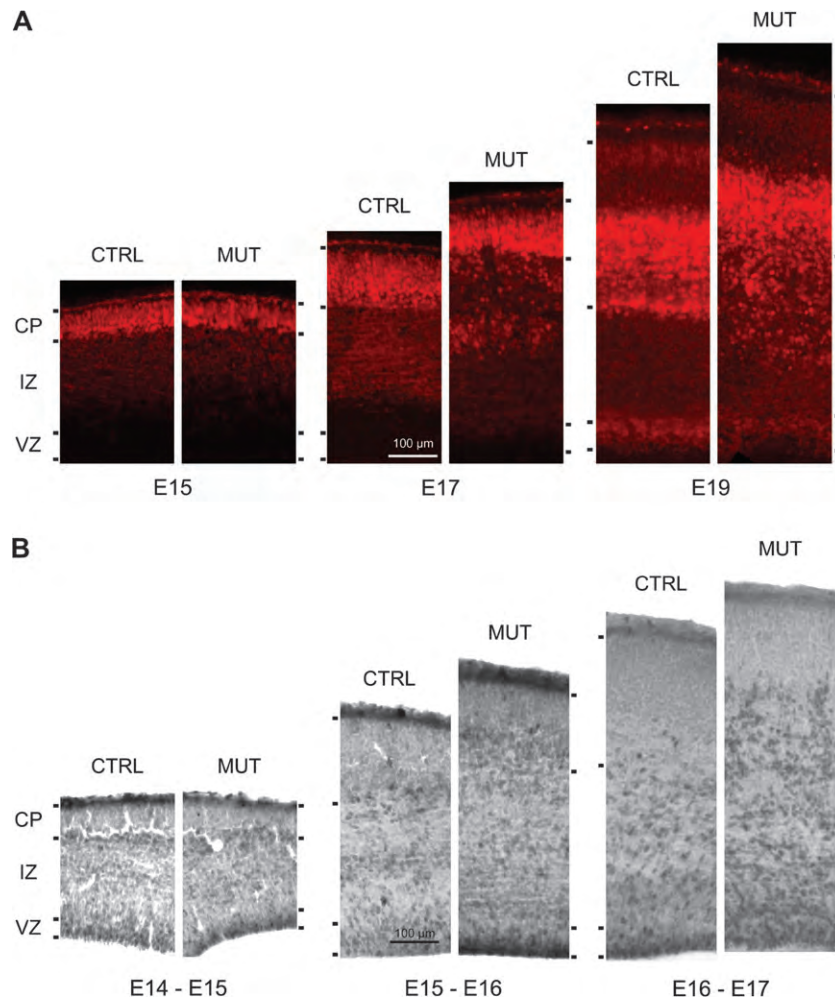


Figure 6. (A) Photomicrographs of coronal sections processed for Tbr-1 immunochrometry through the developing cerebral cortex of control (CTRL) and mutant (MUT) mice at embryonic age 15 (E15), 17 (E17), and 19 (E19). Note the thickness increase of the developing cortex in HeCo animals from E17, the cortical plate being more superficial. This was mainly due to an increase in thickness of the IZ. Note also the more diffuse distribution of Tbr-1 positive cells in HeCo animals at E17 and E19, some of them straggling within the IZ. (B) Photomicrographs of coronal sections processed for BrdU immunochrometry through the developing cerebral cortex of control (CTRL) and mutant (MUT) mice at embryonic age 15 (E15, BrdU injection at E14), 16 (E16, BrdU injection at E15), and 17 (E17, BrdU injection at E16). These images also show the increased thickness of the IZ and the corresponding larger extent of BrdU-positive cells within the IZ in HeCo animals at E16 and E17.

hair growth and eye opening, a slower development of locomotion and a decrease in general activity as assessed by the Y-Maze task. They have a significantly lower performance during task acquisition in the automated radial maze and make significantly more errors in reaching the platform during the Morris water maze task at the age of 7 months.

Discussion

Human neuronal migration disorders are not uncommon pathologies, especially among epileptic patients (Meencke and Veith 1992; Guerrini 2005). Despite the discovery of the doublecortin gene, associated with the majority of cases of subcortical band heterotopia in humans (des Portes et al. 1998) and our current understanding of the mechanisms leading to cortical heterotopias (Clark 2004; Gressens 2006), a complete appreciation of the molecular and cellular events that underlie their pathogenesis is still needed. Different molecular pathways have been determined as important for neuronal migration, some involving the migrating neuron, others being necessary for correct interactions with glia and/or other neurons. Several

molecules of the cytoskeleton, or their associated proteins, have been shown to be involved in the migration of cortical neurons (Gressens 2006). In humans, filamin-A, an actin-binding protein, is mutated in periventricular nodular heterotopia, Dcx, a microtubule-associated protein, is mutated in diffuse subcortical band heterotopia (double cortex) and lissencephaly, and Lis1, a microtubule-associated protein and dynein regulator, is mutated in isolated type 1 lissencephaly and Miller-Dieker syndrome (Gressens 2006). On the other hand, molecules of the reelin pathway, a glycoprotein mutated in lissencephaly associated with cerebellar hypoplasia in humans and in the reeler mouse mutant, are involved in cortical lamination (Gressens 2006). The molecules mentioned above are currently thought to be responsible for only a small percentage of the genetic disorders leading to the altered migration of cortical neurons in humans (Browne and Holmes 2001). To further develop the understanding of these neuronal migration disorders a larger number of animal models are therefore needed. Dcx null mutations in mice neither disrupt isocortical neuronal migration nor cause subcortical band heterotopia formation. In utero RNA interference of Dcx in

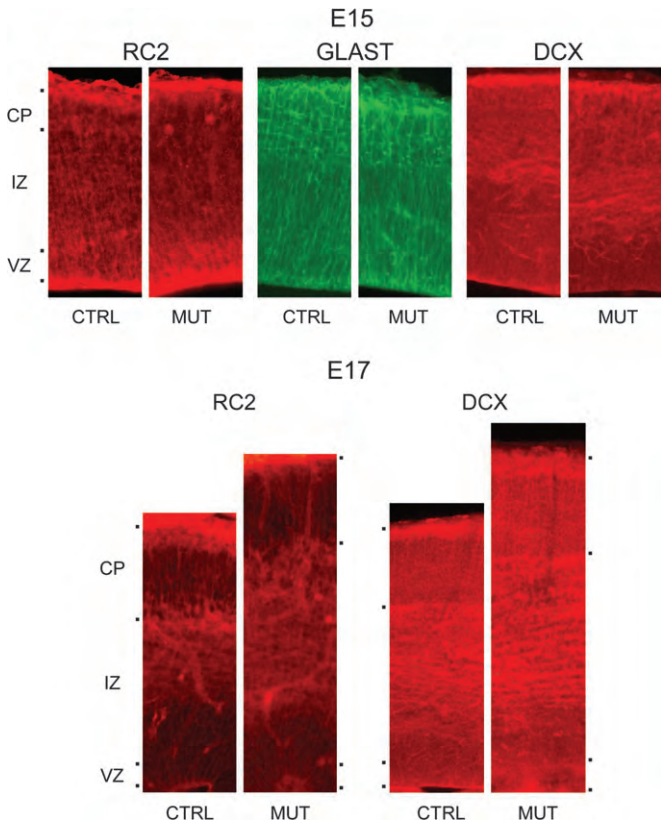


Figure 7. Photomicrographs of coronal sections processed for RC2, GLAST, and Dcx immunochemistry through the developing cerebral cortex of control (CTRL) and mutant (MUT) mice at embryonic age 15 (E15) and 17 (E17). Note again the increase in IZ thickness at E17 and the relatively similar pattern of labeling in both HeCo and control mice.

rats (but not in mice), in contrast, creates an animal model of subcortical band heterotopia (Corbo et al. 2002; Bai et al. 2003; Ramos et al. 2006). Other animal models of cortical malforma-

tions are the reeler mouse, the Lis1 knockout mouse and the spontaneous tish (telencephalic internal structural heterotopia) mutant rat (for review see Ross 2002). The tish rat is a spontaneous mutant that appeared in a colony of Sprague-Dawley rats (Lee et al. 1997). The transmission mode is autosomal recessive. Some of the affected animals present both electrophysiological and clinical seizures. In this mutant it was shown that the heterotopic neurons have connections with both the overlying cortex and deep structures such as the thalamic nuclei (Schottler et al. 1998), as in our model. It was proposed that, in the tish model, the abnormal band of gray matter is generated by an “extra” germinal zone (Lee et al. 1998) during preplate formation (E15). Therefore, the pathogenesis of the tish mutant occurs early during cortical development. Furthermore, the number of PARV+ neurons is decreased in tish rat normotopic and HeCo as compared with control animals and the PARV+ neurons within the HeCo are distributed in patches rather than in distinct layers as in control cortex (Trotter et al. 2006).

In our model however, the cells forming the heterotopia in the adult seem to be born mainly late in development. At P13, a moment where cortical layering is well established, the heterotopia is populated by neurons born at E18, an age that is well beyond the formation of the cortical plate and when the formation of the infragranular layers is already well underway. Furthermore, the results of the morphometric analysis concerning layer thickness, and cell density and size show that the superficial layers of the HoCo, normally populated by neurons born at E17-E18, displayed a decreased thickness and cell density compared with control animals. We also demonstrate that some of the neurons which have their final destination in the infragranular layers and which are born between E13 and E15 display an abnormal migration pattern because a condensed cell layer is already observed in the IZ at E16. However, at P13 these neurons have reached their correct position in the HoCo. The presence of PARV+ neurons within the HeCo together with the abnormal development of supragranular layers within the HoCo and AdCo further suggest that both projection and

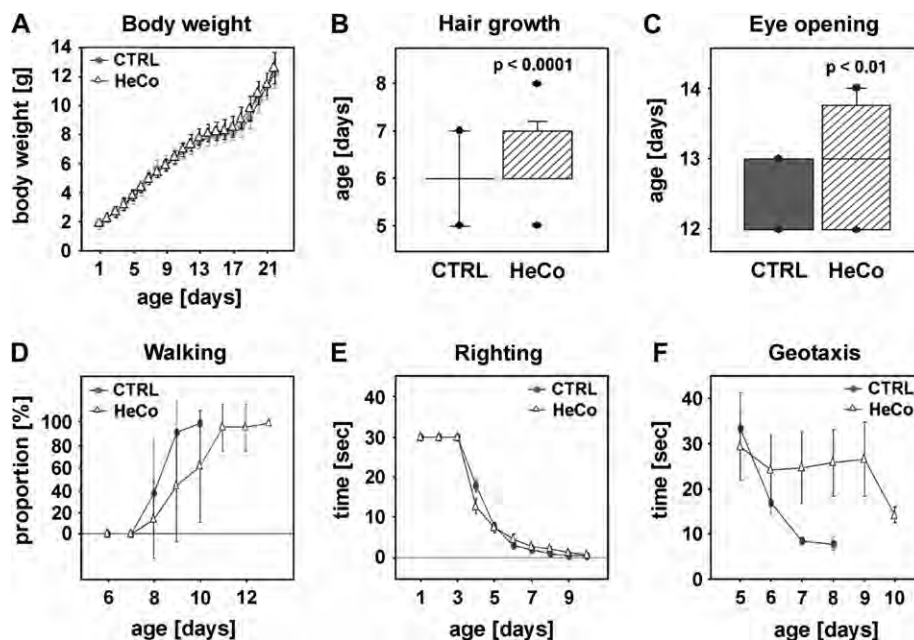


Figure 8. Somatic growth. For details, see text.

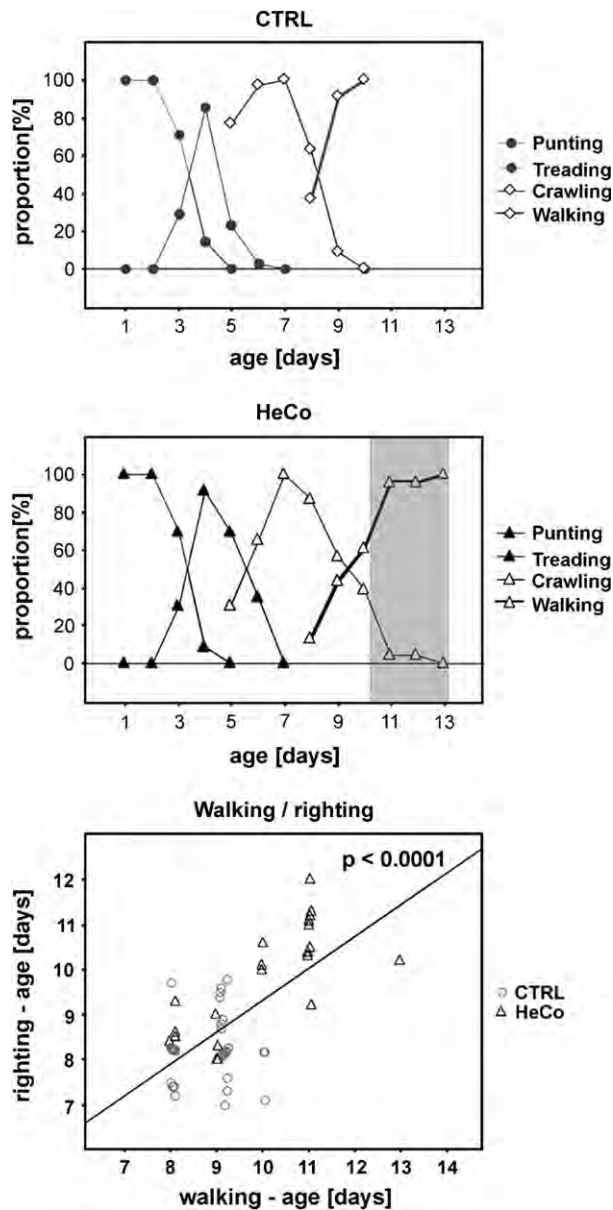


Figure 9. Development of movement. Note that the development of the walk is delayed in HeCo mice and the correlation between the righting test and the apparition of walking. The gray stripe in the middle graph highlights the delay in the development of walking between control and HeCo mice. For details, see text.

interneuron migratory pathways in the forebrain are affected by the mutation.

The detailed comparison between the tish rat and HeCo indicates that cortical band heterotopia in these 2 animal models could be due to different molecular mechanisms. Therefore, the shared morphological and physiological features of the HeCo mouse and the tish rat do not imply necessarily that the mutated gene is identical in both models. To our knowledge the gene responsible for the cortical malformation in tish rat has not yet been identified. We are currently localizing the gene mutation in the HeCo genome using polymorphic marker analyses as part of an ongoing collaboration with the Institut Cochin, France and the French Centre National de Génotypage.

Recently, LoTurco and Bai (2006) hypothesized that the perturbation of early phases of cortical development (e.g., after

loss of filamin-A function), creates nodular periventricular heterotopia because cells remain in the so-called multipolar stage and are unable to polarize and make radial progress through the IZ. By contrast, they hypothesized that failure or delay of the transition out of the multipolar stage, for instance in the case of *Dcx* or *LIS1* mutations, could cause formation of subcortical band heterotopia. The HeCo phenotype seems to be comparable with this second type of subcortical band formation as was shown notably by the birth date analyses and the increase in IZ thickness visualized using the anti-Tbr-1 antibody. Interestingly, when we observe the first signs of HeCo formation, markers of radial glia (RC2 and GLAST), as well as *Dcx*, display a pattern that is roughly similar to that in control mice.

The tendency to develop epilepsy in the tish rat was linked to a disturbance of inhibitory GABAergic neurotransmission before seizure onset, characterized by an altered GABAergic neuron distribution in both heterotopic and normotopic cortex, and a significant reduction in the frequency and amplitude of spontaneous inhibitory currents (sIPSCs) and miniature inhibitory postsynaptic currents (IPSC) recorded from pyramidal neurons (Trotter et al. 2006). Interestingly, the amplitudes of sIPSCs in normotopic cortex were also reduced. In human patients suffering from periventricular nodular heterotopia, interictal spiking activity was found in ectopic gray matter but also in the cortex overlying the nodules and in the mesial temporal structures. The heterotopia was involved in seizure onset in the majority of patients, but some patients had seizures originating in mesial temporal structures only (Aghakhani et al. 2005). We demonstrate here that the density of PARV+ neurons in the HeCo is of the same magnitude as in the overlying HoCo, and as in control cortex. We realize that the density of PARV+ neurons is just one parameter characterizing the GABAergic system, roughly representing 50% of the normal number of GABAergic neurons in cerebral cortex. In addition to such a number, more information is needed on the synaptology of GABAergic innervation of the HeCo, as well as the mode of transmission within this part of the nervous system before a possible link could be proposed on the origin of the lowered threshold for epileptogenesis in the HeCo mouse.

The results of the behavioral experiments indicate a significantly delayed somatic maturation (eye opening and fur growing) in the HeCo mice. This was accompanied by delays in the maturation of locomotor abilities, particularly in the geotaxis response. No genotype effect was evident in the expression of spontaneous alternation in juvenile subjects, but HeCo mice expressed a more marked preference for the cued arm at the age of 20 days, suggesting a marked tendency in cue guidance (see Wiener and Schenk 2005). In the adult subjects the cognitive performance was nearly normal in HeCo mice at the age of 2 months. In the radial maze in particular, it is possible that a cue guidance might have facilitated an optimal performance because the task design required only reference memory capacities. This suggests that HeCo mice were dependent on olfactory or visuo-spatial cues for spatial performance. Thus, HeCo mice appeared more adaptive, selecting the specific cues in comparison with control mice. During the Morris water maze task, no effect of genotype in the 2-month-old group was observed, indicating relatively preserved memory abilities in young animals. This conclusion is in accordance with the results of the neuropsychological assessment reported in children with subcortical band heterotopia due to a mutation

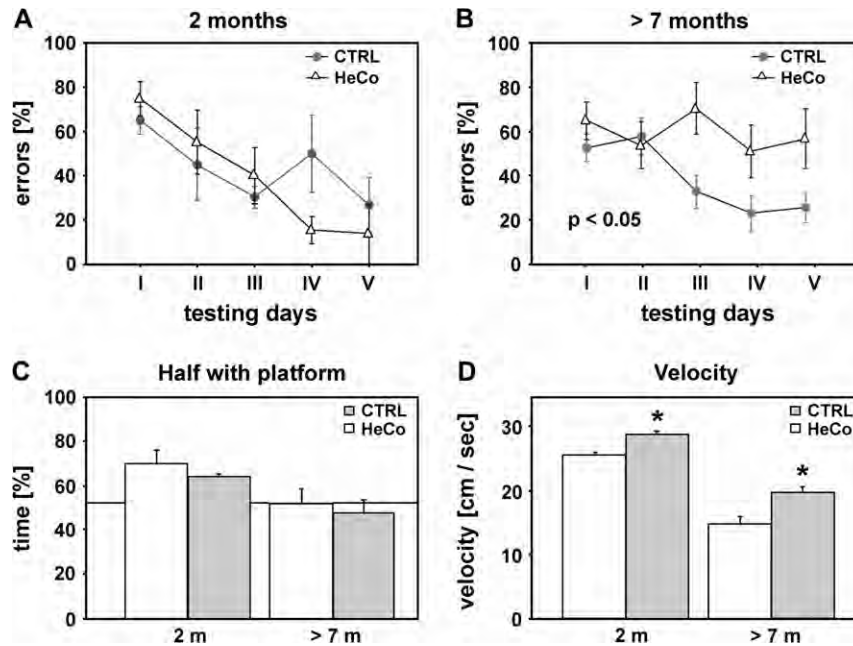


Figure 10. Morris water maze task. (A and B) Average number of errors during acquisition. (C and D) Probe trial on day 5. (C) Mean (\pm SE) time spent in the half containing the platform. At 2 months all animals showed a significant bias toward the quadrant containing the platform. (D) Speed during a 60-s exploration. HeCo mice were significantly slower than control mice. Asterisks highlight statistical significance.

in Dcx, which demonstrated intellectual impairment and deficits in all cognitive domains (processing speed, attention, language, visuomotor skills and fine motor ability) except verbal and visual episodic memory (Hashimoto et al. 1993; Jacobs et al. 2001; D'Agostino et al. 2002; Janzen et al. 2004).

We present here a new and unique mouse model of cortical heterotopia. This model shares with its human counterpart the morphology of the HeCo which lies inside the subcortical white matter, a certain degree of ventricular enlargement, the presence of GABA cells inside the HeCo (Hammers et al. 2001), and a tendency to develop epileptic seizures and SE (Meencke and Veith 1992). It represents therefore a true animal model of cortical heterotopia. The difference in transmission mode (X-linked for human “double cortex,” autosomal recessive for the HeCo mouse), suggests that the gene involved here is part of a new, as yet uncharacterized pathway, and cloning this gene will undoubtedly contribute to our understanding of cerebral cortex development.

Furthermore, the presence of spontaneous epileptic seizures, at least in the younger animals, makes this model a useful tool to study spontaneous chronic epilepsy in the mouse and to examine the relationship between structural abnormalities and epileptogenesis as well as structural modifications after epileptic seizures. It is also likely to provide a new tool to test and develop antiepileptic therapies.

Supplementary Material

Supplementary material can be found at: <http://www.cercor.oxfordjournals.org/>

Funding

Swiss National Science Foundation (310000 - 108246 Egbert Welker); and a “2007 Young Investigator Grant” from the

Faculty of Biology and Medicine, University of Lausanne, Switzerland (Alexandre Croquelois).

Notes

We thank Dr Fiona Francis for her review of this paper and her valuable comments, Caroline Musetti and David Rodriguez for help with the histological processing, Thi Dung Hau Iuliano-Dao for mice inbreeding, Jean-Pierre Hornung for help with the immunohistochemistry procedure and Alain Croquelois for help with BrdU and PARV analysis.

Conflict of Interest: None declared.

Address correspondence to Alexandre Croquelois, MD, Service de Neuropsychologie et de Neuroréhabilitation, Unité Universitaire de Neuroréhabilitation, Centre Hospitalier Universitaire Vaudois (CHUV), Avenue Pierre Decker 5, CH-1011 Lausanne, Switzerland. Email: alexandre.croquelois@chuv.ch.

References

- Aghakhani Y, Kinay D, Gotman J, Soualmi L, Andermann F, Olivier A, Dubeau F. 2005. The role of periventricular nodular heterotopia in epileptogenesis. *Brain*. 128:641-651.
- Altman J, Sudarshan K. 1975. Postnatal development of locomotion in the laboratory rat. *Anim Behav*. 23:896-920.
- Bai J, Ramos RL, Ackman JB, Thomas AM, Lee RV, LoTurco JJ. 2003. RNAi reveals doublecortin is required for radial migration in rat neocortex. *Nat Neurosci*. 6:1277-1283.
- Browne TR, Holmes GL. 2001. Epilepsy. *N Engl J Med*. 344:1145-1151.
- Cavalheiro EA, Santos NF, Priel MR. 1996. The pilocarpine model of epilepsy in mice. *Epilepsia*. 37:1015-1019.
- Clark GD. 2004. The classification of cortical dysplasias through molecular genetics. *Brain Dev*. 26:351-362.
- Corbo JC, Deuel TA, Long JM, LaPorte P, Tsai E, Wynshaw-Boris A, Walsh CA. 2002. Doublecortin is required in mice for lamination of the hippocampus but not the neocortex. *J Neurosci*. 22:7548-7557.
- Croquelois A, Bronchti G, Welker E. 2005. Cortical origin of functional recovery in the somatosensory cortex of the adult mouse after thalamic lesion. *Eur J Neurosci*. 21:1798-1806.
- D'Agostino MD, Bernasconi A, Das S, Bastos A, Valerio RM, Palmieri A, Costa da CJ, Scheffer IE, Berkovic S, Guerrini R, et al. 2002.

- Subcortical band heterotopia (SBH) in males: clinical, imaging and genetic findings in comparison with females. *Brain*. 125:2507-2522.
- des Portes V, Pinard JM, Billuart P, Vinet MC, Koulakoff A, Carrie A, Gelot A, Dupuis E, Motte J, Berwald-Netter Y, et al. 1998. A novel CNS gene required for neuronal migration and involved in X-linked subcortical laminar heterotopia and lissencephaly syndrome. *Cell*. 92:51-61.
- Dobyns WB, Truwit CL. 1995. Lissencephaly and other malformations of cortical development: 1995 update. *Neuropediatrics*. 26:132-147.
- Eriksson SH, Malmgren K, Nordborg C. 2005. Microdysgenesis in epilepsy. *Acta Neurol Scand*. 111:279-290.
- Farrell MA, DeRosa MJ, Curran JG, Secor DL, Cornford ME, Comair YG, Peacock WJ, Shields WD, Vinters HV. 1992. Neuropathologic findings in cortical resections (including hemispherectomies) performed for the treatment of intractable childhood epilepsy. *Acta Neuropathol*. 83:246-259.
- Grandchamp N, Schenk F. 2006. Adaptive changes in a radial maze task: efficient selection of baited arms with reduced foraging in senescent hooded rats. *Behav Brain Res*. 168:161-166.
- Gressens P. 2000. Mechanisms and disturbances of neuronal migration. *Pediatr Res*. 48:725-730.
- Gressens P. 2006. Pathogenesis of migration disorders. *Curr Opin Neurol*. 19:135-140.
- Guerrini R. 2005. Genetic malformations of the cerebral cortex and epilepsy. *Epilepsia*. 46(Suppl 1):32-37.
- Hammers A, Koeppe MJ, Richardson MP, Labbe C, Brooks DJ, Cunningham VJ, Duncan JS. 2001. Central benzodiazepine receptors in malformations of cortical development: a quantitative study. *Brain*. 124:1555-1565.
- Hashimoto R, Seki T, Takuma Y, Suzuki N. 1993. The 'double cortex' syndrome on MRI. *Brain Dev*. 15:57-59.
- Honda T, Tabata H, Nakajima K. 2003. Cellular and molecular mechanisms of neuronal migration in neocortical development. *Semin Cell Dev Biol*. 14:169-174.
- Jacobs R, Anderson V, Harvey AS. 2001. Neuropsychological profile of a 9-year-old child with subcortical band heterotopia or 'double cortex'. *Dev Med Child Neurol*. 43:628-633.
- Janzen L, Sherman E, Langfitt J, Berg M, Connolly M. 2004. Preserved episodic memory in subcortical band heterotopia. *Epilepsia*. 45:555-558.
- Lee KS, Collins JL, Anzivino MJ, Frankel EA, Schottler F. 1998. Heterotopic neurogenesis in a rat with cortical heterotopia. *J Neurosci*. 18:9365-9375.
- Lee KS, Schottler F, Collins JL, Lanzino G, Couture D, Rao A, Hiramatsu K, Goto Y, Hong SC, Caner H, et al. 1997. A genetic animal model of human neocortical heterotopia associated with seizures. *J Neurosci*. 17:6236-6242.
- LoTurco JJ, Bai J. 2006. The multipolar stage and disruptions in neuronal migration. *Trends Neurosci*. 29:407-413.
- Meencke HJ, Veith G. 1992. Migration disturbances in epilepsy. *Epilepsy Res Suppl*. 9:31-39.
- Meencke HJ, Veith G. 1999. The relevance of slight migrational disturbances (microdysgenesis) to the etiology of the epilepsies. *Adv Neurol*. 79:123-131.
- Rakic P. 1988. Defects of neuronal migration and the pathogenesis of cortical malformations. *Prog Brain Res*. 73:15-37.
- Rakic P. 2003. Elusive radial glial cells: historical and evolutionary perspective. *Glia*. 43:19-32.
- Ramos RL, Bai J, LoTurco JJ. 2006. Heterotopia formation in rat but not mouse neocortex after RNA interference knockdown of DCX. *Cereb Cortex*. 16:1323-1331.
- Ross ME. 2002. Brain malformations, epilepsy, and infantile spasms. *Int Rev Neurobiol*. 49:333-352.
- Schottler F, Couture D, Rao A, Kahn H, Lee KS. 1998. Subcortical connections of normotopic and heterotopic neurons in sensory and motor cortices of the fish mutant rat. *J Comp Neurol*. 395:29-42.
- Takahashi T, Nowakowski RS, Caviness VS, Jr. 1992. BUdR as an S-phase marker for quantitative studies of cytokinetic behaviour in the murine cerebral ventricular zone. *J Neurocytol*. 21:185-197.
- Trotter SA, Kapur J, Anzivino MJ, Lee KS. 2006. GABAergic synaptic inhibition is reduced before seizure onset in a genetic model of cortical malformation. *J Neurosci*. 26:10756-10767.
- Van der Loos H, Welker E, Dorfl J, Rumo G. 1986. Selective breeding for variations in patterns of mystacial vibrissae of mice. Bilaterally symmetrical strains derived from ICR stock. *J Hered*. 77:66-82.
- Veenman CL, Reiner A, Honig MG. 1992. Biotinylated dextran amine as an anterograde tracer for single- and double-labeling studies. *J Neurosci Methods*. 41:239-254.
- Wiener SI, Schenk F. 2005. Behavioral studies of directional orientation in developing and adult animals. In: Taube JS, Wiener SI, editors. Head direction cells and the neural mechanisms underlying directional orientation. Cambridge: Massachusetts Institute of Technology Press. p. 247-274.
- Wonders C, Anderson SA. 2005. Cortical interneurons and their origins. *Neuroscientist*. 11:199-205.

Mutations in *EML1/Em1* Lead to Misplaced Neuronal Progenitors during Cortical Development and Massive Heterotopia in Mouse and Human

Michel Kielar*^{1,2}, Françoise Phan Dinh Tuy*³⁻⁵, Cécile Lebrand², Karine Poirier⁶, Robert Olaso⁷, Sara Bizzotto³⁻⁵, Katia Boutourlinsky³⁻⁵, Nadia Bahi-Buisson⁸, Anne Gaele Le Moing⁹, Camino de Juan¹⁰, Dominique Boucher^{4,11}, Victor Borrell¹⁰, Patrick Berquin⁹, Wassila Carpentier¹², Ivo Gut⁷, Egbert Welker², Jamel Chelly⁶, Alexandre Croquelois^{#1,2}, Fiona Francis^{#3-5}

1. Department of Clinical Neuroscience, Centre Hospitalier Universitaire Vaudois and University of Lausanne, 1011 Lausanne, Switzerland
2. Department of Fundamental Neurosciences, University of Lausanne, 1005 Lausanne, Switzerland
3. INSERM UMR-S 839, F75005, Paris, France
4. Université Pierre et Marie Curie, F75005, Paris, France
5. Institut du Fer à Moulin, F75005, Paris, France
6. Inserm U1016, Université René Descartes, Institut Cochin, 75014 Paris, France
7. Plateforme de Transcriptomique, Laboratoire de Recherche Translationnelle, CEA/DSV/IG-Centre National de Genotypage, 91057 Evry, France
8. Hopital Necker Enfants Malades Pediatric Neurology APHP, Université Paris Descartes, 75015 Paris, France
9. Service de neuropédiatrie, CHU Amiens-Nord, 80054 Amiens cedex 1, France
10. Instituto de Neurociencias, CSIC & Universidad Miguel Hernández, 03550 Sant Joan d'Alacant, Alicante, Spain
11. Laboratoire de Biologie du Développement, CNRS UMR 7622, 75252 Paris Cedex 05
12. Plateforme post-génomique de la Pitié-Salpêtrière, Faculty of medicine, 75013, Paris.

* These authors contributed equally to the work.

These authors jointly directed the project.

SUMMARY

Neuronal migration disorders, such as subcortical band heterotopia (SBH), are often associated with pharmaco-resistant epilepsy and intellectual disability. *Doublecortin (DCX)*, *LIS1* and *alpha1-tubulin (TUBA1A)*, are mutated in human SBH, however corresponding mouse mutants do not show heterotopic neurons in the neocortical white matter. On the other hand, the spontaneously arisen *HeCo* mouse mutant displays this phenotype. By genotyping and gene expression studies, we identified *Eml1* as the mutated gene in *HeCo* mice. We show that its ortholog *EML1* is mutated in severe, giant heterotopia in human. Study of *Eml1* and the *HeCo* phenotype reveal novel insights into heterotopia formation. *Eml1* plays a role in neuronal progenitors and our data makes a link for the first time between altered proliferation patterns in the developing cortical wall and severe heterotopia in human.

RUNNING TITLE : *EML1/Eml1* mutations lead to subcortical heterotopia

HIGHLIGHTS

EML1 in association with microtubules plays an essential role in cortical development. Perturbed expression of mouse *Eml1* leads to band heterotopia. Human *EML1* is mutated in atypical globular heterotopia and polymicrogyria. Abnormal spindle orientations and misplaced progenitors lead to heterotopia.

INTRODUCTION

Classical SBH is characterized by the presence of many, aberrantly localized neurons, in the form of a band in the white matter, below a cortex which appears normal by magnetic resonance imaging (MRI, Harding, 1996). The identification of *LIS1*, *DCX* and *TUBA1A* SBH genes, coding for microtubule (MT) associated proteins and a tubulin isoform, highlights the involvement of MT cytoskeletal defects in this neuronal migration disorder (Jaglin and Chelly, 2009). The pathogenesis of SBH however, remains little understood, partly because SBH was until recently rarely observed in mouse models (Hirotsume et al., 1998; Corbo et al., 2002; Kappeler et al., 2007; Keays et al., 2007). Alternatively acute inactivation of *Dcx* by RNAi in the developing rat cortex (Bai et al., 2003), and the spontaneous *tish* rat model (Lee et al., 1997), for which the mutation is unknown, show SBH. Also, *Wnt3a* overexpression in the mouse neocortex (Munji et al., 2011) and conditional knockouts of *Ra-gef1* and *RhoA* (Bilasy et al., 2009; Cappello et al., 2012), as well as spontaneous

HeCo and BXD29 mouse mutants (Croquelois et al., 2009; Rosen et al., 2012), show heterotopic cortical neurons. We set out to identify how heterotopia arises in the *HeCo* mouse, and the nature of the corresponding human malformation.

HeCo mice, which appeared spontaneously in our colony of NOR-CD1 outbred stock, present bilateral bands of heterotopic neurons in the white matter, associated with epilepsy and subtle learning deficits in the adult, thus resembling SBH in human and constituting an interesting genetic model for the pathophysiological study of this malformation (Croquelois et al., 2009). Its mode of inheritance was determined as autosomal recessive (Croquelois et al., 2009). Using whole genome single nucleotide polymorphism (SNP) and transcriptome analyses, we identified *Echinoderm microtubule associated protein-like 1* (*Eml1*) as perturbed in expression in *HeCo* brains. In human, we also identified compound heterozygous mutations in *EML1* in a family with a rare form of giant bilateral, periventricular and subcortical heterotopia. This hence represents the first gene identified for this atypical form of heterotopia. The role of *EML1* in brain development has never previously been characterized. We show here that recombinant *Eml1* has a cell cycle-dependent localization, enriched in abscission regions in mitotic neuronal progenitors. Also, *HeCo* mice show a proportion of abnormally distributed dividing progenitors from early corticogenesis. Abnormal neuronal positioning is likely to be secondary to these progenitor defects. *Eml1/EML1* is thus a novel corticogenesis gene whose disruption highlights ectopic neuronal progenitors in the pathogenesis of severe forms of heterotopia.

RESULTS

A 4.4 Mb candidate region identified by homozygosity mapping on mouse chromosome 12

HeCo mouse crosses were set up as described in Table S1 and Experimental Procedures. Tail DNAs from C57BL/6J wild type (WT) and NOR-CD1 *HeCo* F0 mice, as well as 31 unaffected heterozygote F1, 42 affected F2 and control NOR-CD1 WT mice were used to screen an array of 1536 SNP markers covering the mouse genome (Tables S2 and S3). Only one genomic region on chromosome 12 showed 3 adjacent homozygous NOR allele markers in all affected individuals (Figure 1A). Flanking markers (5' rs13481624 and 3' rs3692361), found heterozygote for some affected F2 individuals, defined a 13.7 Mb region (Figure S1A).

A list of 96 SNPs within this region, and an additional *HeCo* pedigree, were generated for a second round of genotyping (Table S4). This allowed fine-mapping of the mutation to a 4.4 Mb region containing 30 annotated genes (Figure 1A and Tables S5 and S6). Coding exons and intron-exon boundaries of 15 genes selected from the 13.7 Mb region (Figure S1A) were also sequenced.

No mutations were identified in this initial list of genes, however, additional SNPs allowed a further refinement of the candidate region.

Perturbed expression of *Eml1*

Parallel to genetic linkage, we carried out transcriptome experiments. Total RNAs were prepared from 8 WT and 8 *HeCo* embryonic day 18 (E18) hemispheres and hybridized to mouse gene microarrays. *Eml1* transcripts, mapping to the refined 4.4 Mb region, were found differentially expressed. Strikingly, an *Eml1* 3'UTR probe exhibited a 5.5-fold decrease in fluorescence intensity in mutants, whereas a coding sequence probe (exon 5, Figure 1B) showed a 1.9 fold increase (Table S7).

In RT-qPCR analyses (primers in Supplemental Experimental Procedures), confirming the microarray data, *Eml1* transcripts containing exons 3 and 4 were 2.5-fold increased in *HeCo* (0.992 ± 0.084 *HeCo*, versus 0.398 ± 0.084 WT, expressed in relative units, Student *t*-test, $p=7.9 \times 10^{-11}$), whereas full length transcripts containing 3'UTR sequences were decreased more than 96-fold (0.00187 ± 0.00056 *HeCo* versus 0.18052 ± 0.00896 WT, Student *t*-test, $p=3.04 \times 10^{-17}$, Table S8). This dramatic reduction in expression of full length transcripts, together with the location of *Eml1* in the identified genomic region, strongly suggests that *Eml1* is the mutant gene in *HeCo* mice.

Presence of an early retrotransposon in intron 22 of the *HeCo Eml1* gene

To investigate mutation mechanisms, we searched for disruptions of *Eml1* in genomic DNA, and identified abnormalities in intron 22. Primers within exon 22 yielded PCR products of similar size and intensity in *HeCo* and WT, whereas those targeting downstream intronic sequences failed to amplify a product (Figures 1C and S1B). RT-PCRs were performed comparing WT and *HeCo Eml1* transcripts from E18 brains (Figures S1C and S1D). A 420 bp product extending from exon 19 to the 3'UTR was amplified in WT but was undetectable in *HeCo*. A secondary amplification using nested primers revealed two faint smaller bands in *HeCo* (Figure 1D), corresponding to skipping of exon 22, or exons 21 and 22. Both abnormal transcripts are predicted to induce a frameshift and premature stop codon in exon 23, leading of the loss of 84 or 117 C terminal amino acids (aa) out of 814, replaced by 19 or 20 junk aa respectively (sequences in Supplemental Information).

Primers upstream of exon 22 and in exon 23 yielded an expected 910 bp fragment from WT, whereas a >5 kb fragment was amplified from *HeCo* genomic DNAs (Figure 1E). Sequencing revealed a 5.5 kb early retrotransposon (ETn) element (partial sequence in Supplemental

Information) inserted in intron 22, flanked by a 6 bp direct repeat, and highly similar to several ETn type II retrotransposons (Baust et al., 2003).

ETn insertions can cause alternative splicing, premature termination and/or transcription initiation (Zhang et al., 2008). Indeed, we identified chimeric *Eml1*-ETn transcripts, with splicing events between exon 22 and the ETn 5' long-terminal repeat (LTR, Figure S1E), as well as a transcript initiated in the ETn 3'LTR and ending in exon 23, and a transcript not spliced at the exon 22 splice donor sequence (Figure 1F). Thus, although transcripts up to and including exon 22 are detected in *HeCo* brains, normal full length transcripts are absent, replaced by trace levels of shortened transcripts and by chimeric *Eml1*-ETn transcripts, all predicted to lead to truncated *Eml1* with potentially perturbed protein conformation.

Mutations of *EML1* in a human family

Human *EML1* maps to 14q32, and apart from oncogenic chromosomal rearrangements (Hagemeyer and Graux, 2010), and its association with type 1A Usher syndrome, later excluded (Gerber et al., 2006), no other obvious disorders have been linked to this gene (OMIM <http://www.ncbi.nlm.nih.gov>). However, 14q32 telomeric deletions have been associated with intellectual disability (Van Karnebeek et al., 2002; Schneider et al., 2008) and in one girl, lissencephaly was reported (Ravnan et al., 2006). We screened a panel of 47 non-consanguineous and 47 consanguineous sporadic, and 9 familial cortical malformation cases by PCR, sequencing coding exons and intron-exon boundaries (human primers in Supplemental Information). One family showed compound heterozygote mutations in their three affected children (Figures 2A and 2B). A c.481 C>T nucleotide mutation in exon 5, changing an arginine residue (p.R138) into a stop codon, was transmitted from the mother, and a c.796 A>G mutation in exon 8, changing a threonine into an alanine residue (p.T243A), was transmitted from the father. Further nucleotide changes were observed in other patients, either affecting amino acids but present only in the heterozygote state (c.2315 A>G, p.H749R, exon 22; c.292 G>A, p.V75M, exon 2) or present in intronic regions (intron 7, 130 bp after exon 7; intron 21, 10 bp before exon 22).

The three children exhibiting compound heterozygote mutations demonstrated the same MRI pattern, combining giant bilateral periventricular and subcortical heterotopia, most obvious in frontal regions and extending from the lateral ventricles to the white matter in a globular convoluted form, as well as polymicrogyria and corpus callosum agenesis (Figure 2C). Human *EML1* mutations are thus associated with an atypical autosomal recessive form of severe heterotopia, associated with epilepsy and intellectual disability (clinical details in Supplemental Information).

Effect of the T243A patient mutation on Eml1 MT association

Eml1 is a member of the EMAP family containing six members in human and originally identified in the purple sea urchin, in which EMAP represents an abundant MT-associated protein (Suprenant et al., 1993; 2000; NCBI Unigene database <http://www.ncbi.nlm.nih.gov>). The T243A mutation falls in the EML1 *Hydrophobic Echinoderm-Like Protein* (HELP) domain (Figures 2D and S2A), a highly conserved region characteristic of the EMAP family, possibly involved in the MT interaction (Eichenmuller et al., 2002; Pollmann et al., 2006, Tegha-Dunghu et al., 2008). To test the MT association of WT and T243A Eml1, their subcellular localizations were assessed in transfected Vero or COS7 cells. Using standard fixation protocols, Flag-tagged and non-tagged WT Eml1 showed a predominantly cytoplasmic localization during interphase and division (Figures S2B-S2G). Additional mild detergent extraction of soluble proteins revealed MT-associated-Eml1 (Figure 2E). Using purified proteins we also showed a direct association of GST-tagged EML1 with MTs (Figures S3A and S3B).

Cold treatment of transfected cells depolymerized MTs, and Eml1 no longer showed a fibrillar pattern (Figure S3C, 0 min). After restoring the cells to 37°C for 2 min, WT Eml1 was found associated, in the form of puncta, with the aster of newly nucleated MTs in most cells. In contrast, the T243A mutant protein was not found associated with MT asters (Figures 2F and 2G). In cells in which MTs had not been depolymerized, mutant Eml1 was also notably less associated with MTs (Figure S3D). Thus, the T243A mutation affects the MT association of Eml1, suggesting the importance of cytoskeletal interactions for the function of this protein.

***Eml1* expression in progenitors and neurons in developing mouse and ferret brains**

The role of Eml1 during cortical development is unknown. We first checked its expression pattern in the brain using *in situ* hybridization. Mouse *Eml1* transcripts were detected from E13.5 to P1 in cortical neuronal progenitors of the ventricular zone (VZ) and post-mitotic neurons of the cortical plate (CP) (Figures 2H-2M and S4). At E13.5, expression was mainly restricted to the progenitor zones, whereas from E14.5 onwards, an expression was also observed in the CP. At E17.5, no further expression was observed in the VZ. No full-length *Eml1* transcripts were detected in *HeCo* brains, as expected (Figures S4G-S4H'). In the adult, sparse *Eml1* labeling persists in the brain, notably in the cingulate, infra-limbic, prelimbic and piriform cortices, in hippocampal CA1 and dentate gyrus, and in the thalamic nuclei (Figures 2N and S4). To investigate *Eml1* in progenitor zones more similar to those present in primate brains, we further examined expression of *Eml1* in the developing brain of a gyrencephalic species, the ferret. At P0, a developmental stage similar to mouse E15, ferret *Eml1* expression was detected both in the CP and in proliferative layers (Figures

2O and 2P), including the outer subventricular zone (OSVZ), a major neurogenic zone which has expanded during evolution of the neocortex (Hansen et al., 2010; Fietz et al., 2010; Reillo et al., 2011). These combined expression data suggest that *Eml1* may play several roles during cortical development, in proliferation of several progenitor types, and in migration, differentiation and mature neuronal function.

Eml1 expression in primary cultures of progenitors and neurons

Studies of other EMAP proteins have pointed to roles in cell division, mechanotransduction and sensory function (Brisch et al., 1996; Ly et al., 2002; Eichenmuller et al., 2002; Pollmann et al., 2006; Hueston et al., 2008; Bechstedt et al., 2010). To start to question *Eml1*'s role in cortical cells, we first assessed the subcellular localization of the protein in neuronal progenitors and post-mitotic neurons. Due to the lack of specific antibodies for detection in neuronal cells or tissues, YFP- or Flag-tagged *Eml1* was transfected in primary cultures of E12.5 mouse cortices. These cultures show post-mitotic neurons expressing *Dcx*, and progenitor subtypes expressing *Ki-67*, a marker of proliferating cells, and *Pax6* or *Tbr2*, subpopulation markers for radial glial cells (RGCs) and basal progenitors, respectively (Figure S5, Götz et al., 1998; Englund et al., 2005). In progenitors, using standard fixations, a cell cycle-dependent, punctate localization of YFP-EML1 was observed (Figures 3A-C and S5), enriched in perinuclear regions in interphase cells and the region of spindle MTs during metaphase. During telophase and cytokinesis, YFP-EML1 labeled puncta accumulated in the midbody region, a bridge interconnecting the separating cells, which contains vesicles and MTs (Gromley et al., 2005; Guizetti et al., 2011). In neurons, tagged *Eml1* appeared distributed throughout the cell (Figures 3D and 3E), aligning with MTs, and prominent in perinuclear regions and growth cones (Figures 3D'-3E'). A partial co-localisation with dynein was observed (Figure 3F).

Comparing WT and *HeCo* mutant cultures, no significant differences were observed between the genotypes in aspects and numbers of *Dcx*, *Pax6* and *Tbr2* positive (⁺) cells (Figures 3G, S5A and S6). In contrast, considering all proliferating cells together, the percentage of *Ki-67*⁺ cells was found reduced in *HeCo* cultures (Figure 3G).

Development of the heterotopia in the *HeCo* cortex *in vivo*

To characterize heterotopia formation *in vivo*, *HeCo* forebrains were first examined at different stages of development. At E15, there was no obvious accumulation of heterotopic neurons in the *HeCo* intermediate zone (IZ, Croquelois et al., 2009). By E17, neurons forming the heterotopia were evident in the IZ, including both early-born *Tbr1*⁺ and late-born *Cux1*⁺ neurons (Figures 4A-

4D). Nestin⁺ RGC fibres, the guides for migrating neurons, appeared disorganized in heterotopic regions (Figures 4A'' and 4B''). Tbr1⁺ neurons were also abundant between the heterotopia and CP, even though most WT Tbr1⁺ neurons had finished migrating to form layer VI (Figures 4A' and 4B'). Interestingly, although electroporation experiments showed that many mutant cells born at E15.5 did not reach the CP and remained blocked in the lower IZ (Figure 4E and 4F), time-lapse imaging of migrating neurons in the *HeCo* IZ and CP, showed no alteration of speed, or pause frequency and duration compared to WT (Figure S7).

At P3 almost all Tbr1⁺ neurons had reached their final destination in layer VI above the heterotopia, whereas many Cux1⁺ neurons had failed to reach cortical layers II/IV and were present in the heterotopia (Figures 4G-4J). Strikingly at this stage, and to a lesser extent at P7 (Figures S8A and S8B), columns of Cux1⁺ neurons were observed between the heterotopia and the cortex, while the migration of these neurons was already complete in WT (Figures 4I and 4J). The heterotopia is thus sequentially populated by early- and late-born neurons that subsequently migrate in columns between the heterotopia and the CP, having a temporal delay with respect to WT. Some of the last-born neurons remained trapped in the postnatal IZ, the future white matter. Glial cells tended not to be included in the heterotopia (Figure S8).

Proliferation abnormalities in the *HeCo* developing cortex

To further investigate the origin of the defects, we next tested for progenitor abnormalities in *HeCo* brains. Pulsed 5-bromo 2-deoxyuridine (BrdU) injections were initially performed at E15 followed by sacrifice 1 h later, to assess proliferating cells in the developing cortex. In WT, BrdU⁺ cells were largely restricted to VZ and SVZ, whereas in *HeCo* brains they appeared spread throughout the cortical wall (Figures 5A and 5B). BrdU injections were then performed at E13 (Figures 5C-5F). After sacrificing at 30 min post-injection, BrdU⁺ and Ki-67⁺ cells were observed as expected in the VZ and SVZ of WT brains whereas in *HeCo*, in addition to these locations, large numbers of BrdU⁺ and Ki-67⁺ cells were found within the IZ and CP (Figures 5C and 5D). Thus altered distribution of progenitors is observed early in *HeCo* brains, at a time when Tbr1⁺ neurons are being produced.

To assess cell cycle characteristics, we determined the labeling index (percentage of Ki-67⁺ cells also labeled with BrdU, Chenn and Walsh, 2002), which we found significantly higher in *HeCo*, notably in the IZ and CP (Figure 5G). Analysis of embryos sacrificed 24 h after BrdU injection showed that the total number of BrdU labeled cells was increased in *HeCo* compared to WT (Figures 5E, 5F and 5H), due to more labeled cells in the VZ, SVZ and IZ (Figure 5H). A reduced cell cycle exit (quantified by identifying after 24 h those BrdU⁺ cells which showed no Ki-67 expression) was identified in *HeCo* compared to WT, particularly in the SVZ, IZ and CP (Figure

5I). Thus, labeling index and cell cycle exit suggest that misplaced progenitors proliferate actively at E13, displaying characteristics different from WT IZ and CP cycling cells and potentially similar to VZ and SVZ proliferating cells.

At E19, IZ and CP progenitors were still present in *HeCo*, although in lower densities, and mainly positioned around the heterotopia (Figures 5J, 5K and S8G-S8J). Labeling index was also significantly increased in the E19 *HeCo* cortex compared to WT, particularly in the IZ and CP (data not shown), and cell cycle exit significantly reduced in all layers (data not shown). Thus, at early and late stages of corticogenesis, many actively dividing cells are abnormally positioned in *HeCo* brains. We questioned if cell death was also altered, and found increased numbers of caspase-3⁺ cells in E13 *HeCo* versus WT cortices (Figures 5L-5N).

We next questioned if both Pax6⁺ RGCs and Tbr2⁺ basal progenitors were found in ectopic positions. At E13, both cell types were present in the *HeCo* IZ and CP, becoming more pronounced at E16, whereas these markers rarely label cells in these zones in WT (Figures 6A-6H). Also, in order to confirm that ectopic progenitors entered mitosis, co-labeling with phospho(Ser10)-histone 3 (PH3), a mitotic marker, was performed (Figures 6A-6H). At E13 there were no significant differences between overall PH3⁺ cell counts in WT and *HeCo* brains but there was a significantly altered distribution, with less PH3⁺ cells in the *HeCo* VZ and more in SVZ and IZ (Figure 6I). Double labeled Pax6⁺/PH3⁺ or Tbr2⁺/PH3⁺ cells (Figures 6B' and 6F') were also observed in larger proportions in *HeCo* IZ and CP compared to WT, although their total number was not increased (Figure 6J). Thus, both Pax6⁺ and Tbr2⁺ progenitors are abnormally distributed and undergo mitosis in the *HeCo* IZ and CP throughout corticogenesis. They form a misplaced, second source of neurons, potentially contributing to a physical barrier for new migrating cells produced in the VZ and SVZ.

Origin of ectopic progenitors in *HeCo* mice

To further characterize progenitor abnormalities *in vivo*, we first used a cytoplasmic marker of mitotic progenitors, phospho-vimentin (P-vim), revealing their morphologies (Figures 7A-7D). Both Pax6⁺ and Tbr2⁺ populations double-labeled with P-vim were found abnormally distributed at E13 (Figures 7E and 7F). P-vim detection revealed basal processes extending to the pial surface of some Pax6⁺ ectopic progenitors, as well as some horizontally-oriented processes (Figures 7B'' and 7B'''). The ventricular lining, made up of RGC endfeet, has been found perturbed in some mouse mutants (Weimer et al., 2009; Asami et al., 2011). Using β -catenin, which labels adherens junctions between RGCs, we observed an apparently intact ventricle lining in *HeCo* brains at E13 (Figures 7G and 7H). A similar result was also revealed with Par3, a polarity protein present in RGC apical

endfeet (Figures 7I-7K). However, while in WT brains at E13, most metaphasic cells located at the ventricle lining showed vertically oriented DNA (60-90° angle perpendicular to the ventricular surface, Asami et al., 2011), these were significantly reduced in *HeCo* in favor of oblique divisions (Figures 7I-L). Such differences may explain the manner by which ectopic progenitors arise, since oblique and horizontal cleavage orientations are less likely to allow symmetric inheritance of apical membrane attachments and may favor detachment of progenitors. *Eml1*/*EML1* could thus be important in these finely tuned mechanisms and its mutation might perturb spindle orientations and radial glial cell attachment initiating heterotopia formation.

DISCUSSION

We identified here a novel corticogenesis gene associated with severe heterotopia in mouse and human. Patients with mutations in *EML1* exhibit an autosomal recessive, complex cortical disorder combining giant bilateral periventricular and subcortical heterotopia, as well as polymicrogyria, macrocephaly and corpus callosum agenesis. Our converging data strongly suggest that ectopic proliferation is the major underlying event contributing to this severe form of heterotopia, which hence differs from classical forms of SBH, caused by problems of neuronal migration (Barkovich et al., 2012). In *HeCo* mice, a retrotransposon insertion was responsible for perturbed *Eml1* expression and interestingly, a previous insertion of an ETn II element has been described in the same NOR-CD1 stock (Welker et al., 1996; Abdel-Majid et al., 1998). *Eml1* or genes coding for proteins of the same pathway could also be good candidates for the spontaneously arisen *tish* and BXD29 mutants (Lee et al., 1997; Rosen et al., 2012).

The association of *Eml1* with MTs re-emphasizes the importance of a correctly functioning cytoskeleton during cortical development (Jaglin and Chelly, 2009). Human *EML1* shares 58% identity with sea urchin *EMAP*, found to localize to the mitotic spindle, as well as to interphase MTs (Suprenant et al., 1993). *EMAP* family members have been reported to either destabilize or stabilize MTs (Eichenmuller et al., 2002; Houtman et al., 2007) and several are regulated by phosphorylation during the cell cycle (Brisch et al., 1996; Pollmann et al., 2006). In epithelial cells, we observed both cytoplasmic and MT localizations of *Eml1* and we showed that the T243A mutation, occurring in the *HELP* domain, altered the MT association. In neuronal progenitor cultures, we found *Eml1* localization to be cell cycle-dependent and enriched at the equatorial, interzonal region and at the midbody during anaphase and telophase. *EML3*, another member of the *EMAP* family, was also reported to co-localize with midbody MTs in HeLa cells (Tegha-Dunghu et al., 2008). The midbody is a transient structure showing active vesicle trafficking and MT

rearrangements, both necessary for membrane addition during abscission of the daughter cells (Gromley et al., 2005; Guizetti et al., 2011). Our data suggest that *Eml1* could associate with vesicles in these subcellular regions. In RGCs *in vivo*, the midbody is situated at the apical membrane, and its fate is different during symmetric and asymmetric division (Kosodo et al., 2004; Dubrueil et al., 2007). Indeed, spindle dynamics and orientation, midbody function and cell cycle properties are coordinated during brain development, and dynein, which we found partly colocalized with EML1, has been reported to be involved in these activities (Kosodo et al., 2004; Paramasivam et al., 2007; Dubreuil et al., 2007; Asami et al., 2011, Horgan et al., 2011). Although other features of RGC function could also be affected in *HeCo* brains, our data already point to spindle orientation abnormalities, which could represent the primary defect (Figure 8).

Subcortical heterotopias are classically linked to problems of migration, but primary abnormalities in progenitor number, type or localization may also lead to ectopic neurons (Lee et al., 1998; Fitzgerald et al., 2011; Munji et al., 2011; Cappello et al., 2012). In *HeCo* mice, many neurons are unable to reach the CP. However, we found that migration speed and parameters of E15-born neurons were unchanged compared to WT. Several hypotheses might account for these data: i) a possible migration defect may affect only some neurons; ii) migration *per se* may not be affected, but the accumulation of ectopic progenitors and local neuron production within the IZ may subsequently hinder migration; iii) neurons may be unable to migrate due to disorganized nestin⁺ RGC fibers (Cappello et al., 2012). Our data in the *HeCo* model seem most consistent with the last two possibilities (Figure 8).

Concerning a role in progenitors, *in situ* hybridizations suggest similarities in the expression profiles of *Eml1* and *Pax6*, the latter expressed in RGCs between E13.5 and E16.5, with a high-lateral to low-medial gradient (Stoykova et al., 2000). In *Pax6* mutants, ectopic proliferating RGCs are present in the IZ during the same developmental period as *HeCo* mice (Götz et al., 1998), and ectopic Tbr2⁺ cells also occur (Quinn et al., 2007) although *Pax6* is not expressed in Tbr2⁺ basal progenitors. Lack of full-length *Eml1* in *HeCo* RGCs is likely to lead to their abnormal position and function, as indicated by the presence of many ectopic Pax6⁺ cells in the IZ. We found that ectopic RGCs also express Sox2, and are rarely double-labelled with Tbr2 (data not shown).

In addition to classical RGCs, *Pax6* is also expressed in basal radial glia progenitors (bRGs), recently identified abundantly in the developing cortex of primates, including human, and other species (Fietz et al., 2010; Hansen et al., 2010; Reillo et al., 2011; Kelava et al., 2012). They are also present in mouse brain where they are quite rare (Wang et al., 2011; Shitamukai et al., 2011). Expression of *Eml1* in the ferret OSVZ suggests that this gene could be expressed in bRGs. These cells, proposed to be important for gyri formation, retain many features of classical RGCs,

including a radially-extended basal process contacting the pia, but they lack contact with the ventricular surface. *HeCo* ectopic progenitors, which do not seem to be apically attached, may resemble such cells. *HeCo* RGCs, which show cleavage orientation differences compared to WT, could produce an excess of bRG-like cells, with however, sufficient RGCs remaining apically attached to retain ventricular lining integrity. Further studies are required to characterize the exact nature and origin of *HeCo* ectopic progenitors.

We find that a heterotopic cluster of neurons forms early in corticogenesis. Ectopic progenitors and cleavage orientation abnormalities are already present at E13 and heterotopic cells obvious in the IZ several days later. Detached apical progenitors proliferate actively in ectopic positions and are likely to give rise to ectopic Tbr2⁺ basal progenitors. Intrinsic abnormalities could also alter the distribution of SVZ Tbr2⁺ cells, although *Eml1*, like *Pax6*, may not normally be expressed in such cells. The increased labeling index and reduced cell cycle exit of ectopic mutant cells may also induce increased cell death. At later stages, as the IZ increases in size during corticogenesis, progenitors positioned above the heterotopia may eventually convert into neurons that will reach the CP, or alternatively could be attracted and contribute to the development of a heterotopic cell mass.

Our data reveal further novel insights into the formation of the heterotopia. Tbr1 and Cux1 labelings during corticogenesis show that probably all types of neurons, early to late born, sequentially populate the heterotopia during development and continue to migrate to the CP, with a temporal delay in comparison with WT neurons expressing the same markers. At late stages (P3, P7) columns of mutant migrating neurons are observed and finally only upper layer neurons remain trapped in the heterotopia, probably due to a shutdown of migration (Manent et al., 2009). As neurogenesis occurs in a lateral to medial gradient (Takahashi et al., 1999), upper layer neurons in medial regions are the last to be formed and hence, the most susceptible to remain trapped in the IZ after the migration period.

Our data reinforce the concept that ectopic proliferation during corticogenesis can contribute to the pathogenesis of rodent heterotopia (Lee et al., 1998; Munji et al., 2011; Cappello et al., 2012). Here we link this phenotype to combined periventricular and subcortical heterotopia in human, associated with polymicrogyria, thus highlighting that progenitors can be involved in the pathogenesis of these disorders. Further studies are still required to identify the relative contributions of normally positioned and ectopic progenitors to neurons destined for the heterotopic, homotopic or polymicrogyric cortex. Progenitor abnormalities distinguish the severe and atypical heterotopia observed in patients with mutations in *EML1* from those most probably largely due to intrinsic neuronal migration defects, and giving rise to classical SBH in human and a preserved neocortex in the mouse (Hirotsune et al., 1998; Corbo et al., 2002; Kappeler et al., 2007;

Keays et al., 2007). Identification of *EML1* provides a new entry point into understanding the molecular and cellular mechanisms underlying normal cortical development.

EXPERIMENTAL PROCEDURES

Animals. Research was conducted according to national and international guidelines (EC directive 86/609) with protocols followed by local ethical committees. WT and *HeCo* mice on a NOR-CD1 genetic background were used for developmental analyses. For primary neuronal cultures and *in situ* hybridization, Swiss and NOR-CD1 mice were used. For staging of embryos, the day of vaginal plug was considered as E0.5. Methods for DNA and RNA preparation, immunohistochemistry and *in situ* hybridization are detailed in Supplemental Experimental Procedures.

Mouse crosses. Previous mouse crosses established the autosomal recessive nature of the *HeCo* phenotype (Croquelois et al., 2009). For genotyping studies, *HeCo* mice on the NOR-CD-1 background were crossed to C57BL/6J mice, giving rise to an unaffected heterozygote F1 population. Brother-sister matings generated an F2 population with 25 % affected homozygous individuals (pedigrees in Table S1). Brain sections of each F2 mouse (n= 240) were analyzed in order to identify mutants.

Whole genome and second round chromosome 12 SNP analyses. SNP markers were selected based on naturally occurring polymorphisms between C57BL/6 and Sv129 strains, the latter showing the strongest similarity to the NOR-CD-1 background. An array of 1536 SNPs was created and screened using Golden Gate Illumina technology (Illumina, GmbH). New SNP markers between rs13481624 and rs3692361 on mouse chromosome 12 were screened using the same technology.

PCR amplification. Genomic DNA amplifications were performed for each exon and flanking sequences of mouse *Eml1* from *HeCo* and NOR-CD1 WT samples using standard PCR (primer sequences in Supplemental Experimental Procedures). Intron 22 was amplified using Pfu turbo DNA polymerase (Agilent Technologies). RT-PCRs were performed from random-hexamer primed cDNAs using standard protocols. PCR products were checked by agarose gel electrophoresis and sequenced using standard Sanger sequencing (Beckmann Coulter Genomics).

Differential gene analysis. Quality analyses of E18 RNAs showed a mean RNA integrity number of 9.81 +/- 0.12 and a coefficient of variation of 1.26 %. Labeled cRNAs were hybridized to

MouseWG-6 v2 expression BeadChips (Illumina, GmbH). Differential analysis *per gene* was performed with Student t-tests. In microarray analyses, quality controls (reference samples, principal component analyses before and after normalization) showed neither batch nor beadchip effect. Bead-averaged data was normalized using quantile normalization (BeadStudio software, Illumina, GmbH). For real time qPCRs, total RNA samples were treated by the DNase RQ1 (Promega) and the SYBRgreen method was used, following MIQE guidelines (Bustin et al., 2009). Values were normalized to the geometric mean of 3 normalization factors found to be the most stable through all samples using the geNorm approach (Vandesompele et al., 2002). First strand cDNA was synthesized using 50 ng/ μ l of total RNA, oligo(dT) and the Superscript III Reverse Transcriptase kit (Invitrogen) following the manufacturer's recommendations. Gene-specific primers were designed using Primer Express Software (PE Applied Biosystems). The 3 genes used for normalization were histone deacetylase 3, Hdac3; Endoplasmic reticulum protein 29, Erp29; ATP synthase, H⁺ transporting, mitochondrial F0 complex, subunit c (subunit 9), isoform 3, Atp5g3. Amplicon sizes were between 54 and 79 bp. Standard curves were generated from assays made with serial dilutions of cDNA to calculate PCR efficiencies (90 % < efficiency < 105%, with $r^2 \geq 0.998$). Threshold cycles (Ct) were transformed into quantity values using the formula $(1 + \text{Efficiency})^{-\text{Ct}}$. Only means of triplicate with a coefficient of variation of less than 10 % were analyzed. Inter-plate variation was below 8 %.

Patients and analysis of human *EML1*. Patient DNAs or blood samples, and informed consent (from all patients' parents) were obtained according to the guidelines of local institutional review boards. Sporadic or familial cases were selected with clinical and brain imaging features compatible with a diagnosis of either lissencephaly or heterotopia. Prior to *EML1* analysis, patients were found negative for mutations in *DCX* (RefSeq NM_181807), *LIS1* (RefSeq NM_000430), *ARX* (RefSeq NM_139058), *TUBA1A* (RefSeq NM_006009) or *TUBB2B*. The family with compound heterozygote mutations was also negative for filamin A mutations. Genomic DNA amplifications were performed for *EML1* using standard procedures (primers listed in Supplemental Experimental Procedures) and PCR products were analyzed by direct sequencing using an ABI3700 DNA analyzer (Applied Biosystems, Foster City, CA).

Plasmids and transfections. Full length mouse *Eml1* (canonical sequence RefSeq NM_001043335) was obtained from the IMAGE clone 6400458 (MGC 62485) and cloned into the pCAGIG vector (Addgene), or the p3X FLAG vector (Sigma-Aldrich) with the FLAG N terminal to *Eml1* sequences. Site directed mutagenesis was performed using a Quik Change kit (Stratagene).

The pcDNA3.1-YFP-*EML1* construct was a kind gift from A.M. Fry (University of Leicester, UK). Plasmid DNAs were amplified using a Qiagen maxiprep Endofree kit (Qiagen). Details of cell cultures, transfections and immunodetection are provided in Supplemental Experimental Procedures.

BrdU injections and assessment of proliferation. Timed-pregnant females received a single intraperitoneal injection of BrdU (Sigma-Aldrich, 50 $\mu\text{g/g}$ body weight; 8 mg/ml in 0.15 M phosphate buffer, 0.9% w/v NaCl, pH 7.4) at E13, E15 and E19. Mice were sacrificed 30 min, 1 h, or 24 h later (Martynoga et al. 2005) and brains processed for immunohistochemistry. Alternate sections were chosen for BrdU and Ki-67 or BrdU and Tbr1 double-labeling and preincubated with 2% methanol v/v to improve BrdU detection.

Confocal microscopy (brain sections). Fluorescent-stained sections were imaged with confocal microscopes (Zeiss LSM 710 Quasar or Leica SP5) equipped with 10x, 20x, 40x oil Plan-NEOFLUAR, and 63x oil Plan-Apochromat objectives. Fluorophore excitation and scanning were performed with an Argon laser 488 nm (blue excitation for GFP, Alexa 488), with a HeNe1 laser 543 nm (green excitation for Alexa 594) and a Diode laser 405 nm (for Hoechst staining). To get the whole Z-stack dataset, we used the mode “Surpass” and single sections of a Z-stack were displayed by using the “Slice” mode of Imaris.

Cell counting and quantification. After immunohistolabeling Z-stacks were acquired for each coronal section in a multitrack mode avoiding crosstalk artifacts of the fluorochromes. All Z-stacks and image processing were performed with Imaris 4.3 software (Bitplane). In general, image stacks contained approximately 40 confocal planes each, for optimal z-axis. Counting was performed for each layer (VZ, SVZ, IZ, CP) in 3 sections per animal (3 to 4 per genotype and per age). Labeled cells were counted in a region of interest (ROI), a 100 μm wide and 10 μm deep stripe across VZ, SVZ, IZ and CP, in which thickness was defined by the different layers. Caspase-3⁺ cells were counted in at least 3 cortical sections of 50 μm per genotype, in a defined volume stack using Imaris manual volume tool.

Statistical analysis. Statistical analysis was performed using the IBM SPSS Statistics version 19 (SPSS Inc.). Data were checked for the normality of distribution. Comparisons of means in 2 groups were made using the unpaired Student *t*-test. The χ^2 test was used for frequency comparisons. For cell count quantifications, data were analyzed with the multiple factors ANOVA using the

generalized linear model (GLM) procedure (layers x strains). Simple main effects (univariate tests) were based on the linearly independent pairwise comparisons among the estimated marginal means.

ACKNOWLEDGEMENTS

We thank the Inserm Avenir program, the French Agence National de la Recherche (ANR- 08-MNP-013), the Fondation Bettencourt Schueller and the Federation pour la recherche sur le cerveau (FRC) for grants awarded to FF, the FRC Rotary for an equipment grant awarded to the IFM, and the Swiss National Science Foundation (SNSF)-SPUM-33CM30-124089 and 33CM30-140332, the Fondation Gianni Biaggi de Blasys and the SNSF-31003A-135574 for grants awarded to AC and SNSF 31003A-125379 to EW. We are particularly grateful to French families and clinicians for access to their DNA samples. We also thank B. Barry, C. Walsh and American clinicians for access to certain of their severe heterotopia cases. We thank the imaging and animal house platforms at the IFM and the Région Ile-de-France for support. We thank J. Lemarchand, Y. Saillour, D. Derbala, M. Foglio, A. Boland, D. Zelenika, J.P. Hornung, D. Valloton, N. Narboux-Neme, A. Cabrera, E. Bruel-Jungerman, R. Belvindrah, R. Khalaf, X. Jaglin, T.D.H. Iuliano, M. Karababa, N. Magalhaes for their contributions to this work. We are very grateful to A. Houdusse, C. Moores, R. Bayliss, A. Fry, S. Cappello, M. Götz and W. Krezel for interesting discussions.

REFERENCES

- Abdel-Majid, R.M., Leong, W.L., Schalkwyk, L.C., Smallman, D.S., Wong, S.T., Storm, D.R., Fine, A., Dobson, M.J., Guernsey, D.L., and Neumann, P.E. (1998). Loss of adenylyl cyclase I activity disrupts patterning of mouse somatosensory cortex. *Nat. Genet.* *19*, 289-291.
- Asami, M., Pilz, G.A., Ninkovic, J., Godinho, L., Schroeder, T., Huttner, W.B., and Götz, M. (2011). The role of Pax6 in regulating the orientation and mode of cell division of progenitors in the mouse cerebral cortex. *Development* *23*, 5067-5078.
- Bai, J., Ramos, R.L., Ackman, J.B., Thomas, A.M., Lee, R.V., and LoTurco, J.J. (2003). RNAi reveals doublecortin is required for radial migration in rat neocortex. *Nat. Neurosci.* *6*, 1277-1283.
- Barkovich, A.J., Guerrini, R., Kuzniecky, R.I., Jackson, G.D., and Dobyns, W.B. (2012). A developmental and genetic classification for malformations of cortical development: update 2012. *Brain* *135*, 1348–1369.

- Baust, C., Gagnier, L., Baillie, G., Harris, M., Juriloff, D., and Mager, D. (2003). Structure and expression of mobile ETnII retroelements and their coding-competent MusD relatives in the mouse. *J. Virol.* 77, 11448-11548.
- Bechstedt, S., Albert, J.T., Kreil, D.P., Müller-Reichert, T., Göpfert, M.C., and Howard, J. (2010). A doublecortin containing microtubule-associated protein is implicated in mechanotransduction in *Drosophila* sensory cilia. *Nat Commun.* Apr 12;1:11. doi: 10.1038/ncomms1007.
- Bilasy, S.E., Satoh, T., Ueda, S., Wei, P., Kanemura, H., Aiba, A., Terashima, T., and Kataoka, T. (2009). Dorsal telencephalon-specific RA-GEF-1 knockout mice develop heterotopic cortical mass and commissural fiber defect. *Eur. J. Neurosci.* 29, 1994-2008.
- Brisch, E., Daggett, M.A., and Suprenant, K.A. (1996). Cell cycle-dependent phosphorylation of the 77 kDa echinoderm microtubule-associated protein (EMAP) in vivo and association with the p34cdc2 kinase. *J. Cell Sci.* 109, 2885-2893.
- Bustin, S.A., Benes, V., Garson, J.A., Hellemans, J., Huggett, J., Kubista, M., Mueller, R., Nolan, T., Pfaffl, M.W., Shipley, G.L., Vandesompele, J., and Wittwer, C.T. (2009). The MIQE guidelines: minimum information for publication of quantitative real-time PCR experiments. *Clin. Chem.* 55, 611-622.
- Cappello, S., Böhringer, C.R., Bergami, M., Conzelmann, K.K., Ghanem, A., Tomassy, G.S., Arlotta, P., Mainardi, M., Allegra, M., Caleo, M., van Hengel, J., Brakebusch, C., and Götz, M. (2012). A radial glia-specific role of RhoA in double cortex formation. *Neuron* 73, 911-924.
- Chenn, A. and Walsh, C.A. (2002). Regulation of cerebral cortical size by control of cell cycle exit in neural precursors. *Science* 297, 365-369.
- Corbo, J.C., Deuel, T.A., Long, J.M., LaPorte, P., Tsai, E., Wynshaw-Boris, A., and Walsh, C.A. (2002). Doublecortin is required in mice for lamination of the hippocampus but not the neocortex. *J. Neurosci.* 22, 7548-7557.
- Croquelois, A., Giuliani, F., Savary, C., Kielar, M., Amiot, C., Schenk, F., and Welker, E. (2009). Characterization of the HeCo mutant mouse: a new model of subcortical band heterotopia associated with seizures and behavioral deficits. *Cereb. Cortex* 19, 563-575.

- Dubreuil, V., Marzesco, A.M., Corbeil, D., Huttner, W.B., and Wilsch-Bräuninger, M. (2007). Midbody and primary cilium of neural progenitors release extracellular membrane particles enriched in the stem cell marker prominin-1. *J. Cell Biol.* *176*, 483-495.
- Eichenmüller, B., Everley, P., Palange, J., Lepley, D., and Suprenant, K.A. (2002). The human EMAP-like protein-70 (ELP70) is a microtubule destabilizer that localizes to the mitotic apparatus. *J. Biol. Chem.* *277*, 1301-1309.
- Englund, C., Fink, A., Lau, C., Pham, D., Daza, R.A., Bulfone, A., Kowalczyk, T., and Hevner, R.F. (2005). Pax6, Tbr2, and Tbr1 are expressed sequentially by radial glia, intermediate progenitor cells, and postmitotic neurons in developing neocortex. *J. Neurosci.* *25*, 247-251.
- Fietz, S.A., Kelava, I., Vogt, J., Wilsch-Bräuninger, M., Stenzel, D., Fish, J.L., Corbeil, D., Riehn, A., Distler, W., Nitsch, R., and Huttner, W.B. (2010). OSVZ progenitors of human and ferret neocortex are epithelial-like and expand by integrin signaling. *Nat. Neurosci.* *13*, 690-699.
- Fitzgerald, M.P., Covio, M., and Lee, K.S. (2011). Disturbances in the positioning, proliferation and apoptosis of neural progenitors contribute to subcortical band heterotopia formation. *Neuroscience* *176*, 455-471.
- Gerber, S., Bonneau, D., Gilbert, B., Munnich, A., Dufier, J.L., Rozet, J.M., and Kaplan, J. (2006). *USH1A*: Chronicle of a slow death. *Am. J. Hum. Genet.* *78*, 357-359.
- Götz, M., Stoykova, A., and Gruss, P. (1998) Pax6 controls radial glia differentiation in the cerebral cortex. *Neuron* *21*, 1031-1044.
- Gromley, A., Yeaman, C., Rosa, J., Redick, S., Chen, C.T., Mirabelle, S., Guha, M., Sillibourne, J., and Doxsey, S.J. (2005). Centriolin anchoring of exocyst and SNARE complexes at the midbody is required for secretory-vesicle-mediated abscission. *Cell* *123*, 75-87.
- Guizetti, J., Schermelleh, L., Mäntler, J., Maar, S., Poser, I., Leonhardt, H., Müller-Reichert, T., and Gerlich, D.W. (2011). Cortical constriction during abscission involves helices of ESCRT-III-dependent filaments. *Science* *331*, 1616-1620.
- Hagemeijer, A., and Graux, C. (2010). ABL1 rearrangements in T-cell acute lymphoblastic leukemia. *Genes Chromosomes Cancer* *49*, 299-308.

- Hansen, D.V., Lui, J.H., Parker, P.R., and Kriegstein, A.R. (2010). Neurogenic radial glia in the outer subventricular zone of human neocortex. *Nature* 464, 554-561.
- Harding, B. (1996). Gray matter heterotopia. In *Dysplasias of cerebral cortex and epilepsy*, R. Guerrini, F. Andermann, R. Canapicchi, J. Roger, B.G. Zifkin, P. Pfanner, ed. (Philadelphia, USA: Lippincott-Raven), pp. 81–88.
- Hirotsune, S., Fleck, M.W., Gambello, M.J., Bix, G.J., Chen, A., Clark, G.D., Ledbetter, D.H., McBain, C.J., and Wynshaw-Boris, A. (1998). Graded reduction of Pafah1b1 (Lis1) activity results in neuronal migration defects and early embryonic lethality. *Nat. Genet.* 19, 333-339.
- Horgan, C.P., Hanscom, S.R., and McCaffrey, M.W. (2011). Dynein LIC1 localizes to the mitotic spindle and midbody and LIC2 localizes to spindle poles during cell division. *Cell Biol. Int.* 35, 171-178.
- Houtman, S.H., Rutteman, M., De Zeeuw, C.I. & French, P.J. Echinoderm microtubule associated protein like protein 4, a member of the echinoderm microtubule-associated protein family, stabilizes microtubules. *Neuroscience* 144, 1373-1382 (2007).
- Hueston, J.L., Herren, G.P., Cueva, J.G., Buechner, M., Lundquist, E.A., Goodman, M.B., and Suprenant, K.A. (2008). The *C. elegans* EMAP-like protein, ELP-1 is required for touch sensation and associates with microtubules and adhesion complexes. *BMC Dev. Biol.* 8:110.
- Jaglin, X.H., and Chelly, J. (2009). Tubulin-related cortical dysgeneses: microtubule dysfunction underlying neuronal migration defects. *Trends Genet.* 25, 555-566.
- Kappeler, C., Dhenain, M., Phan Dinh Tuy, F., Saillour, Y., Marty, S., Fallet-Bianco, C., Souville, I., Souil, E., Pinard, J.M., Meyer, G., Encha-Razavi, F., Volk, A., Beldjord, C., Chelly, J., and Francis, F. (2007). Magnetic resonance imaging and histological studies of corpus callosal and hippocampal abnormalities linked to doublecortin deficiency. *J. Comp. Neurol.* 500, 239-254.
- Keays, D.A., Tian, G., Poirier, K., Huang, G.J., Siebold, C., Cleak, J., Oliver, P.L., Fray, M., Harvey, R.J., Molnár, Z., Piñon, M.C., Dear, N., Valdar, W., Brown, S.D., Davies, K.E., Rawlins, J.N., Cowan, N.J., Nolan, P., Chelly, J., and Flint, J. (2007). Mutations in alpha-tubulin cause abnormal neuronal migration in mice and lissencephaly in humans. *Cell* 128, 45-57.

- Kelava, I., Reillo, I., Murayama, A.Y., Kalinka, A.T., Stenzel, D., Tomancak, P., Matsuzaki, F., Lebrand, C., Sasaki, E., Schwamborn, J.C., Okano, H., Huttner, W.B., and Borrell, V. (2012). Abundant occurrence of basal radial glia in the subventricular zone of embryonic neocortex of a lissencephalic primate, the common marmoset *Callithrix jacchus*. *Cereb. Cortex* 22, 469-481.
- Kosodo, Y., Röper, K., Haubensak, W., Marzesco, A.M., Corbeil, D., and Huttner, W.B. (2004). Asymmetric distribution of the apical plasma membrane during neurogenic divisions of mammalian neuroepithelial cells. *EMBO J.* 23, 2314-2324.
- Lee, K.S., Schottler, F., Collins, J.L., Lanzino, G., Couture, D., Rao, A., Hiramatsu, K., Goto, Y., Hong, S.C., Caner, H., Yamamoto, H., Chen, Z.F., Bertram, E., Berr, S., Omary, R., Scrable, H., Jackson, T., Goble, J., and Eisenman, L. (1997). A genetic animal model of human neocortical heterotopia associated with seizures. *J. Neurosci.* 17, 6236-6242.
- Lee, K.S., Collins, J.L., Anzivino, M.J., Frankel, E.A., and Schottler, F. (1998). Heterotopic neurogenesis in a rat with cortical heterotopia. *J. Neurosci.* 18, 9365-9375.
- Ly, C.D., Roche, K.W., Lee, H.K., and Wenthold, R.J. (2002). Identification of rat EMAP, a delta-glutamate receptor binding protein. *Biochem. Biophys. Res. Commun.* 291, 85-90.
- Manent, J.B., Wang, Y., Chang, Y., Paramasivam, M., and LoTurco, J.J. (2009). Dcx reexpression reduces subcortical band heterotopia and seizure threshold in an animal model of neuronal migration disorder. *Nat. Med.* 15, 84-90.
- Martynoga, B., Morrison, H., Price, D.J., and Mason, J.O. (2005). Foxg1 is required for specification of ventral telencephalon and region-specific regulation of dorsal telencephalic precursor proliferation and apoptosis. *Dev. Biol.* 283, 113-127.
- Munji, R.N., Choe, Y., Li, G., Siegenthaler, J.A., and Pleasure, S.J. (2011). Wnt signaling regulates neuronal differentiation of cortical intermediate progenitors. *J. Neurosci.* 31, 1676-1687.
- Paramasivam, M., Chang, Y.J., and LoTurco, J.J. (2007). ASPM and citron kinase co-localize to the midbody ring during cytokinesis. *Cell Cycle* 6, 1605-1612.
- Pollmann, M., Parwaresch, R., Adam-Klages, S., Kruse, M.L., Buck, F., and Heidebrecht, H.J. (2006). Human EML4, a novel member of the EMAP family, is essential for microtubule formation. *Exp. Cell Res.* 312, 3241-3251.

Quinn, J.C., Molinek, M., Martynoga, B.S., Zaki, P.A., Faedo, A., Bulfone, A., Hevner, R.F., West, J.D., Price, D.J. (2007). Pax6 controls cerebral cortical cell number by regulating exit from the cell cycle and specifies cortical cell identity by a cell autonomous mechanism. *Dev Biol.* 302, 50-65.

Ravnan, J.B., Tepperberg, J.H., Papenhausen, P., et al. (2006). Subtelomere FISH analysis of 11688 cases: an evaluation of the frequency and pattern of subtelomere rearrangements in individuals with developmental disabilities. *J. Med. Genet.* 43, 478-489.

Reillo, I., de Juan Romero, C., García-Cabezas, M.A., and Borrell, V. (2011). A Role for Intermediate Radial Glia in the Tangential Expansion of the Mammalian Cerebral Cortex. *Cereb. Cortex* 21, 1674-1694.

Rosen, G.D., Azoulay, N.G., Griffin, E.G., Newbury, A., Koganti, L., Fujisaki, N., Takahashi, E., Grant, P.E., Truong, D.T., Fitch, R.H., Lu, L. and Williams, R.W. Bilateral Subcortical Heterotopia with Partial Callosal Agenesis in a Mouse Mutant. *Cereb. Cortex* 2012 March 27. [Epub ahead of print].

Schneider, A., Benzacken, B., Guichet, A., Verloes, A., Bonneau, D., Collot, N., Dastot-Le-Moal, F., Goossens, M., Taine, L., Landais, E., Gaillard, D., and Doco-Fenzy, M. (2008). Molecular cytogenetic characterization of terminal 14q32 deletions in two children with an abnormal phenotype and corpus callosum hypoplasia. *Eur. J. Hum. Genet.* 16, 680-687.

Shitamukai, A., Konno, D., and Matsuzaki, F. (2011). Oblique radial glial divisions in the developing mouse neocortex induce self-renewing progenitors outside the germinal zone that resemble primate outer subventricular zone progenitors. *J. Neurosci.* 31, 3683-3695.

Stoykova, A., Treichel, D., Hallonet, M., and Gruss, P. (2000). Pax6 modulates the dorsoventral patterning of the mammalian telencephalon. *J. Neurosci.* 20, 8042-8050.

Suprenant, K.A., Dean, K., McKee, J., and Hake, S. (1993). EMAP, an echinoderm microtubule-associated protein found in microtubule-ribosome complexes. *J. Cell Sci.* 104, 445-450.

Suprenant, K.A., Tuxhorn, J.A., Daggett, M.A., Ahrens, D.P., Hostetler, A., Palange, J.M., VanWinkle, C.E., and Livingston, B.T. (2000). Conservation of the WD-repeat, microtubule-binding protein, EMAP, in sea urchins, humans, and the nematode *C. elegans*. *Dev. Genes Evol.* 210, 2-10.

- Takahashi, T., Goto, T., Miyama, S., Nowakowski, R.S., and Caviness, V.S. Jr. (1999). Sequence of neuron origin and neocortical laminar fate: relation to cell cycle of origin in the developing murine cerebral wall. *J. Neurosci.* *19*, 10357-10371.
- Tegha-Dunghu, J., Neumann, B., Reber, S., Krause, R., Erfle, H., Walter, T., Held, M., Rogers, P., Hupfeld, K., Ruppert, T., Ellenberg, J., and Gruss, O.J. (2008). EML3 is a nuclear microtubule-binding protein required for the correct alignment of chromosomes in metaphase. *J. Cell Sci.* *121*, 1718-1726.
- Vandesompele, J., De Preter, K., Pattyn, F., Poppe, B., Van Roy, N., De Paepe, A., and Speleman, F. (2002). Accurate normalization of real-time quantitative RT-PCR data by geometric averaging of multiple internal control genes. *Genome Biol.* *3*, research0034.1-research0034.11.
- Van Karnebeek, C.D., Quik, S., Sluijter, S., Hulsbeek, M.M., Hoovers, J.M., and Hennekam, R.C. (2002). Further delineation of the chromosome 14q terminal deletion syndrome. *Am. J. Med. Genet.* *110*, 65-72.
- Wang, X., Tsai, J.W., Lamonica, B., and Kriegstein, A.R. (2011). A new subtype of progenitor cell in the mouse embryonic neocortex. *Nat. Neurosci.* *14*, 555-561.
- Weimer, J.M., Yokota, Y., Stanco, A., Stumpo, D.J., Blackshear, P.J., and Anton, E.S. (2009). MARCKS modulates radial progenitor placement, proliferation and organization in the developing cerebral cortex. *Development* *136*, 2965-2975.
- Welker, E., Armstrong-James, M., Bronchti, G., Ourednik, W., Gheorghita-Baechler, F., Dubois, R., Guernsey, D.L., Van der Loos, H., Neumann, P.E. (1996). Altered sensory processing in the somatosensory cortex of the mouse mutant barrelless. *Science* *271*, 1864-1867.
- Zhang, Y., Maksakova, I.A., Gagnier, L., van de Lagemaat, L.N., Mager, D.L. (2008). Genome-wide assessments reveal extremely high levels of polymorphism of two active families of mouse endogenous retroviral elements. *PLoS Genet.* *4*(2):e1000007.

LEGENDS TO FIGURES

Figure 1. Genetic Linkage of the *HeCo* Mutation and Identification of a Retrotransposon in *Eml1*

(A) The 12q *HeCo* candidate region identified by first (1) and second (2) rounds of genotyping and the final candidate region (3) between rs29151683 and a non referenced SNP in *Dlk1*. ▼, internal SNPs homozygous for the NOR-*HeCo* alleles in all affected F2 mice; ▽, flanking boundary SNPs and additional informative SNPs from genes *Dlk1*, *Dync1h1*, *Mark3*, and *Adam6*, heterozygous (HZ) in some F2 individuals. Black bars, regions of homozygosity; grey bars, excluded regions; dotted bars, non-excluded regions (informative SNPs and individuals in Table S6).

(B) *Eml1* gene structure (assembly NCBI37/mm9, July 2007). The canonical isoform (NCBI NM_001043335.1) begins in exon 2.

(C) *Eml1* exon 22 could not be PCR amplified from *HeCo* genomic DNA.

(D) Aberrant transcripts were detected by nested RT-PCR between exons 19 and 23, from two distinct *HeCo* (1 and 2) samples; RT, reverse transcriptase.

(E) An ETn element insertion in intron 22 was identified by sequencing a >5 kb PCR product from *HeCo* genomic DNA.

(F) Schema of the ETn element in *Eml1* intron 22 with chimeric transcripts detected by RT-PCR. Some *Eml1* transcripts finish in the ETn, others start in the ETn and finish in *Eml1* exon 23. Black bars, PCR products; ⇔, *Eml1* primers; →, ETn primers; SD, splice donor, SA, splice acceptor, pA, potential polyadenylation sites; STOP, in frame stop codons; ATG, potential start codons (the ETn contains additional SD, SA and pA sites, not represented here). See also Figure S1.

Figure 2. Mutations in Human *EML1* and *Eml1* Expression

(A-C) *EML1* mutations in a family with giant bilateral heterotopia. (A) Schema of a non-consanguineous family with unaffected parents and three affected boys. (B) Sequence chromatograms showing the 2 mutations (black bars). (C) Patient axial T1 weighted MRI sections (upper row, left and centre) show huge subcortical masses (left, arrowhead) that start at the ventricles (centre) and expand to the subcortical white matter. The cortex close to the lesion is polymicrogyric (left, arrow). White matter is present between the heterotopia and cortex. Corpus callosum agenesis and mild brainstem hypoplasia are obvious when comparing patient (upper right) and control (ctrl, lower right, 6 years old) T1 sagittal sections (arrowhead, corpus callosum; arrow, brainstem). Moderate ventricular enlargement, most prominent in the left lateral ventricle, is

observed. Cerebellum and hippocampus are normal. Patient and control images are at the same scale.

(D) Predicted domains of the Eml1 protein (Hueston et al., 2008; Bechstedt et al., 2010). CC, coiled-coil; HELP domain; 1-11, predicted WD40 motifs.

(E-G) Expression of recombinant WT and mutant Eml1 in Vero cells. (E) A fraction of WT tagged Eml1 is associated with the MT cytoskeleton (right, higher magnification of boxed area). After cold treatment, WT Eml1-labeled puncta (F left, G) strongly associate with repolymerizing MTs at the MT asters (arrows) while mutant Eml1 (T243A) is not associated (F middle and right, G) although asters are detected with antibody to α -tubulin (insets).

(H-P) *Eml1* expression in brains of mouse (H-N) and ferret (O,P). (H-L) *Eml1* is present in the VZ of the dorsal cortical wall at E13.5 (H, L, blue staining, arrow) and in both the VZ and CP at E14.5 (I) and E15.5 (J). At E17.5 a strong CP expression is observed with no further expression in the VZ (K). The dorsal thalamic neuroepithelium is also labeled at E13.5 (L, asterisk). At E17.5 (M) thalamic nuclei (upper arrow) and the lateral olfactory tract nucleus (lower arrow) are labeled. In adult mouse brain (N) labeling is observed in thalamus and piriform cortex (arrow). (O-P) Ferret *Eml1* in the P0 forebrain is detected strongly in the CP and in the proliferative layers (O, arrows). MZ, marginal zone; SP, subplate; IZ, intermediate zone; OSVZ, outer subventricular zone; ISVZ, inner SVZ. H-N, coronal sections, O-P, sagittal section. Scale bars 500 μ m (O), 400 μ m (M and N), 200 μ m (H-L, P), 10 μ m (F), and 5 μ m (E). See also Figures S2-S4.

Figure 3. Eml1 Localization in Dissociated Neuronal Progenitors and Cortical Neurons *In Vitro* and Analysis of WT and *HeCo* Cultures

(A-C) In neuronal progenitors in interphase (A) YFP-EML1 is distributed throughout the cell in the form of puncta. In telophase (B) it accumulates in the region of the midbody ring at either side of intercellular bridges. YFP-EML1 labeled midbody ring remnants are sometimes observed asymmetrically after cell separation (C). Co-labeling with Pax6 (A), γ tubulin (B), KIF1A (C) and Hoechst. A', A'', B' and C', enlargements, B'' and C'', schematic representations, of boxed areas.

(D) Flag-Eml1 puncta in a neuron, partially co-localizing with MTs traversing the nucleus and accumulating in growth cones (D', arrow) and at positions along the neuronal process (D'').

(E) YFP-EML1 partially colocalizes with tyrosinated tubulin in perinuclear regions. Punctate labeling aligns with MTs in a growth cone (E'), where little co-localization is observed.

(F) YFP-EML1 partially co-localises with dynein in a neuron at 1 DIV.

D', D'', E' and F' are enlargements of boxed areas in D, E and F (confocal images).

(G) The percentage of Ki-67⁺ proliferating cells is significantly reduced in *HeCo* compared to WT cultures (Student *t*-test, * $p=0.023$). Quantification of Pax6⁺, Tbr2⁺ and Dcx⁺ cells individually showed no significant differences. Data are shown as mean \pm SEM. Scale bars, 10 μ m (D, E, F), 8 μ m (A, B, C), 5 μ m (D', D'', E'), and 1 μ m (A', B', C'). See also Figures S5 and S6.

Figure 4. Cell Accumulation in the Dorso-Medial Regions of Developing *HeCo* Cortex

(A-D) At E17, in the *HeCo* cortex, early born Tbr1⁺ (B and B') and late born Cux1⁺ (D) neurons are trapped within the heterotopia (#). Nestin labeling shows disorganized RGCs processes throughout the heterotopia (B'' and B''').

(E-F') After *in utero* electroporation at E15.5, less EGFP⁺ cells have reached the cortex in *HeCo* embryos at P3, and they fail to form a distinct cortical layer II/IV although the morphology of cells reaching the CP is similar to WT (E' and F'). Many of them remain sequestered in the heterotopia (#).

(G-J) At P3, Tbr1⁺ neurons have reached layer VI (H) whereas many Cux1⁺ neurons remain trapped within the heterotopia (J) and the radial extent of the Cux1⁺ cortical layer II/IV is reduced above the heterotopia in the *HeCo* cortex compared to WT. A column of Cux1⁺ cells is present between the heterotopia and layer II/IV (J and J', arrow).

A''', B''', E', F', H' and J' are higher magnifications of A'', B'', E, F, H and J, respectively. Cell nuclei of coronal brain sections were counterstained with Hoechst. Ctx, cortex; Hip, hippocampus; LV, lateral ventricle. Scale bars, 400 μ m (G-J), 200 μ m (A-D, H', J', E, F), 100 μ m (E', F') and 25 μ m (A', B'). See also Figures S7 and S8.

Figure 5. Proliferation Defects in the Cortex of *HeCo* Mice

(A-B') At E15, BrdU⁺ progenitors are observed in all zones of the *HeCo* cortex and intermix with Tbr1⁺ neurons of future layer VI, while WT BrdU⁺ cells are mostly restricted to the VZ and SVZ.

(C-I) At E13, increased numbers of BrdU⁺ cycling progenitors are present in the *HeCo* forebrain. After a 30 min BrdU pulse (C and D) ectopic *HeCo* progenitors are observed in the IZ and CP as in (B), with an increased labeling index (G). After a 24 h BrdU pulse (E and F) the total number of BrdU⁺ progenitors is increased in *HeCo* brains (H) with a reduced cell cycle exit index in the SVZ, IZ and CP (I).

(J-K'') At E19, *HeCo* ectopic progenitors surround the heterotopia (#) and are often BrdU⁺ and Ki-67⁺ (K'').

(L-N) E13 Caspase 3 immunostaining reveals a significant increase in the total number of apoptotic cells in *HeCo* (N).

A', B', K' and K'' are higher power views of A, B and K, respectively. Cell nuclei of coronal brain sections were counterstained with Hoechst. Scale bars, 200 μm (A, B, J, K), 100 (A', B', C-F, K', L, M) and 50 μm (K''). Data are shown as the mean + SEM. Student *t*-test are used for all layers and Multiple Factor ANOVA with post-hoc univariate analysis based on estimated marginal means, MFA, for each layer. * $p < 0.05$, ** $p < 0.01$, *** $p < 0.001$. See also Figure S8.

Figure 6. Altered Distribution of Apical and Basal Progenitors in IZ and CP of *HeCo* Mice

PH3/Pax6 (A-D) and PH3/Tbr2 (E-H) double staining, at E13 and E16. At E13 the distribution of mitotic progenitors was altered in *HeCo* brains, with a decrease in the VZ and a concomitant increase in the other zones (I). However overall numbers of labeled cells were similar in WT and *HeCo*. Both apical Pax6⁺ and basal Tbr2⁺ progenitors divide ectopically in the *HeCo* IZ and CP, shown by PH3 labeling (B', F', arrow heads, and J). B' and F' are higher power views of B and F, respectively. Cell nuclei of coronal brain sections were counterstained with Hoechst. Scale bars 100 μm (A-H) and 20 μm (B', F'). Data are shown as the mean \pm SEM. MFA, * $p < 0.05$, ** $p < 0.01$, *** $p < 0.001$.

Figure 7. Features of Radial Glia and Ectopic Progenitors in *HeCo* Cortices

(A-F) At E13, the number of P-vim⁺ RGCs is decreased in the VZ while increased in the IZ and CP of *HeCo* brains, resulting in a similar number overall compared to WT (E). P-vim⁺/Pax6⁺ cells are increased in the *HeCo* SVZ, IZ and CP (F, left). Some P-vim⁺ basal processes appear misoriented (B'' and B''', arrows). P-vim⁺/Pax6⁺ cells are shown by filled arrow heads in B' and B'''. Pvim⁺/Tbr2⁻ are indicated by empty arrow heads in D' and D''. Rare P-vim⁺/Tbr2⁺ cells were identified and found in similar overall numbers in WT and *HeCo* brains, but with an altered layer distribution in the latter, including in the VZ (F, right).

(G and H) β -catenin labeling shows apparently normal RGC endfeet at the ventricle lining in *HeCo* brains with typical honeycomb apical membrane structure.

(I-L) The proportion of metaphasic nuclei with a vertical cleavage plane (K) is significantly decreased in mutant brains (L) in favor of oblique cleavages (J).

A', B'-B''', D' and D'' are higher power views of A, B and D, respectively. Cell nuclei of coronal brain sections were counterstained with Hoechst. Scale bars 100 μm (A-D), 20 μm (A', B'-B''', D', D'', G and H) and 5 μm (I-K). Data are shown as the mean + SEM. χ^2 test is used in J, MFA in E and F. * $p < 0.05$, ** $p < 0.01$, *** $p < 0.001$.

Figure 8. Graphic Summary of Heterotopia Development in *HeCo* Mutant Mouse Brain

Schemas of cortical development in WT (upper) and *HeCo* (lower) mouse brains are indicated, at E13, E16 and E19. In WT, progenitors are restricted to the VZ and SVZ, whereas in *HeCo*, as early as E13, a proportion of progenitors is abnormally distributed in the IZ and CP. At E16, an accumulation of neurons begins in the IZ, and RGC processes are perturbed in this region. Columns of neurons are present between the heterotopia and CP at later stages when the heterotopia becomes populated by superficial neurons. Below, vertical and oblique mitotic cleavages at the ventricle lining are schematized. In *HeCo* progenitors, a defect of *Eml1* induces a relative increase of oblique cleavages, likely to modify apical membrane inheritance and to lead to increased numbers of detached progenitors which continue to divide ectopically.

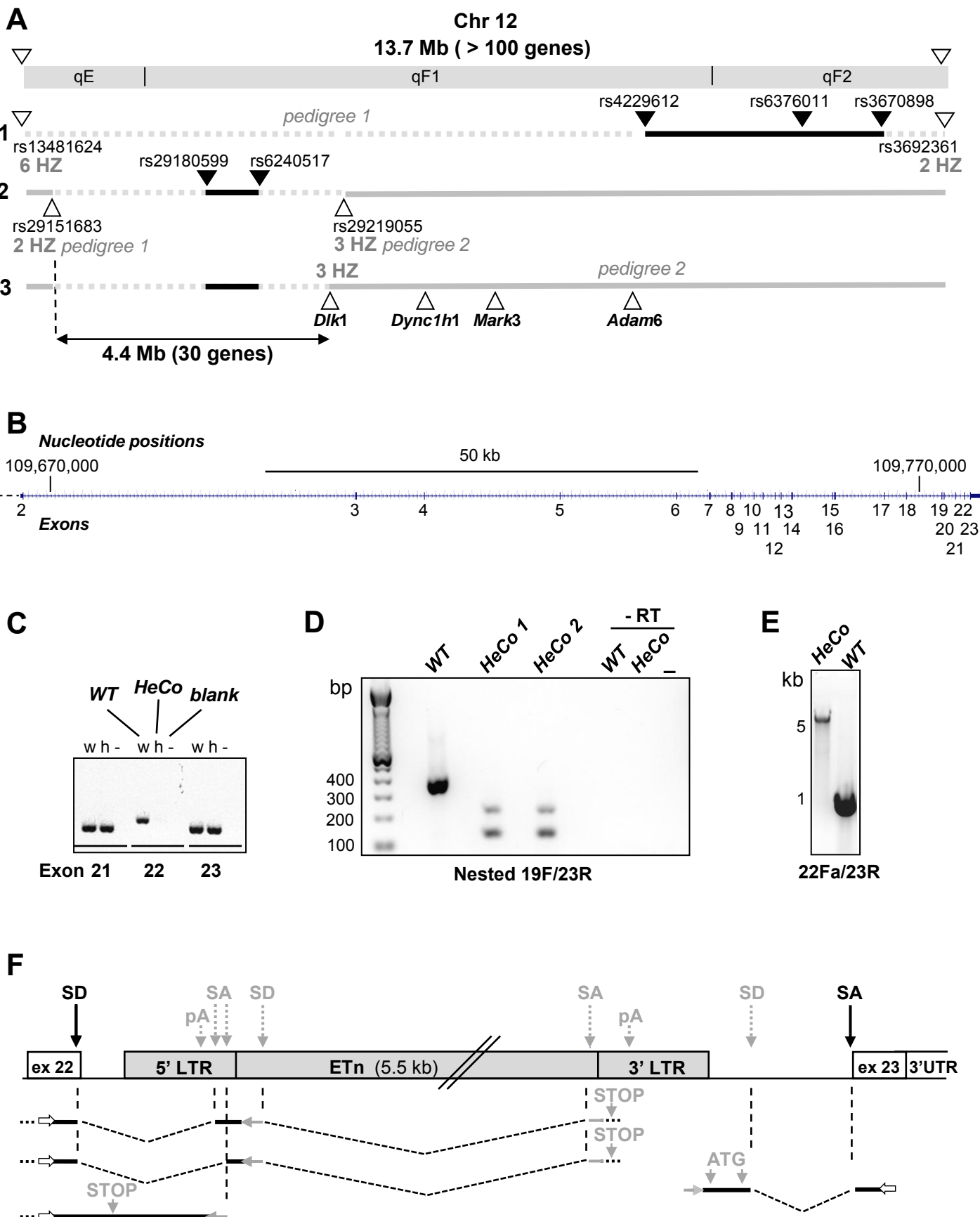


Figure 1

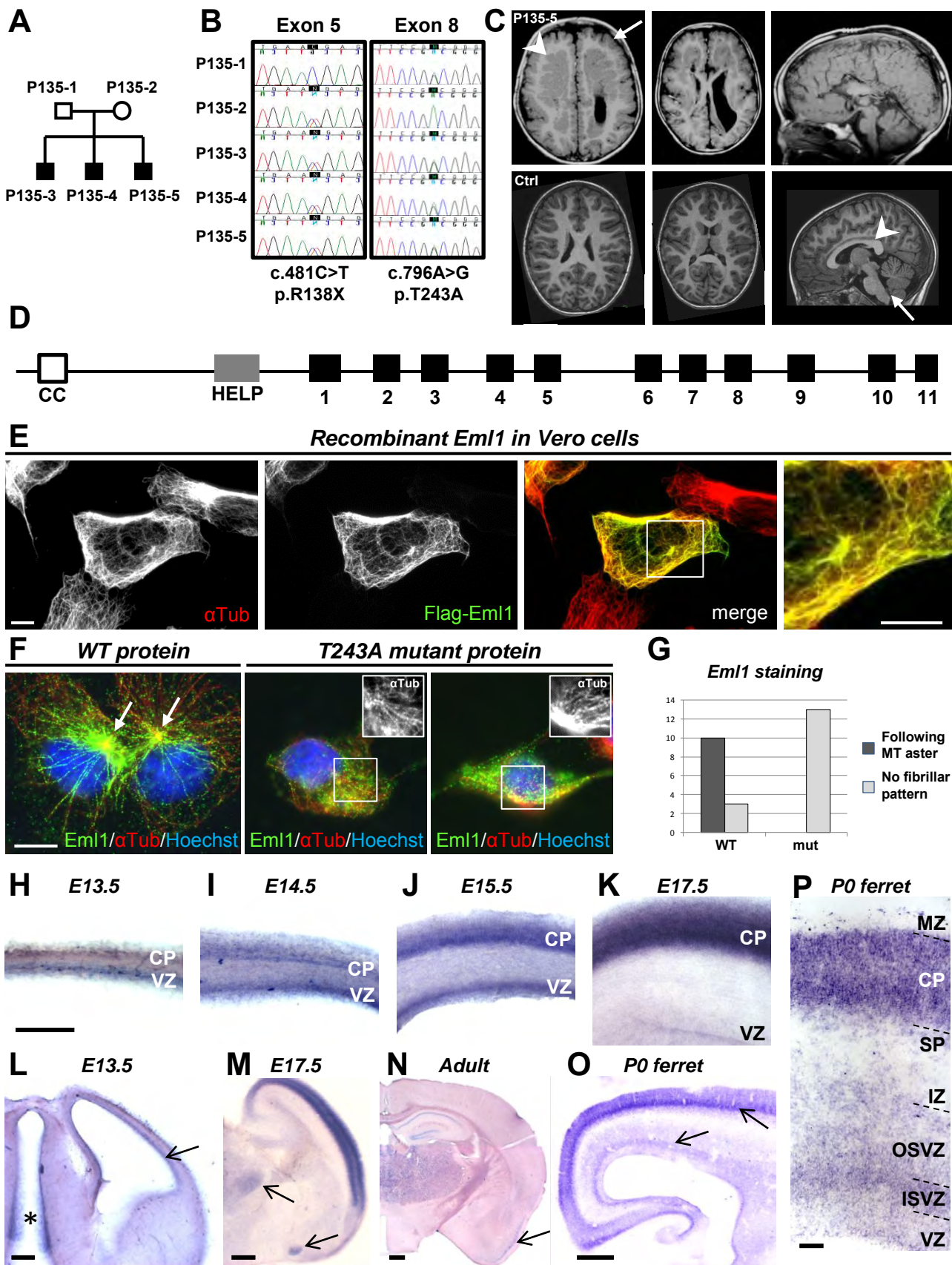
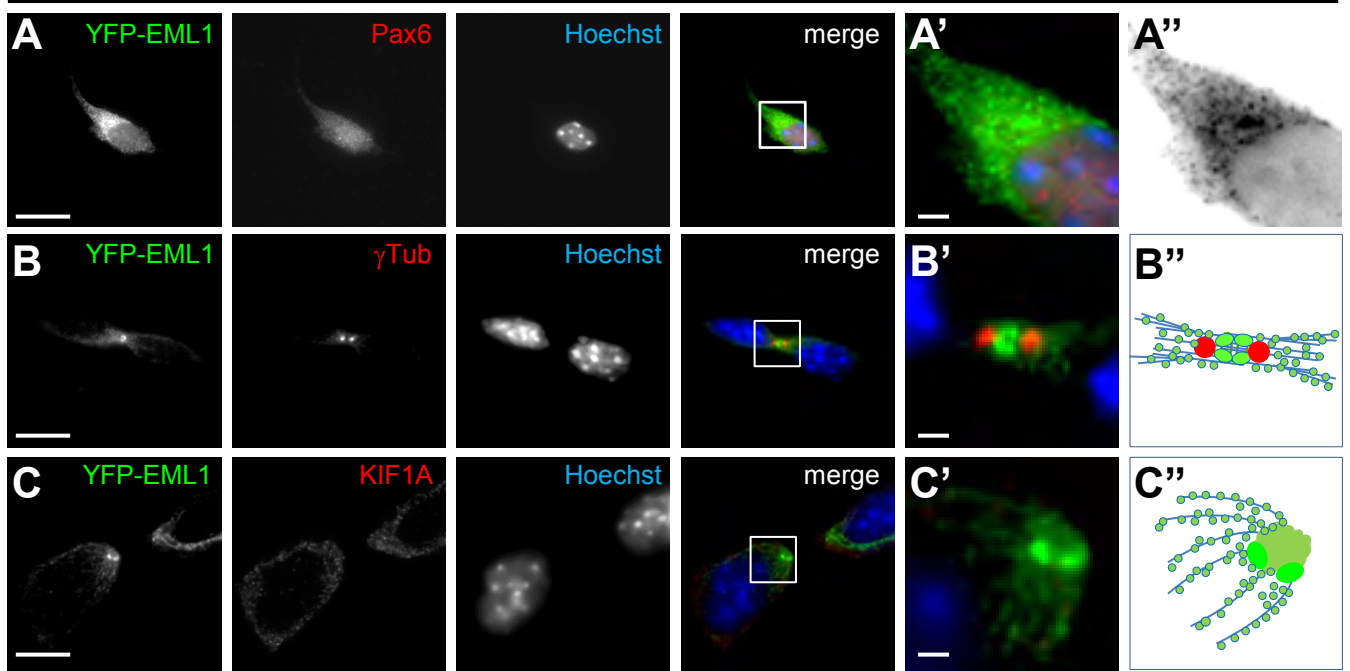


Figure 2

Recombinant Eml1 in neural progenitors



Recombinant Eml1 in post-mitotic neurons

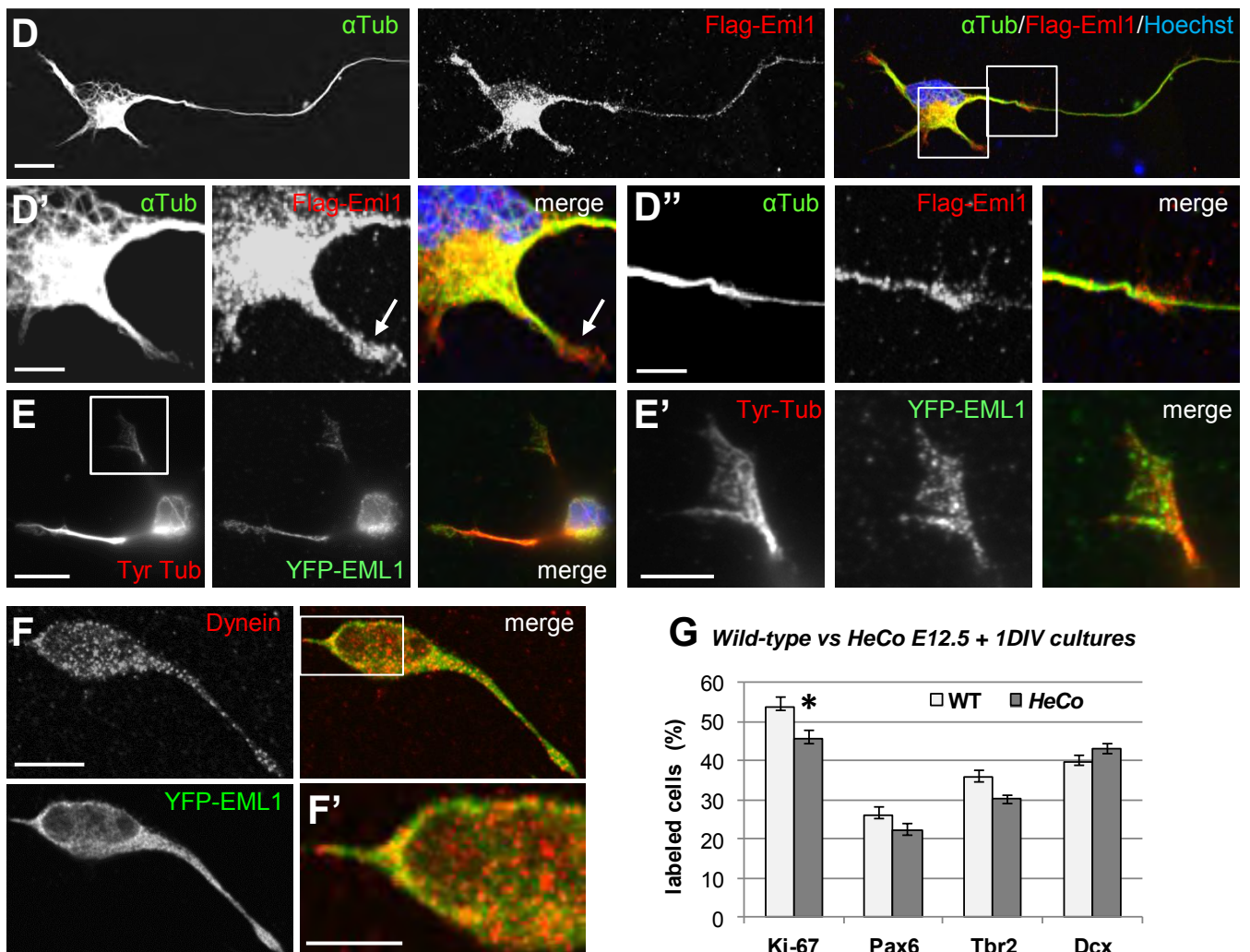


Figure 3

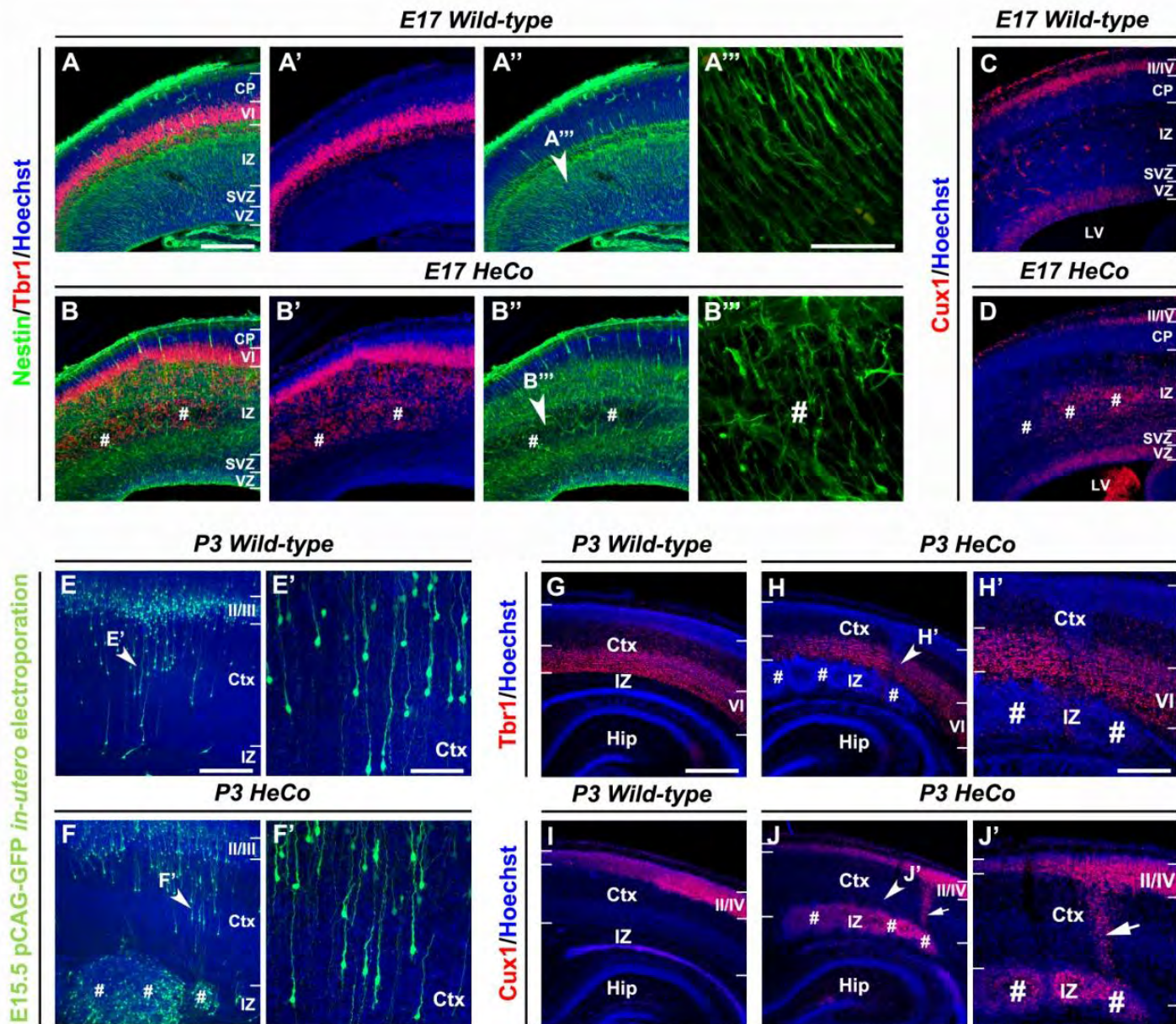


Figure 4

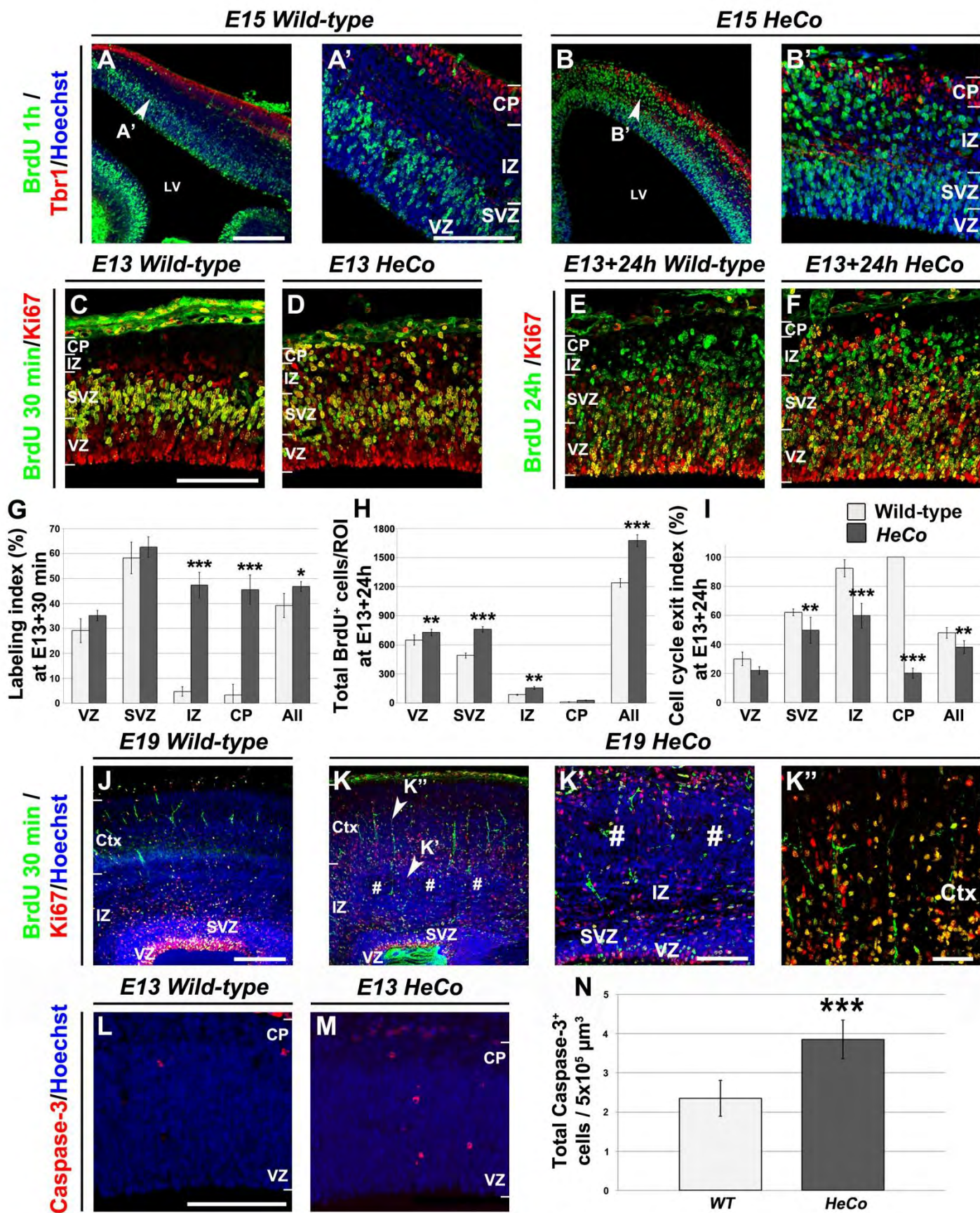


Figure 5

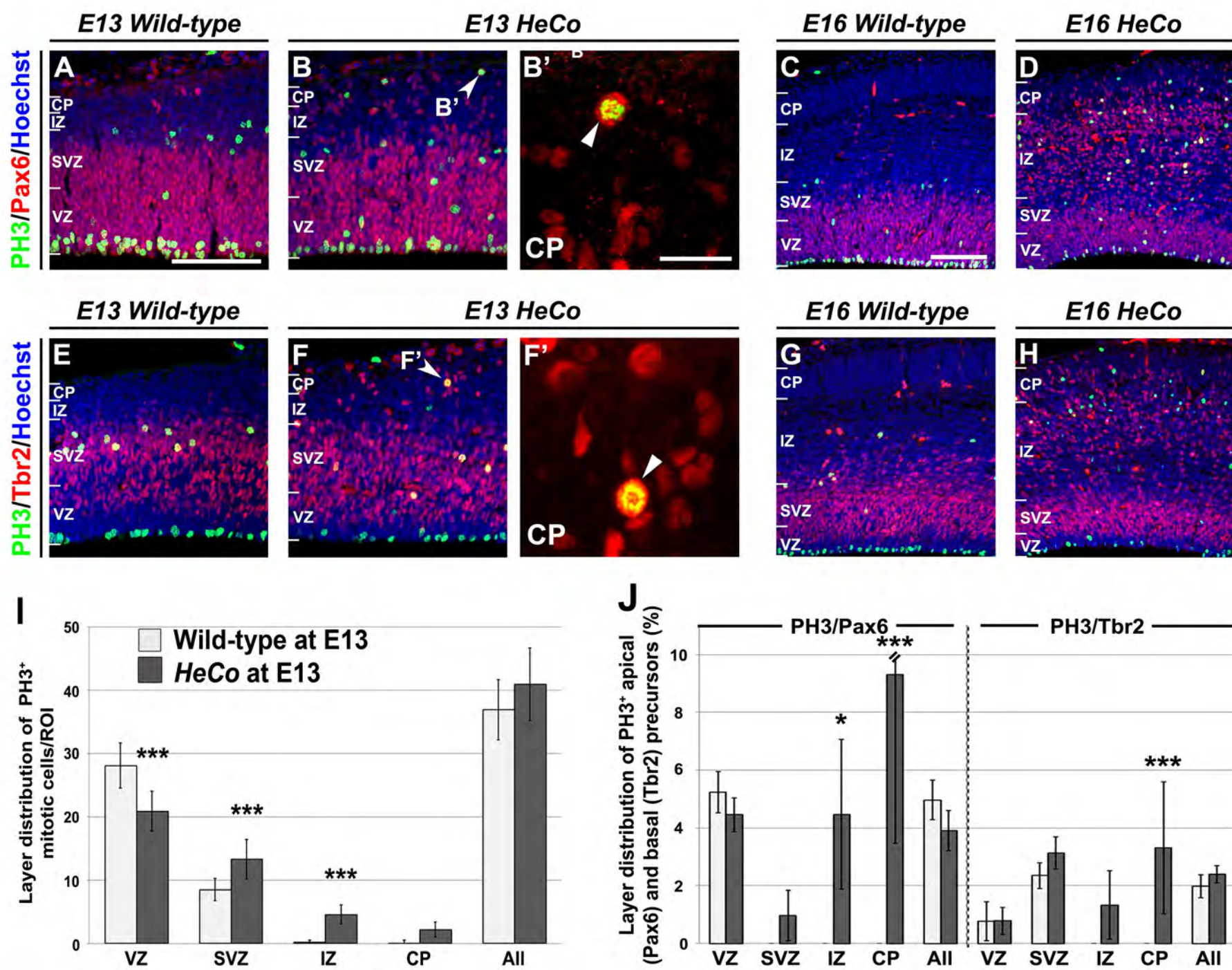
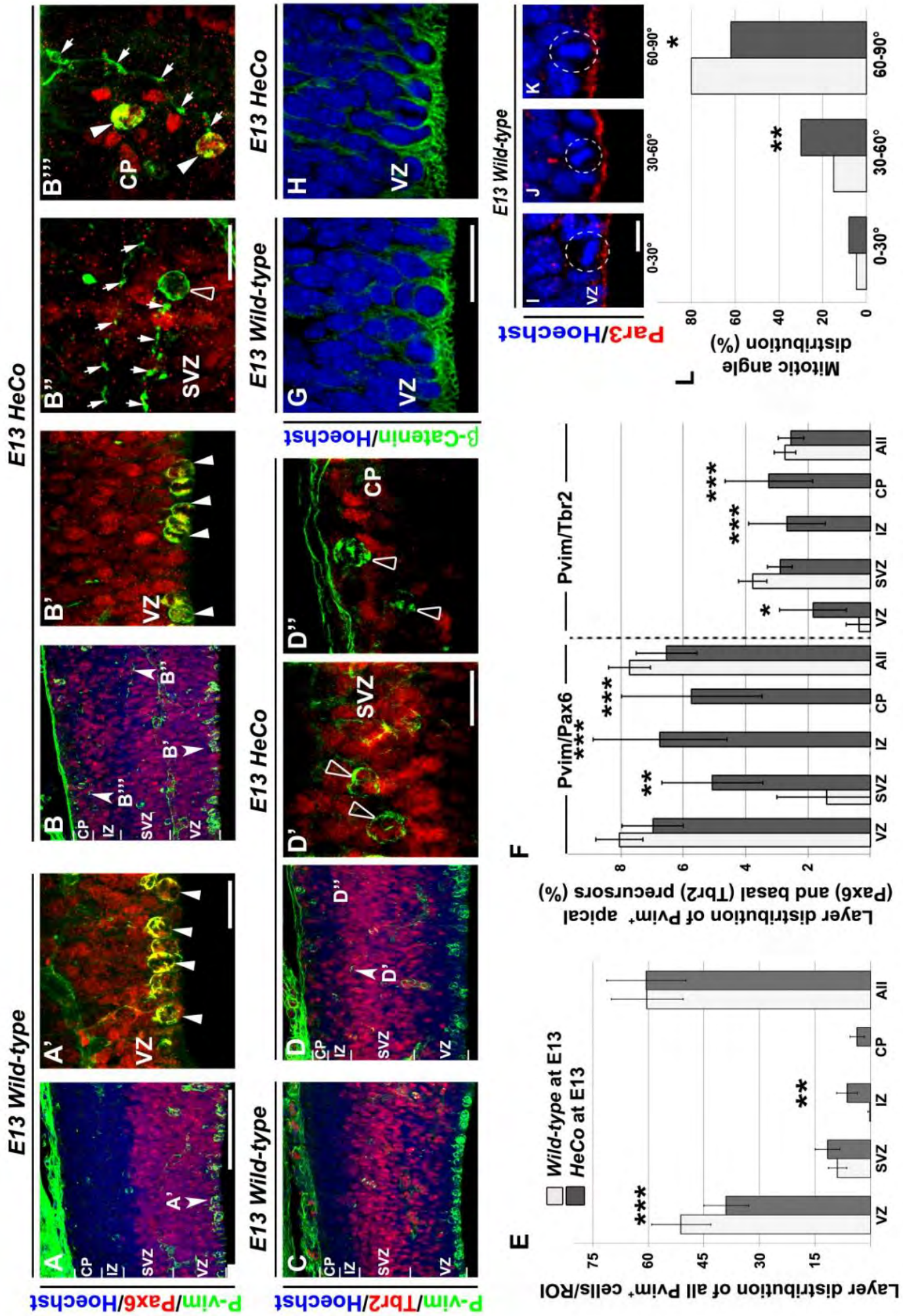


Figure 6

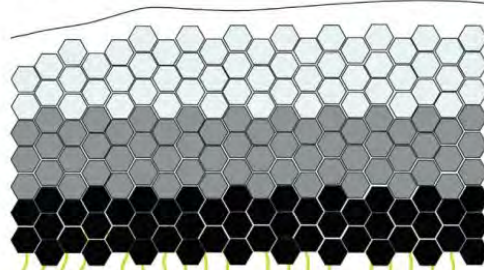


Wild-type

E19

E13

E16



CP

IZ

SVZ

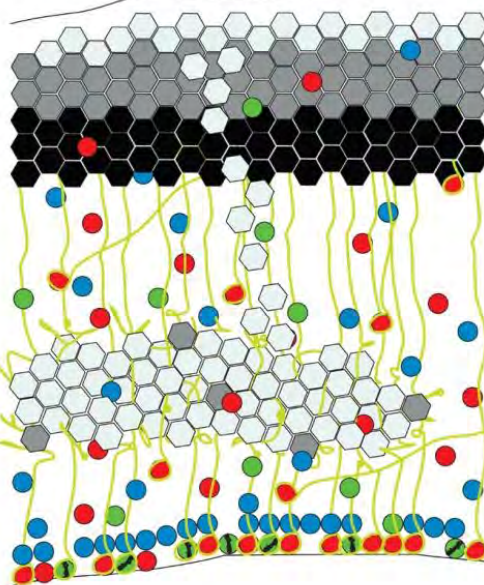
VZ

HeCo

E19

E13

E16



CP

IZ

SVZ

VZ

● Pax6

● Tbr2

● PH3 (Pax6 or Tbr2)

⊥ Metaphasic DNA

⊖ Midbody

● Neuron layer VI

● Neuron layer V

● Neuron layer IV/II

Vertical:

2 attached progenitors

Oblique:

1 detached progenitor

1 attached progenitor

VZ

RGC: Disorganized Misoriented

Figure 8

Mutations in *EML1/Eml1* Lead to Misplaced Neuronal Progenitors during Cortical Development and Massive Heterotopia in Mouse and Human

Michel Kielar, et al.

SUPPLEMENTAL INFORMATION

Supplemental Figure S1. Schema of the 13.7 Mb *HeCo* Candidate Region and Analysis of *Eml1* in WT and *HeCo* DNAs. Related to Figure 1.

(A) Schema of the chromosomal region identified during the first round of genotyping with key SNPs (▼, internal homozygotes; ▽, flanking heterozygotes) with Refseq genes indicated (captured image from Genome Browser, <http://genome.ucsc.edu/>; assembly NCBI37/mm9, July 2007). This region shows synteny with human chromosomes 14q and 7q. *Eml1* is boxed in red. The 15 genes initially sequenced which showed no mutations are *Clmn*, *Tcl1*, *Yy1*, *Dlk1*, *Mark3*, *Adam6b*, *Tmem121*, *Adam6a*, *Zfp386*, *Vipr2*, *Wdr60*, *Esyt2*, *Ncapg2*, *Ptprn2*, *Rapgef5*.

(B) Schema showing genomic region containing *Eml1* exons 22 and 23. PCR products and sequences were identical between WT and *HeCo* except for exon 22 which could not be amplified from *HeCo* DNAs, using primers annealing to nucleotides -85 to -66 upstream and +117 to +96 downstream of exon 22 (→, primers; ✕, PCRs which failed to give a product).

(C) RT-PCR between the exon 17-18 boundary and within exon 22 shows identical amplification products from *HeCo* and WT RNAs. RT, reverse transcriptase.

(D) RT-PCR between exons 19 and 23 shows an amplification product from WT RNAs only.

(E) A junction fragment between *Eml1* exon 22 and the ETn 5'LTR is amplified specifically from *HeCo* genomic DNA and not from WT DNA of the same genetic background.

Supplemental Figure S2. Sequence of the HELP Domain and Expression of Recombinant *Eml1*. Related to Figure 2.

(A) *Eml1* (814 aa, Uniprot Q05BC3-1) contains a conserved HELP domain in its N terminus (aa 183-259). This domain is shown from human proteins EML1, 4, 2, the purple sea urchin *Strongylocentrotus purpuratus* (EMAP Sp), the ELP protein from *Caenorhabditis elegans* (ELP Ce), ciliary WD repeat-containing protein Ctxp80 from the protist *Euplotes octocarinatus* (Ctxp Eo) and *Drosophila melanogaster* (Droso). The mutated threonine residue identified in patients (T243A, arrow) is conserved in mammalian EML1, 2 and 4, as well as in ELP Ce and EMAP Sp (Li and Suprenant, 1994; Eudy et al., 1997; Lepley et al., 1999; Heidebrecht et al., 2000; Hueston et al., 2008). Other family members contain a serine

(Droso and EML3, Bechstedt et al., 2010; Genbank accession AK093146) or an asparagine (Ctxp80 Genbank accession AJ251505), suggesting that a polar aa is important at this position (<http://www.ncbi.nlm.nih.gov/Structure/cdd/cdd.shtml>).

(B-E) Western blot expression of transfected recombinant proteins in non-neuronal cells. (B) Untagged Eml1 expressed from pCAGIG vector, detected with an antibody to Eml1. (C) WT Eml1 protein compared to mutated T243A Eml1 (extracts from two different transfection experiments for each plasmid, control with an antibody to α -tubulin). (D) Flag-Eml1 expressed from pNter3xFLAG-CMV vector, detected with an antibody to Flag. (E) Same construct detected with an antibody to Eml1. Western blots also confirmed soluble and non-soluble fractions of the recombinant protein (not shown). Western blot analyses to characterize normal and mutant proteins in mouse brain and human fibroblasts were unsuccessful due to the lack of specificity of different antibodies to Eml1 tested in these cells. (F) Vero cells transfected with Flag-Eml1 constructs and fixed with PFA, without detergent extraction. Flag-Eml1 shows a largely cytoplasmic labeling not resembling the MT network. Right, higher magnification of the boxed region.

(G) COS7 cells transfected with Flag-Eml1 constructs and fixed with methanol. Two different stages of cell cycle are shown. As in F, Flag-Eml1 is mainly cytoplasmic, although a faint accumulation at the spindle poles is observed (lower panel), without detergent extraction. Scale bar, 5 μ m (F).

Supplemental Figure S3. Eml1 Association with MTs, in Sedimentation and Re-Polymerization Experiments, Effect of T243A Mutation. Related to Figure 2.

(A and B) GST-EML1 interacts directly with MTs *in vitro*. (A) When incubated in the presence of taxol-stabilized MTs assembled from 10 μ g of purified tubulin (left), a major fraction of GST-EML1 (MW 116 kDa) cosediments with the MT pellet (P), whereas in the presence of the same amount of unpolymerized tubulin (right), GST-EML1 largely remains in the supernatant (S). (B) After incubation with MTs under the same conditions as in (A), the GST control protein (MW 26 kDa) remains in the supernatant. Upper Western blots, antibody to GST and lower Western blots, antibody to α -tubulin.

(C) Cold-treated Vero cells (0 min, after 30 min depolymerization at 4°C) were restored to 37°C for 2, 4, 7 or 15 min as indicated, before detergent extraction and fixation. At 2 min, a strong localization of untagged WT Eml1 is observed at the aster of nascent MTs (arrows) and then progressively extends to the overall array of MTs.

(D) Untagged recombinant Eml1 is detected in untreated Vero cells with the antibody to Eml1 after detergent extraction. A MT-association is observed for the WT version (upper row) whereas localization of the T243A mutant version (lower row) is altered, showing less association with the MTs and a more predominant punctate appearance. This result was consistently obtained in multiple experiments. Scale bars, 20 μm (C) and 5 μm (D).

Supplemental Figure S4. *In situ* Hybridization of *Eml1* in the Developing Mouse Brain, Additional Images. Related to Figure 2.

(A) Expression in E13.5 dorsal cortex (upper, antisense probe; lower, sense probe).

(B and C) At E13.5 and E14.5, expression is observed in the VZ at the dorsal-ventral telencephalon boundary but tapers off in ventral telencephalon VZ (left, antisense probe; right, sense probe).

(D and E) Labeling of *Eml1* at E14.5 and E15.5 in both the VZ and the CP (arrows). A high lateral to low medial gradient is obvious.

(F) Strong two-layered expression in the CP at E17.5 with no further expression in the VZ. Faint expression in the hippocampus.

(G-H') No *Eml1* transcript is detected in the *HeCo* developing brain at E17.5 (H and H') compared to WT sections (G and G').

(I and J) Labeling of the medial edge of the developing striatum (arrow) at E15.5 and E17.5, suggesting that *Eml1* may be expressed in retinoic acid synthesizing cells (Li et al., 2000).

(K) At P1 the expression resembles E17.5, with a stronger expression in superficial layers II and III and a lower expression in deeper layers.

(L) Expression continues in the adult in some cells of the isocortex, and in CA1 pyramidal and dentate gyrus (DG) cells of the hippocampus.

(M) Strong rostral labeling of *Eml1* at E15.5, particularly in more lateral regions (upper). On the right are schematized the levels of the sections shown on the left according to The Mouse Brain in Stereotaxic Coordinates (Paxinos and Franklin, 2001). r, rostral; c, caudal.

(N-S) Antisense (N-P) and sense (Q-S) probes hybridized to adjacent mouse adult cortex sections. Faint labeling is observed in superficial and deeper layers of the somatosensorial cortex (N, arrows) and in the cingulate cortex (O, arrows). Labeling in the CA1 and DG regions of the hippocampus and little labeling in the CA3 region (P). Coronal sections except in (M), sagittal. Scale bars, 400 μm (G, I, J, N-S) and 200 μm (A-F, G', K, L).

Supplemental Figure S5. Characterization of Mixed Progenitor and Neuronal Cultures and Recombinant Eml1 in Neuronal Progenitors. Related to Figure 3.

(A) Ki-67, Pax6, Tbr2 and Dcx immunolabelings of cultures derived from WT E12.5 dissociated cortex and fixed after 1 DIV. (B-F) Recombinant YFP-EML1 in neuronal progenitors at different stages of the cell cycle. Co-labeling with tyrosinated tubulin (B), Pax6 (C), γ tubulin (D), and γ adaptin (E). Antibody to spastin gave no specific labeling (F). In metaphase (B) YFP-EML1 is ubiquitously distributed in the form of puncta. During anaphase, telophase and cytokinesis, an enrichment of YFP-EML1 is observed at the midbody and surrounding region (C-F). Right column images in B-F are higher magnifications of boxed areas. Scale bars, 100 μm (A), 8 μm (B-F, left) and 1 μm (B-F, right).

Supplemental Figure S6. Recombinant Eml1 in Dissociated Cortical Neurons and Pax6 and Tbr2 Populations in *HeCo* versus WT Progenitor Cultures. Related to Figure 3.

(A-B') Analysis of Dcx⁺ neurons (see Supplemental Experimental Procedures). No obvious differences were observed globally in neuron morphologies with approximately equal proportions of monopolar, bipolar and multipolar neurons present in WT and *HeCo* cultures. A representative growth cone from each genotype is shown. No significant differences were observed in mean surface areas (WT, 52.8 μm^2 (range 24.8–129.3), *HeCo*, 51.4 μm^2 (range 23.5–133.3) or mean perimeters (WT, 83 μm (range 63.8–96.3), *HeCo*, 83 μm (range 78.1–90.4).

(C-L) WT and *HeCo* dividing neuronal progenitors labeled with Pax6 and Tbr2. Centrosomes were identified by γ -tubulin labeling. No obvious centrosome abnormalities were observed in Pax6⁺ *HeCo* cells. No major differences in the staining patterns of acetylated tubulin were observed in dividing Pax6⁺ and Tbr2⁺ *HeCo* versus WT cells. Scale bars, 10 μm (A, C, G and K) and 5 μm (A' and K').

Supplemental Figure S7. Characterization of Migrating EGFP Expressing Cells in *HeCo* and WT Mice. Related to Figure 4.

(A-K) The density of EGFP⁺ cells (A and E, and indicated with white spots in B and F) having reached the IZ and CP, 3 DIV after E15.5 *ex vivo* electroporation, was reduced in *HeCo* slices although motility parameters in the IZ and CP were similar for WT and *HeCo* neurons (J and K). Similar trajectories of WT and *HeCo* EGFP⁺ neurons within the CP are illustrated by cell tracking paths (C and G) and 3 sequential pictures (D1-D3, H1-H3, arrow heads). Some stationary *HeCo* EGFP⁺ cells with horizontal orientation were observed (H1-

H3, arrow). Cell nuclei of coronal brain sections were counterstained with Hoechst. Scale bars, 50 μ m (B-D3), 25 μ m (A and B). Data are shown as the mean \pm SEM. * p < 0.05.

Supplemental Figure S8. Additional Characterization of the Heterotopia at Late Embryonic and Postnatal Stages in *HeCo* Mice. Related to Figures 4 and 5.

(A-B') Cux1 immunohistochemistry at P7 demonstrating columns of superficial layer neurons (arrows) potentially migrating in between the heterotopia (#), and between the heterotopia and the cortex layer II-IV in *HeCo* brains.

(C-D') GFAP labeling and (E-F') S100 β /Ki-67 co-labeling at P3 showing subpopulations of glial cells around but not inside the heterotopia (#).

(G and H) PH3/Pax6 and (I and J) PH3/Tbr2 double-stainings at E19 showing proliferating apical and basal progenitors largely excluded from the heterotopia (#). B', D' and F', higher power views of B, D and F, respectively. Cell nuclei of coronal brain sections were counterstained with Hoechst. Scale bars, 400 μ m (A-F), 200 μ m (B', D', G), 100 μ m (F').

Supplemental Table S6. Key SNPs and Informative Individuals in the Fine Mapping of the *HeCo* Mouse Candidate Region.

Heterozygote genotypes are highlighted in grey. SNPs rs4229612, rs6376011, rs3670898 for the first round and SNPs rs29180599, rs6240517 for the second round were found homozygous for the NOR alleles in all F2 affected individuals. After the second round of screening rs29151683 and rs29219055 were identified as flanking markers (underlined). The region was slightly further reduced by the identification of a non-referenced SNP in the *Dlk1* gene. Non informative genotypes are noted '-'. '.

SNP	nucleotide	F0 C57 WT		F0 NOR	F2 tree 1								F2 tree 2			
		Tree 1	Tree 2	HeCo	71	124	160	224	164	250	186	194	368	395	552	
rs13481624	105,246,728	CC	-	GG	CG	CG	CG	CG	CG	CG	GG	GG	-	-	-	5' boundary (1 st round)
<u>rs29151683</u>	106,303,360	AA	-	GG	GG	GG	GG	AG	AG	GG	GG	-	-	-	-	Final 5' boundary (2 nd round)
rs29180599	108,884,307	CC	-	AA	AA	AA	AA	AA	AA	AA	AA	-	-	-	-	Internal homozygous (2 nd round)
rs6240517	109,744,829	AA	-	GG	GG	GG	GG	GG	GG	GG	GG	-	-	-	-	Internal homozygous (2 nd round)
non ref	110,693,217	-	CC	TT	-	-	-	-	-	-	-	CT	CT	CT	-	Final 3' boundary (<i>Dlk1</i>)
<u>rs29219055</u>	110,727,094	-	CC	GG	-	-	-	-	-	-	-	CG	CG	CG	-	3' boundary (2 nd round)
rs4229612	114,496,842	GG	-	AA	AA	AA	AA	AA	AA	AA	AA	-	-	-	-	Internal homozygous (1 st round)
rs6376011	116,788,762	GG	-	TT	TT	TT	TT	TT	TT	TT	TT	-	-	-	-	Internal homozygous (1 st round)
rs3670898	117,956,773	CC	-	GG	GG	GG	GG	GG	GG	GG	GG	-	-	-	-	Internal homozygous (1 st round)
rs3692361	118,957,587	TT	-	CC	CC	CC	CC	CC	CC	CT	CT	-	-	-	-	3' boundary (1 st round)

Supplemental Table S7. Differential Expression of *Eml1* in WT versus *HeCo* E18 Brains.

Upper two lines show microarray results and lower two lines, qPCR results. The average values \pm standard deviations are presented (individual values are provided in Supplemental Table 8). WT/*HeCo* ratios and *P* values calculated using the Student T-test are indicated. The fluorescence intensities measured for the exon 5 and *Eml1* 3'UTR probes in WT and *HeCo* samples respectively, were close to detection threshold in the microarray experiment.

	WT	<i>HeCo</i>	WT/<i>HeCo</i>	<i>P</i>-value
<i>Eml1</i> 3' UTR	428.6 \pm 37.2 (n=8)	77.5 \pm 3.5 (n=8)	5.5	1.09 E-13
<i>Eml1</i> ex5	79.8 \pm 3.3 (n=8)	155.0 \pm 24.2 (n=8)	0.5	2.51 E-07
<i>Eml1</i> 3' UTR	0,18052 \pm 0,00896 (n=7)	0,00187 \pm 0,00056 (n=8)	96.6	3.04 E-17
<i>Eml1</i> ex3-4	0,398 \pm 0,027 (n=7)	0,992 \pm 0,084 (n=8)	0.4	7.90 E-11

Sequences of Normal and Exon Skipped Versions of *Eml1*. (See next page)

Nucleotide and protein sequences of *Eml1* from exon 21 to the stop codon in exon 23. Predicted WD repeats are indicated by grey shading. Below the normal sequence are the skipped exon 22 (sk22) and skipped exons 21 and 22 (sk2122) versions where frameshifts occur just after the junction with exon 23. Junk amino acids are shown in grey lettering before premature stop codons (TGA or TAG). Both WD10 and WD11 are absent in sk22 and sk2122 and the 11 last residues of WD9 are also absent in sk2122. Skipping of these two regions is also likely to affect protein conformation.

Sequences of Normal and Exon Skipped Versions of *Eml1*.

| ex21

2465 CTCTACTGGGTTCCGTCTGCCTGTAAGCAAGTCGTGAGTGTGGAAACCACAAGGGACATC

696 -L--Y--W--V--P--S--A--C--K--Q--V--V--S--V--E--T--T--R--D--I-

WD9

sk22 CTCTACTGGGTTCCGTCTGCCTGTAAGCAAGTCGTGAGTGTGGAAACCACAAGGGACATC

-L--Y--W--V--P--S--A--C--K--Q--V--V--S--V--E--T--T--R--D--I-

sk2122 CTCTACT-----

-L--Y--

| ex22

2525 GAGTGGGCCACCTATACCTGCACCTTGGGATTCCACGTCTTTGGAGTGTGGCCGGAGGGC

716 -E--W--A--T--Y--T--C--T--L--G--F--H--V--F--G--V--W--P--E--G-

sk22 GAGTGGGCCACCTATACCTGCACCTTGGGATTCCACGTCTTTG-----

-E--W--A--T--Y--T--C--T--L--G--F--H--V--F--

sk2122 -----

2585 TCCGATGGGACAGACATCAACGCCGTCTGCCGGGCTCACGAGAGAAAAGCTCTTGTGCACA

736 -S--D--G--T--D--I--N--A--V--C--R--A--H--E--R--K--L--L--C--T-

WD10

sk22 -----

sk2122 -----

| ex23

2645 GGCGATGACTTCGGCAAAGTGCACCTCTTCTCATACCCGTGCTCACAGTTCCGGGGCTCCA

756 -G--D--D--F--G--K--V--H--L--F--S--Y--P--C--S--Q--F--R--A--P-

sk22 -----GCTCCA

G--S--

sk2122 -----GCTCCA
-----C--S--

2705 AGCCACATCTACAGTGGACACAGCAGCCACGTCACCAACGTGGACTTCCTCTGTGAAGAC
776 -S--H--I--Y--S--G--H--S--S--H--V--T--N--V--D--F--L--C--E--D--

WD11

sk22 AGCCACATCTACAGTGGACACAGCAGCCACGTCACCAACGTGGACTTCCTCTGTGA
K--P--H--L--Q--W--T--Q--Q--P--R--H--Q--R--G--L--P--L--=* =

sk2122 AGCCACATCTACAGTGGACACAGCAGCCACGTCACCAACGTGGACTTCCTCTGTGA
K--P--H--L--Q--W--T--Q--Q--P--R--H--Q--R--G--L--P--L--=* =

2765 AGCCACCTTATCTCCACGGGTGGGAAAGACACAAGCATCATGCAGTGGCGAGTCATTTAG
796 -S--H--L--I--S--T--G--G--K--D--T--S--I--M--Q--W--R--V--I--=* =

Retrotransposon Partial Sequence.

The early retrotransposon (ETn) sequence identified in an *Eml1* intron is highly similar to several ETn II elements. 5' and 3' LTRs are identical (underlined), indicative of its recent origin (Baust et al., 2003). The ETn is flanked by 6 bp *Eml1* direct repeats, indicated in upper case letters with their chromosomal position (Genome Browser, <http://genome.ucsc.edu/>). In lower case letters is the partial sequence of the *Eml1* ETn determined by sequencing of PCR products amplified between an ETn primer and an *Eml1* primer. Bases are numbered according to the sequence of an ETn described in SELH/Bc mice (NCBI accession Y17106, Hofman et al., 1998) which was further identified as a member of the ETnII β group (Baust et al., 2003) and which displayed the greatest homology with the partial sequence of the *Eml1* ETn (98% for the 1192 bp upstream of the 3' LTR and 99% for the remaining partial sequence).

109,775,748 GAAATG

5'LTR and 1058 bp immediately downstream

1 tgtagtctcc cctcccctag cctgaaacct gcttgctcgg ggtggagctt cctgctcatt
61 cgttctgcca cgcccactgc tggaacctga ggagccacac acgtgcacct ttctactgga
121 ccagagatta ttcggcgagg atcgggtccc ctcccccttc cttcataact ggtgtcgcaa

181 caataaaaatt tgagccttga tcagagtaac tgtcttggct acatttcttc ttttgccccg
 241 tctagattcc tctcttacag ctcgagcggc cttctcagtc aaaccgttca cgttgcgagc
 301 tgctggcggc cgcaacattt tggcgcccga acagggacct gaagaatggc agagagatgc
 361 taagaggaac gctgcattgg agctccacag gaaaggatct tcgtatcgga catcgaggca
 421 acggacaagt acacatgcta gcgctagctt aaaatttcag ttttgtaaag tgttgctgag
 481 gatgcggtag gatacgaatt aagcttgaat cagtgtctaac ccaacgctgg ttctgcttgg
 541 gtcagcagcg tgттаатсgg aactagaaac ggaaacaggc aggttagccg cagcttttta
 601 ggaagctgct taggtgaaag aagaaagggт ttaaagtcат agatcaggcg gtaggccgta
 661 gctctccgaa gctacatgag gtgtgagaaa agaaagggтt таттааааgg аатaggcgga
 721 ttgccccagt таатаааааа тacatcataa gggaggaaaa tgtcccaaaa agcagagaga
 781 aatatctctc tgggccttat agcaggagta ctctgttccc ctttgtgtct tgtctaатgt
 841 ccggtgcacc аатctgttct cgtgttcgat tcatgtatgt tcgtgtccag tctgtatgaa
 901 tgaatgttct atgttttgtg ttggataata aagatggтat аааааacttt атctgcaааg
 961 ccgagagctg ccacgtgttt cagccaagaa tcagacacgt ggcgagaggg cccctgctgg
 1021 ааааactgtt cgttttagaa аатаagggcg агtgcacagc ctctaagttt cagagtaaaa
 1081 aagctaataa atggttcатg аттаатgtgt ttgacaatgg тааagtgtt tttattttat
 1141 gattgtagct аcaaaaatta ttattctctg attggtctaa atgтаactgc ttcatттgtt
 1201 tcttttttat tggтаатgtg ctctaagтgt tttcacaatc агctcataag ttgttggtta
 1261 agattaataa ttgttacatt gctacagatg gttagtgtta ааттгатаа ctcaagtтta
 1321 gagtccttcc gacacatggc атаaggcagc ccaagaggct gggтctctaa agata ...

826 bp in the internal region

a cgttttaact

1921 gтаagtcатc ттаааааага gtatcaaaat тtagaggcgt agacagttat атgtттtctc
 1981 таааатсggт ccttattaca ggagggccag gatgctcaga ттааааагта тtttacgttt
 2041 aagtcaatgc agggctctgg gcagcccaa агсggcttgt ggcctttctt ttgtттtgca
 2101 aacagtgcct gagaaagatt тttccctgtg тtcaaaaaaa атtcttttta acagtgttgc
 2161 агatctатtc агatgtttaa аатаатgctt аааттcaааg агttttgctt ctagtgaact
 2221 gтаатcacta ааааатттг cctctaggta tggctaатgt аactttacat тatgтаагаа
 2281 ааатттtatt gtttctgctt ctatacaaaa агccaagagt тttaatcttt cagtgtatat
 2341 tgtttcctaa gtgaaaagta тtttattaac таатgcttct тааagtтtac cttaaатcct
 2401 tgctctcacc caаааgатtc агagacaata тccttttatt acttagggтt тtagттtact
 2461 аcaaaaagttt тtacaааааа тааagctttt атааттgтta ттааттggta аттааааатт
 2521 ggttgтgccc ааааcaатtc тttggccaaa аааааааacat тattgтаааg тcattттtct
 2581 catcctcca gccaatgтt ggcccacgtg ggcccaacta gcttctgtgg ggcggagtct
 2641 тааgacacag тttccctgt тccagcacag атgatctagt tgtgtgctgt агatggтgtt
 2701 ттаааатgct ааacaатcaa acctтааттt gtata ...

3'LTR and 1192 bp immediately upstream

ccccgc cccctagag cacacaggтg gcagctgtta cccccagtct

4081 caagacattt ccagcatgtg gctttcagtc tgagttaaaa аттtaggttt acctagaggg
 4141 ctagaagagt агатттттtct ататтаатаа агаттggттt тtattттtgat агacaggctt
 4201 агcccccttag ctgacctctg gcttttcacc cttgctgtta ctgcaaggтg тccttagctc

4261 aataggctgt ggaaaaaaca gggatgagga gaaacgactt ccagctccta ttttaccac
 4321 aaatcgtggt gttattaacg acataattct tgcttaggct ttgctaattc tgaggttgat
 4381 aattctcctt taggagctgc acagcactca aaactgtaca tactggtttg tgattgtaca
 4441 aattcagtat gggcacgct tgggtgcagag atacttactg caaggggaag tccggcttga
 4501 ccatttctga gtttctctgt agataaaccc ggtttaaag aggttggtac caaattttgg
 4561 ttaaaaataa aaaatattct cgggctctac ctgcctccc caaaaggtag caagagccac
 4621 atgtgtgggt tttaccacg agaaaaatcg ggtccatgtc cacccaagcc aaggttaaaa
 4681 gccactcat ctacggatga gaaaatcatt tgatcacctc agttaagcgt tgccttattt
 4741 aacttaatta atagggggga gagagattgg agacatacta ttgaaagggc aagcccttca
 4801 ctgcctcca cccaaataaa aaggccaatt ggccttgtag tacaagagcc ggtcactcct
 4861 tctccctggt tcccacctat cttccaaaaa tgcggaggaa ttcaacttag tgttattttc
 4921 acatccttca gtcaaactta gccagagttc caaacgcctt acttaaaatt caactagaaa
 4981 gttacctacc aagtactaat tagcattata aagtcagagt gtgcagctcc aggcctttca
 5041 gttgtttact agaaaggaca gtcttaagcc agatacagtt taccataaga aaagttaaag
 5101 attcccagta aagcaagttt tttcttttagc cctagattcc aggcagaact attgagcata
 5161 gataattttc cccctcagg ccagcttttt tttttttttt ttattttggt aataacaggg
 5221 aggagatgta gtctcccctc ccctagcctg aaacctgctt gctcggggtg gagcttctg
 5281 ctcattcggt ctgccacgcc cactgctgga acctgaggag ccacacacgt gcacctttct
 5341 actggaccag agattattcg gcggaatcg ggtcccctcc cccttcttc ataactgggt
 5401 tgcgaacaat aaaatttgag ccttgatcag agtaactgtc ttggctacat ttcttctttt
 5461 gccccgtcta gattcctctc ttacagctcg agcggccttc tcagtcaaac cgttcacggt
 5521 gcgagctgct ggcggccgca aca
 GAAATG 109,775,753

Clinical Information for Giant Heterotopia Patients Mutated in *EML1*. Related to Figure 2.

The first boy was initially referred for severe developmental delay with congenital macrocephaly. He acquired ambulation at 4 years of age with mild spasticity. At the same age, he developed refractory epilepsy with a combination of atypical absences, atonic falls and tonic seizures. At his most recent evaluation at 16 years, he was severely delayed intellectually and presented severe behavioral and sleep disturbances. His brother aged 14 years was initially referred at 8 years of age for severe intellectual disability and epilepsy. Clinical features were similar to his brother, with generalized epilepsy starting at 8 years of age. The third brother, now aged 8 years, developed neurological symptoms from the neonatal period. He was admitted for severe hypotonia. Subsequently he made constant progress and walked independently at 3 years, but developed behavioral and sleep disturbances. No seizures have yet been reported. Macrocephaly was also noted from birth (head circumference 37.5 cm).

SUPPLEMENTAL EXPERIMENTAL PROCEDURES

1. General methods

DNA and RNA preparation. DNA samples were prepared from mouse tail biopsies according to recommendations of genotyping platforms, with phenol extraction followed by isopropanol precipitation. Total RNA samples were extracted from single hemispheres dissected from NOR-CD1 *HeCo* and WT E18 embryos, using a Qiagen RNeasy Protect mini kit (Qiagen, S.A.). Genomic DNA and RNA samples were tested for quality control using an Agilent Bioanalyzer.

MT sedimentation experiments. MTs were polymerized from 10 μg of purified porcine brain tubulin (Cytoskeleton Inc.) in the presence of taxol and GTP (Francis et al., 1999) and incubated 20 min at 37°C with 1 μg of precleared GST-EML1 or control GST proteins (ProteoGenix). Soluble tubulin (10 μg) was incubated with GST-EML1 under the same conditions. MTs were separated from soluble proteins by ultracentrifugation through a 60% v/v glycerol cushion (10 min at 30,000 g on Airfuge, Beckman). Samples were analyzed by SDS-PAGE and Western blotting using antibodies to GST and to α -tubulin.

Cell cultures, transfections and immunodetection. Transfections in COS7 cells (ATCC) or Vero cells (ATCC), grown in Dulbecco's modified Eagle's medium containing 10% v/v fetal calf serum, were performed using Nanofectin (PAA Laboratories GmbH). Cells were fixed 24 h after transfection with either 4 % w/v paraformaldehyde (PFA, 5 min, 37°C) or ice cold methanol (6 min, -20 °C), or subjected to a detergent extraction in PHEM buffer (60 mM PIPES, 25 mM HEPES, 10 mM EGTA, and 2 mM MgCl_2 , pH 6.9) + 0.5 % v/v Triton X-100 (according to Audebert et al., 1993) for 1 min prior to fixation with cold methanol. For repolymerisation experiments cells were incubated on ice for 30 min 24 h post-transfection, thereafter restored to 37°C for various intervals before detergent extraction and fixation. Primary cultures of E15.5 cortical neurons were maintained in a standard Neurobasal/B27 medium. Primary cultures from E12.5 cortices were maintained in a B27/N2 medium (Gaspard et al., 2009) which is a mixture (1:4) of Neurobasal/B27 medium without vitamin A and DDM medium (DMEM/F12 with GlutaMAX, supplemented with N2, 0.1 mM non-essential amino-acids, 1 mM sodium pyruvate, 500 $\mu\text{g}/\text{ml}$ BSA, 0.1 mM 2-mercaptoethanol and penicillin/streptomycin 100 U/ml). Electroporation was performed using an Amaxa mouse Nucleofector kit (Lonza). Cells were fixed in PFA or cold methanol 24 h after

electroporation. Immunocytochemistry was performed according to standard procedures and results observed and photographed using either epifluorescence (Leica DM6000) or confocal microscopy (Olympus FV10i). All cell culture media were from Life Technologies Corporation. For quantification of Ki-67, Pax6, Tbr2, and Dcx expressing cells in E12.5 cultures, 15 to 19 fields were counted for each marker, representing more than 1600 cells, from 3 independent cultures for each genotype.

***In situ* hybridization.** PFA-fixed embryonic, neonate and adult mouse brains were embedded in 4% (w/v) agarose. Free floating vibratome sections (200 μ m for up to P1 and 60 μ m for adult brains) were hybridized following a protocol adapted from from Bailly-Cuif and Wassef (1994). Digoxigenin-labeled sense and antisense riboprobes were generated by *in vitro* transcription of a fragment amplified from the *Eml1* 3'UTR region (chr12 nt 109,776,616 to 109,777,469, Genome Browser, <http://genome.ucsc.edu/>) subcloned in pBluescript II KS vector. To generate complementary DNA (cDNA) plasmids for the *Eml1* ferret probe, total RNA from P0 ferret brain was isolated using the RNeasy protect mini kit (Qiagen). First-strand cDNA was synthesized using AMV Reverse Transcriptase (Finnzymes). The primers used to amplify cDNA fragments were: fEml1F, CTTTTCTATGAACTCTTC, and fEml1R, AAGGATACATACAAACAG. The PCR products were purified (Wizard SV Gel and PCR Clean-Up System, Promega) and ligated into pGEM-T-easy vector (pGEM-T-Easy vectorSystem, Promega). *In situ* hybridization on ferret brain sections was performed as described previously (Reillo et al., 2011).

Growth cone analysis. Using progenitor and neuronal cultures at 1 DIV, stained for doublecortin (Dcx) and phalloidin (detecting F-actin), we selected immature post-mitotic neurons for growth cone image acquisition and analysis (WT and *HeCo* cultures, n=3 of each). No obvious differences were observed in global neuron morphologies with approximately equal proportions of monopolar, bipolar and multipolar neurons present in WT and mutant cultures. To avoid artifacts generated by comparing inhomogeneous neuronal populations, cells with relatively uniform morphologies were selected, with a recognizable predominant neurite tipped with a main growth cone. The major neurite had a length between 2 and 4 somal lengths. Neurons for analysis were selected in the Dcx channel, to avoid biased cell selection on the basis of growth cone size. The image was acquired after focusing on the neuronal process extremity. Image J was used to visualize the growth cone region, to draw around the phalloidin labeling and calculate the surface area and perimeter. This was

performed 3 times for each growth cone. At least 10 cells were analyzed in each of the 6 cultures (Total n= 43 for WT and 45 for *HeCo*).

Immunohistochemistry. Embryos were collected by Caesarean and killed by decapitation. Brains were fixed by immersion overnight at 4°C in 4% w/v PFA in 0.1M phosphate buffer, pH 7.4. Postnatal mice were anaesthetized with sodium pentobarbitone and perfused with the same fixative, and their brains postfixed 2 h. Brains were cryoprotected in 30% w/v sucrose, and cut in coronal 30-50 µm frozen sections with a cryotome (Microm). Preincubation and incubations with the primary and secondary antibodies were performed in 0.1 M phosphate buffer containing 0.6 % w/v NaCl, 0.3% v/v Triton X-100, and 2% v/v normal horse serum (see the list of antibodies below). Sections were counterstained with Hoechst 33258 (Invitrogen) and mounted on glass slides with Mowiol 4-88 (Calbiochem).

***Ex vivo* electroporation and confocal time-lapse microscopy.** Pregnant mice were sacrificed with pentobarbital, E15.5 embryos collected in cold dissecting medium (MEM, Gibco, with 15 mM glucose and 10 mM Tris, pH 7.4). 30µl of the expression vector pCAGGS-GFP (0.5µg/µl) in sterile PBS (0.1 M, 0.9% w/v NaCl, pH 7.4) with 20% w/v Fast-blue (Sigma-Aldrich) were pressure injected into the ventricular region of embryonic brains by a pneumatic picopump (Picospritzer III, Parker Hannifin Corporation; time of injection: 15ms) through a syringe. Embryos were placed into HBSS 1X medium (Gibco), electrodes (System CUY650P5 Nepa Gene Co) were maintained around the embryo head with a 45° angle and plasmids electroporated by discharging a 4000 µF capacitor charged to 45 V (5 electric pulses at 50 ms intervals) with a CUY21 electroporator. After electroporation brains were embedded in 3% w/v low-melting point agarose (Invitrogen). For imaging migrating neurons, an *in vitro* model of organotypic slices was used (modified from Niquille et al., 2009). Coronal sections (250µm-thick) were cut using a vibratome and cultured for 3 DIV on nucleopore Track-Etch membranes (1µm pore size; Whatman) in tissue dishes containing 3 ml of slice culture medium (SCM: BME/HBSS, Invitrogen) supplemented with glutamine, 5% v/v horse serum, and penicillin/streptomycin (Lopez-Bendito et al., 2006). Neuron migration paths and dynamics were studied in cortical slices of WT and *HeCo* mice. Temperature was maintained at 37°C (microscope incubator system Life Scientific) and slices were perfused with SCM medium containing a gas mixture of 5% CO₂/ 95% O₂. EGFP⁺ neurons were imaged for 10 hrs with a 20X and a 60X immersion lens at 15 min intervals using the fast scan function of the Leica SP5 confocal microscope resonant scanner. Image

captures and all peripherals were controlled with Leica software. Pictures were processed and converted into *.AVI movies using Imaris and Metamorph 6.0. Migration parameters (basal rate of migration, frequency and duration of the intervening pauses) of IZ and CP migrating neurons were assessed. Using the tracking function of Metamorph software 6.0, a total of 3091 WT and 3180 *HeCo* neuron traces were analyzed. For quantification of electroporated cells, overall fluorescence intensities were measured manually with Imaris software and EGFP⁺ cells in the CP were counted in at least 3 cortical sections of 50 μ m per genotype, in a defined volume stack using Imaris manual volume tool.

***In utero* electroporation.** We adapted the protocol previously described by Cancedda et al. (2007). E15.5 timed-pregnant NOR-CD1 mice were anesthetized with isoflurane (3 % during induction and 2 % during surgery) and embryos were exposed within the intact uterine wall after sectioning the abdomen. The expression vector pCAG-GFP (2 μ g/ μ l) together with Fast Green (0.3 mg/ml; Sigma-Aldrich) was pressure injected focally (2 μ l) into the lateral ventricle of embryos through a glass micropipette using a PicoSpritzer III picopump (Parker Hannifin Corp.). Each embryo head was placed between electrodes (System CUY-650P5) and electroporated with five electrical square unipolar pulses (amplitude: 45 V; duration: 50 ms; intervals: 950 ms) powered by a BTX electroporation apparatus (model BTX ECM 830; Harvard Apparatus). The tweezer-type electrodes were oriented in order to preferentially electroporate dorsal pallium precursors that give rise in part to pyramidal projecting neurons (Molyneaux et al., 2007). The embryos were placed back in the abdominal cavity and the muscular and skin body wall layers were sutured. Development was allowed to continue until P3.

2. Antibodies. Antibodies used were mouse monoclonal antibodies to α -tubulin (1:10,000 for western blot and 1:1,000 for immunocytochemistry, Sigma-Aldrich), GFP (1:400, Sigma-Aldrich), γ -tubulin (1:800, Sigma-Aldrich), γ -adaptin (1:200, BD Transduction Laboratories), KIF1A (1:75, BD Transduction Laboratories), tyrosinated tubulin (1:10,000, Sigma-Aldrich), dynein (intermediate chain, 1:50, Sigma-Aldrich), Ki-67 (1:200, BD Pharmingen), spastin (1:50, Santa Cruz Biotechnology), acetylated tubulin (1:10,000, Sigma-Aldrich), BrdU (1:100, Monosan), β -catenin (1:200, BD Transduction Laboratories), nestin (1:200, DSHB), P-vim (1:200, Abcam); rabbit polyclonal antibodies to FLAG (1:500, Sigma-Aldrich), EML1 (1:300, GeneTex), GFP (1:700, Invitrogen), GST (1:1,000, Sigma-Aldrich), caspase-3 (1:200, Cell Signaling), Cux1 (1:400, Santa Cruz Biotechnology), Ki-67 (1:200,

Novocastra), Par-3 (1:200, Millipore), Pax6 (1:500, Covance), Tbr1 (1:500, Millipore), Tbr2 (1:500, Abcam), GFAP (1:400, Dako), S100 β (1:2,000, Sigma-Aldrich); goat polyclonal antibodies to Dcx (1:300, C-18, Santa Cruz Biotechnology), Sox2 (1:500, R&D Systems); and rat monoclonal antibody to phospho-Histone3(Ser10) (1:200, Abcam). Secondary antibodies were goat or donkey Alexa Fluor® 488, 568 and 594 (1:300 for immunohistochemistry, 1:1,200 for immunocytochemistry, Invitrogen). For actin staining, Phalloidin Alexa Fluor 647 was used (1:1,500, Invitrogen).

3. Primers

qPCR primers

mE1utr For1 : CACAGACAGCATGCAGCATAACA

mE1utr Rev1 : CTTCTCGACACCTTCAGACCCTAC

mE1_34 For1 : CTCAACAGGAAAGGACCTACCAA

mE1_34 Rev1 : GTTGACGGTGGTTCTCAATGG

mHdac3 For1 : CGCATCGAGAATCAGAACTCAC

mHdac3 Rev1 : TCAAAGATTGTCTGGCGGATC

mAt5g3 For2 : GCAGTCTTATCATTGGTTATGCCA

mAt5g3 Rev2 : AGAACAGCTGCTGCTTCAGTGA

mErp29 For1 : CCTTCCCTTGGACACAGTCACT

mErp29 Rev2 : GTCGAACTTCACCAAGACGAACTT

Mouse genomic DNA primers

Exon 1_NM_001043336 (non coding)

cccatctgcctacatacca = eml_1F_336

ccgtcagtaaagccatccat = eml_1R_336

Exon 2 (NM_001043335)(BC053094)(isoform ozs.1) sequenced on cDNA

GCGCAGTGTGTGGGTGA (= AFbis)

CGCTGACTTGAGCAGTTGAA =Primer cDNA3R

Exon3

TCATGGGCTGTACGTCCTC
GAGATTGGTTCAGTGGGTGG

Exon4

GGATCGTTCCTGCTGCTATG
GCTGCTTTGAGAAGTCAGGTG

Exon5

CTCAGTACACTGGGCAATGAAG
GGCTTGACTCATCAAGAGGG

Exon6

CACACATGCAAGCACACATC
TTCCCCACTCAGTCAAGGTC

Alternative exon6a (in isoform ovr.1)(not in cDNA BC053094)

CCCTTGTTCCCTTGTCCC
TATGAGAACAGCCTCAGGGG

Exon7

GTGTTTGCTTTCGGAGCG
TGGCCACATCTGAAATTTG

Exon8

ATCTTTGGGCCTGTTGAATG
TGATGCTGAATTCTTTTGGC

Exon9

GAAGCTAGGCAGTGTGGATTTC
ATGTCGCCAGGAGGTTGTC

Exon10

TTTATGGTTCCAAGGTAAAGAGAAG
ATGCCTTGAGAAAGGCTGG

Exon11

TCGTGTTGGTCCCCTTG
GCAGGTCTTAGGCAGGGTC

Exon12

CTTGAGAGACTCAGTGCCCC
CTCAGCGCTCCCTTATAACC

Exon13

CAAATAAAAGGCTGTCTTCGG
GGTTGTCCTGTTCGTAACTCC

Exon14

CAAAGTGAAGTGGGTTTCGG
GAATCCAAACGGCCAGC

Exon15-16

GCCTCGCTTGACACAGTAAGT
TGTTAATTCATACAAAGATATATCCCA

Exon17

GAGTCTGAGAAGAGCAGGGC
CTCAGCCGTCTAACTGCTCC

Exon18

TCTGTAGAGAAAGCTGTGGGG
GTTCGCTGTCTAGTGAGCCC

Exon19-20

CCAGCCTTTCCTCTTACGAC

CCCATGGGAATGTCAGAGTG

Exon21

AGGACTCTGCCTGACTCCAG

TGGAGAAGGTATGGTCTCGG

Exon22

TGAAGGTGGATTTCTGTCCC

TTAACAGGGTCATATGCAGGC

Exon23

GACTGATTTAGTGCTCGGGG

GAAATCACAGTGACCAAGCG

3'UTR

TGCAGTGGCGAGTCATTTAG EML3utr 1F

TTAACCAGGGAGAGCACAGC EML3utr 1R

GCTTTCCTTGGCCATGTATC EML3utr 2F

TGTATGCTGCATGCTGTCTG EML3utr 2R

CCTTTGAGGCTCTGGGTGTA EML3utr 3F

GGGAACAGGATGTAGTGTGGA EML3utr 3R

Primers for PCR in the region of mouse *Eml1* exon 22 and for RT-PCR

Supp Fig S1B

- . F and R primers for exon 22 sequencing
- . AGAGATGCAGGGCTTCTCAG (Eml22Fbis1)
and GGAAGTGTGAGCACGGGTAT (22R)
- . CCGATGGGACAGACATCAAC (Eml22Fter)
and R primer for exon 23 sequencing
- . F and R primers for exon 23 sequencing

Supp Fig S1C

ACTGACTGGGAGGTGGTTTG (17-18F)

GGAAGTGTGAGCACGGGTAT (22R)

Supp Fig S1D

TGGAGTTACCGACAATGGAAG (19F)

AGGAAGTCCACGTTGGTGAC (23R)

Fig 1D

ACACGAGTTGGCAAGTGCTC (Nested 19F)

CCACTGTAGATGTGGCTTGG (Nested 23R)

Primers for retrotransposon amplifications

Fig 1E

F primer for exon 22 sequencing (22Fa)

AGGAAGTCCACGTTGGTGAC (23R)

Supp Fig S1E

CCGATGGGACAGACATCAAC (22Fb)

CCGCTCGAGCTGTAAGAG (ETnR)

Fig 1F

CAAGTGCTCCGGCCATTC RT19-20F

GAGACTACATCTCCTCCTTG ETnSD-7R (double sequence readable)

CTCGAGCGGCCTTCTCAGTC ETnF2

CCACTGTAGATGTGGCTTGG Nested23R

CAAGTGCTCCGGCCATTC RT19-20F

TGAGAAGGCCGCTCGAGTTG ETnSD261R

Human *EML1* primers (according to NCBI RefSeq NM_004434.2)

Exon	forward 5'-3'	Reverse 5'-3'	Amplicon length(bp)
1	AGCTCAGTGTGTGGTGAGCG	CCCCGCGGCTCCAACACAAT	320
2	GCTTAAGAGCAGTATCTGTAGTCCG	TTAAAGAGCACAAATGTGTTTGC	406
3	GGTAACATGAGTGATGGGTA	CACACTGTGGTTTTAGCCAG	543
4*	GTGCGTCCTGCAATTTACTG	CACTGGACAAGACCTTGAAGC	254
5	GACGTTCTATGTATATATTT	TGTTTGATTAGTCCTATAAA	380
6	GGCTTTGGGGTCTGAAGTG	AAGCTCCTGTGTGTCCAAGG	216
7	CAAAGCAAACAAGATGCAAAC	GGAATGATAAGTTGGTTCTCCTG	564
8	CTGCATGCCTTTTGGGG	TGACCGTGTTCCTGCTAATGC	505
9	TTGAAATGGTATTTTCCCAGC	CACCCTGCCACACAATAAGTC	505
10	GTCCGAGTTACTGCCCAAG	CCCCTCTTCAACCCTGAG	281
11	GTCTCAAAAGCAATGGATGAG	ACCACTATGCCAGGGCG	306
12	TTTGTGGCTCACATTTTACTTG	GATCCCAAGGGATTGTGTTG	326
13	CAGAAATGCAAGGTGTGCAG	TCTCCGCTTTTCCTCTGTTC	450
14	ATTGCAATGATGTGCTCACG	TGTGATTTACCTAAACAATTTTC	389
15-16	AAGTGTTTTGAATGACTGAGCTAAC	AACATTTGCTTTGGGACAAC	706
17	GCCCTAAGGAATTAGAAGTGTG	GCCTGTTTCTGGGGAAATAG	262
18	TAAGCAAATCTGAGTATTT	CATGGGCTCACTTATAAGTG	500
19-20	GGTGGCAGCTACCGTTATCC	GGAGGTGGGTTCCTCACAGAG	475
21	CCAGGAAGGGCTCTGTACC	TGGTGACCATGAGACTCCG	294
22	TCATGTTTCCAGACCGTTCAG	TAGTCTCCAAACAGGTCCGG	297
23	ATTCAAGCACTTTCCCATCC	CTGAAGTGATCTGTCCTTTTAGG	657

* exon 4 is present in the mRNA NM_001008707 not in the mRNA NM_004434.

Human and mouse genes have the same structure overall with some distinct alternative exons.

SUPPLEMENTAL REFERENCES

Audebert, S., Desbruyeres, E., Gruszczynski, C., Koulakoff, A., Gros, F., Denoulet, P., and Edde, B. (1993). Reversible polyglutamylation of alpha- and beta-tubulin and microtubule dynamics in mouse brain neurons. *Mol. Biol. Cell* 4, 615-626.

- Bally-Cuif, L. and Wassef, M. (1994). Ectopic induction and reorganization of Wnt-1 expression in quail/chick chimeras. *Development* 120, 3379-3394.
- Cancedda, L., Fiumelli, H., Chen, K., and Poo, M.M. (2007). Excitatory GABA action is essential for morphological maturation of cortical neurons in vivo. *J. Neurosci.* 27, 5224-5235.
- Eudy, J.D., Ma-Edmonds, M., Yao, S.F., Talmadge, C.B., Kelley, P.M., Weston, M.D., Kimberling, W.J., Sumegi, J. (1997). Isolation of a novel human homologue of the gene coding for echinoderm microtubule-associated protein (EMAP) from the Usher syndrome type 1a locus at 14q32. *Genomics* 43, 104-106.
- Francis, F., Koulakoff, A., Boucher, D., Chafey, P., Schaar, B., Vinet, M.C., Friocourt, G., McDonnell, N., Reiner, O., Kahn, A., McConnell, S.K., Berwald-Netter, Y., Denoulet, P., Chelly, J. (1999). Doublecortin is a developmentally regulated, microtubule-associated protein expressed in migrating and differentiating neurons. *Neuron* 23, 247-256.
- Gaspard, N., Bouchet, T., Herpoel, A., Naeije, G., van den Aemele, J., and Vanderhaeghen, P. (2009). Generation of cortical neurons from mouse embryonic stem cells. *Nat. Protoc.* 4, 1454-1463.
- Heidebrecht, H.J., Buck, F., Pollmann, M., Siebert, R., Parwaresch, R. (2000). Cloning and localization of C2orf2(ropp120), a previously unknown WD repeat protein. *Genomics* 68, 348-350.
- Hofmann, M., Harris, M., Juriloff, D., and Boehm, T. (1998). Spontaneous mutations in SELH/Bc mice due to insertions of early transposons: molecular characterization of null alleles at the nude and albino loci. *Genomics* 52, 107-109.
- Lepley, D.M., Palange, J.M., and Suprenant, K.A. (1999). Sequence and expression patterns of a human EMAP-related protein-2 (HuEMAP-2). *Gene* 237, 343-349.
- Li, H., Wagner, E., McCaffery, P., Smith, D., Andreadis, A., and Dräger, U.C. (2000). A retinoic acid synthesizing enzyme in ventral retina and telencephalon of the embryonic mouse. *Mech. Dev.* 95, 283-289.

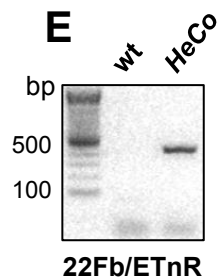
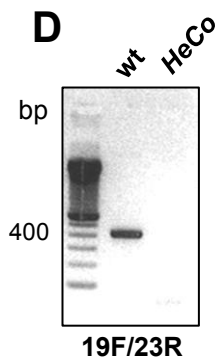
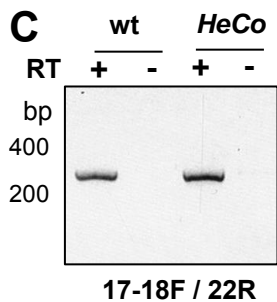
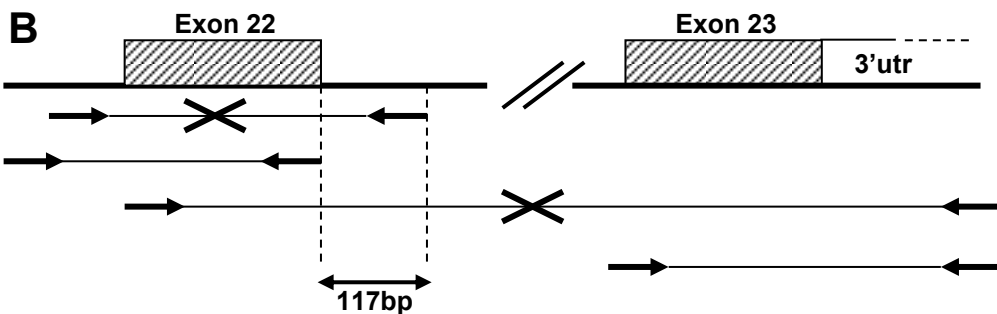
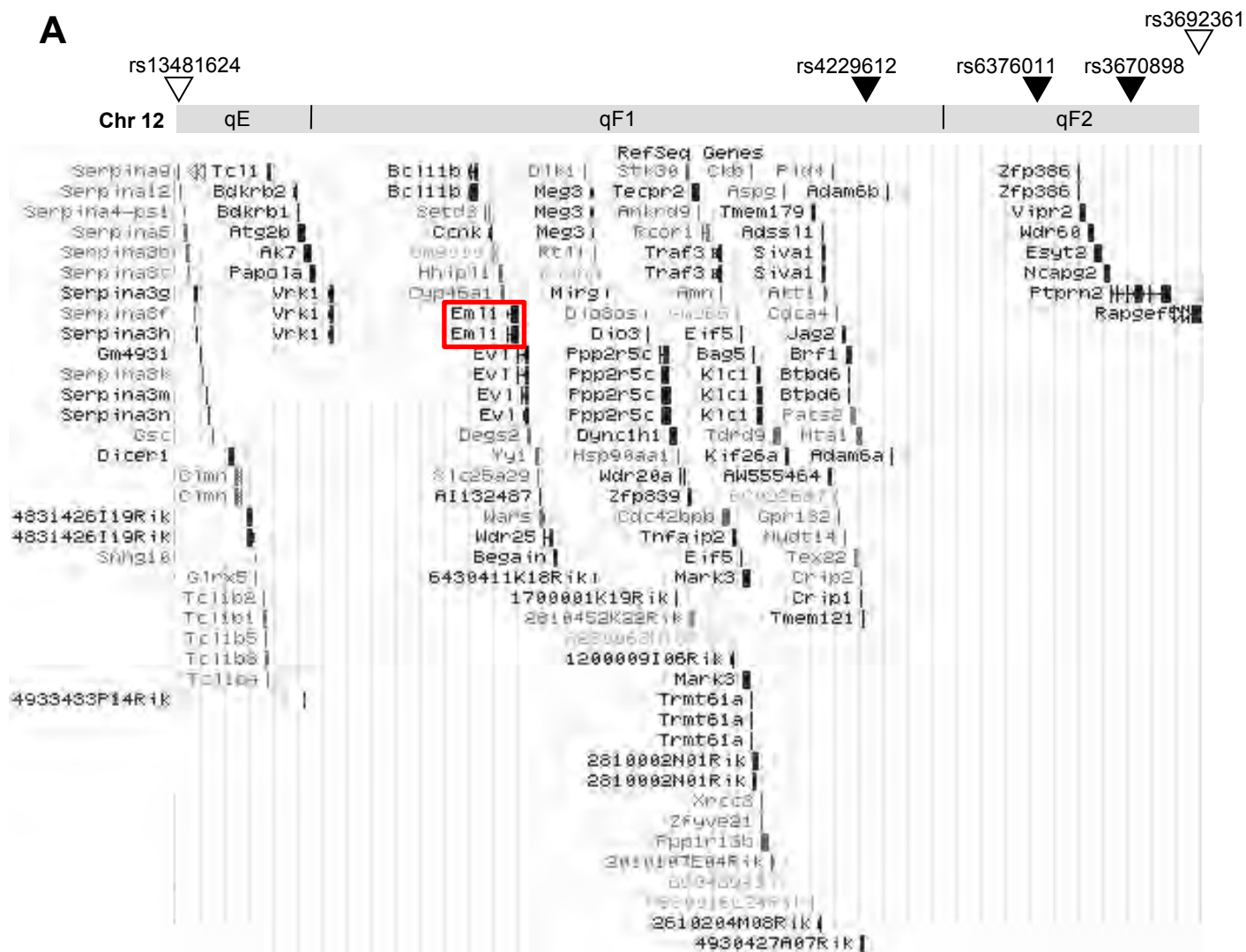
Li, Q., Suprenant, K.A. (1994). Molecular characterization of the 77-kDa echinoderm microtubule-associated protein. Homology to the beta-transducin family. *J Biol Chem.* 269, 31777-31784.

López-Bendito, G., Cautinat, A., Sánchez, J.A., Bielle, F., Flames, N., Garratt, A.N., Talmage, D.A., Role, L.W., Charnay, P., Marín, O., and Garel, S. (2006). Tangential neuronal migration controls axon guidance: a role for neuregulin-1 in thalamocortical axon navigation. *Cell* 125,127-142.

Molyneaux, B.J., Arlotta, P., Menezes, J.R., and Macklis, J.D. (2007). Neuronal subtype specification in the cerebral cortex. *Nat. Rev. Neurosci.* 8, 427-437.

Niquille, M., Garel, S., Mann, F., Hornung, J.P., Otsmane, B., Chevalley, S., Parras, C., Guillemot, F., Gaspar, P., Yanagawa, Y., Lebrand, C. (2009). Transient neuronal populations are required to guide callosal axons: a role for semaphorin 3C. *PLoS Biol.* 7(10):e1000230.

Paxinos, G., and Franklin, K.B.J. (2001). *The Mouse Brain in Stereotaxic Coordinates*, 2nd ed. (San Diego: Copyright Academic Press).

A**Supp Fig 1**

HELP motif

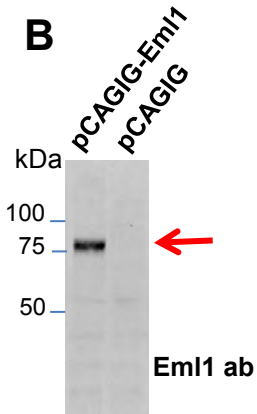
A

gi	Accession	Protein	Start	End	Species
gi 254763417	183	EEGVKMF...VDSYSLEAKVELP...VWVYGRGDCRMNLYLLPTGETVYF...VAVLVNVE	183	260	EML1
gi 18202954	223	EGEYIKM...IPSD-VNVD-DIRTEL...VWVYGRGDCRANVLLPTGEIVYF...VAVLVNVE	223	298	EML 4
gi 17374910	17	EDGSVMF...IPDEIAPTYSIDTRSEL...VWVYGRGDCRANLYLLPTGEIVYF...VAVLVNVE	17	94	EML 2
gi 18202520	57	EEGVVRI...IPSD-VEDYDINAKHP...VWVYGRGDCRCNLYLLPTGEEIYF...VAVLVNVE	57	133	EMAP Sp
gi 18202045	243	GGGHLPI...IPVPTG-YENNDpTNDQP...VWVYGRGDCRANLYLLPTGELVFF...VAVLVNVE	243	319	ELP Ce
gi 18203308	70	GSGEQFM...IPVPAQ----HhEPSKD...VWVYGRGDCRANLYLLPTGELVFF...VAVLVNVE	70	142	Ctxp80 Eo
gi 195590322	238	KEEPTKV...IPVPH----HhPADNS...VWVYGRGDCRANLYLLPTGELVFF...VAVLVNVE	238	310	Droso

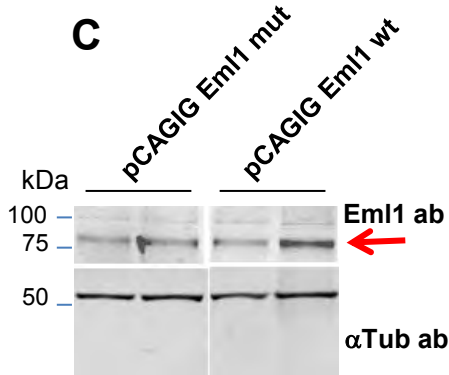
Citing CDD

Marchler-Bauer A et al. (2009), "CDD: specific functional annotation with the Conserved Domain Database.", *Nucleic Acids Res.* 37(D):205-10.

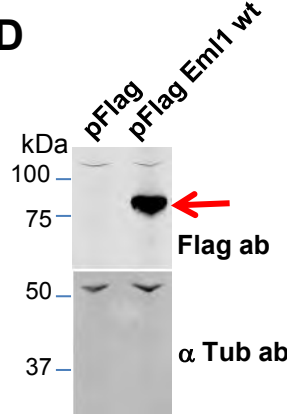
B



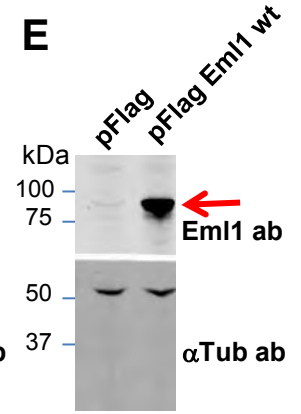
C



D

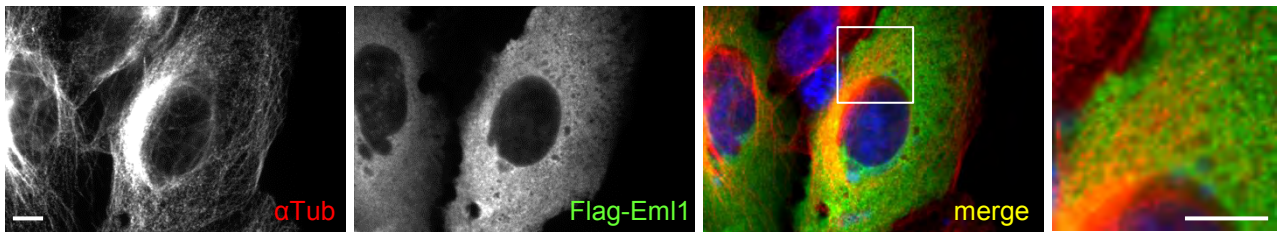


E



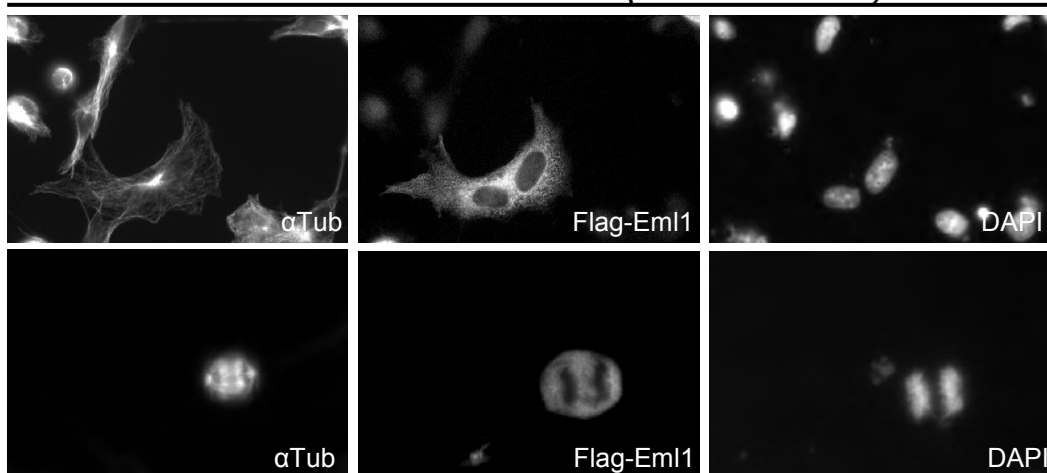
F

Recombinant Eml1 in Vero cells (standard fixation)

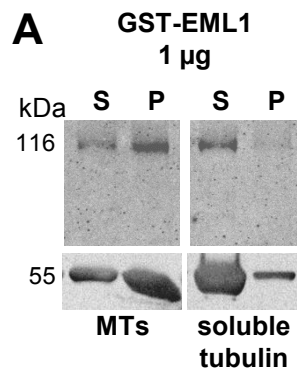


G

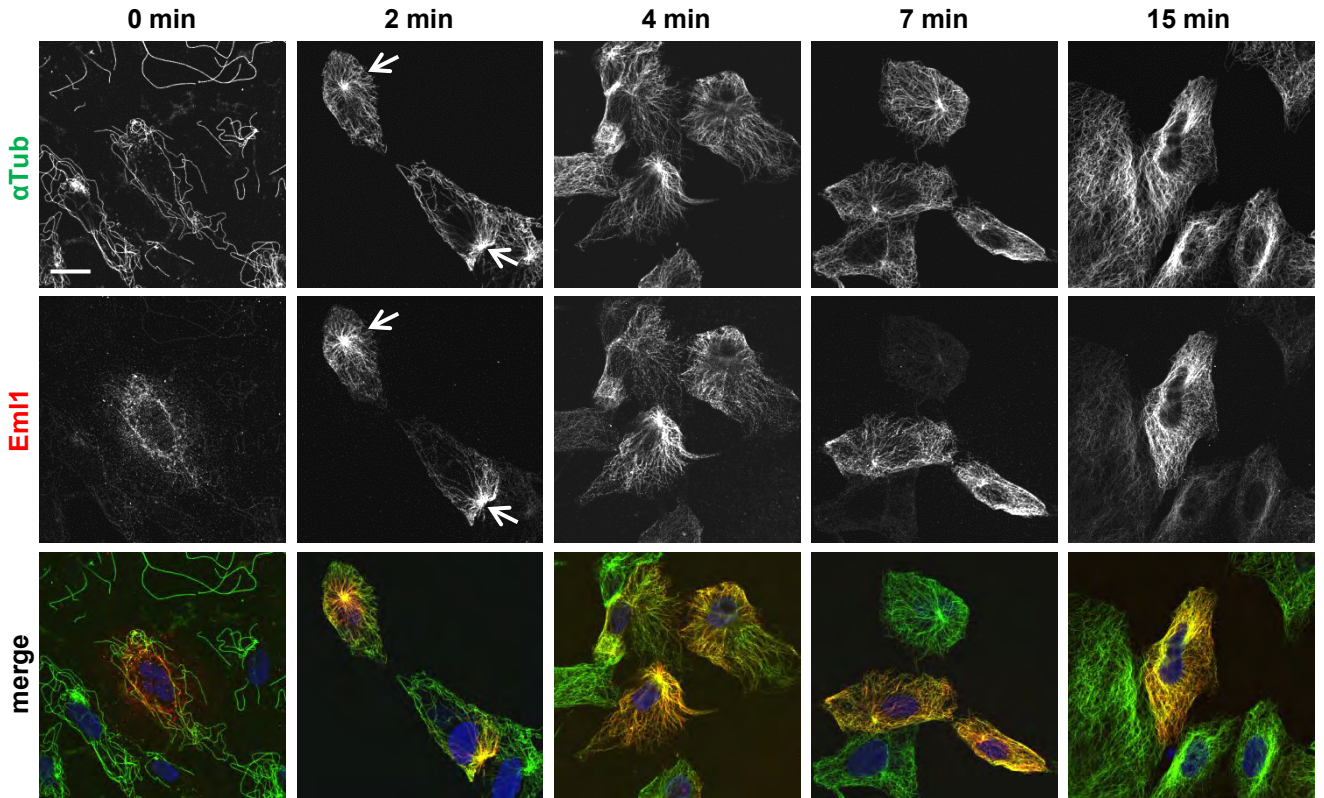
Recombinant Eml1 in COS7 cells (standard fixation)



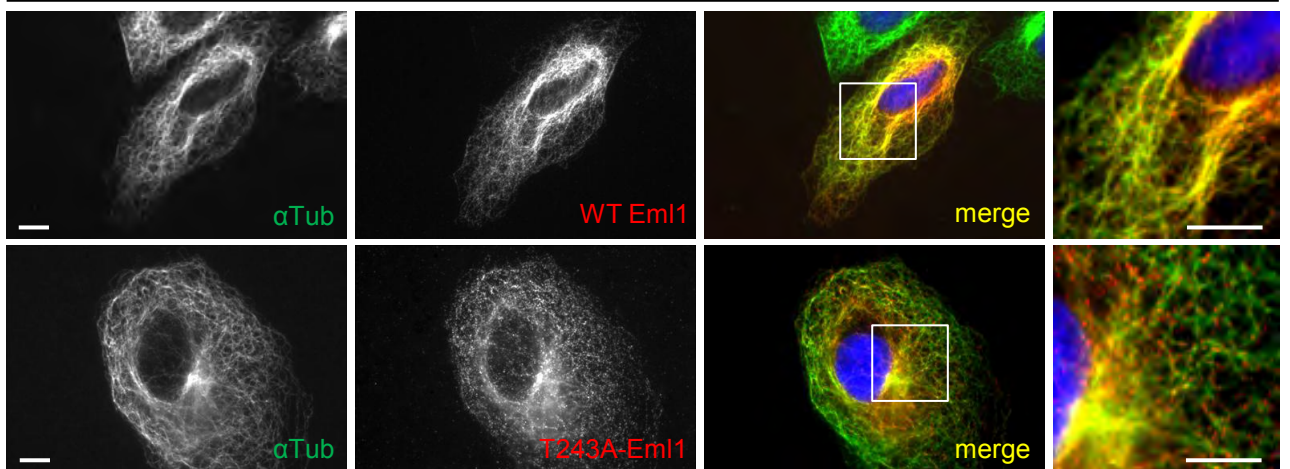
Supp Fig 2



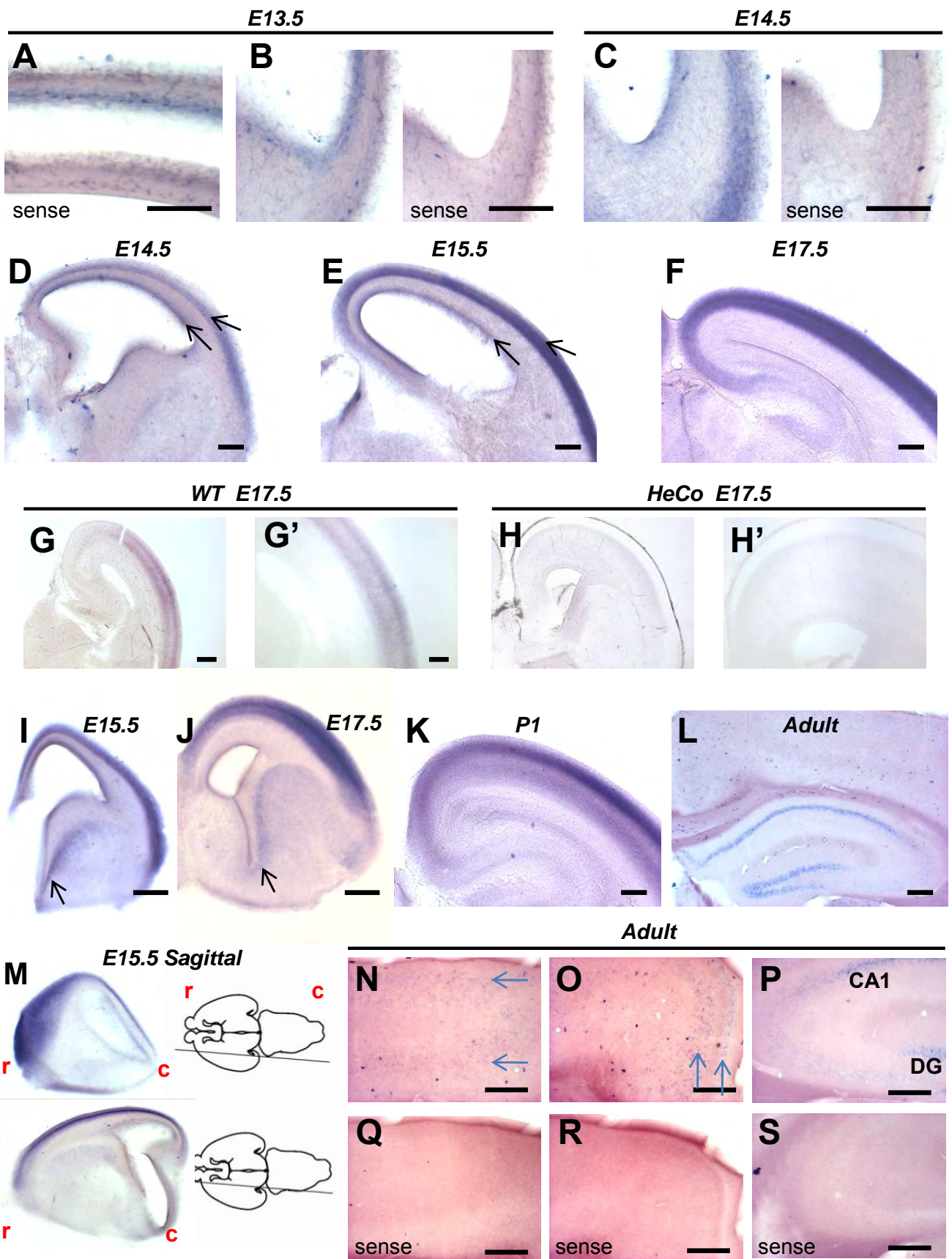
C *Recombinant Eml1 in Vero cells (repolymerization experiment)*



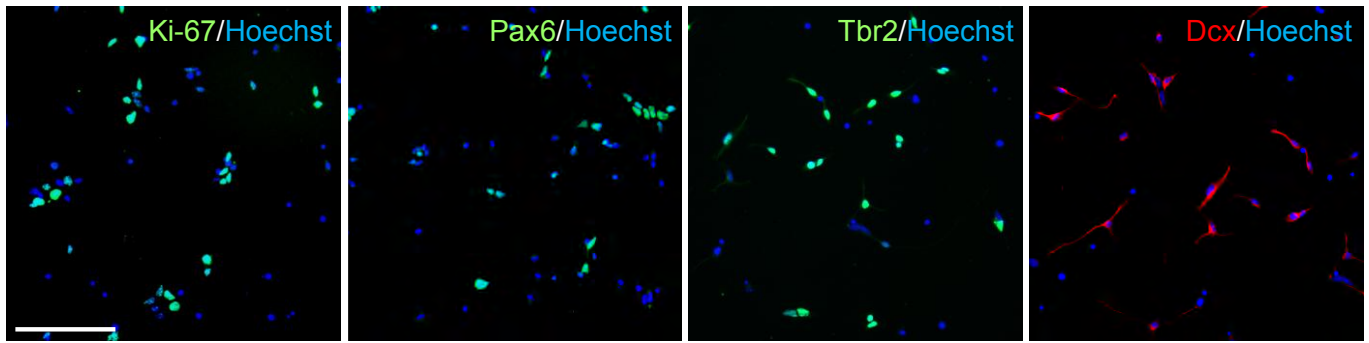
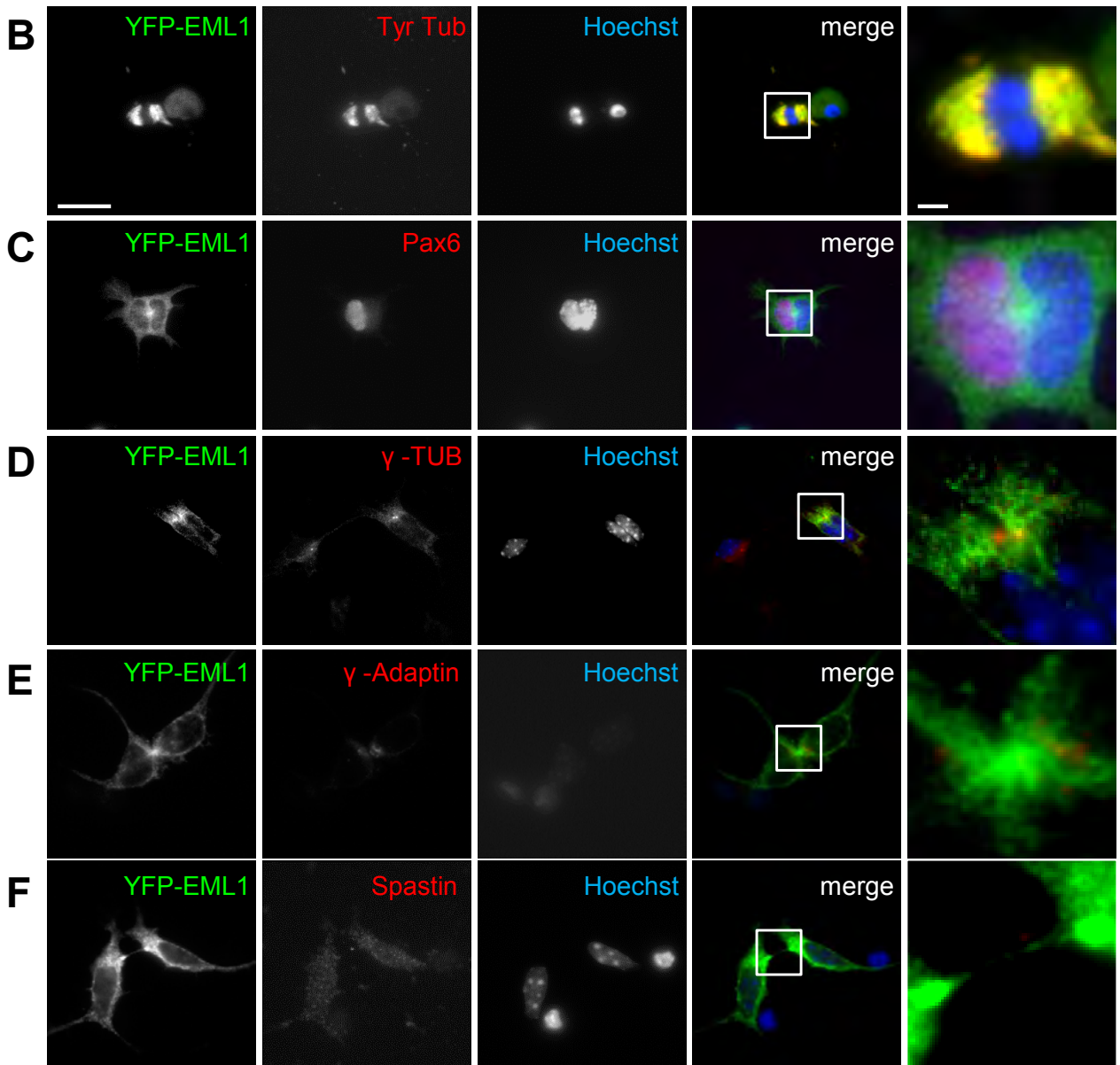
D *WT and T243A mutant Eml1 in Vero cells*



Supp Fig 3

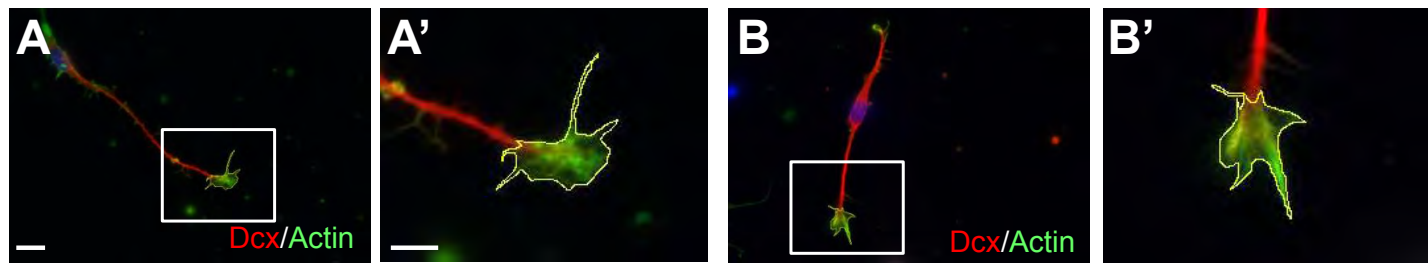


Supp Fig 4

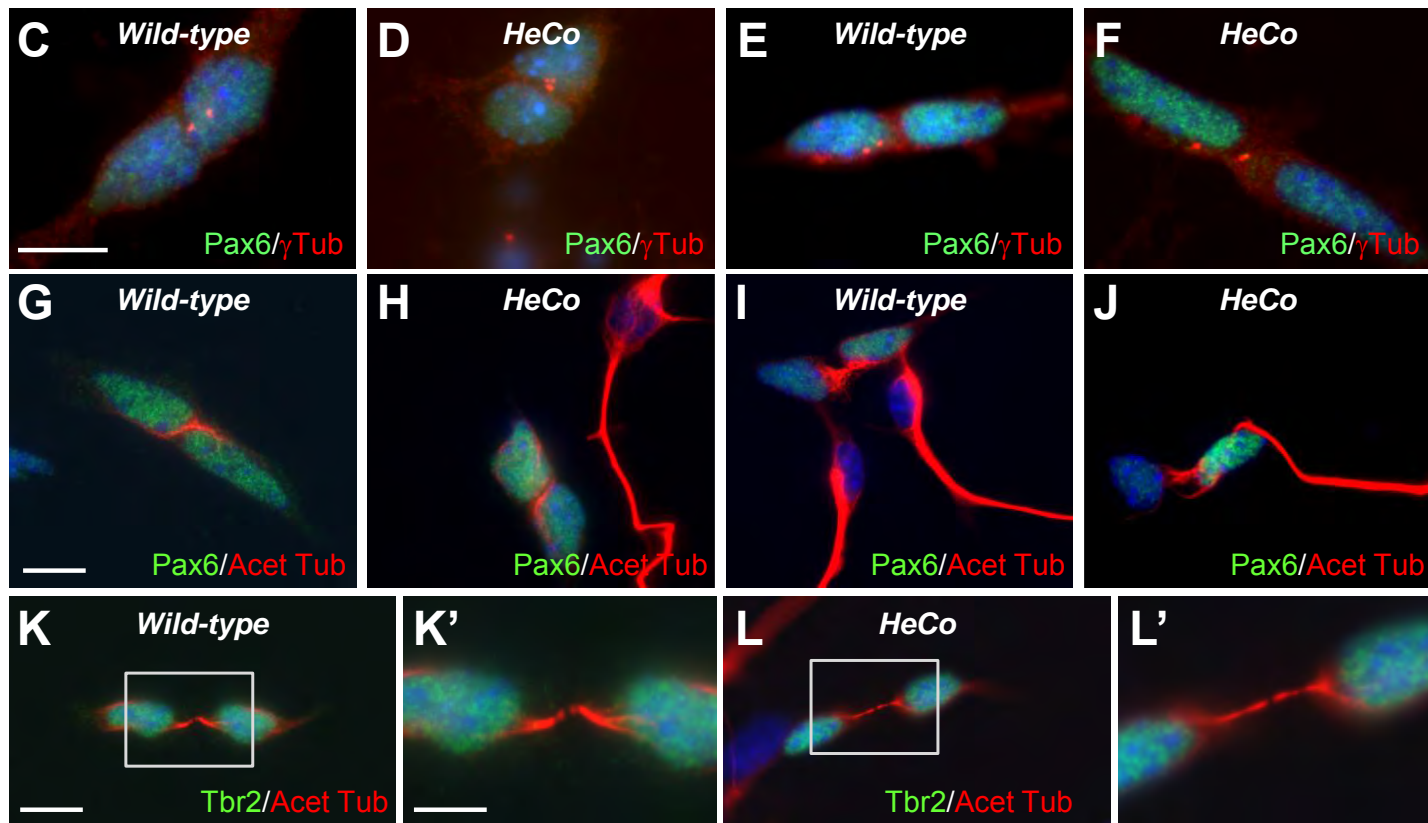
A***E12.5 progenitor and neuronal cultures******Recombinant EML1 in progenitors******Supp Fig 5***

Wild-type post-mitotic neurons

HeCo post-mitotic neurons

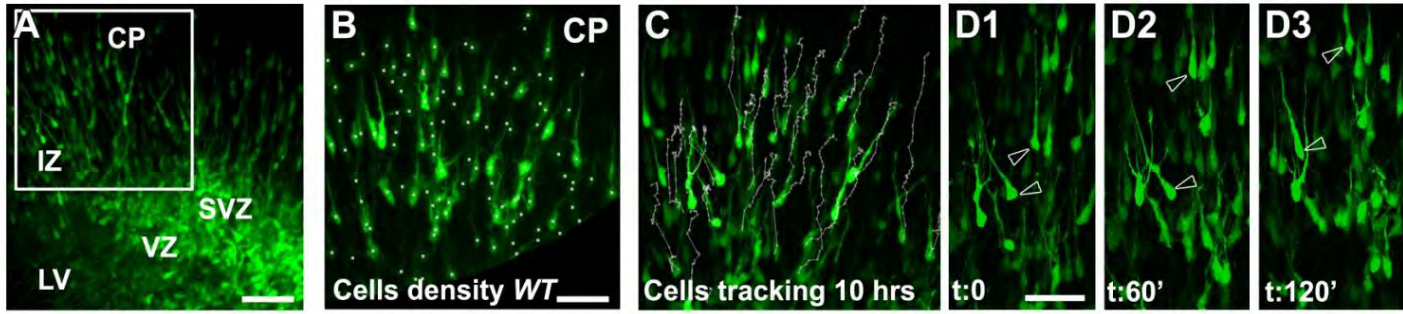


Pax6⁺ and Tbr2⁺ neuronal progenitors

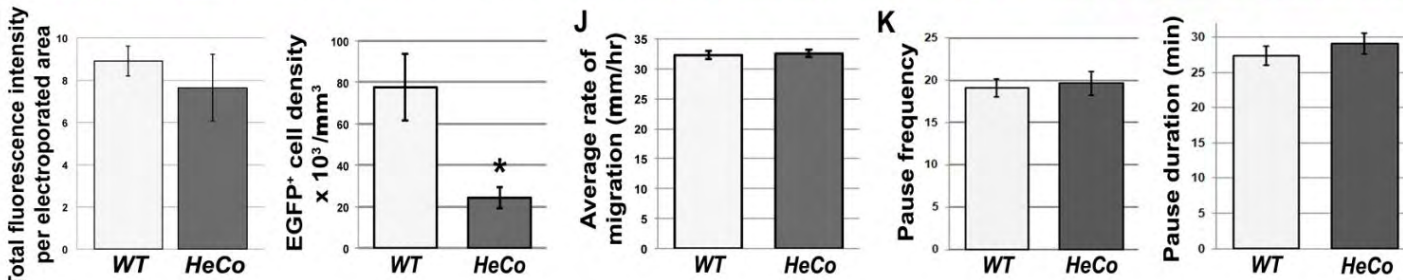
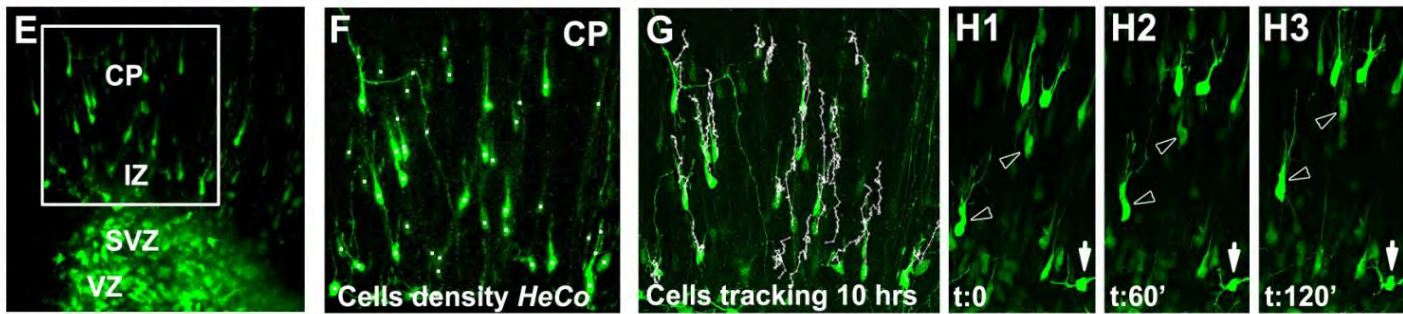


Supp Fig 6

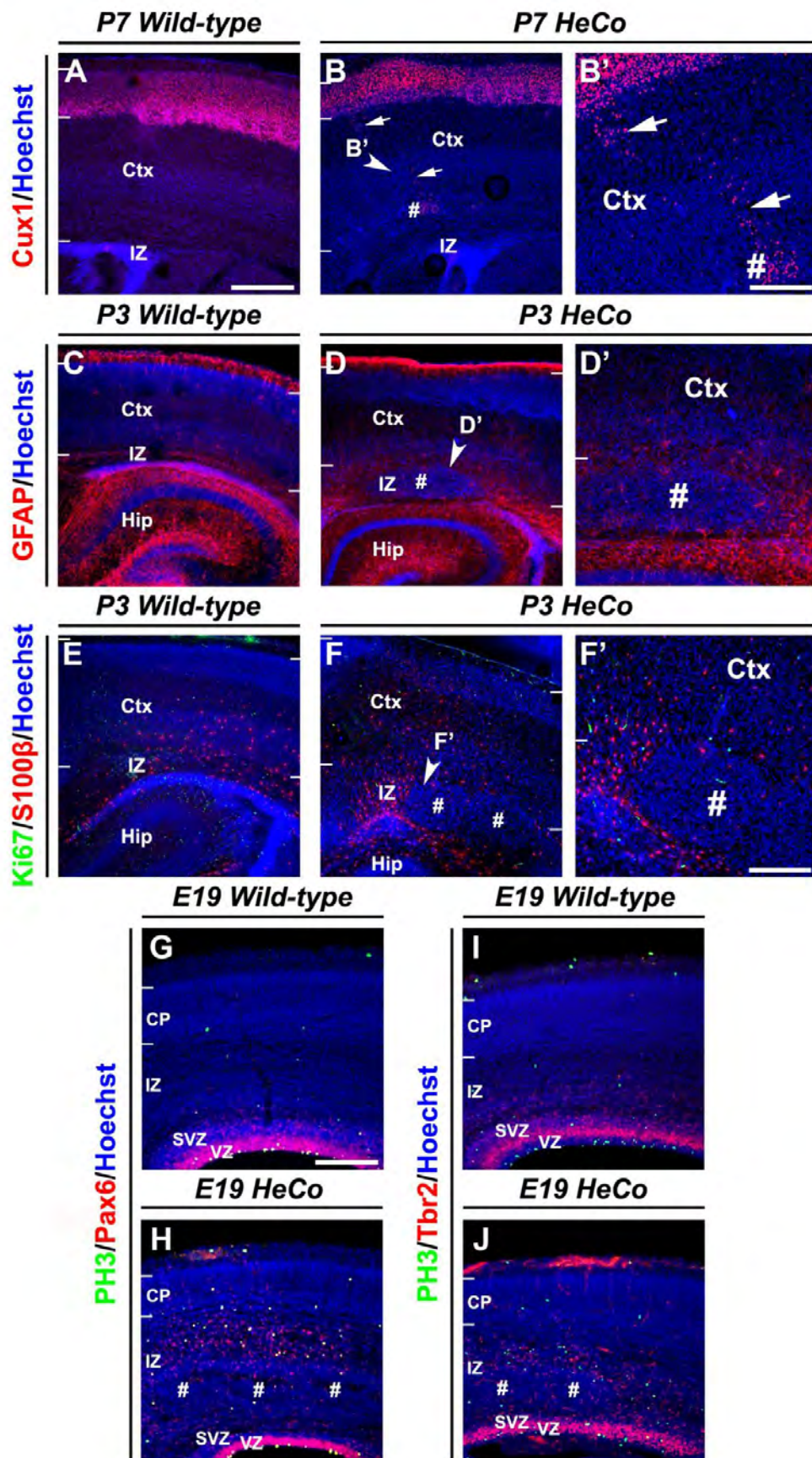
E15.5 ex-vivo pCAG-GFP electropo + 3DIV: time lapse on *Wild-type* slice



E15.5 ex-vivo pCAG-GFP electropo + 3DIV: time lapse on *HeCo* slice



Supp Fig 7



Supp Fig 8